Novel Strategies for Cleaning-in-Place Operations

Yang, Jifeng

Publication date:
2018

Document Version
Publisher's PDF, also known as Version of record

DTU Chemical Engineering
Department of Chemical and Biochemical Engineering

Novel Strategies for Cleaning-in-Place Operations

Jifeng Yang
PhD thesis
November 2018

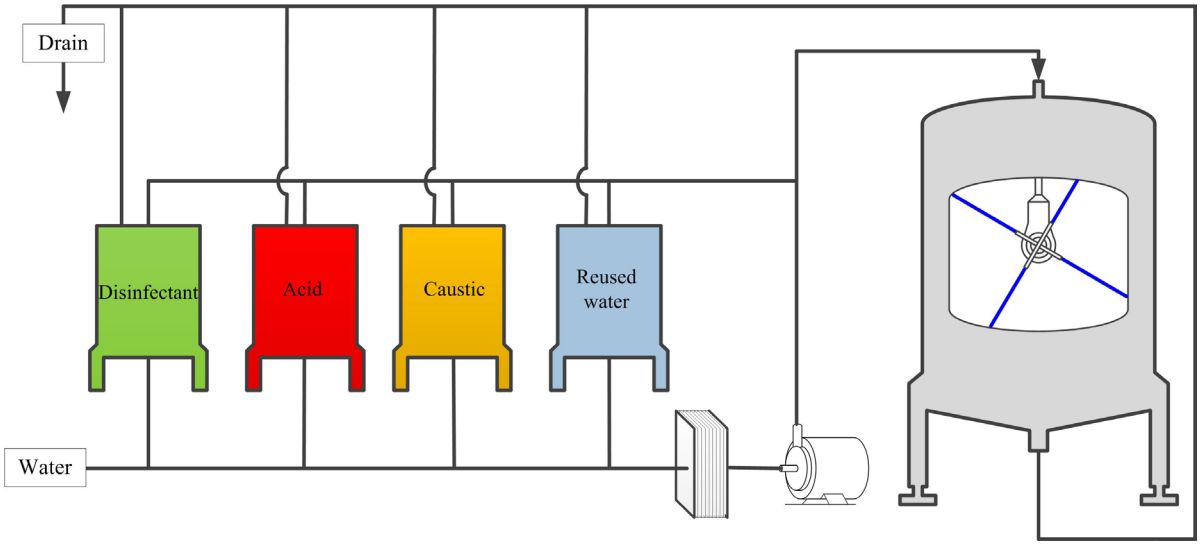

Technical University of Denmark

Novel Strategies for Cleaning-in-Place Operations

Ph.D. Thesis

Jifeng Yang

Supervisors

Ulrich Krühne (DTU)
Krist V. Gernaey (DTU)
Mikkel Nordkvist (Alfa Laval)

Department of Chemical and Biochemical Engineering
Technical University of Denmark
2800 Kgs. Lyngby
Denmark

November, 2018

Address: Process and Systems Engineering Center (PROSYS)

Department of Chemical and Biochemical Engineering

Technical University of Denmark

Building 229

Dk-2800 Kgs. Lyngby

Denmark

Phone: +45 4525 2800

Web: www.kt.dtu.dk/forskning/prosys

Print: STEP

Email: jifeng.yang@outlook.com

DTU Chemical Engineering
Department of Chemical and Biochemical Engineering

Summary

Cleaning-in-place (CIP) is a widely used technique in food and pharmaceutical industries. The execution of CIP is critical for food safety and public health. Since the introduction of CIP, various studies have been performed in order to reduce the cleaning costs without compromising the cleaning quality.

The starting point for this thesis was a mapping study at the world-leading brewery, Carlsberg Danmark A/S (Fredericia), in which the most time- and resource-consuming CIP operations were identified. The suggestions for improving the existing CIP systems in the brewery are representative for the processes where similar CIP systems are utilized in other fields. The findings from the mapping study led to the topics explored in this Ph.D study.

The objective of this thesis is to investigate different approaches for reducing the resource consumption and cleaning costs during CIP operations. A number of parallel projects were defined and conducted for this purpose. All of these projects can stand alone when reading this thesis.

Firstly, a study based on the cleaning of an industrial brewery fermenter demonstrates how to analyse historical cleaning data to improve cleaning operations in the future. The proposed analysis approach detects anomalies in a CIP system online and offline. A trouble-shooting process is advised to guide the operators to diagnose the likely anomaly or fault.

Secondly, Computational Fluid Dynamics (CFD) was used to simulate the displacement of cleaning agent by water during the intermediate and final rinses of pipe systems. The results obtained include the identification of dead zones and the calculation of rinsing time, minimum water consumption, minimum generation of waste water, and pressure drop, etc. The cross-comparison of different pipe geometries indicates the key factors that determine the cleanability of various pipe elements. CFD proves to be an effective tool for the hygienic design of pipe systems and the optimization of pipe rinsing.

Thirdly, burst cleaning technique to clean the tank surfaces soiled by egg yolk was studied. The experimental observations were compared with the conventional cleaning method using continuous flows. Different cleaning parameters were investigated and optimised for removing the soil material at the lowest cleaning costs. The primary findings from pilot-scale studies were then examined in scale-up tests.

Fourthly, a three-stage measurement-based partial recovery CIP system was designed.

The purpose of the design was to prolong the lifetime of cleaning liquid by only recycling the clear liquid from the CIP outlet. The proposed approach was compared with other cleaning scenarios for economic analysis.

Lastly, the cleaning of toothpaste soil from vessel surfaces by impinging liquid jet and falling film was studied. The properties of the soil material and the removal force were investigated. The adhesive removal model presented by other researchers was applied to describe the experimental results. This study is the first work to integrate the effect of soil soaking and the cleaning by falling film into the existing model.

Dansk Resume

Cleaning-in-place (CIP) er en udbredt teknik inden for fødevare- og farmaceutiske industrier. Gennemførelsen af CIP er meget vigtig for fødevaresikkerhed og folkesundhed. Siden introduktionen af CIP er der blevet foretaget en række undersøgelser for at reducere rengøringsomkostningerne uden at gå på kompromis med rengøringskvaliteten.

Udgangspunktet for denne ph.d.-afhandling var en kortlægningsundersøgelse på det verdensledende bryggeri, Carlsberg Danmark A/S (Fredericia), i hvilket de mest tidskrævende og ressourcekrævende trin i CIP-operationer blev identificeret. Forslagene til forbedring af de eksisterende CIP-systemer i bryggeriet kan overføres til processer, hvor lignende CIP-systemer bruges på andre områder. Resultaterne fra kortlægningsundersøgelsen afødte emnerne for dette ph.d.-studie.

Formålet med denne afhandling er at undersøge forskellige metoder til at reducere ressourceforbrug og rengøringsomkostninger under CIP-operationer. En række parallelle projekter blev defineret for at møde dette formål. Alle disse projekter kan stå alene, når man læser denne afhandling.

Først viser et studie baseret på rengøringen af en industriel bryggerifermenter hvordan man kan analysere historiske rengøringsdata for at forbedre rengøringsprocesserne i fremtiden. Den foreslåede analysemetode gør det muligt at detektere anomalier i et CIP-system, både online og offline. En fejlfindingsproces anbefales for at guide operatørerne til at diagnosticere sandsynlige anomali eller fejl.

I anden del af afhandlingen bruges Computational Fluid Dynamics (CFD) til at simulere fjernelsen af rengøringsmiddel med vand under mellemliggende og slutskyl af et rørsystem. De opnåede resultater omfatter identifikation af 'døde' zoner og beregning af rensningstid, mindste vandforbrug, mindste generening af spildevand og trykfald etc. Sammenligningen af forskellige rørgeometrier indikerer de nøglefaktorer, der bestemmer rengøringsvenligheden af forskellige rørelementer. CFD viser sig at være en effektiv metode til hygiejnisk design af rørsystemer og optimering af rørrensning.

I tredje del studeres en 'burst' rengøringsteknik til rengøring af tankoverflader, der er tilsmudset af æggeblomme. De eksperimentelle resultater sammenlignes med den konventionelle rengøringsmetode, hvor der bruges kontinuerligt flow. Forskellige rengøringsparametre undersøges og optimeres til fjernelse af smudsmaterialet til de laveste rengøringsomkostninger. De primære resultater fra pilotskalaundersøgelser undersøges herefter i opskaleringstest.

I fjerde del designes et tretrins målebaseret partielt genvinding CIP system. Formålet

med designet er at forlænge rengøringsvæskens levetid ved kun at genbruge den klare væske fra CIP udløbsstrøm. Den foreslåede tilgang sammenlignes med andre rengøring scenarier i en økonomisk analyse.

Endelig studeres rensningen af tandpasta fra tankoverflader med jet-væskestråler og faldende film. Besmudsningsmaterialets egenskaber og fjernelseskraften undersøges. Den klæbende fjernelses-model fremlagt af andre forskere anvendes til at beskrive de eksperimentelle resultater. Denne undersøgelse er det første eksperimentle studie, der integrerer effekten af jordopblødning og rensning med faldende film i den eksisterende model.

Preface

This thesis is prepared at the department of Chemical and Biochemical Engineering at the Technical University of Denmark (DTU) in fulfilment of the requirements for acquiring a Ph.D degree. The project was carried out from December 2015 to November 2018, in cooperation with Alfa Laval Copenhagen A/S.

I would like to express my heartfelt gratitude to my academic supervisors Ulrich Krühne and Krist V. Gernaey from DTU, and my industrial supervisor Mikkel Nordkvist from Alfa Laval. All of them have devoted lots of time and efforts to my work. I keep their untiring and sincere teachings in my mind. It has been a great pleasure to work together and witness my research progress.

I would also like to thank my industrial collaborators Bo Boye Busk Jensen, Kim Kjellberg and Jesper Sundwall from Alfa Laval for thoughtful discussions and for helping me to learn advanced technologies. Also, thanks to Peter Rasmussen, Bjarne Pedersen and Anders Kokholm from Carlsberg and Lars Jensen from Ecolab for allowing me to perform industrial on-site studies and sharing their interest and experiences with me. I am also truly grateful to Professor Ian Wilson and his Ph.D students Rajesh Bhagat, Rubens Rosario Fernandes, Melissa Chee, Ru Wang and Harry Ayton at the University of Cambridge, who all have made me feel like a part of the team during my research visit in the summer of 2018.

I have also received help from many other colleagues at the PROSYS Research Group at DTU. I would like to thank everyone who has helped me by answering my questions. Especially, I would like to thank secretary Gitte Læssøe and former secretary Eva Mikkelsen for helping me with administration stuff, as well as Ph.D students Mengzhe Wu and Pau Cabañeros López for sharing unforgettable experiences in office 231 in building 227.

This project is part of the INNO+DRIP (Danish partnership for Resource and water efficient Industrial food Production) project. The fundings from the Innovation Fund Denmark (IFD) under Contract 5107-00003B and DTU are acknowledged. The passionate assistance from the partnership manager Hanne Skov Bengaard and the kind discussions with other collaborators within the partnership are greatly appreciated.

Last but not least, I will never forget the patience and support from my friends and loving family, in particular my wife Wenbo.

Jifeng Yang, November 2018

List of Abbreviations

AFM	Atomic Force Microscopy
ANOVA	Analysis of Variance
ATP	Adenosine TriPhosphate
BLFR	Boundary Layer Formation Region
CBR	Case Based Reasoning
CFD	Computational Fluid Dynamics
CIP	Cleaning-In-Place
COD	Carbon Oxygen Demand
COP	Cleaning-Out-of-Place
CPV	Cumulative Percent Variance
CTS	Confocal Thickness Sensor
DF	Degree of Freedom
DN	Nominal Diameter
DoC	Degree of Cleaning
DRIP	Danish partnership for Resource and water efficient Industrial food Production project
DTW	Dynamic Time Warping
EHEDG	European Hygienic Engineering and Design Group
ERT	Electrical Resistance Tomography
FDA	Functional Data Analysis
FDG	Fluid Dynamic Gauge
FN	False Negative
FP	False Positive

FTIR	Fourier-Transform Infrared Spectroscopy
GCV	Generalized Cross-Validation
MPCA	Multiway Principal Component Analysis
NIR	Near-InfraRed spectroscopy
NIZO	Nederlands Instituut voor ZuivelOnderzoek (Dutch)
PBL	Problem-Based Learning
PCA	Principal Component Analysis
PENSSE	Penalized Sum of Squares
PIV	Particle Image Velocimetry
PVC	PolyVinyl Chloride
RFZ	Radial Flow Zone
RJH	Rotary Jet Head
RO	Reverse Osmosis
RSH	Rotary Spray Head
RSM	Response Surface Methodology
RTD	Residence Time Distribution
SDBS	Sodium Dodecyl Benzene Sulfonate
SEM	Scanning Electron Microscope
SRC	Stepwise Regression Control
SS	Stainless Steel
SSB	Static Spray Ball
STD	STandard Deviation
TMP	Trans-Membrane Pressure
TN	True Negative
TOC	Total Organic Carbon
TP	True Positive
VFD	Variable Frequency Drive
WFM	Wide-Field fluorescence Microscopy
WSS	Wall Shear Stress

Contents

Part I

Background

CHAPTER 1

Introduction

Fouling is a critical problem in food and pharmaceutical industries. Cleaning aims to remove the product residuals and fouling materials that remain in the process line after production. The act of cleaning is crucial to ensure product quality and production safety. Industrial users often expect to minimize the cleaning costs without compromising cleaning quality. The purpose of this chapter is to present:

1. Fouling problems in industries;
2. The definition and implementation of cleaning-in-place;
3. Legislative guidelines of cleaning and hygienic design;
4. Typical cleaning-in-place systems;
5. The definition of cleaning assessment methods;
6. Typical challenges in the studies of cleaning;
7. The aim and structure of this thesis.

1.1 Fouling

During the production and transfer of food and pharmaceuticals, materials stick to the surfaces of the equipment and pipes. This build-up process is known as fouling. These unwanted material depositions, called soils, need to be removed before the next production can take place. Fouling is formed due to the adhesion of materials to the surfaces as well as the cohesion between elements of the materials being processed [1]. Fouling can be classified according to the means of formation, such as crystallization, particulate deposition, biological growth, chemical reaction, corrosion and freezing or solidification [2, 3].

Fouling results in increased operating costs of equipment. Moreover, a potential cross-contamination can threaten the product quality, which can be catastrophic to public health and operational safety. Therefore, cleaning is of great significance to the food and pharmaceutical industries. It is estimated that, for a food and beverage plant, nearly 20% of each work day is spent on cleaning [4].

1.2 Cleaning-in-Place

Cleaning-in-Place (CIP) is now a common cleaning practice for pipe systems, vessels, filters, process and associated equipment. It originated in the 1950s on dairy farms and was adopted by the brewing, dairy, beverage, pharmaceutical and food industries during the subsequent 15 years [5]. The concept of CIP is to clean the components of a plant without dismantling or opening the equipment, and with little or no manual involvement of operators.

Typical CIP systems utilize vessels for the storage and recovery of cleaning solutions. A series of pipelines, pumps, along with valves and field instruments are used to transfer and control the flows of liquids. The cleaning efficiency and cost effectiveness depend on the complexity and degree of automation of the cleaning system. Cleaning processes, either manual or automated and in all industries, tend to consist of a series of similar steps, including [6]:

1. *Product recovery* to drain product from the system;
2. *Pre-rinse* to remove excessive soils by using water;
3. *First detergent circulation* to loosen soils from surfaces and dissolve or suspend the soils in the alkaline detergent solution;
4. *First intermediate rinse* to remove the first detergent and entrained soils by means of water;
5. *Second detergent circulation* to remove harsher soils or mineral scales by acid;
6. *Second intermediate rinse* to remove the second detergent and soils by means of water;
7. *Disinfection (optional)* to kill microorganisms if sterile or aseptic environment is required for subsequent processes;
8. *Final rinse* to remove residual cleaning and/or disinfection agents.

CIP is more suitable than conventional manual cleaning methods for large scale operations, where complex plant and equipment are involved. CIP allows for high temperature, high chemical concentration and harsh chemicals, which are difficult to apply in manual cleaning operations.

1.3 Legislation and Hygienic Design

The design of food processing equipment requires the equal consideration of production purpose and cleaning possibility. The criteria for the hygienic design of food processing equipment have been described by the Machinery Directive 2006/42/EC and the amending Directive 2009/127/EC, part of which has been incorporated in the standards EN 1672-2:2005+A1:2009 and EN ISO 14159:2008 [7]. The European Hygienic Engineering

and Design Group (EHEDG) provides guidelines as authority on hygienic engineering and design. It is created by an international expert panel with diverse representatives of equipment manufacturers, food industries, research institutes and public health authorities. The EHEDG offers standardized tests for the cleanability of components. In the USA, prescriptive standards for dairy production have been amended for equipment design and sanitation, called 3-A standards. These standards are also adopted in other branches in the food industries in the USA. The ASME BPE standard used for Bioprocessing Equipment provides guidelines applicable to the specific parts with relatively high levels of hygienic requirements.

Stainless steel is the most frequently used material for processing equipment. In the hygienic industries, the selected stainless steel should meet the requirement: carbon content (C) $\leq 0.05\%$, molybdenum content (Mo) $\geq 2.0\%$. The inside surface roughness should be with the acceptance criterion of $Ra \leq 0.8$ µm [8]. The tanks, pipes, internal angles and corners need to be mounted to be fully drainable, or with drain valves installed as low as possible. Dead spaces shall be avoided, or at least should be capable of performing proper cleaning and disinfection. However, in reality, some production plants are not completely hygienically designed, especially when a new system is built by adding onto an existing layout. Therefore, the inspection of pipes and equipment is suggested periodically for detecting the potential defects or weaknesses.

1.4 CIP System

In all hygienic industries (e.g., food, beverage, pharmaceutical), similar CIP systems and equipment are used in CIP practices. Typical CIP systems can be divided into single-use and reuse [6]. For a single-use CIP system, the cleaning medium needs to be prepared freshly, and drained after finishing cleaning. The single-use CIP system should be installed as close as possible to the facilities that need to be cleaned. It reduces the possibility of cross-contamination and potential spore formation, which is more hygienic and flexible than the reuse CIP system. But single-use systems tend to be very expensive to operate. For a reuse CIP system, the cleaning medium is recovered partially or completely, depending on whether an intermediate storage is used or not. This type of system usually comprises large storage tanks and one or more recovery loops, as shown in Figure 1.1. The tanks and associated pipes and instruments to be cleaned can be cleaned simultaneously without delay.

1.5 Assessment of CIP Cleaning Efficiency

The assessment of cleaning efficiency can be divided into validation, verification and monitoring [6].

- *Validation* ensures that the information supporting the cleaning process is correct. It is the method that determines whether the cleaning process is correct. Validation

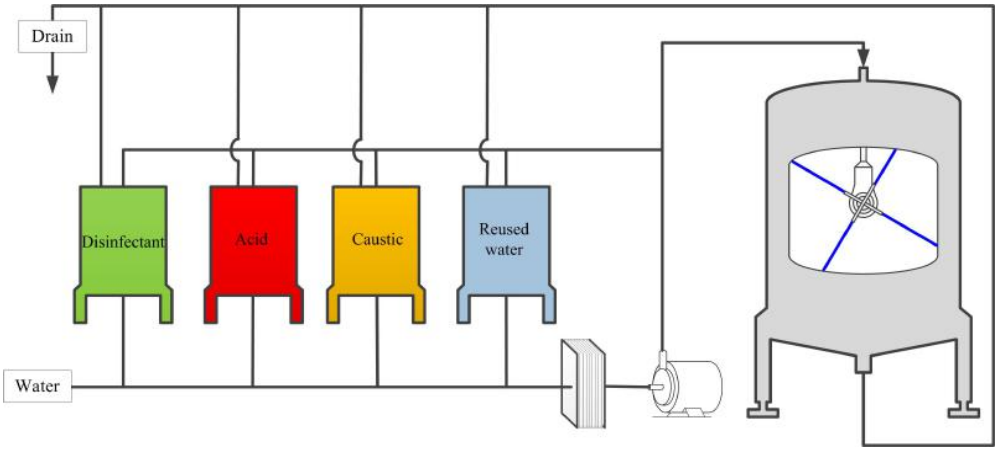

Figure 1.1: A typical reuse CIP system in industries for cleaning a fermenter

takes place before implementation and after alterations of a CIP system that is going to be used;

- *Verification* is the procedure that determines whether the fouling deposits have been removed as expected after performing a validated cleaning process. Verification takes place after the production or cleaning run, with low frequency;

- *Monitoring* refers to the regular measurements taken during the cleaning process for detecting the end point of each cleaning stage and indicating whether the process is in a state of control. It should ideally be easy to perform the monitoring, and the results are obtained fast.

1.6 Challenges of CIP Optimization

During the past 60 years, studies of CIP have mainly been carried out with focus on the fouling and cleaning mechanisms, the design of new hygienic equipment, the assessment of cleaning efficiency and the optimization of operating conditions. However, there are still a number of challenges in current industrial practices:

- Cleaning results and process parameters are directly related to hygienic design. The design and installation of the plant should avoid the presence of pits, crevices, gaps, sharp edges, visible threads and dead ends, because these structures are difficult to clean and disinfect due to the lack of fluid movement in these areas. The presence of porous or rough surfaces may also proliferate bacterial colonies [6, 9]. The application of Computational Fluid Dynamics (CFD) in hygienic design has a future in improving the processing equipment through predicting the adhesion of deposits and the cleaning performance of surfaces [10].

- Despite the high automation of current CIP systems, most cleaning operations proceed semi-empirically and far from optimal. This is because (1) the confirmation of cleanliness is mostly achieved by offline measurement in an open-loop control, and (2) there is no effective measurement method to exactly detect the end point of cleaning [11]. Therefore, current CIP systems are normally controlled with fixed cleaning times and/or fixed volumes of cleaning agents [12]. The cleaning time is merely predictable using a series of adjustable variables [5], and usually determined from experience. Thus, excessive amounts of water and chemicals are used in order to ensure complete cleanliness, which causes large operating costs and high environmental impact.
- Cleaning operations generate large amounts of waste water containing corrosive pollutants, nutrients, organic loadings, biochemical oxygen components and heat. Minimizing the environmental impact of cleaning has become of great importance due to the legislative pressure towards the establishment of zero emission processes [13]. In addition to waste water treatment, another possibility is to take into account the mass balance and energy balance in the whole system. This can be realized through three steps: (1) investigating the current water balance; (2) optimizing the water consuming processes; and (3) optimizing the overall process with zero discharge of water and the minimal consumption of energy [14].
- It is problematic to compare and transfer results from lab scale experiments to industrial scale equipment. The deposits observed in experiments are often not representative of real soils. The relationship between the cleaning rate and the effectiveness of cleaning at different scales is still unclear [15].
- In some industries, the CIP systems have been employed for many years and are relying on outdated methods. Early CIP systems typically had a one-size-fits-all cleaning cycles. But the different sets of processing equipment need individual CIP recipes and cleaning requirements. In addition, the age of pipelines and the rearrangement of process equipment have often reduced the efficiency of the originally designed CIP capacity, which requires the renovation of the pipes. Meanwhile, a CIP process should be considered together with the production process in order to achieve the final goal of an efficient, robust, and validated CIP operation, named integrated CIP design.

1.7 Thesis Aims and Structure

This Ph.D project is a part of the INNO+DRIP (**D**anish partnership for **R**esource and water efficient **I**ndustrial food **P**roduction, `http://drippartnership.com/`) project. The partnership involves a number of food companies and technology providers, three universities and two GTS institutes (research and technology organizations). The ambition of INNO+DRIP project is to produce more with less water at leading Danish food producers. The goal is a reduction in water consumption of 15 – 30%.

The objective of this Ph.D thesis is to shed light on the opportunities for reducing water usage during CIP. This Ph.D work was performed in close collaboration with the partners

including a technology provider, a food end-user, a chemical supplier and an academic partner. The primary intention of the project is to provide practical solutions for saving cleaning costs in industrial CIP applications.

This thesis is divided into three parts. Part I (Chapters 1 and 2) focuses on the background including the basic knowledge of CIP and the present status of the research activities about CIP. Part II (Chapters 4 to 8) describes the research conducted in this Ph.D work. Each chapter can be read separately and some are written as scientific articles with additional information added in the thesis. Chapter 3 describes a mapping study of the CIP systems in a brewery and serves as an introduction to the following investigations. Chapters 4 and 5 aim to optimize existing CIP operations by analysing industrial monitoring data and simulating the displacement process in pipe systems. Chapters 6 to 8 are focused on designing new CIP systems. The conclusions and perspectives of this work are presented in Part III (Chapters 9 and 10).

In this thesis, a “List of Abbreviations” (pages vii - viii) summarizes all abbreviations appearing in the whole thesis. Each chapter contains its own nomenclature, where sometimes the same letters are used in different chapters but have different meanings.

CHAPTER 2
Literature Review

Chapter 1 has highlighted the challenges encountered during the industrial implementation of CIP. This thesis aims to investigate different approaches for reducing resource consumption and cleaning costs during CIP operations. To achieve this, a literature review in this chapter is conducted, including:

1. The understanding of soil materials and study methods;
2. The cleaning mechanisms for typical soil types;
3. The effects of different cleaning parameters on the cleaning performance;
4. The monitoring techniques for measuring a cleaning process online or offline;
5. The studies and techniques about tank cleaning and open surface cleaning;
6. The application of mathematical modelling and data analysis tools in cleaning studies;

2.1 Soil Studies

2.1.1 Soil Types

Fouling is a result of the adhesion of species to a surface and the cohesion between the elements contained in the deposits [1]. According to the complexity of the physiochemical properties of the soils and the types of cleaning fluid, cleaning problems can be classified through a diagram representation (Figure 2.1) [15].

The horizontal axis in Figure 2.1 indicates the soil complexity ranging from non- or low-viscosity fluids to high viscous fluids and even cohesive solids. The vertical axis determines which fluid should be used for cleaning, including cold water, hot water and hot chemical solutions. Figure 2.1 demonstrates that clusters of similar problems are found with respect to cleaning issues from the food and personal care product industries. According to Fryer et al. (2009), the shaded area shows three types of soils that are most difficult to clean [15]):

- *Type 1* soils refer to viscous or viscoelastic or viscoplastic fluids that can be removed by water, such as toothpaste, shampoo, cream and mustard;

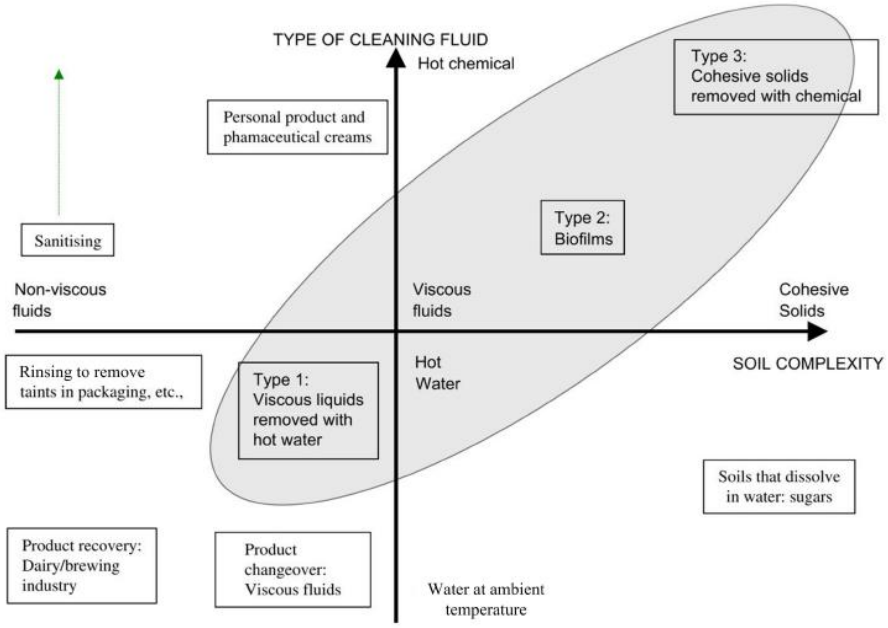

Figure 2.1: Cleaning map; a classification of cleaning problems based on soil type and cleaning chemical use. (Adapted from Fryer et al. (2009) [15])

- *Type 2* soils are biofilms that require biocide to kill the adhered organisms and then water to remove them, such as bacteria, spores and yeast species;
- *Type 3* soils are cohesive solids that require chemicals for cleaning, such as whey protein concentrate, egg yolk/albumin, sweet condensed milk and starch.

2.1.2 Soil Study Methods

The removal of deposits from surfaces mainly consists of two processes: (i) if the deposit is soluble in the cleaning liquid, it is removed during dissolution even in a static condition; (ii) regardless of the solubility of the deposit, fluid mechanical forces can remove soil materials by overcoming the cohesive and adhesive forces [13]. Table 2.1 lists some methods for studying soil properties. The main purposes of studies conducted to investigate soils often include:

- Measurements to understand the cleaning mechanism. Scanning electron microscope (SEM) has been used to investigate the change of soil surface under different NaOH concentrations and temperatures [16, 17]. Fluid dynamic gauge (FDG) can be used to measure the soil thickness and contribute to developing an understanding of the swelling process of the material. Wide-field fluorescence microscopy (WFM)

Table 2.1: Summery of soil study methods

Techniques	Characteristics	Soil types and references
SEM	Surface topography	Whey and whole milk protein [16, 17]; *Bacillus* spores [19]
FDG	Soil thickness	Egg yolk [20]; Gelatine and egg yolk [21]; β-lactoglobulin gel and whey protein [22]; Whey protein [23]; *Bacillus* spores [19]
WFM	Fluorescence of proteins	Whey protein hydrogels labelled with fluorescent tracer [24]
Micromanipulation	Cohesive force and adhesive force	Egg albumin [25]
Millimanipulation	Cohesive force and adhesive force	Carbohydrate-fat food soil [26]
AFM	Adhesive force	Whey protein concentrate [27]; Toothpaste, sweetened condensed milk, Turkish delight and caramel [18]
Rheology	Viscosity; Yield stress; Microstructure property	Toothpaste [28]; Food product (i.e., dairy, emulsion gels) [29]
Microindenter	Shear modulus	Whey protein hydrogels [30]

can also provide swelling and dissolution information by detecting the protein concentration in the liquid phase.

- Measuring the required force to remove deposits from surfaces. Both micromanipulation and millimanipulation techniques have been developed to study the adhesive and cohesive forces required to deform and displace soil layers. The latter can measure larger forces and deeper layers than the former. Atomic force microscopy (AFM) is more sensitive to determine adhesive forces and can work in nano-scale, which can help the studies of anti-fouling surfaces [18].

- Measuring the internal properties of deposits. The application of rheology measurement and microindenter provides information about the structural change of soils for example by soaking. The understanding of the internal resistance of soil is valuable to select an optimal cleaning method.

There are also spectroscopic techniques available to investigate biofilms, such as confocal microscopy, reflective Fourier-transform infrared spectroscopy (FTIR) and near-infrared spectroscopy (NIR). However, the application of these methods has yet to be reported because of the challenges of speed, resolution, and cost [31].

2.1.3 Soil Soaking and Swelling

Fundamentally, the cleaning process of protein or starch deposits consists of three phases [23, 32]. First, the initially dry soil contacts with the cleaning liquid and swells to be a weakened and mobilised soil layer. The removal rate in this phase is insignificant. Second, the weakened layer is exposed to mechanical stress and chunks of deposits are removed at a high rate. The main mechanism in this phase could be viscous shifting or cohesive separation. Third, the cleaning mechanism switches to the decay phase, where the removal of small soil particles is limited by the continuous diffusive swelling process. This induces a substantial increase in the time scale.

Swelling comes together with soaking, which is a combined result of chemistry, temperature and time. As a consequence, the force required for cleaning can be reduced greatly. For example, the force to detach carbohydrate-fat based soil is reduced by 95% after submerging the dry material into sodium dodecyl benzene sulfonate (SDBS) solutions. The understanding of soaking and swelling helps to implement burst technology in tank cleaning and to design new tank cleaning devices for example by combining the advantages of liquid fans to wet the soil and nozzles to mechanically detach the soil in one rotary jet head [33]. The concept of burst cleaning is to perform cleaning operations by interrupting a continuous flow with several breaks between shots of fluid, with the goal to reduce cleaning cost by using less chemicals to achieve a certain level of cleanliness.

2.2 Cleaning Mechanisms

Long time scale soluble deposits can be removed by diffusion-reaction without the involvement of mechanical forces. Liquid forces mainly contribute to the breakup of cohesive and adhesive strength from deposits and surfaces [34]. A comparative overview of four relevant cleaning mechanisms is shown in Figure 2.2, namely diffusive dissolution, cohesive separation, viscous shifting and adhesive detachment [32].

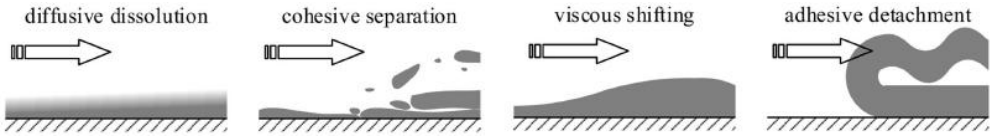

Figure 2.2: Overview of cleaning mechanisms. (From Joppa et al. (2017) [32])

However, for the same soil type, the cleaning mechanism may change under different operating conditions and cleaning phases. For instance, when rinsing a pipe filled with toothpaste using water, the toothpaste is initially displaced as chunk and then eroded away (cohesive failure) gradually [35]. On the other hand, when cleaning toothpaste by impinging jets and falling films, an adhesive failure model works to illustrate the cleaning process, which is discussed in Chapter 8.

2.3 The Effects of Cleaning Parameters

The key parameters affecting cleaning effectiveness have traditionally been illustrated by Sinner's circle, involving temperature, time, chemicals and mechanical forces [6]. Sinner's circle has later been revised by the Nederlands Instituut voor Zuivelonderzoek (NIZO, Dutch Institute for Dairy Research), as shown in Figure 2.3, combining the equipment design and the product related factors [36].

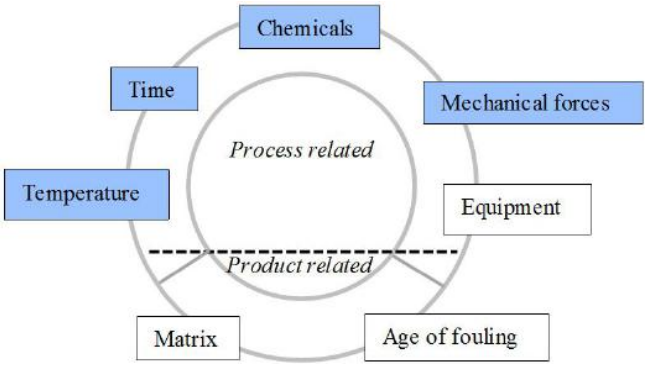

Figure 2.3: Sinner's circle by NIZO illustrating the cleaning parameters. The shaded factors are the parameters in the original Sinner's circle. (Adapted from Asselt et al. (2012) [36])

When designing a cleaning method, the initial consideration is the nature of the product [31]. The matrix of the soil structure mainly refers to the components of soils, which determines the degree of difficulty of the cleaning process, see Figure 2.1. Heating the soil can lead to more energy required to clean it, particularly for protein-based materials [37]. Generally, ageing may yield a stronger and more resistant deposit due to phenomena such as drying and reaction [31]. The equipment should have smooth surfaces with no dead zones and should be easy to dismantle. The process related parameters that affect cleaning behaviour are reviewed in the following subsections.

2.3.1 Chemistry

CIP relies substantially on the proper usage of chemicals like alkalis, acids, disinfectants, and surfactants. Alkaline solutions are mainly used to react with carbohydrate and protein-based soils as well as to make fats and oils soluble. Sodium hydroxide is a commonly used alkaline detergent, supplemented with additives to increase the removal capability to specific soils. Acid can dissolve mineral deposits that are introduced by hard water or heating products. Formulations of acids may contain phosphoric acid and organic acid (lactic, gluconic, glyconic), etc. Surfactants are added in alkaline and acid solutions mainly for an anti-foam purpose. Anionic, cationic or non-ionic surfactants are normally employed as effective surfactants [38].

If a sanitary environment is required, the acid step is generally followed by a disinfection

treatment to kill microorganisms or decrease the number of microbes to a safe level. The common disinfection methods include heating, oxidising solutions (e.g., chlorine-based, iodophors, and peroxide-based) and non-oxidising surfactant-based solutions (e.g., quaternary ammonium compounds, acid anionic, amphoteric disinfectants) [6]. Hydrogen peroxide is a suitable candidate for industrial purposes because the remaining disinfectant can easily break down into water and oxygen.

Generally, a higher detergent concentration contributes to a higher cleaning rate. However, an optimal detergent concentration may exist for specific soil materials. The increase in chemical concentration above the optimum can only result in limited improvement of the cleaning efficiency, sometimes even decreased efficiency. For example, Bird et al. (1991, 1992) indicated the existence of an optimal concentration of NaOH (ca. 0.5 wt%) to clean cooked whey protein [16, 17]. They explained that high alkali concentrations changed the deposit structure rapidly to form a very thick translucent layer, which was difficult to remove. A negative performance by increasing alkaline concentration has also been observed when studying other protein- and lipid-based soils like egg yolk [39], and was also found in the study reported in Chapter 6.

2.3.2 Temperature

Even though it is often expected to perform cleaning at room temperature, some industries apply heating to increase the cleaning rate and to remove harsh deposits. Using high temperature in a cleaning process should be thoroughly considered along with the chemical effectiveness, system complexity, operating cost and risk, etc. Heating the cleaning media and maintaining them at a certain temperature level is one of the biggest energy consuming steps in a cleaning process [40].

Higher media temperature can increase the diffusion rate of chemicals and the reaction rate, henceforth improve the chemical effectiveness. For example, pink guava puree fouling cannot be effectively cleaned at 35 °C even with high NaOH concentration (up to 2.0 wt%). However, when the temperature is increased to 50 °C or 70 °C, fouling is removed completely [41]. For yeast soil, an increase in temperature from 30 to 50 °C does not decrease the cleaning time. However, chemical cleaning at 70 °C can shorten the cleaning time greatly [42].

An extremely high temperature may sometimes make the cleaning unprofitable. For instance, changing water temperature from 22 to 45 °C can improve the rinsing effectiveness significantly when flushing reconstituted skim milk from stainless steel pipes. A further increase to 67 °C only improves the cleaning rate slightly but increase the operating cost hugely [43]. Furthermore, the increase in temperature can change the structure of deposits. Goode et al. (2013) found that the dependence of adhesive force on temperature was related to the types of deposits and surfaces. For whey protein concentrate deposits, the adhesive force became high after being heated to a temperature above 70 °C due to the denaturation of proteins. On the contrary, caramel deposits turned to be less adhesive to stainless steel surfaces with temperature increasing from 30 to 90 °C [44].

Another application of heating is to disinfect surfaces. For example, in the dairy industry,

high temperature is often used after caustic and acid treatments to kill microorganisms or decrease the microbe amount to a safe level.

2.3.3 Time

Cleaning time is usually regarded as a characteristic to evaluate the performance of a cleaning recipe. In a cleaning practice, the cleaning time is generally determined by assuming that the area that is the most difficult to clean can still be cleaned, which is called the "worst case" scenario. In most cases, a long cleaning time results in better cleaning results. The exceptions are the cases where soil materials become restructured to be harsher under extreme chemical and heating conditions, like the denaturation of proteins. However, longer cleaning time also means more resource consumption.

For industrial cleaning operations, a short cleaning time is normally associated with high cleaning efficiency. This is because industries expect a minimized cleaning downtime in order to produce more products in a fixed period. It is estimated that a food and beverage plant spends approximately 20% of each day on cleaning the equipment. A 20% reduction in cleaning time therefore delivers approximately an extra hour of production time to each day [4].

2.3.4 Mechanical Force

The mechanical force, normally referring to the physical impact that acts on soil layers, is mainly discussed in the cleaning of pipe or pipe-like (e.g., flow cells) systems. The general rule is that high flow rates lead to high removal rates because of the high impact and shear force on the deposit layer. A critical wall shear stress of 3 Pa is used for the standardised EHEDG cleaning test method [45].

Asteriadou et al. (2009) coated sweet condensed milk on a lab scale stainless steel coupon and fit the soiled coupon in a flow cell. The test coupon was flushed with water. It has been found that the cleaning time decreases greatly by increasing the Reynolds number from 2,500 to 15,000. Interestingly, a further increase only results in a limited reduction of the cleaning time [46]. Gillham et al. (1999) investigated the contribution of each cleaning factor in different cleaning phases of whey protein concentrate deposits by using alkaline solutions. They found that the protein removal rate was strongly dependant on the swelling of the deposit layer in the beginning while the decay phase was more sensitive to the flow rate (or the wall shear stress) [47].

2.3.5 Coverage

In tank cleaning operations, coverage is related to the total flow of the cleaning liquid but also related to the selection of the particular tank cleaning device (see Section 2.5.1). The coverage of internal surfaces includes: (1) direct coverage, which is the result of the jets or fans of cleaning liquid hitting the surface to be cleaned directly, and (2) indirect coverage, which is provided either by a splash-back effect or by the effect of a falling film

[6]. Coverage is the prerequisite of other parameters like chemistry, temperature, time and mechanical force.

The coverage of tank surface is dependent on the cleaning time and flow rate. In burst cleaning operations, the period of each burst should ensure that the whole internal surface is covered after each cycle. A fast coverage of the tank surface enables fast wetting of soil layers. As a result, the cleaning costs are potentially reduced by minimizing chemical consumption [33].

2.4 Cleaning Monitoring

This section discusses the monitoring techniques that can be used to evaluate the cleaning result and to determine the end point of each cleaning stage, for example, by sensors. An ideal technique should not only be accurate and fast, but also automatic, applicable to industrial practices and low cost. The measurement results need to represent the overall cleaning performance instead of the clenaing of a local point or area. If possible, the inclusion of a sensor should be noninvasive, which means the sensor cannot become the source of contamination or the area that is difficult to clean. Table 2.2 summarizes some measurement methods that can be used to assess the cleaning performance.

In general, more than one monitoring method is utilized to assess the cleaning results. Christian et al. (2006) studied the cleaning of a pilot scale plate heat exchanger fouled by whey protein, which was rinsed by water and NaOH solutions of different concentrations. The cleaning was monitored through both the reduction in pressure drop and the increase of the heat transfer coefficient. The positive overshoot of the pressure drop and the negative overshoot of the heat transfer coefficient indicated the swelling of deposits caused by chemical diffusion. Both measurements resulted in steady values after the cleaning had been done. The cleaning times determined by the pressure drop data were shorter than those determined by the heat transfer coefficient, suggesting that the last part of deposits to be removed had greater effect on heat transfer than on flow characteristics [51]. Goode (2012) investigated the cleaning of stainless steel pipes in a pilot plant, which was fouled by yeast slurry (to mimic Type 1 and Type 2 deposits) or cooked caramel (to mimic Type 3 deposits) in brewing processes. Inductive conductivity sensors were located before and after the test section, and a turbidity sensor was placed after the test section. The turbidity measurement increased from a low value to saturation, which suggested the cleaning of the deposit. The conductivity values fluctuated significantly due to the poor mixing of deposits at low flow rates. The author concluded that the inductive conductivity measurements were not reliable when the volume of deposit relative to the volume of cleaning water was very small. Turbidity measurements were recommended for CIP optimization purposes [59].

In industrial practices, the selection of measurement methods depends on various factors, such as the process, the plant, the type of fouling and the operating conditions. Among these techniques, the online measurement of bulk liquid rather than a surface is the most employed strategy. For example, the company Ecolab A/S has developed a CIP monitoring system (3D TRASAR^{TM}) [65]. The online continuous monitoring is realized

Table 2.2: Monitoring techniques for fouling and cleaning in CIP systems. (After Wilson (2005) [31])

Methods and References	Measuring	Timescale	Issues
Visualization [37, 48, 49]	Local contaminated surface	Real-time or Retrospective	Easy to do; Rapid; Subjective assessment; Accuracy and resolution; Training and cost; Non-quantitative; Hard for large scale
Overall pressure drop [50, 51]	Hydraulic performance across the contaminated section	Real-time	Accuracy (differential pressure); Interpretation for complicated units; Dependent on flow pattern
Overall heat transfer coefficient [46, 50, 51]	Thermal performance of contaminated area	Real-time	Accuracy; Interpretation; Dependent on process model
Local heat flux [52]	Thermal performance of local contaminated area	Real-time	Reliability; Local-scale up; Material model
ATP bioluminescence [53, 54]	Microbiological activity on contact surface or in liquid	Retrospective	Time lag; Specificity of detection; Dormant cells
Microbiological counting [53, 55, 56]	Microbiological activity on contact surface	Retrospective	Soluble and insoluble materials on surfaces; Time lag and time consuming; Skilled operators; Invasive; Sample location
Protein concentration [57]	Foulants in disassembled pipe sections	Retrospective	Invasive; Time lag and time consuming; Complex disassembly and assembly
Conductivity, pH, or Turbidity [58, 59, 60, 61]	Foulants and chemicals in bulk liquid	Real-time	Cheap; Rapid; Sensitivity varies for different contaminants; Bulk liquid detection so uncertainty is high; Specificity
TOC [62]	Organic foulants in bulk liquid	Real-time	Sensitivity; Bulk liquid detection so uncertainty is high; Tolerance of TOC analyzer; Require short residence time in the analyzer
COD [61]	Foulants and chemicals in bulk liquid	Retrospective	Bulk liquid detection so uncertainty is high; Specificity of foulant
Ultrasonics [63]	Foulant thickness on contaminated surface	Real-time	Local; Hard for scale-up; Intrusion into flow; Calibration for foulants
ERT [64]	Foulants and chemicals in bulk liquid	Real-time	Noninvisive; 2D visualization; Size of cross section; Sensitivity varies for different foulants; Bulk liquid detection so uncertainty is high; Specificity

through measuring the temperature, time, flow rate, pH, and turbidity, etc. The turbidity measurement controls the quality of cleaning. The other measurements are measuring the processing parameters in cleaning cycles. A similar CIP optimization approach, called OptiCIP, has also been proposed by NIZO [66]. Offline measurements are only applied for stand-alone systems. Conductivity probes have also been installed at present commercial CIP plants [54]. Using such probes, it is possible to monitor the blending phase between cleaning detergents and rinsing water. The challenge of conductivity analysis is the two distinctly different conductivity ranges of detergent solutions (acid or caustic) and water. Typically, two sensors with different conductivity ranges are required. Recently, a single multi-channel analyser with multi-range measurement capabilities or a single sensor with the full dynamic range from low to high has been applied [67].

The measurement of adenosine triphosphate (ATP) has also been more and more popular for cleaning verification, because it directly determines the biological cleaning/contamination. ATP is the chemical compound in which energy is stored in all living cells. It is also present in most food debris. Some quick methods to test the presence of ATP have been developed, for example by using the enzyme luciferase that emits light when in contact with ATP. The level of luminescence can be measured easily, displaying the presence of living organisms or food debris [44, 54]. Despite its offline manipulation, ATP measurements have proven to be an efficient and effective approach to assess cleaning results when used in combination with other techniques.

2.5 Cleaning Tank Surface and Open Surface

2.5.1 Tank Cleaning Devices

Tank cleaning is one of the most common CIP operations in food industries and accomplished with the help of tank cleaning devices. The purpose of installing a cleaning device is to distribute liquid on the tank surface. There are three main choices for tank cleaning tasks, as illustrated in Table 2.3.

A static cleaning head like a static spray ball (SSB) sprays large volumes of low-pressure liquid onto the tank surface at fixed spots. A single axis rotary spray head (RSH) distributes the cleaning liquid using a rotating fan. A rotary jet head (RJH) distributes the cleaning liquid through a number of nozzles, which rotate around both the vertical and horizontal axes to ensure full coverage of the tank surface. The comparison of these three cleaning devices is described in Table 2.3.

2.5.2 Cleaning by Impinging Jets

Water jet flows are extensively used for the removal of deposits from surfaces for example by static spray balls and rotary jet heads. When jet flows travel in air, cylindrical jets tend to break into small drops after a certain distance due to air entrainment that causes flow instability [68]. The critical distance, where the jet starts to break up, is determined by the nozzle diameter, flow velocity, liquid properties, etc. [69]. This jet

Table 2.3: Comparison of typical tank cleaning devices. The images are obtained from online sources.

Devices	Static spray ball	Rotary spray head	Rotary jet head
Image			
Rotation	No rotation	Single axis rotation	Two-axis rotation
Method	Cleaning by spot and falling film	Cleaning by fans of water	Cleaning by high-impact jets
Mechanical impact	Low	Middle	High
Flow rate	High	Middle	Low
Operating costs	High	Middle	Low
Applications	Low initial cost; Limited hygiene requirement; Small tank size; Weak soil	Low operating cost; Good hygiene requirement; Small tank size; Weak soil	Low operating cost; High hygiene requirement; Large tank size; Harsh soil

breakup phenomenon can happen at both low and high flow velocities (Figure 2.4). It has been found that jet breakup promotes cleaning by enlarging the pressurised area [70, 71]. However, the impact of a water jet decreases after a certain throw length, leading to reduced cleaning performance. Therefore, an understanding of the stability of liquid jets is of importance in the design of devices and the optimization of operations in order to remove the largest quantity of deposits with minimized water consumption.

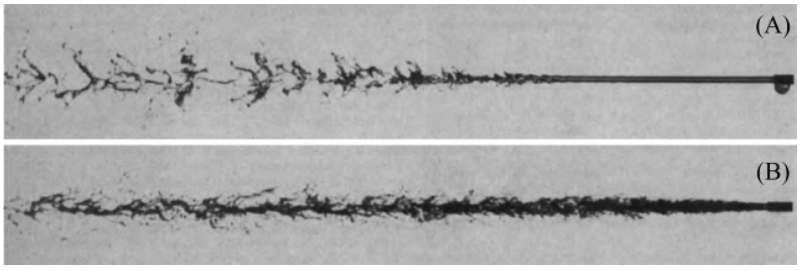

Figure 2.4: Anatomy of water jet breakup in air: (A) Laminar jet, (B) Turbulent jet. (Adapted from Grant et al. (1966) [69])

Wilson et al. (2012), Bhagat et al. (2016) and Chee et al. (2018) studied the flow patterns of liquid from static or moving impinging jets on flat or curved surfaces in pilot scale [72,

73, 74]. Numerical solutions could be used to describe the velocity profiles on flat surfaces with different inclination angles. An adhesive removal model was further developed to describe the cleaning radius of different soil types (soft, intermediate and hard) as a function of the cleaning time, based on a momentum balance between liquid and deposit at the cleaning front [75, 76, 77]. However, this model neglected the effect of jet breakup at long distance and flow splash-back at high flow rate. Therefore, a discrepancy between the predicted cleaning radius and experimental results was found when applying the model in large scale [78].

The splash-back of liquid occurs at high flow rates, where the liquid expels a shower of droplets from the liquid film formed on the surface [79]. It becomes significant when the jet Reynolds number is above 12,000 [80]. On the one hand, splash-back can help with the indirect coverage within a tank. On the other hand, it reduces the impact at the point where the jet impacts directly [6]. The ratio of splashed flow rate to the incoming flow rate is dependent on the jet velocity, jet distance to the surface, nozzle diameter as well as liquid properties (liquid density and surface tension) [79]. One way to deal with liquid splash-back is to use an effective flow rate term to predict the cleaning performance rather than the actual flow rate [78].

2.5.3 Cleaning by Falling Films

Falling films contribute significantly to the indirect coverage of tank surfaces where the jets or fans of cleaning liquid cannot hit directly. When liquid initially flows away from the point of impingement and then drains downwards, three flow regions are evident (Figure 2.5), depending on the flow and surface conditions. A gravity flow without dry patch formation (Figure 2.5A) is preferred in cleaning operations because it provides a large wetting area. However, when surface tension effects associated with non-wetting behaviour are significant, the film narrows and forms a rivulet (see Figure 2.5B). Non-wetting behaviour can even promote the splitting of a wide film and form a dry path (see Figure 2.5C).

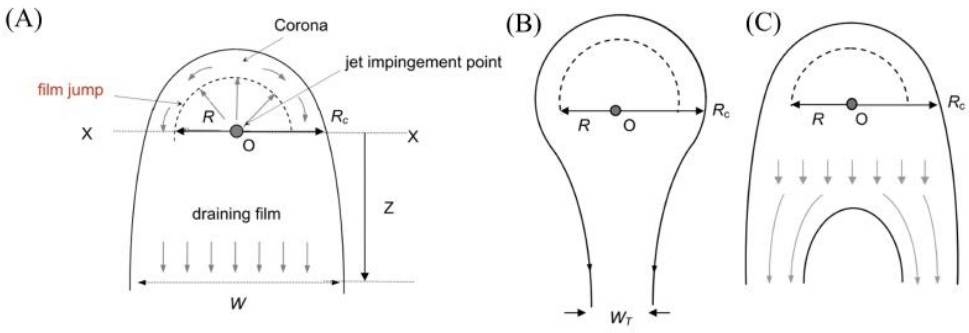

Figure 2.5: Schematics of flow patterns generated by an impinging jet: (A) gravity flow without dry patch formation, (B) rivulet flow, and (C) gravity flow with dry patch formation. (Adapted from Wang et al. (2013) [83])

The wetting rate, Γ [kg m^{-1} s^{-1}], is defined to quantify the peripheral flow rate by $\Gamma = \dot{m}/W$, where $\dot{m}$ is the mass flow rate and W is the wetted width. Hartley et al. (1964) presented the criteria for initiating a dry patch on a vertical surface based on both force balance and energy balance theories at the break-point [81]. This threshold depends on the liquid density (ρ), dynamic viscosity (μ), surface tension (γ), and the contact angle (β) which is a property of the liquid/surface interaction. This criterion can be used to calculate the minimum wetting rate (Γ_{min}) required to maintain a wide film of liquid for cleaning purposes, see Equation 2.1. Morison et al. (2002) investigated the falling films on acrylic and stainless steel surfaces generated by a static spray ball, and estimated that the minimum wetting rate ranged from 0.1 to 0.3 kg m^{-1} s^{-1} [82].

$$\Gamma = \dot{m}/W \geq 1.69(\mu\rho/g)^{0.2}[\gamma(1-\cos\beta)]^{0.6} = \Gamma_{min} \tag{2.1}$$

Nusselt (1916) first presented the important film flow theory, assuming that the film surface is flat and the flow is truly laminar [84]. However, it has been shown that the liquid may produce a wave motion at extremely low flow rates and within the viscous flow region [85]. A wall shear stress maximum was found to be located either in front of the wave crest or behind it [86]. For cleaning operations, a large wall shear stress favours deposit removal by shearing the deposit layers. It is of great importance to quantify the thickness and velocity profile of the film as well as the wall shear stress caused by the film.

Fuchs et al. (2015, 2013) measured the film thickness using a fluorescence method and found that the film thickness was strongly affected by the inclination angle of the surface, which, hence, had a major impact on the wall shear stress and the cleaning rate [87, 88]. Aouad et al. (2016) measured the surface velocity of draining film generated by liquid jets using particle image velocimetry (PIV) , and revised a model to predict the film velocity in the central part of the film [89]. The level of wall shear stress could also be determined directly for example by using a dual electrodiffusion friction probe system [90]. Furthermore, it has been found that the stream-wise velocity is strongly disturbed by the presence of an obstacle on the surface like a small deposit [91].

2.6 Mathematical Modelling and Data Analysis

In the past decades, a number of experiments and models have been made to understand how cleaning occurs. The objectives for constructing models are to optimize the equipment design and control variables and to predict the end point of cleaning, which further result in significant reduction in environmental impact of cleaning operations. Most studies focus on predictive mathematical models and advanced Computational Fluid Dynamics (CFD) models. The predictive models are efficient for cleaning practices related to monitoring and control purposes. The great computational demand of CFD limits its application for real-time monitoring and control. But it has proven to be a powerful tool for understanding and improving cleaning processes and equipment design. Since all of the systems should be controlled without the occurrence of errors, a risk analysis model is also introduced here to improve the reliability and safety of operations.

2.6.1 Predictive Models

2.6.1.1 Response Surface Methodology

The response surface methodology (RSM) approach investigates the functional relationship between a response of interest, y, and a series of input variables denoted by x_1, x_1,..., x_k [92]. The most commonly used RSM is the second-order model:

$$y = \beta_0 + \sum_{i=1}^{k} \beta_i x_i + \sum_{i=1}^{k} \sum_{j=i+1}^{k} \beta_{ij} x_i x_j + \sum_{i=1}^{k} \beta_{ii} {x_{ii}}^2 + \epsilon \qquad 2.2$$

where y is the estimated response of interest (e.g., cleaning cost and soil removal percentage); x_i is the input variables (e.g., temperature, flow rate, time); β_0 is the average value of the response at the center point; β_i,β_j,β_{ij} are the coefficients of the linear, interaction and quadratic terms; and ϵ is the statistical error. The regression coefficients for the variables are obtained by fitting the experimental data. The significance of the model can be analysed using an analysis of variance.

The effects of cleaning water temperature and flow rate on the cleaning time, energy and water consumptions were studied by RSM in the removal of toothpaste from a pilot plant pipe [1]. The flow rate had considerable effects on the cleaning performance. However, the influence of temperature was initially little and increased afterwards. The CIP protocol was optimized based on the model. The cleaning time and the amount of waste water were reduced by 53% and 50%, respectively. In another study of the removal of biofilm from a chilling tank, the log reduction in biofilm cells was characterized as response. The input variables were cleaning time, temperature and NaOH concentration [55]. An optimized CIP regime was achieved: 1.5 wt% NaOH at 65 °C for 30 min $\longrightarrow$ water rinse $\longrightarrow$ 1 wt% HNO_3 at 65 °C for 10 min $\longrightarrow$ water rinse. The optimized CIP resulted in a 4.77 log reduction in biofilm cell count, compared with a 3.29 log reduction in biofilm cell count in the reference CIP. Jurado Alameda et al. (2016) used the RSM to investigate the cleaning of starch films using nonionic and zwitterionic surfactant solutions [93]. Similar to RSM, Piepiórka-Stepuk et al. (2016) defined a cleaning degree factor and an energy consumption factor, and correlated them with temperature, flow rate and cleaning time. These two factors were introduced as a new multicriterial function to find the optimal operating conditions with high cleaning efficiency and low energy input [94].

RSM is a useful method to evaluate the effects of different variables and their interactions from the minimum number of experiments. It is very effective to model and optimize CIP operations. The design of experiments is very important in any RSM investigation, because the choice of the variable matrix needs to be representative.

2.6.1.2 Function Fitting Models

One aim of predictive models is to predict the end point variation of cleaning. One of the most common predictive models is based on the functional form, which uses the cleaning data collected from an ongoing operation to predict the future cleaning behaviour when cleaning has commenced. For example, the existing removal curve of toothpaste can be

fitted as [95]:

$$C_{out} = k_1 e^{a \cdot t} + k_2 e^{b \cdot t} \tag{2.3}$$

where C_{out} is the soil concentration in the outlet; t is the cleaning time; k_1, k_2, a and b are the function coefficients. The functional forms of particular soils and plants differ from one process to another, which is the biggest challenge in adopting this type of models.

Another type of function fitting uses a case based reasoning (CBR), which involves comparing the measurement during a cleaning operation and using that along with historical information to predict the remaining profile [95]. The fit of the measurement and the historical case library can be determined in the expression:

$$fit = \sqrt{\sum_{i=t_1}^{t_2} (n \cdot y_{lib_i - t_{corr}} - y_{meas_i})} \tag{2.4}$$

where t_1 and t_2 are the start and end times of the measurement that are used for comparison; t_{corr} is the time correction aligning the starting time of the two profiles; n is the stretch coefficient which requires to be calculated and modified; y_{lib} and y_{meas} are the monitoring data from the library and the measurement, respectively. An example of the CBR based forecasting model is given in Figure 2.6, which predicts the turbidity intensity during the cleaning of toothpaste from a test pipe [95]. The original and modified library profiles are shown alongside the profile of the current cleaning. The time shift and stretching effect are clear from these profiles. This CBR based model approach indicates the same concept of big data that analyses the data change over an extended period of time, such as the detergent amount and the energy consumption. It enables to monitor the CIP effectiveness and to improve the process efficiency [96].

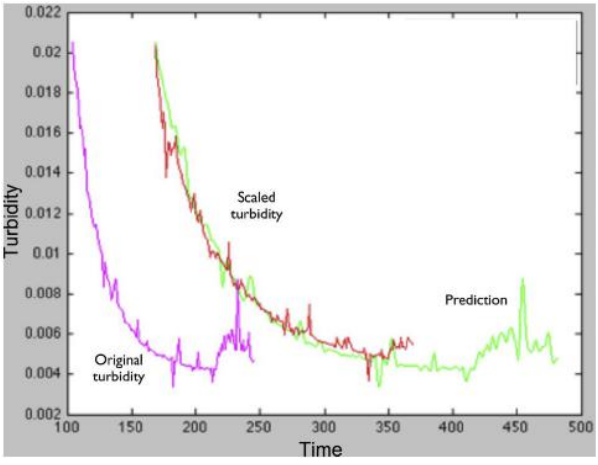

Figure 2.6: Example of a CBR based forecasting model that uses the closest fit in a library. (From Martin et al. (2013) [95])

2.6.1.3 Mechanism-Based Models

In the aforementioned function based forecasting models, the functions are obtained by fitting the current curve, which may be meaningless to describe how the cleaning occurs. Another type of model is based on a mechanism, which tries to explain the process. For example, a hybrid model with a simple mechanistic structure and empirical kinetics described the cleaning of whey protein, based on the assumption that the cleaning involved the top swollen layer removal and the residual soil removal. The model could be represented as Equation 2.5 [16, 97]:

$$\frac{dl_s}{dt} = R_s - R_r, R_s = a - b \cdot l_s, \frac{dl_r}{dt} = R_r = k \cdot l_s, F = R_\tau \cdot \rho_{soil} \tag{2.5}$$

with initial conditions $l_s(0) = 0$, $l_r(0) = L$. l_s and l_r are the thickness of the swollen layer and the residual soil; R_s and R_r are the rate of change of these two layers; a, b and k are the constants related to the cleaning kinetics; ρ_{soil} is the density of the removed soil; F is the mass rate of the removed soil; and L is the initial thickness of the soil prior to cleaning. This model includes the forecasting concept as well.

A cleaning model can be derived based on different cleaning steps as well. For example, in the cleaning of milk systems, the total remaining deposit can be expressed as [98]:

$$m_{TOT}(t) = m_{WAT}(t) + m_{ALK}(t) + m_{ACD}(t) + m_{RES}(t) \tag{2.6}$$

where $m_{TOT}(t)$ is the total remaining mass at any time t in the CIP process; $m_{WAT}(t)$ is the deposit removed by warm water rinsing; $m_{ALK}(t)$ is the deposit removed by alkaline washing; $m_{ACID}(t)$ is the deposit removed by acid washing; and $m_{RES}(t)$ is the residual amount at time t. Each step includes a fast removal rate of the tightly bonded deposit and a slow removal rate of the loosely bonded deposit. For example, the removal rate in the warm water rinsing step can be written as follows:

$$\begin{aligned} \frac{dm_{WAT,F}(t)}{dt} &= -k_{WAT,F} \cdot m_{WAT,F}(t) \\ \frac{dm_{WAT,S}(t)}{dt} &= -k_{WAT,S} \cdot m_{WAT,S}(t) \end{aligned} \tag{2.7}$$

where $m_{WAT,F}(t)$ and $m_{WAT,S}(t)$ are the fast and slow removal rate, respectively. The coefficients $k_{WAT,F}$ and $k_{WAT,S}$ are correlated to the experimental results. Similar functions also apply to the alkaline rinsing and acid rinsing steps. The mechanistic models are difficult to construct, as they require deeper understanding of the process. But they are very useful to make efficient cleaning strategies.

2.6.1.4 Kinetics-Based Models

Another type of forecasting models with physical meaning that are constructed is the kinetics-based model. An example is demonstrated from the removal of *Bacillus cereus* strains from pipes rinsed by a NaOH solution [99]. This work assumes that removal and deposition occur at the same time, applying the pseudo-first-order models. The removal part can be expressed as:

$$\frac{dN(t)}{dt} = k_1(N(t) - N_R) \tag{2.8}$$

and the deposition of spores can be expressed as:

$$\frac{dN(t)}{dt} = k_2(N_0 - N(t)) \tag{2.9}$$

where $N(t)$, N_R and N_0 are the surface density of adhering spores at time t, at infinite time and at initial time, respectively; k_1 and k_2 are model coefficients, representing constants of removal and deposition, respectively. The value of k_2 is related to the total area of contamination and the detergent volume. The removal and deposition occur concurrently. Then the equations can be associated as follows:

$$\frac{dN(t)}{dt} = k_2(N_0 - N(t)) - k_1(N(t) - N_R) \tag{2.10}$$

This equation can be solved by integrating between time 0 and t. Parameters are identified using experimental values. It is hypothesized that the removal rate constant, k_1, becomes smaller if water is used instead of NaOH solution.

2.6.2 Computational Fluid Dynamics

The removal of soils and microorganisms is affected by the local flow conditions (e.g., wall shear stress and its fluctuating rate), detergent mixing, and heat distribution, etc. [56, 100]. CFD has become an effective tool to predict these local properties [101]. The main advantages of using CFD are that: (1) it is possible to test different designs without building prototypes; (2) it is possible to calculate the local properties where measurements cannot reach. Therefore, CFD has been carried out in early design works to improve hygienic design, showing the effects of wall shear stress and fluctuation on cleaning behaviour.

Figure 2.7 shows a T-joint with a dead end geometry, which is unwanted but inevitable in food processing lines [102]. Detergents and fluid may be stagnant in these areas due to low velocity and low wall shear stress, consequently resulting in ineffective cleaning performance. CFD simulates the distribution of velocity and wall shear stress at different flow rates. It has been found that an increase in the incoming flow rate can increase local velocities generally, but the influence on the stagnant area is very small (the blue areas in Figure 2.7B). The fluctuation rate of wall shear stress is linked with the turbulence intensity, which can be obtained from steady-state simulations as well [101]. Therefore, the CFD results are helpful to improve the hygienic design of equipment by avoiding stagnant zones, and to optimize the operating conditions.

Another application of CFD is to simulate the displacement process of soils. Figure 2.8 displays the displacement of yoghurt by water in a dairy pilot line of 60 mm inner diameter at average flow rate of 170 kg/min [64]. Both the measurement and the CFD simulation describe a clear tailing effect of yoghurt removal at the lower section of the pipe, which is caused by the density difference between yoghurt and water. The CFD model can be further used to investigate the effects of pipe length, water flow rates, yoghurt rheology and wall slips, as well as yield stress.

CFD has become a valuable supplement to EHEDG tests. It is currently the only alternative to testing different sizes of the same piece of equipment. For example, CFD has

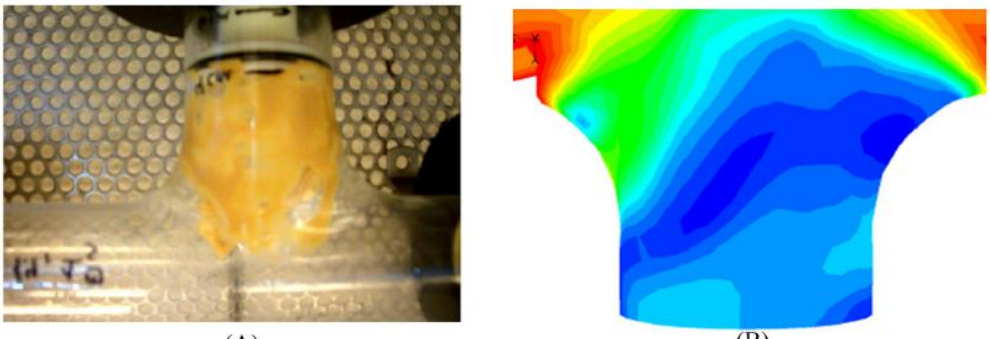

Figure 2.7: (A) Actual upstand geometry (T-joint) made out of glass and used for investigating the influence of different flow rates during CIP. (B) Predicted shear stress at a constant inlet velocity of 1.5 m/s by using CFD (illustrated as a downstand by Jensen et al. (2007)). In Figure B, the flow direction is from right to left. Blue color denotes low wall shear stress of 0 Pa and red color denotes high wall shear stress of 5 Pa. (Adapted from Jensen et al. (2007) [102])

.

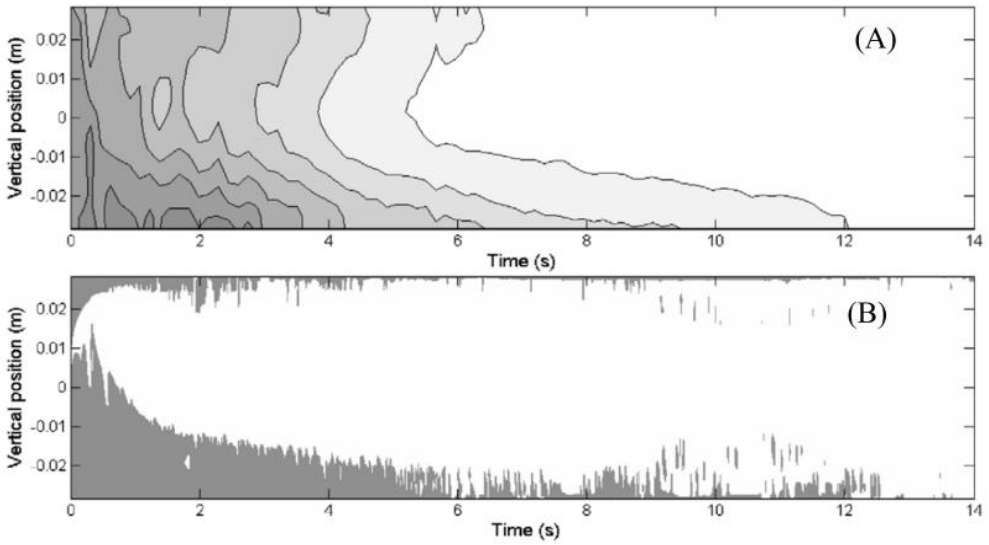

Figure 2.8: Distribution of yoghurt (grey) and water (white) as a function of time in a vertical pipe: (A) measurement with ERT, (B) simulation using CFD. Time zero is defined as the breakthrough time. (From Henningsson et al. (2007) [64])

been used to optimize the design of a 4-lobed swirl pipe by enhancing the swirl intensity and wall shear stress downstream with minor pressure loss [103, 104, 105]. However, the application of CFD is still limited in CIP practices because: (1) most of the studies have focused on simple geometries (e.g., pipes, valves) and one phase systems in small scales. It

is still difficult to simulate complex equipment (e.g., heat exchangers, tanks, reactors) and multiphase problems; (2) the fluid exchange and heat exchange near the surface still need more investigations; (3) the transient phenomena (e.g., detergent mixing and blending phase) have not been fully understood in either measurement or CFD modelling; (4) the CFD model cannot be directly utilized for process control due to its huge computational requirement.

2.6.3 Risk Assessment

CIP failure can be defined as the unexpected survival of pathogens and food-spoiling microorganisms. It might be due to not only the operational mistakes by workers, but also some accumulating random errors within the system. Such risk of failure can be modelled by mathematical functions, like *Friday 13th failure modelling* (*Fr 13*), based on an underlying unit-operations model and Monte Carlo simulations. Davey et al. (2013) gave an example of using the *Fr 13* risk model for CIP operations [106], developed from the two-stage CIP unit-operations model and extensive experimental data from previous studies [16, 17]. The cleaning includes the alkaline washing of a proteinaceous milk deposit. The first stage is the break-up of the swelled x-layer with the removal rate:

$$R_{S1} = k_y[1 - exp(-k_x \cdot t)], 0 < t < t^* \tag{2.11}$$

where R_{S1} is the first order removal rate; k_x and k_y are constants; t^* is the time to reach the maximal removal rate. The second stage applies for all $t > t^*$, with the removal rate:

$$R_{S2} = R_{max} exp[-k_x(t - t^*)], t > t^* \tag{2.12}$$

where R_{S2} is the second order removal rate; R_{max} is the maximal removal rate at time t^*. For automation control, the overall cleaning time is defined as the time when the removal rate falls to $0.02R_{max}$, that is:

$$t_T = t^* - \frac{ln(0.02)}{k_x} \tag{2.13}$$

where t_T is the auto-set cleaning time. The parameters k_x, k_y and the Reynolds number Re can be correlated with temperature over the reported range of experimental conditions. The actual cleaning time, $t_T{}'$, varies from t_T, due to random errors. A risk factor p is defined as:

$$p = -\%tolerance + 100(\frac{t_T{}'}{t_T} - 1) \tag{2.14}$$

A latent failure occurs for all values at $p > 0$, which means the deposit has not been removed beyond the tolerated cleaning time. Typically, the tolerance is specified as 5% for operations.

Traditional analysis methods input the parameters with a defined distribution of values, probably resulting in a distribution of output values. The *Fr 13* model uses the Monte Carlo method to generate sampling input and process parameters. It allows the calculation of combined impact of systematic errors (variability) and random errors (uncertainty). The simulation results reveal that the CIP plant is a mix of success and failure

as a result of random system errors. The risks come from not only the auto-set cleaning time, but also the auto-set cleaning fluid temperature.

Besides the two-stage CIP model, the *Fr 13* model can also be used in combination with the more complicated three-stage CIP model from Xin (2003, 2004): the swelling of deposit by alkaline, the uniform removal with constant removal rate and the decay [107, 108, 109]. The application of risk analysis helps to assess control and other process intervention strategies and improve the reliability and safety of operations [106, 109].

2.7 Conclusions

Several fouling problems and cleaning techniques have been discussed in the scientific literature. Three soil types have been classified according to the complexity of soil properties and the difficulty of removal. For type 1 soil, it is enough to solely use water as cleaning media. For type 2 soil, removal needs to be preceded by the destruction of biofilm. Type 3 soil is the most reluctant deposit that requires chemicals to remove. Various measurement techniques can be used to study soils in order to (1) understand the cleaning mechanism, (2) measure the required force to remove deposits from surfaces, and (3) measure the internal properties of deposits. These techniques are very helpful to investigate how cleaning occurs at micro scale. Especially, the understanding of soil soaking and swelling may introduce the novel development of burst technique in tank cleaning operations. Furthermore, four cleaning mechanisms have been proposed to describe a cleaning process, namely diffusive dissolution, cohesive separation, viscous shifting, and adhesive detachment. These mechanisms may occur synchronously, depending on soil types, cleaning methods and cleaning phases, etc.

The main parameters that determine cleaning results include temperature, time, chemicals, mechanical forces, surface coverage as well as soil properties like structure matrix and ageing. Generally speaking, higher temperature, higher detergent concentration and higher mechanical impact are helpful to shorten the cleaning time. However, above some temperatures, the extra heat may generate more elastic deposits which are even more difficult to remove. Excessive flow rates and chemical consumption may result in limited improvement of cleaning efficiency, but increase the operating cost significantly. For some protein-based soils like whey protein and egg yolk, an optimal alkali concentration is observed, above which the soil layers become less penetrable to the cleaning agent.

Several monitoring techniques have been developed to assess the cleaning results and to determine the end point of each cleaning stage. The monitoring methods can be either real-time or retrospective. Each method has its own field of application. Among the methods, the measurement of bulk liquid using pH, conductivity and turbidity sensors surpasses the others due to its applicability in large scale. ATP measurement is another remarkable technique for detecting the existence of residual microorganisms and food debris.

For the cleaning of tank surfaces, a cleaning device is required to distribute cleaning liquid on the surface with high impact. The coverage of the internal surface can be achieved by either direct hitting of liquid jets or indirect flow by falling films. The cleaning by

impinging jets can be modelled by numerical equations. However, the application of the present models needs the consideration of jet breakup and splash-back if proposed for large scale. The studies of falling films have been mainly associated with the wetting rate for a wide film and film characteristics (i.e., thickness, velocity profile, and wall shear stress).

In the end of this chapter, some mathematical modelling and data analysis methods were presented. Four predictive models are discussed, in regard to predicting the cleaning profile and possibly a cleaning end point. CFD models are not applicable for real-time monitoring and control due to their huge computational demand, but they are helpful in the optimization of operations and equipment design. A CIP operation is less tolerant of a potential failure because any cleaning failure may result in a catastrophic disaster to public health. Therefore, failure analysis of CIP becomes of great importance in this respect.

Part II

Case Studies

CHAPTER 3

Mapping CIP Systems in a Brewery

3.1 Introduction

3.1.1 Brewing Process

The purpose of brewing is to produce beer through a series of process steps. As shown in Figure 3.1, the process starts with the milling of raw materials such as barley malt and rice grains. Then these raw materials are mashed into a sugary fermentable liquid called wort. The wort is boiled with hops added, and cleared to remove solid particles. Next, this liquid medium is converted into an alcoholic, carbonated beverage by yeast, followed by maturation. Afterwards, the matured green beer is filtrated to get bright beer. As a result of the above process steps, the product is ready to be filled into bottles, cans or kegs, before being shipped to distributors [110].

As indicated in Figure 3.1, a brewing process includes many equipments that need to be cleaned after use. For example, the operations prior to fermentation take place in a brew house, where there are silos, millers, filters, boilers, heat exchangers, etc. Fermentation and maturation generally occur in either a vertical cylinder with a conical bottom or a horizontal tank. In a packaging plant, beer containers and crates should be cleaned before filling with beer. In addition, shipment vehicles like trucks need to be washed as well. There are still cleaning operations that are not indicated in Figure 3.1, such as the cleaning of pipes, pumps, valves, as well as water purification systems.

Most of the cleaning operations in large scale breweries can be accomplished through automated CIP recipes by installing several CIP systems to clean different equipments or processes. Though, manual cleaning and cleaning-out-of-place (COP, to dismantle a device and wash it separately) operations are still used for other parts. Small scale breweries may choose movable CIP stations to clean small facilities one by one rather than a big and fixed CIP system. However, soil types and cleaning cycles are similar from small scale to large scale.

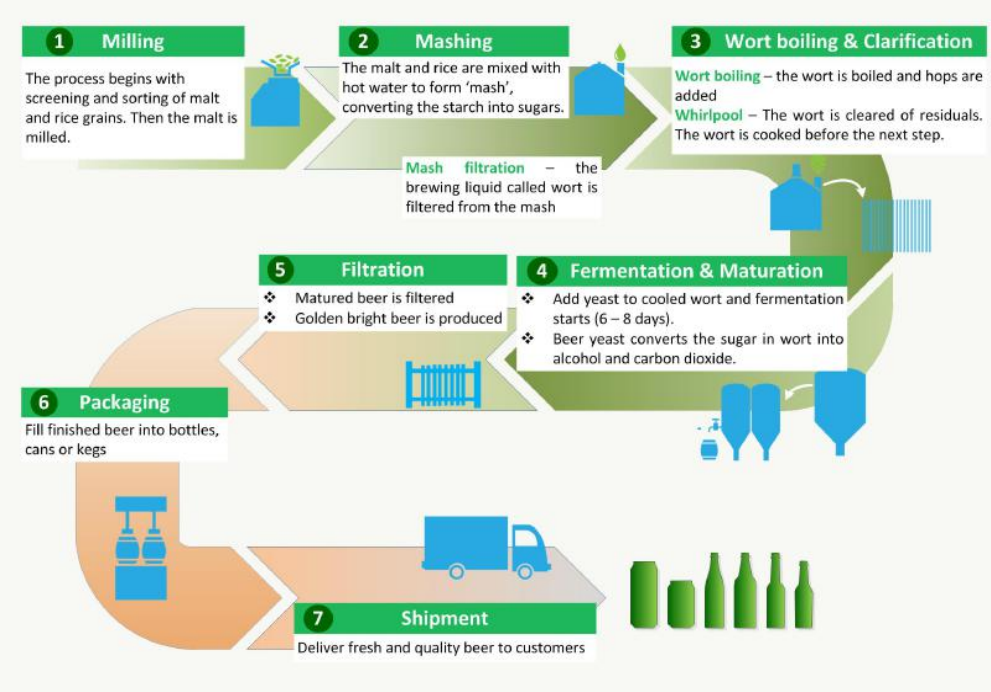

Figure 3.1: Schematic of a brewing process (reproduced based on an online resource from the Carlsberg website [111])

3.1.2 Soils in Brewery

According to the soil classification by Fryer et al. (2009) (see Figure 2.1), all of the three types of fouling exist in a brewery, as shown in Table 3.1. Yeast soils can be both type 1 and type 2 because yeast is actually easily removed by water but becomes difficult to remove if foaming takes place in a fermenter. Furthermore, in brewery tanks where yeast is used to ferment sugar, two different forms of soil materials are found above and below the liquid level [42]:

- *Type A* is formed above the beer liquid level (ca. 20% of the tank volume) due to foam. It is filled with yeast, wort residues with protein and hop components. This type of deposit can age on the tank surface for up to 12 days;

- *Type B* is the residual yeast below the liquid level and attached to the wall and cone during emptying. It consists of the same compositions as *Type A* soils, and can age on the surface for up to 5 h.

Table 3.1: Different fouling materials and fouling types in a brewery (adapted from Goode (2012) [59])

Plant geometries	Fouling materials	Fouling types
Wort boilers	Protein, beer stone	Type 3
Fermenters and maturation tanks	Yeast protein, slight beer stone	Type 2
Yeast storage tanks	Yeast protein, slight beer stone	Type 1
Bright beer storage tanks	Traces of beer and foam	Type 1

3.1.3 Purpose of Mapping in Carlsberg Danmark A/S

Carlsberg Danmark A/S is a global brewer with the headquarter located in Copenhagen, Denmark. The Carlsberg brewery in Fredericia is one of the main production sites to produce beer and soft drinks. Mapping of the CIP systems in the Carlsberg brewery in Fredericia is the preliminary step in the INNO+DRIP project in order to upgrade the existing CIP operations.

According to a pre-assessment report about water efficiency in Carlsberg's Fredericia site, CIP processes (only including part of the CIP systems) are the third largest sink of water, following the water used in the production of soft drinks and beer. Significant potentials have been identified related to the optimization of CIP operations. The complexity of CIP systems varies site by site, line by line and unit by unit. Therefore, this mapping case study is conducted in order to understand the performance of these CIP systems and to identify potential savings.

However, due to the complexity of the overall process, this mapping study exclusively assesses the CIP systems in the brewery plant. To be exact, the results and conclusions are mainly focusing on the cleaning of tanks (fermenters, storage tanks, etc.) and transfer lines (pipes, pumps, valves, etc.). In this thesis chapter, CIP processes and data values are not reported for confidentiality reasons. Nevertheless, the findings in this case are very representative of common industrial CIP practices in other industries like dairy, beverage and pharmaceutical. This case study also provides the factual basis for implementing the research projects described in the remaining chapters.

3.2 Methods

This mapping study was performed through on-site review and data analysis that recorded historical cleaning operations. A mapping report was accomplished to document CIP systems, chemical supplies, cleaning recipes, water and energy consumptions, cleaning frequencies, measurements and CIP equipment, etc. This thesis only presents examples about cleaning time and annual costs, which were calculated according to the aforementioned information through Equation 3.1.

$$\delta_{Total} = \delta_{Fresh\ water} + \delta_{Detergent} + \delta_{Electricity} + \delta_{Heat} + \delta_{Waste\ water} \tag{3.1}$$

The term δ with subscripts denotes the cost of each item. The costs of fresh water, detergent, electricity, sensible heat and waste water treatment were computed as follows:

$$\delta_{Fresh\ water} = Q \cdot t \cdot \varphi_{Fresh\ water} \tag{3.2}$$

$$\delta_{Detergent} = Q \cdot t \cdot C \cdot \varphi_{Detergent} \tag{3.3}$$

$$\delta_{Electricity} = (P_f + P_s) \cdot t \cdot \varphi_{Electricity} \tag{3.4}$$

$$\delta_{Heat} = Q \cdot t \cdot \rho \cdot c_P \cdot (T - T_0) \cdot \varphi_{Heat} \tag{3.5}$$

$$\delta_{Waste\ water} = Q \cdot t \cdot \varphi_{Waste\ water} \tag{3.6}$$

where Q is the flow rate; t is the cleaning time; C is the detergent concentration; P_f and P_s are the powers of forward and scavenge pumps; ρ and c_P are the density and heat capacity of the liquid; T and T_0 are the cleaning temperature and room temperature, respectively. The unit cost of each cleaning resource, φ with subscript (i.e., water, detergent, heating energy, electricity, waste water treatment), was based on the prices in Danish industries. If there were recoveries of water or detergent solutions, the costs were reduced by replacing the flow rate Q as the difference in flow rates between the feeding flow and the recovery flow, neglecting the dilution effect and reaction loss.

3.3 Mapping Results

3.3.1 A Cleaning Example

Figure 3.2 displays the cleaning time spent on each step for a typical cleaning example. The current recipe is time-based, meaning that each step is performed for a pre-defined period. The times for detergent circulations (alkali, acid and disinfectant) contribute to over 80% of the overall cleaning time. The pre-rinse and intermediate rinse steps are generally shorter than the final rinse, which makes sense because the final rinse is essential in order to remove all residual soils and detergents from the system.

Figure 3.3 shows the cost of each cleaning resource using cleaning times from Figure 3.2 and Equations 3.2 to 3.6. It can be seen that nearly 98% of the cleaning costs attribute to detergent solutions, particulary disinfectant and alkaline solutions. Taking a recovery ratio of 95% based on the estimation of the actual processes, the overall cleaning costs can be reduced by ca. 93% through the recovery of detergent solutions. Then, the costs of water (the sum of pre-rinse, intermediate rinses and final rinse) become the second contributor to the overall costs besides disinfectant. The costs of electricity and waste water treatment are very low compared with other factors.

3.3.2 Annual Cleaning Costs

The annual cleaning costs of each process can be calculated as the product of cleaning frequency per year and costs per cleaning. It is found in Figure 3.4A that ca. 70% of the cleaning operations are performed for pipes, because pipes are frequently used for the transfer of materials, products, yeast, etc. There are two cleaning recipes for fermenters, named CIP of fermenters and disinfection of fermenters, because a cleaned fermenter

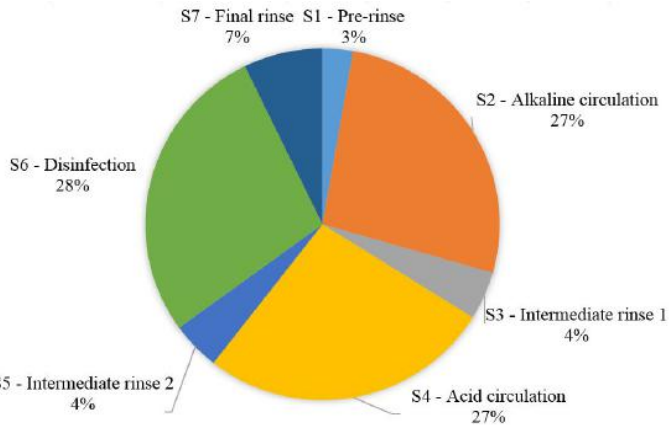

Figure 3.2: The cleaning time of each step in a typical pipe cleaning example.

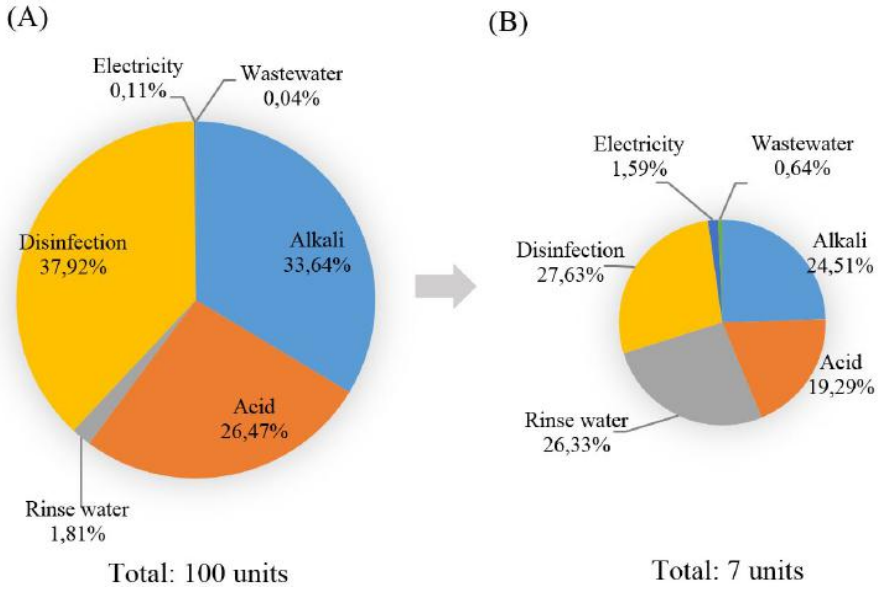

Figure 3.3: An example of the costs of each cleaning resource in pipe cleaning: (A) the costs without the recovery of detergent solutions, (B) the costs with 95% recovery of detergent solutions.

needs to be cleaned again before filling if it is held for a long time without use. In this situation, only a short disinfection procedure is necessary rather than a full CIP recipe in order to save costs.

In Figure 3.4B, tank cleaning operations contribute to ca. 40% of annual cleaning costs.

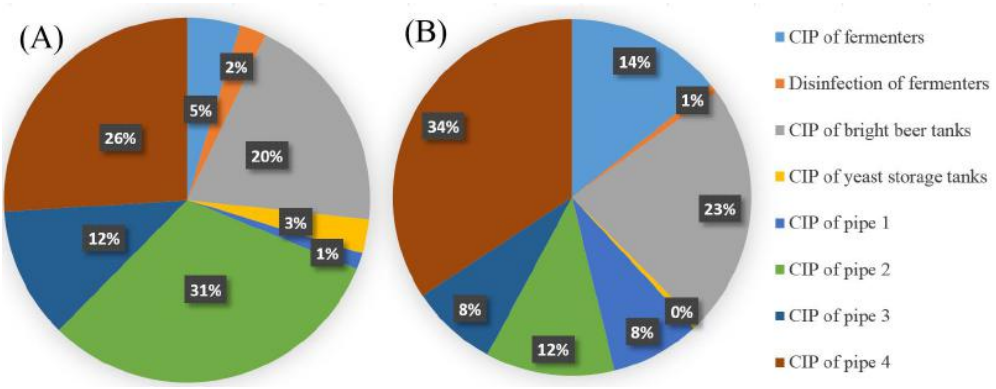

Figure 3.4: (A) Percentage of annual cleaning frequency and (B) percentage of annual cleaning costs of tanks and pipes in the brewery. The reduction of cleaning costs by the actual recovery of water and detergent solutions have been considered in calculation.

Through comparing the two plots in Figure 3.4, some important information can be gained:

- CIP of pipe 1 results in the highest cleaning costs per operation, as its contribution to the annual overall costs (ca. 8%) increases most compared to its contribution to the cleaning frequency (ca. 1%), as shown Figure 3.4A.
- Similar cleaning devices are used for cleaning fermenters, bright beer tanks and yeast storage tanks. But the recipes differ from each other. The CIP recipe of fermenters is the most expensive. The recipe of yeast storage tanks is the cheapest.
- In order to reduce the annual overall cleaning costs, it is worth optimizing the CIP operations of pipe 4 and tanks (bright beer tanks and fermenters), which makes over 70% of the total costs.

However, the present mapping study does not consider the cleaning operations in the brew house or of the filters, the self-cleaning of CIP systems, or the dilution of detergent solutions in recovery processes, etc. Therefore, the actual cleaning costs in the whole brewery can be higher than presented in Figure 3.4B. Though, the cleaning of tanks and pipes are very representative of CIP operations occurring in various industries.

3.4 Suggestions for Upgrade

The best practice of CIP refers the following principles given by Hatlar Group Pty Ltd (2010) [112]:

- Minimise the usage of water, energy and detergents, and select proper chemicals to minimise the damage to the environment;

- Operate the CIP systems by ensuring various interface boundaries by instrumentation (pH, conductivity, turbidity, etc.) rather than time or visual inspection;
- Optimise the operating conditions based on need;
- Use single-use systems for small or rarely used equipment or where the cleaning solutions are grossly contaminated.

According to the CIP best practice guidelines and the need of the industrial CIP user, the improvement of current CIP systems in the mapped brewery can be implemented in five aspects as follows [112], which can also be regarded as reference in other breweries and other industries:

1. Improve product removal
    a) Inspecting the draining capability of the equipment, allowing gravity draining of the product for recovery;
    b) Using turbidity or other forms of measurements to determine whether the product has been sufficiently removed rather than time-based;
    c) Recovering the product prior to CIP to avoid drying fouling;
    d) Using carbonated water and product mixture to assist product removal and recovering the liquid in the product.
2. Minimise rinsing water use
    a) Intalling spray devices as close as to the foam part in fermeters, which is the most difficult to remove;
    b) Selecting the water of proper quality (“fit-for-use”) and treating the water for applicable purpose (“fit-for-purpose”), and reusing water from intermediate rinse and final rinse for use in the pre-rinse of next cleaning;
    c) Optimising the flow rate and rinsing time and implementing measurement-based rinse instead of time-based.
3. Minimise chemical use
    a) Optimising chemical conditions (i.e., concentration, flow rate, temperature and time), as most cleaning parameters are determined based on experiences without examination in specific applications;
    b) Using alternative chemicals like potassium hydroxide (KOH) and enzymes in order to reduce the environmental impact;
    c) Holding frequently used chemical solutions at required temperature to shorten the cleaning time that is spent on raising the temperature prior to CIP;
    d) Recovering chemicals at a proper ratio (ca. 80%) to reduce volume loss (if recovering too little) and dirt accumulation in the tanks (if recovering too much).

4. Improve equipment performance

    a) Checking the proper use of cleaning devices and inspecting the dead ends in the systems;

    b) Separately cleaning the equipment difficult to clean, e.g., centrifuges, rotational parts, and heat exchangers;

    c) implementing in-line measurements to monitor the process and determine the end point of cleaning.

5. Other aspects

    a) Checking the cleaning recipes of some processes where expensive recipes are used to clean easy soils;

    b) Rearranging the orders of detergent tanks so that the earlier used liquid should be closer to the forward pump, in order to avoid cross-contamination in CIP feeding pipes. For example, if the cleaning recipe is "pre-rinse $\longrightarrow$ alkaline $\longrightarrow$ acid $\longrightarrow$ disinfection $\longrightarrow$ final rinse", the ideal order of CIP tanks should be:
    (Forward pump -) Reused water tank - Alkali tank - Acid tank - Disinfectant tank - Fresh water

    c) Simplifying the cleaning process by for example combining the disinfection step with the acid circulation step to reduce the cleaning time;

    d) Implementing a smart production schedule to avoid long holding times of equipment and repeated cleaning operations before new productions.

3.5 Inspirations for This Ph.D Thesis

This mapping study has provided a number of possibilities to reduce the annual cleaning costs in a brewery. This Ph.D thesis is motivated by this case study and aims at providing practical solutions to upgrade CIP systems and processes using academic knowledge. Four projects have been defined in this respect and were organised as follows:

1. For an existing CIP system

    a) Analyzing historical data of CIP operations is essential to avoid potential operation failures in the future. Chapter 4 presents a three-level approach of analysis based on the CIP of a brewery fermenter at Carlsberg to describe how to analyse the historical data in steps for detecting anomalies. The potential application of the analysis approach is to integrate a reference model into the control system for automatically indicating and diagnosing likely anomalous events;

    b) Pipe cleaning is one of the main costs in cleaning operations. Reducing the use of rinsing water and improving the recovery of detergent solutions can potentially decrease the operating costs of pipe cleaning. Chapter 5 presents

how CFD tools can be applied to simulate the displacement of detergent solutions by water. The purpose is to understand the blending phase within pipe systems and to optimise flow conditions and detergent/water recovery;

2. For designing a new system

   a) The costs of alkali are the main costs in the cleaning of fermenters because alkaline solution is not recovered due to deactivation by CO_2. In Chapter 6, the burst technique is investigated in tank cleaning operations and compared with conventional continuous flows. The goal of burst cleaning is to improve the effectiveness of alkali usage and to reduce the detergent consumption henceforth reduce the cleaning costs;

   b) The current recovery of cleaning liquid is controlled based on time or conductivity measurements. Chapter 7 develops a measurement-based recovery system. A turbidity sensor is applied to measure the quality of water for switching between water recovery and draining. The goal is to only reuse clear liquid and increase the lifetime of reused water.

3.6 Conclusions

CIP is commonly used in industrial breweries. All of the three fouling types, classified according to Fryer et al. (2009) [15], exist in different brewing processes. Yeast is the main fouling material in wort boilers, fermenters, yeast and bright beer tanks, as well as transfer lines. For a beer fermenter, yeast soils above liquid level are more difficult to remove than the soils below liquid level because of foaming. This mapping study assessed the main CIP systems at the Carlsberg brewery, with special attention paid on the cleaning of tanks and pipes. This thesis mainly presents the economic evaluation of cleaning operations.

In general, the CIP systems at Carlsberg are highly automated and efficient. The treatment of cleaning detergents (alkali, acid and disinfectant) contributes significantly to the overall cleaning time and cleaning costs. The recovery of cleaning detergents can reduce the cleaning costs by over 90%. The annual costs of pipe cleaning (ca. 60%) are higher than the costs of tank cleaning (ca. 40%), because pipe cleaning operations occur more frequently.

Based on the mapping results, suggestions for implementing the best practice of CIP have been provided to Carlsberg by improving product removal, minimising rinsing water use, minimising chemical use, upgrading equipment, and some other aspects. These suggestions can also be useful to improve the CIP systems in other industries where similar processes are applied.

In the end, based on the mapping study in the brewery case, four projects are defined in this Ph.D thesis. The aim of this thesis is to provide practical solutions to upgrade existing CIP systems or design new systems.

List of Nomenclature in Chapter 3

The following nomenclature is only valid for this chapter. Some symbols are used in other chapters but with different meanings. Otherwise, the symbols are specifically explained in the text if there is no nomenclature in some chapter.

Roman Letters

c_P	Heat capacity of liquid, [kg m^2 $°C^{-1}$ s^{-1}]
C	Detergent concentration, [kg m^{-3}]
P_f, P_s	Power of feed pump and scavenge pump, [kW]
Q	Flow rate, [m^3 min^{-1}]
t	Time, [min]
T	Cleaning temperature, [°C]
T_0	Room temperature, [°C]

Greek Letters

δ with subscript	Cleaning cost (of resource), [Euro]
ρ	Liquid density, [kg m^{-3}]
φ with subscript	Unit cost of a cleaning resource, [Euro per unit resource]

CHAPTER 4

Anomaly Analysis in CIP Operations of a Brewery Fermenter

In this chapter, the historical data from the cleaning of a brewery fermenter at Carlsberg is analysed with the purpose to detect anomalies in monitoring and diagnose the potential causes. The work was performed in collaboration with Alfa Laval Copenhagen A/S, Carlsberg Danmark A/S and Ecolab Danmark A/S. This chapter of the thesis has been published and reproduced with permission from [113]

Anomaly Analysis in Cleaning-in-Place Operations of an Industrial Brewery Fermenter
Yang, J., Jensen, B. B. B., Nordkvist, M., Rasmussen, P., Pedersen, B., Kokholm, A., Jensen, L., Gernaey, K. V., Krühne, U.
Industrial and Engineering Chemistry Research, 57 (38): 12871 - 12883. (2018)
DOI: 10.1021/acs.iecr.8b02417

4.1 Introduction

Chapter 3 describes a mapping study of CIP systems at the Carlsberg Fredericia brewery site. There are lots of monitoring data from historical cleaning operations. A potential application of the data is to establish forecasting models to identify the likely future CIP performance by comparing the current observations with previously stored experiences, as described in Section 2.6.1.2 [95]. Another method to use the data is to evaluate and optimize the system by examining the current parameters or processes manually and periodically. For instance, a CIP specialist, sometimes an auditor, can check if the cleaning duration or flow rate is insufficient or over demand by reading the record. This kind of analysis is normally conducted by external experts infrequently (e.g., once per year). Industry anticipates a more efficient and automatic approach to evaluate a cleaning operation and detect abnormal events right after cleaning or even immediately when it occurs.

In present, the analysis of historical cleaning data is usually experience-based. It is expected that this fact will remain in the near future. The aforementioned methods to use the data have the aim to investigate only one parameter at once, which is called a univariate statistical approach [114]. However, in complex processes, a large data set is generated, containing many interacting variables. Then, multivariate methods become essential, allowing monitoring and analysing multiple variables simultaneously [115].

In this chapter, the introduced three-level approach to analyse CIP monitoring data applies both univariate and multivariate approaches. The aim is to benchmark how to use historical cleaning data to evaluate anomalies occurring in CIP, by taking an example from the cleaning of a brewery fermenter.

4.2 Description of the CIP Practice of a Brewery Fermenter

The proposed analysis benchmark was based on the cleaning of a 500 m^3 brewery fermenter at Carsberg's Fredericia site. The vertical fermenter, mainly soiled by yeast, was cleaned with help of a rotary jet head (Alfa Laval, Denmark). There were 27 CIP operations for the same fermenter implemented over the past two years. The data were recorded by a CIP diagnosis system from Ecolab A/S, allowing an analysis in this chapter.

Table 4.1 shows the CIP procedure of the fermenter. The available data contain both quantitative and qualitative forms, shown in Table 4.2. Quantitative data are measured on a numeric scale. Qualitative data denote categorical or discrete variables [116].

Table 4.1: CIP procedure of the analysed brewery fermenter

No.	Steps	Approx. time, min
1	Alkaline without circulation	20
2	Alkaline circulation	35
3	Intermediate rinse	6
4	Acid circulation	20
5	Intermediate rinse	9
6	Disinfectant circulation	30
7	Final rinse	17

However, some challenges exist when dealing with the data, including:

1. The feed pump is controlled dynamically, which means that the pump stops and restarts or the flow rate varies during cleaning. This kind of flow pattern helps to accumulate liquid to clean some elements at the tank bottom but creates fluctuations in the data.

2. Only the overall cleaning time is documented. Whereas, the period and interval of each step need to be determined manually. A step starts when both the valve and

Table 4.2: Process monitoring data by the CIP diagnosis system

Types of data	Names	Units	Sampling frequency	Notes
Quantitative	Feed flow rate	m^3/h	ca. every second	
	Return flow rate	m^3/h	ca. every second	
	Conductivity in feed flow	mS/cm	ca. every second	
	Conductivity in return flow	mS/cm	ca. every second	
	Pump outlet pressure in feed flow	bar	ca. every second	
Qualitative	Date and time	Dimensionless	Once per cleaning	
	Recipe number	Dimensionless	Once per cleaning	
	Pump status	Dimensionless	Once per change	Binary data (on and off)
	Valve status	Dimensionless	Once per change	Binary data (on and off)

pump are “on”. Meanwhile, a step stops when either the valve or pump is “off”.

3. Even though the same recipe is applied, the real step times differ on a minute scale from batch to batch. This difference can be caused by for example the delay to reach the critical control point, liquid filling in transfer lines, pump failure, etc.

4. Both quantitative and qualitative data exist. However, all data are exported as discrete data sets. For the quantitative data, different variables are documented with their own time series, which are different among each other in terms of sampling indices and intervals.

5. The cleaning recipe is time-based. The measurement of cleaning quality is missing. Thus, the cleaning time is set over need, assuming the most difficult area to be cleaned can still be cleaned.

6. Some modifications in the past two years are not recorded. Some data related to the process are unknown, like the tank liquid volume and the pump power.

4.3 Three-Level Approach for Anomaly Analysis

A CIP operation can be regarded as a batch process. Each batch comprises several steps, which are assumed to be independent of each other. A three-level approach was designed for the data analysis, forming the main highlight of the chapter.

1. *First level, prior-to-batch analysis*
   This was performed before cleaning took place, with the purpose to ensure that the cleaning requirements could be met. The factors to be analysed included but were not limited to (i) the interval to the last production or cleaning for assessing the soil age or if the cleaning was repeated; (ii) the recipe number to ensure a right program was selected; (iii) the off-line measurement of chemical samples to ensure the chemical solution was active; and (iv) the accumulated equipment errors to ensure that the system was effective. In this cleaning of the fermenter, cleaning was assumed to be performed at the right time, meaning the cleaning interval was correct. The procedure selection (recipe number) and chemical solutions were confirmed to be correct as well. Therefore, only the performance of the feed pump was assessed, which was one of the most important factors for a successful cleaning operation.

2. *Second level, process monitoring*
   The purpose of process monitoring was to ensure that the cleaning program was under a state of control. Process monitoring included an end-of-batch monitoring and an online monitoring. End-of-batch monitoring was carried out when the whole trajectories were available. Online monitoring was the ultimate goal of process monitoring, which provided the process information while the deviation took place and served the real-time quality control [117]. In both monitoring methods, a multivariate analysis approach was applied by simultaneously monitoring the pressure, flow rate, and conductivity measurements. It was optional to enable the recording of more variables into the model if data were available (e.g., temperature).

3. *Third level, end-of-batch performance evaluation*
   End-of-batch performance evaluation was made in the end of the cleaning operations. A standard procedure was defined based on good batches (defined in Section 4.4.2.3), in terms of cleaning step time, water and chemical consumption, pump and valve status, etc. The purpose of this level was to find if the cleaning operation was performed consistently. After cleaning, an operator could compare these factors with the reference and evaluate if the cleaning was finished normally or abnormally.

In the present analysis, the three-level approach only indicates the existence of anomalous events and the likely causes. The operators should be trained to identify the root cause of an anomaly and then solve the problem. Ideally, the anomalies can be automatically detected and solved through the integration of the proposed approach with control systems, which, however, is not a topic of this study.

4.4 Methods

4.4.1 Feed Pump Analysis

The feed pump output was dynamically adjusted during cleaning. There were short periods when the flow rate was stable at the required level, though. Therefore, the

working flow rate when the pump was operated at a static pressure and the start-up transition time to reach the steady state were captured for analysis. Both characteristics formed indicators of the pump performance. The two-year results were divided into four groups with data collected during each half year as a group. The average flow rate and transition time in each group were calculated and plotted together for analysis.

4.4.2 Multivariate Monitoring Analysis

The multiway principal component analysis (MPCA) method is a common batch monitoring technique extending the ordinary principal component analysis (PCA). It is equivalent to performing PCA on a large two-dimensional matrix constructed by unfolding the three-way array. The implementation of MPCA or PCA requires a complex data preprocessing treatment. In this work, MPCA was applied, and the procedure is described in Figure 4.1. All calculations were carried out in Matlab (Mathworks, Inc., Natick, USA).

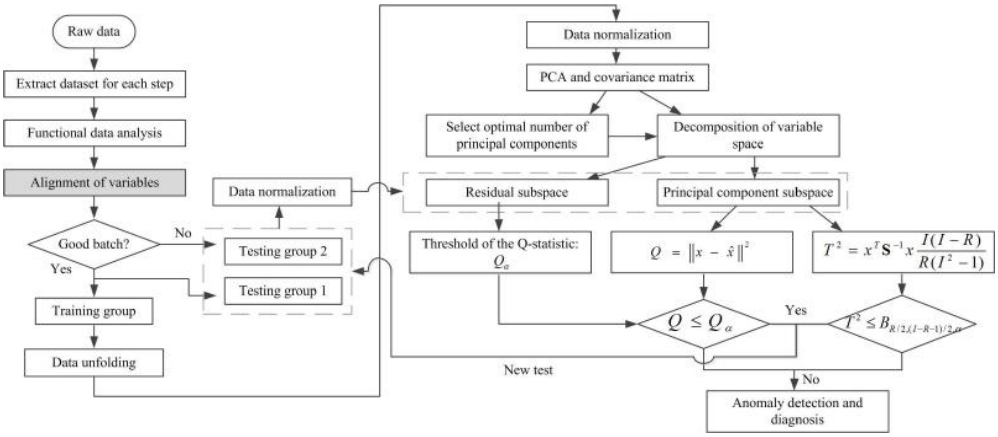

Figure 4.1: Proposed methodology for multivariate analysis in the level 2 analysis. The step "Alignment of variables" is eliminated when performing nonsynchronization analysis.

4.4.2.1 Functional Data Analysis

Each cleaning step was analysed separately. The start and end points of each step were manually determined based on the qualitative pump or valve status data. The starting time of a step was defined as time zero. In this level, five quantitative variables (see Table 4.2) were analysed. Due to the uneven length of time series for each variable, the first treatment of data was to project all measurement variables into uniform time indices and intervals, as illustrated in Figure 4.2. Functional data analysis (FDA) was applied to produce a smooth functional data set from the discrete records by reducing random errors [118]. The standard form of FDA is the "signal plus noise" model as Equation 4.1 shows:

$$\boldsymbol{y} = x(\boldsymbol{t}) + \boldsymbol{\varepsilon} \tag{4.1}$$

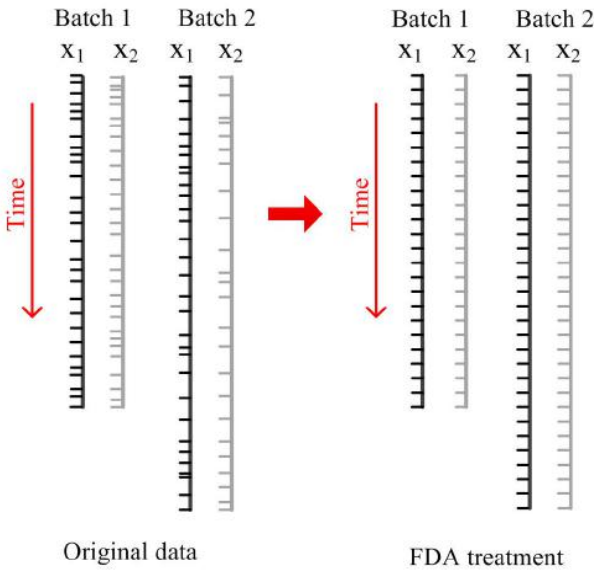

Figure 4.2: Illustration of unifying the time stamps of different variables by means of FDA. The new data set after FDA treatment has a one second time interval.

where the observed data set $\boldsymbol{y}$ is expressed by the function $x(\boldsymbol{t})$ and noise $\boldsymbol{\varepsilon}$. $x(\boldsymbol{t})$ represents a linear expansion of a series of basic functions. The best known basic expansions are the Fourier series for periodic data and the spline basic system for open-ended data [118]. Only the spline basis was used in this work, as shown:

$$x(t) = \sum_{i}^{M} c_i \Phi_i(t) \tag{4.2}$$

$\Phi_i(t)$ are fourth-order polynomials with the ith term coefficient c_i. The number of basic functions was resolved as follows [119]:

$$Number\ of\ functions = knots + order - 2 \tag{4.3}$$

The knots equalled the time trajectory of the measured variable. The coefficients, c_i, for spline functions were obtained by fitting the measurement data by minimising the penalized sum of squares (PENSSE) with an additional penalty term, $J[x]$, to impose smoothness in the function output. The function's roughness was the integrated squared second derivative $[D^2x(t)]^2$, as calculated by Equation 4.5. The smoothing parameter, λ, was defined to be 1, which was close to the optimal value determined by means of the

generalized cross-validation (GCV) criterion [118, 119].

$$PENSSE = \sum_{i}^{n}(y_i - x(t_i))^2 + \lambda \times J[x] \quad 4.4$$

$$J[x] = \int [D^2 x(t)]^2 dt \quad 4.5$$

In order to unify the time trajectories for all variables, a new time vector with one second interval was defined. The values of different variables in the new time series were evaluated from the smoothed functions.

4.4.2.2 Alignment of Variable Trajectories

FDA aligns different variables within a batch. However, following FDA, the unequal and unaligned data across batches still exist because the original data were collected with independent lengths. Three approaches were tested to solve the problem:

1. The first and the simplest method was to cut all batches to the minimum length or a specific length. This method kept the nature of batches, at the expense of losing all information after the cutting point. However, the shifts of variable profiles caused by the dynamic operation of the pump could still lead to the challenges of data analysis.

2. The second method was the indicator variable technique, the concept of which was to replace time by another process or derived variable to indicate the progress of a batch [120]. In this study, the liquid volumetric consumption, calculated from time and flow rate data, was chosen as the indicator variable to quantify the percent completion of cleaning. Linear interpolation was used to transform the time dimension into the indicator variable dimension.

3. The third method was to locally translate, compress, and expand the pattern of one sequence to match another sequence of similar features, called dynamic time warping (DTW) [121]. DTW non-linearly warps two data series in such a way that similar events are aligned and the distance between them is minimized [117]. In this study, pressure was an active variable, whose variance influenced the patterns of other variables. Therefore, the warping path was obtained by aligning all pressure measurements to a reference batch demonstrating good performance, and other variables within a batch were aligned in the same warping path.

4.4.2.3 Training and Testing Data Sets

The CIP batches were labeled as “good” or “bad” operations. A CIP batch was regarded as bad when possessing at least one of the following characteristics:

- the pump stopped for an uncommonly long time during a step;
- there were more or less pump stops than foreseen in a normal operation procedure;

- a cleaning step was missing, or the duration of a step was extremely long or short;
- the ionic properties of chemical solutions were abnormal;
- unreasonable flow rates were observed (i.e., zero flow rate due to pump idling).

Ca. 15 good batches, the number of which varied when analysing different cleaning steps, were used as training data set for constructing the reference models. The rest, consisting of both good and bad batches, were used as testing data set for validating the models.

4.4.2.4 Data Unfolding and Normalization

The functional data were provided as a three-dimensional (3D) matrix with I batches, J time indices, and K variables. MPCA requires that the 3D matrix is unfolded to a two-dimensional (2D) matrix. There are normally two ways to unfold batch data: a batch-wise unfolding results in an $(I \times JK)$ matrix and a variable-wise unfolding yields an $(IJ \times K)$ matrix. Most statistical process monitoring techniques apply the batch-wise unfolding approach, allowing one to analyse the variability among batches with respect to variables and their time variation. However, when being used online, it is required to estimate the future portions of variable trajectories. On the contrary, the variable-wise unfolding does not require such estimation, making it applicable for online monitoring [115, 122, 123]. Wold et al. (1998) concluded that the former was oriented to evaluating the completed batch as normal or abnormal, while the latter focused more on the monitoring of individual time points [124]. The primary objective of this study was to identify the occurrence of an anomalous event online. Therefore, only the variable-wise unfolding method was applied to the data.

The new unfolded matrix was then mean-centered and variance scaled. Mean centering was applied to the raw data by subtracting the average variable values for each time point. Then the variance scaling was carried out to the centered data by a slab-scaling method, by dividing with a unit root-mean-square of each variable. We noted that other scaling methods, like column-scaling by dividing the root-mean-square of each time point, led to different results. In pre-studies, lower variability was explained when scaling with column-scaling, because this method caused significant deviations when data were unsynchronized or inadequately synchronized. Therefore, only the robust slab-scaling method was used in this study, which was also recommended when dealing with an industrial data set [125].

4.4.2.5 Multivariate Analysis

PCA is a commonly used multivariate statistical analysis method for monitoring purposes, which defines the principal components through a linear transformation of the original variables and explains the maximum variance. Instead of analysing all variables, the PCA method focuses only on analysing the principal components when monitoring the system and thereby reduces the dimensionality of data [122, 124]. In this work, PCA was applied to the normalized data matrix X, which was decomposed into a score matrix T and a principal loading matrix P:

$$X = TP^T \tag{4.6}$$

Only the eigenvectors, Q ($Q \in \Re^{K \times M}, M < K$), in P were retained in the PCA model. The number of selected principal components in this model was $M = 3$, which explained approximately 90% of the cumulative percent variance (CPV). The new validation data were normalized in the same way as the training data set. The estimate of the testing groups of data was done according to:

$$\hat{X}_{new} = X_{new} Q Q^T \tag{4.7}$$

4.4.2.6 Anomaly Detection

Two commonly used indexes to detect anomalies or faults are the Q-statistic [122] and the Hotelling's T^2 statistic [115, 126]. The Q-statistic and its threshold (δ^2) are computed as follows [114]:

$$Q - statistic = ||X_{new} - \hat{X}_{new}||^2 \leq \delta^2 \tag{4.8}$$

$$\delta^2 = \theta_1 \left[\frac{h_0 c_\alpha \sqrt{2\theta_2}}{\theta_1} + 1 + \frac{\theta_2 h_0 (h_0 - 1)}{{\theta_1}^2} \right]^{1/h_0} \tag{4.9}$$

where $\theta_i = \sum_{j=M+1}^{K} {\sigma_j}^{2i}$, $h_0 = 1 - \frac{2\theta_1 \theta_3}{3{\theta_2}^2}$ and c_α is the normal deviate corresponding to the $(1-\alpha)$ percentile. σ_j is the jth eigenvalue. When there is no anomaly, the Q-statistic is less than δ^2, representing the normal dynamics and noises which are unavoidable. On the other hand, if an anomaly or fault exists, the Q-statistic is higher than the threshold.

The Hotelling's T^2 statistic and its threshold, $B_{R/2,(I-R-1)/2,\alpha}$, are given by [117]:

$$T^2 = \hat{X}_{new} S^{-1} \hat{X}_{new}^T \frac{R(R-K)}{K(R^2-1)} \tag{4.10}$$

$$B_{R/2,(I-R-1)/2,\alpha} \sim \frac{(K/(R-K-1))F_{K,R-K-1,\alpha}}{1 + (K/(R-K-1))F_{K,R-K-1,\alpha}} \tag{4.11}$$

where S is the $(K \times K)$ covariance matrix, R is the number of batches in the reference set. F is the F-distribution value with R and $(I - R - 1)$ degrees of freedom at the α significance level. The interpretation of the T^2 statistic is similar to the Q-statistic, that is, an out-of-threshold signal denotes an anomalous event.

4.4.2.7 Anomaly Diagnosis

The diagnosis of a detected anomaly can be performed by a univariate method to analyse the monitoring variables one by one, or by a multivariate method like contribution plot. A contribution plot indicates the contribution of each variable to the deviation from a normal operation. For the Q-statistic, the contribution of variable k at time j is calculated from the residual, e, as follows[117, 127]:

$$C_{Q,jk} = e_{jk}^2 \tag{4.12}$$

For the Hotelling's T^2 statistic, the contribution of each variable is given by [127]:

$$C_{T^2,jk} = \sum_{m=1}^{M} x_{jk} p_{km} \tag{4.13}$$

where p_{km} is the loading for variable k in dimension m.

4.4.3 End-of-Batch Performance Evaluation

For level 3 of the approach, a standard range was defined for the cleaning time, liquid consumption or on−off ratio (the period when the pump is "on" divided by the whole step time) of each step on the basis of some good batches. The standard was made for each cleaning step, including the means, standard deviations (STD), and a parameter γ, to allow a judgement range as described in Equation 4.14.

$$Reference = mean \pm \gamma \times STD \tag{4.14}$$

The testing groups of data were used for validation, which included both good and bad batches (defined in section 4.4.2.3). During the test, a cleaning was regarded as "normal" if the indexes were within the reference range. On the contrary, a cleaning was "abnormal" if the indexes were out of the range. However, wrong judgement might occur. For example, a good operation was denoted as bad or a bad operation was denoted as good. Therefore, there are four possible outcomes [128]: (1) true positive (TP) correctly recognizes a good operation as "good"; (2) true negative (TN) correctly recognizes a bad operation as "bad"; (3) false positive (FP) wrongly recognizes a bad operation as "good"; and (4) false negative (FN) wrongly recognizes a good operation as "bad".

The judgement decision depends on the value of γ. Therefore, a new index, η, was defined to quantify the ratio of the number of correct judgements over the total number of testing batches, as present in Equation 4.15. A high value of η represents a high probability to make a right decision.

$$\eta = 1 - \frac{FP + FN}{All} \tag{4.15}$$

4.5 Results and Discussion

4.5.1 Precleaning: Performance of the Feed Pump

Figure 4.3 displays the performance of the feed pump over a two-year period. The start-up transition time for the feed pump to reach the working flow rate has not changed significantly ($p = 0.23$), but the static flow rate reveals a clearly decreasing trend ($p < 0.01$). The decrease of flow rate may result in insufficient mechanical force to remove soils from the surface, or make the cleaning costs extremely high. This decreasing trend of flow rate can be due to the mechanical variance of the pump, leaking of liquid, fouling of the transfer pipe, low level of liquid in the storage tank, calibration of sensors, etc. Since the variance of flow rate is a long-term performance metric, the occasional faults can be ignored, like the leaking problem and the liquid level. However, it is still difficult to find an exact cause of the anomaly due to the lack of measurement.

The differential pressure (the difference between the suction and discharge heads) is critical for a pressure-controlled pump, as in this case. For example, the outlet pressure is controlled to be constant. However, if there is fouling in the suction line, the inlet pressure

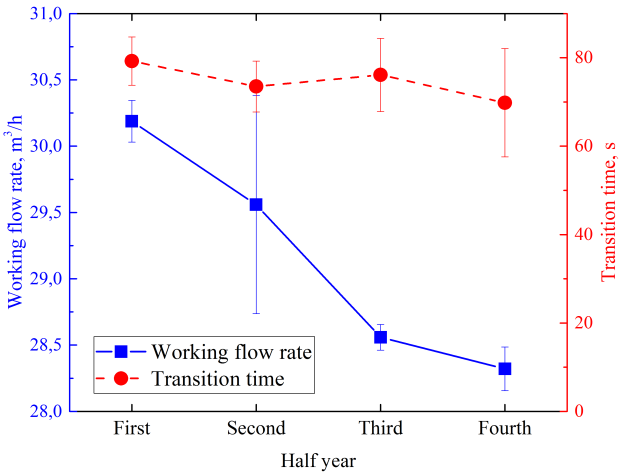

Figure 4.3: Working flow rate and start-up transition time of the feed pump over the past two years.

drops and the differential pressure increases, and consequently the flow rate drops. On the other hand, the fouling in the discharging line (which is to be cleaned) can increase the system friction and reduce the flow rate as well [129]. Besides, the cavitation of the pump and the change of impeller clearance can influence the pump performance. As a result, the observation in Figure 4.3 reminds the operators to perform an inspection of the pump or of the whole system. There is a risk of failure once the flow rate is less than the critical point.

The above-mentioned analysis can be accomplished automatically if the system can extract the flow rate information based on previous cleaning operations by coupling the pump status and output, thereby displaying the performance of the feed pump before a new operation starts. A similar analysis can be applied to other systems besides the feed pump. For example, checking heat exchangers' working temperature and heating time to reach the critical temperature can characterize the performance of heat exchangers (though irrelevant in this study). Keeping the whole system in high performance is a prerequisite to avoid a potential cleaning failure.

4.5.2 Cleaning or Post Cleaning: Data Pretreatment and MPCA Model

The multivariate analysis was performed for each step separately. An example of the FDA results for the alkaline treatment without circulation step is shown in Figure 4.4. The smoothness is controlled by the penalty coefficient, λ, in Equation 4.4. For the alkaline step, the optimal λ determined by the GCV criterion varies from batch to batch and variable to variable, most of which lie in the range of $10^{-1} \sim 10^{1}$. Choosing a small value

of λ, the function fits the raw observations better but the smoothness becomes less. On the contrary, as λ becomes larger, the function places more emphasis on the smoothness and less on fitting the observations. However, in this study, the influence of changing λ between 0.1 and 10 is visually small, because the measurement noise is not significant. Therefore, a fixed value of 1 was selected for all computations.

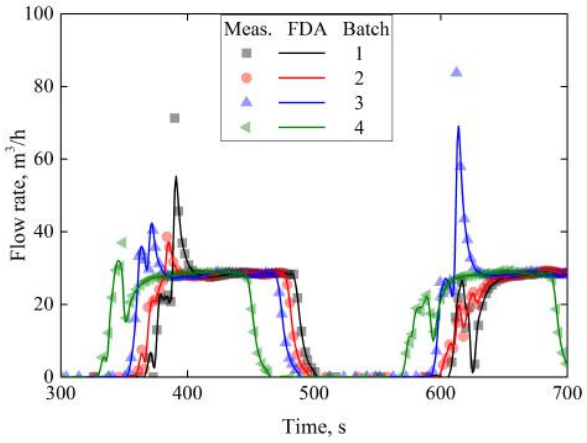

Figure 4.4: Raw discrete data (symbols) and the FDA results (curves) of the alkaline treatment step without circulation. The roughness penalty coefficient in FDA, λ, is 1.

After FDA treatment, similar curves are obtained for different batches. However, there is still a shift or delay of the pattens (see Figures 4.4 and 4.5A). Without trajectory alignment, it is necessary to keep different batches of the same length, for example, by cutting the remaining measurements after a specific time point (Figure 4.5B). However, this kind of treatment eliminates information after the cutting point. On the other hand, the shape differences can be reduced by applying an indicator variable or time warping of the data, as displayed in Figure 4.5C and D, respectively. Both techniques retain the whole trajectories of data. Nevertheless, variances and fluctuations still exist, especially when the pump starts. This transition problem will further lead to large variances at these time points.

PCA was then performed to the unfolded and normalized data matrix. In accordance with Lehman et al. (2013) [130], the selection of the number of PCs should explain at least 80% of CPV. The final model uses three PCs to meet this criterion.

4.5.3 Post Cleaning: End-of-Batch Anomaly Detection and Diagnosis Based on the Multivariate Analysis

A good and a bad batch are introduced for showing the validation of the MPCA model. Figures 4.6 to 4.8 display the off-line anomaly detection with trajectories either unaligned or aligned by two methods. Since there are spike disturbances in measurements, it makes

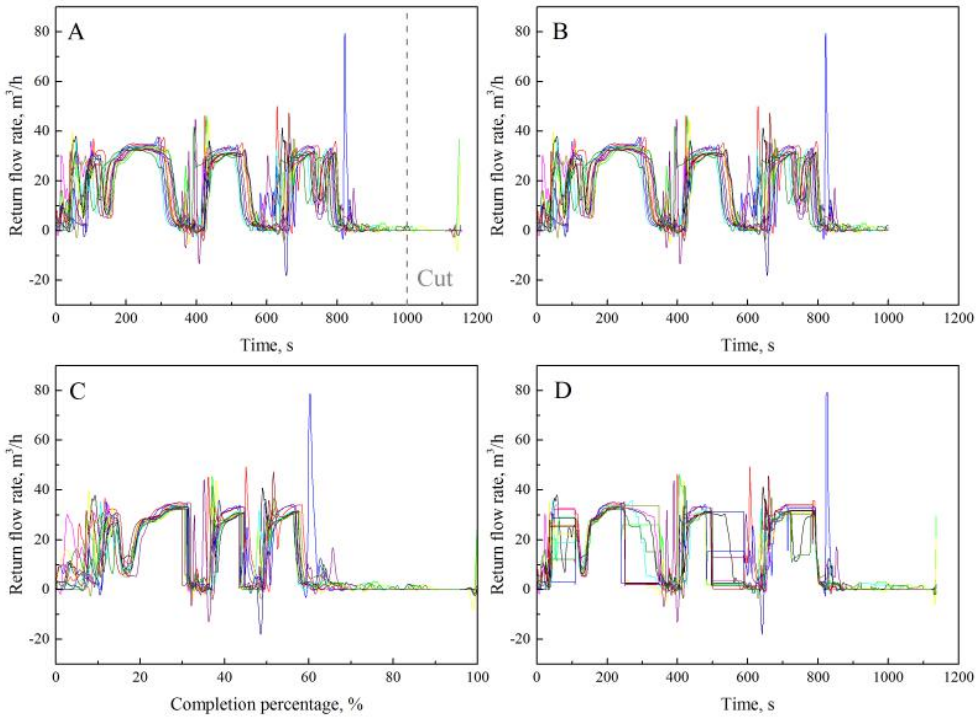

Figure 4.5: An example of the alignment of variables for the alkaline treatment step without circulation. (A) is the original measurement. (B) is obtained by cutting the data after 1000 s. (C) is based on the indicator variable technique. (D) is based on DTW.

no sense to recognize an anomaly when only one or a few samples jump above the threshold [126]. Thus, an anomaly is determined when a continuous series of points are out of the control region. Increasing the significance level α lifts the detection threshold [117].

For both Q and T^2 statistics, there are none or only a few anomaly alarms triggered for the good test batch. Some out-of-threshold points at the beginning of cleaning can be mostly caused by the various initial states in different batches, like product or liquid filling in pipes. If neglecting some short-term out-of-threshold observations, all models successfully avoid wrong detection by recognizing a normal situation as abnormal. On the contrary, the detection of the bad test batch is very sensitive to the selected statistical method and alignment approach. The T^2 statistic triggers more alarms than the Q-statistic, meaning the former is more sensitive to anomalous events. The large peaks of values are the results of dynamic pump profiles. Applying trajectory alignment can increase the robustness of the model, because after alignment all batches are adjusted to be as close as possible to the reference. Therefore, the normal time shift between batches, which causes the firm alarms in Figure 4.6B, becomes no longer the source of anomalies. Aligning the data

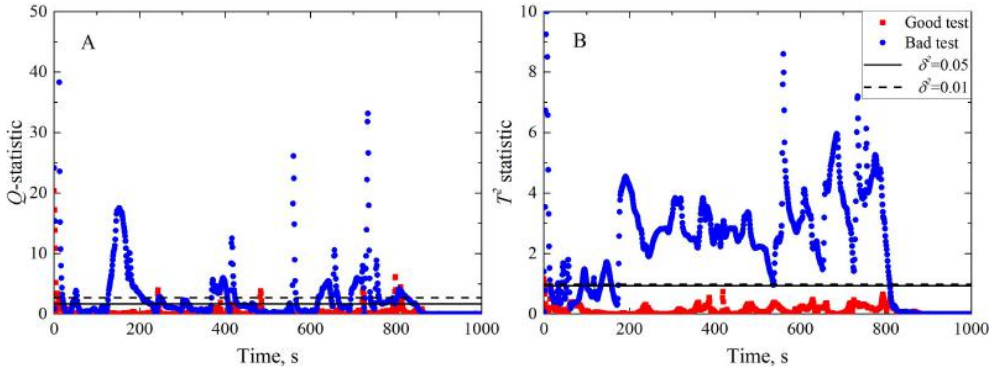

Figure 4.6: Anomaly detection plots by (A) the Q-statistic and (B) the Hotelling's T^2 statistic with the unaligned trajectory discarding the part of the data set that is cut off. The example is based on the alkaline treatment step without circulation.

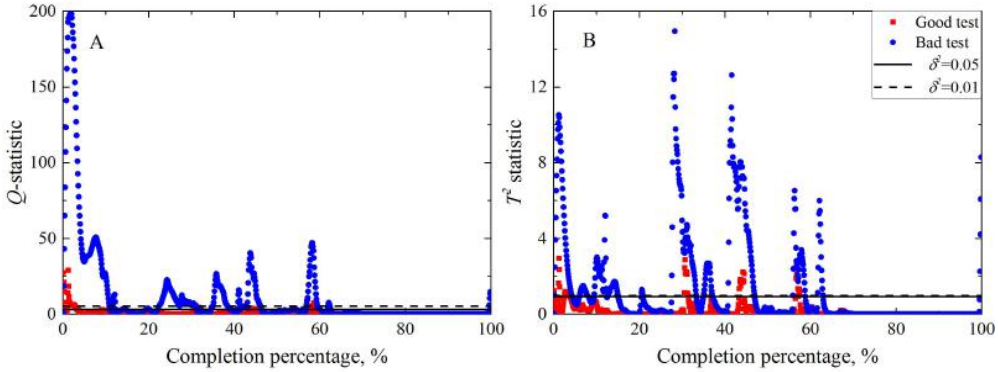

Figure 4.7: Anomaly detection plots by (A) the Q-statistic and (B) the Hotelling's T^2 statistic with the trajectory aligned by indicator variable. The example is based on the alkaline treatment step without circulation.

by the indicator variable is more applicable for detecting a sudden variation. For the alignment by DTW, however, a long-term anomaly occurs as a gradual change.

Once an anomaly is detected, it is necessary to understand which measurement deviates most and why it occurs. This can be done by analysing the measurement values one by one or by using the contribution plot [127]. When there are many measurements or more than one measurement is deviating from the reference, the troubleshooting approach using contribution plots becomes more effective.

Figures 4.9 and 4.10 display the contributions of each variable to the Q and T^2 statistics for the data set with trajectories aligned by the indicator variable technique and DTW, respectively. Both represent the same events at 300 s and 400 s reference times in Fig-

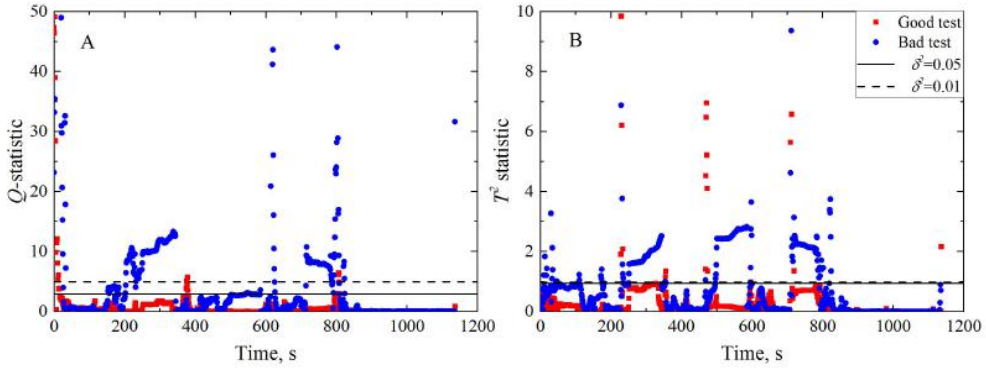

Figure 4.8: Anomaly detection plots by (A) the Q-statistic and (B) the Hotelling's T^2 statistic with the trajectory aligned by DTW. The example is based on the alkaline treatment step without circulation.

ure 4.8 when aligning the trajectory using DTW. The two alignment methods are almost identical with regard to diagnosing the observations. At 300 s, an anomaly occurs to the bad batch. At 400 s, both batches are in the state of control. The axis scaling of the bad test at 28.3% completion or 300 s is greater than the other normal tests in all plots, indicating that the absolute difference of each measurement value in the abnormal state is larger than in the normal states. This anomalous event is mostly caused by the significant deviations of the conductivity measurements in either feed flow or return flow. However, the current analysis cannot figure out the exact causes of the anomaly. But the operator is led to checking the chemical solution to diagnose the problem. A detailed off-line diagnosis of the system confirms that the real cause is due to the extreme dosage of concentrated caustic. Therefore, the troubleshooting approaches presented in Figures 4.9 and 4.10 indicate the right tracing of the fault.

Note that contribution plots suffer from a smearing effect, under which the contribution of a variable is affected by the interferences with other variables [131]. As a result, the diagnosis accuracy can sometimes be reduced. Despite some available modified or alternative methods, it is advisable to interpret the diagnosis task based on both contribution plots and univariate isolation (i.e., analysing the deviation of each variable from its expected value) for the sake of safety [132].

4.5.4 Cleaning: Online Anomaly Detection and Diagnosis Based on the Multivariate Analysis

The advantage of variable-wise unfolding is to treat the new monitoring data directly online without estimating the future variable measures that are required when unfolding in the batch-wise direction. In order to implement online analysis, a coupled measurement system is necessary, where all measurements are made in the same time series or can be functionalized to estimate the variable values at consistent time points. Without

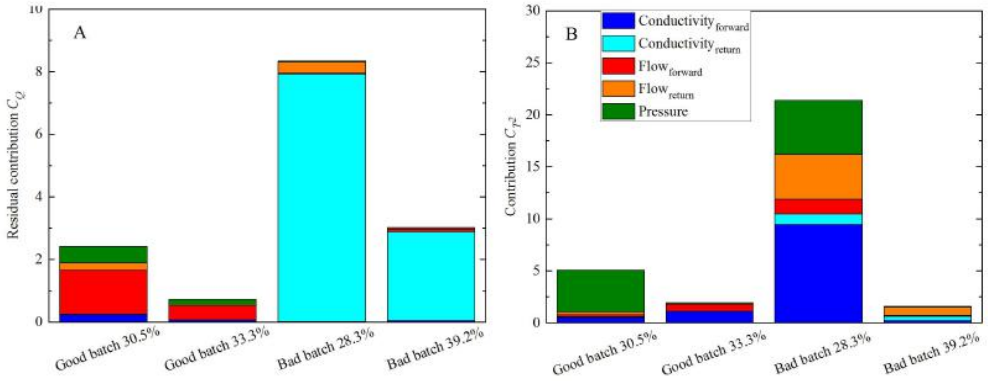

Figure 4.9: Anomaly diagnosis of aligned data sets by the indicator variable technique. (A) represents the residual contributions to the Q-statistic. (B) represents the absolute contributions to the T^2 statistic. The selected percentages of completions correspond to 300 s and 400 s reference times, respectively, when aligning the trajectory by DTW. Only the "bad batch 28.3%" is a detected anomaly state. The others are under the control limit.

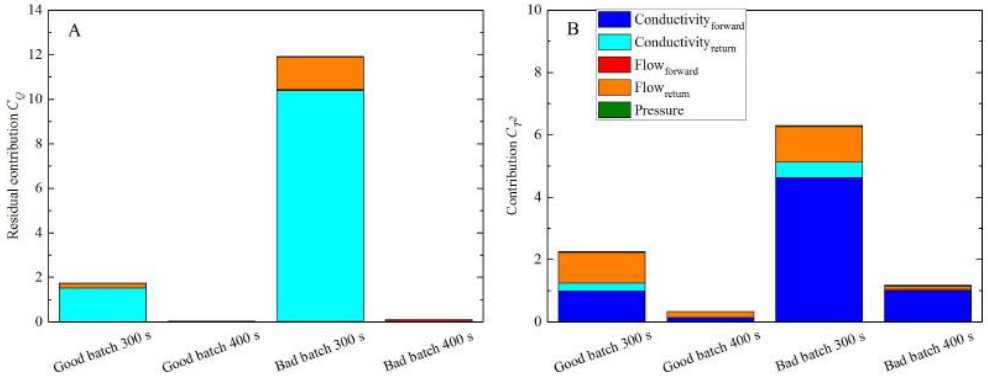

Figure 4.10: Anomaly diagnosis of aligned data sets by DTW. (A) represents the residual contributions to the Q-statistic. (B) represents the absolute contributions to the T^2 statistic. The selected reference times correspond to the completion percentages in Figure 4.9 when aligning the trajectory using the indicator variable technique. Only the "bad batch 300 s" is a detected anomaly state. The others are under the control limit.

trajectory alignment, the new monitoring variables can be directly unfolded, normalized, PCA transformed, and analysed by statistics as illustrated in Figure 4.1. Similar results can be obtained as shown in Figure 4.6. However, the unaligned approach results in high uncertainty once normal time shifting is significant in the new batch. In this regard, trajectory alignment becomes more credible, plus more challenging.

For the alignment according to an indicator variable, the completion percentage is calculated from the consumption of liquid volume divided by the total consumption. However, the actual total consumption of liquid is unknown until the end of the batch. Therefore, a constant value of the average consumption in reference batches is used for the new batch. This value can be altered to the real consumption when performing an end-of-batch analysis.

For the alignment using DTW, the challenge in online monitoring is to pair the current observation time to an end point in the reference in order to synchronize the new trajectory with the reference timeline. Kassidas et al. (1998) introduced lower and upper bounds for searching the optimal path that provides the best matching between the reference and the uncompleted batch [133]. The point resulting in the minimal accumulated distance is determined as the end point corresponding to the current observation. In the study of this chapter, the alignment path can be obtained by aligning the pressure intensity along the reference timeline. This procedure is one-way incremental and repeated when each new measurement comes in.

To explain online monitoring, an example is shown in Figure 4.11 based on functionalized data. In Figure 4.11A, the difference between the online and offline aligned data is due to the fact that the real overall consumption may differ from the expected value. However, the deviation only causes a slight shift of the profile. The alignment based on DTW can also effectively reduce the time difference (see Figure 4.11B). However, caution should be taken when defining the searching bounds of the end point, which should lie internally between the lower and upper bounds. To sum up, the indicator variable based approach surpasses the DTW method in terms of computation efficiency because the latter requires accumulative calculations of all likely points in the range in order to obtain the minimal distance. After alignment, the new monitoring variables can be further transformed for anomaly detection, as described in Figure 4.1.

4.5.5 Post Cleaning: Validation of Performance

Operators expect a simple method to evaluate a CIP operation, by indicators which can be easily measured or computed, such as the step time, the liquid consumption, and the on−off ratio of the pump. Therefore, the operators only need to compare these values with the standard ranges and get an idea about whether the cleaning is performed accordingly. The standard range is related to the safety margin parameter, λ, which further influences the judgement of the cleaning performance.

As shown in Figure 4.12, the increase in λ generally improves the correctness of the judgement, as more good cleaning operations are covered in the range. However, if the value of λ is beyond a specific limit, the correctness of the judgement is reduced, because

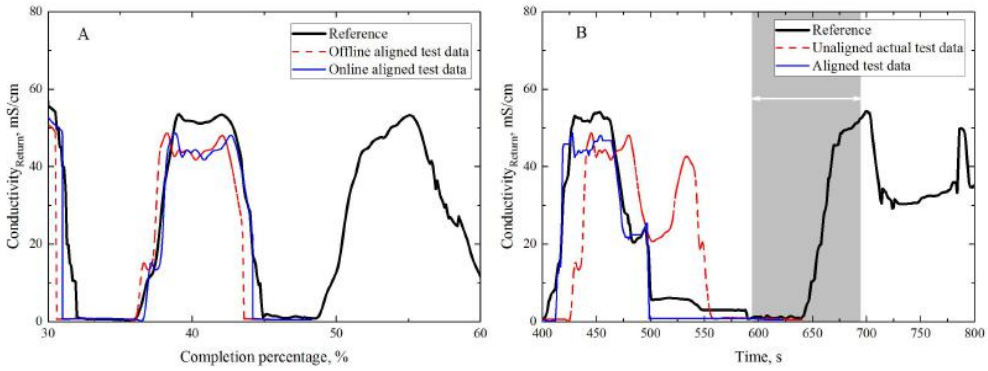

Figure 4.11: An example demonstrating online alignment of the variable trajectory based on (A) indicator variable technique and (B) DTW. The current observation time is 640 s, corresponding to 47.6% completion of the batch. The grey region in figure B refers to the searching range of the end point with ±50 s bounds

more and more bad cleaning operations are wrongly considered as good. Therefore, it is recommended to select the value of λ between 2 and 3. Using the step cleaning time or the on−off ratio is more effective than using the liquid consumption to make a decision, where the accuracy is up to 80%. This can be understood by the fact that the current recipe is based on time, and the main anomalies in the studied CIP system result from the feed pump or accessory valves. Once a low flow rate occurs, the system automatically takes an action by controlling the flow rate at the predefined value and adjusting the cleaning time to be long enough. As a result, the cleaning time deviates from the reference range but the total consumption does not vary significantly. Therefore, the operator is advised to use the cleaning time or on−off ratio of the pump to evaluate the cleaning results. Once there is a rising trend of the number of abnormal events in a period, it is time to perform an overall inspection of the CIP system.

4.6 Practical Applications and Future Perspectives

The proposed three-level approach provides a benchmark in the analysis of historical data for evaluating a CIP system. The above analysis was based on the cleaning of a brewery fermenter. However, the application is not limited to the brewery case. The potential applications could be the following:

- *Training of operators*: the operator is the most important person to implement a CIP operation. If the operator gets some simple indexes to assess a CIP cycle (i.e., the step time), a potential failure can be evaluated immediately after cleaning, thereby avoiding potential delays in the production process.

- *Maintenance of the equipment*: it mainly refers to pumps and valves (as well as heat

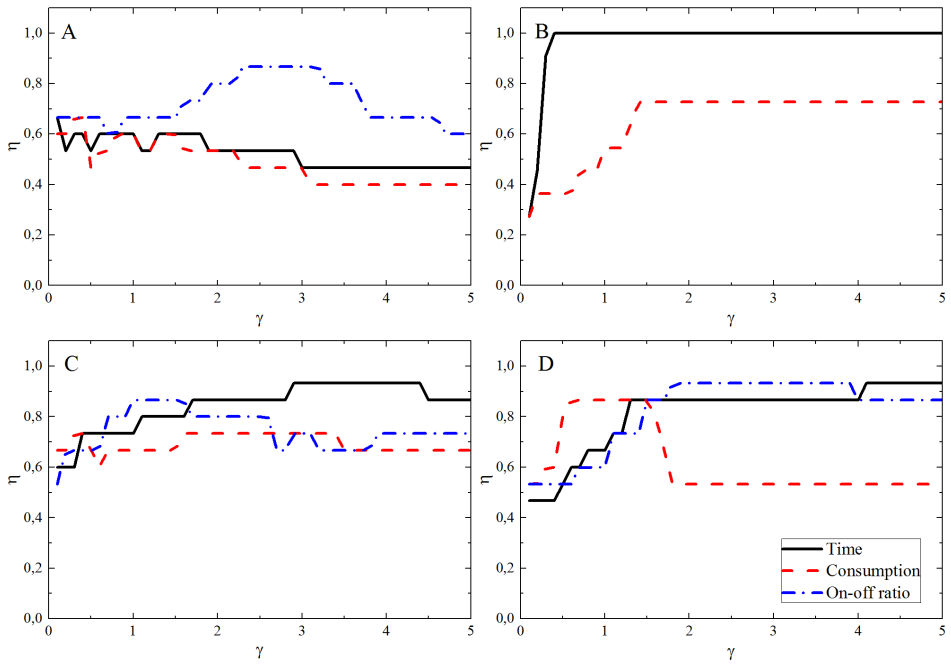

Figure 4.12: Ratio of the correct judgement of cleaning performance against the margin parameter λ: (A) alkaline step without circulation, (B) alkaline circulation, (C) acid circulation, and (D) disinfectant circulation. There are no pump stops during the alkaline circulation step.

exchangers, though not involved in this chapter). A systematic shift of observations (i.e., flow rate and transition time) may indicate an accumulated error or damage of the equipment.

- *Optimization of the system*: a reference model has been established based on historical data of good cleaning operations. Optimization could therefore be achieved by altering one parameter once and comparing the new measurements with the reference.

- *Flexible selection of cleaning recipes*: in some processes where the equipment is used to produce different products, there are multiple recipes to remove different soiling materials when altering products. A reference model helps to examine if a complex recipe is selected to clean a loose soil or a simple recipe is selected to clean a harsh soil. Sometimes, a short cleaning recipe should be selected before production if the equipment is held for a long time. Choosing a full recipe in this case will waste considerable money and resources. A reference model helps to recognise the recipe, because an improper selection of recipe results in unexpected monitoring outputs when comparing with the reference.

- *Alarm of system anomaly*: conventionally, the alarm is triggered when one or more monitoring variables are out of range, meaning that the failure or error already happens. A multivariate analysis approach can not only capture such an existing problem but also identify abnormal trends that may suggest a potential failure. Early detection of anomalies reduces the damage of equipment and saves cleaning resources.

- *Counting of anomalous events*: end-of-batch analysis can be performed periodically by counting anomalies over a specific period, in order to gain a better understanding of the system.

There are some considerations associated with the existing study to support an effective application in the future. First, only the two-year data set of one brewery fermenter is investigated. As a benchmark case, the model is flexible to involve other systems and more data sets. Second, the current system does not consist of any online monitoring of cleaning quality, which is a common problem in most CIP practices. New sensor technology (i.e., turbidity) allows to detect the residues in the liquid phase. Involving the quality indicators of the cleaning operation into the second level analysis will deliver more information and potentially allow to predict the end point of cleaning operations [115]. Finally, an advanced monitoring and control system is required to implement the analysis automatically. Especially, monitoring all variables of the same trajectory and equal time space should allow simplifying the model construction and reducing the uncertainty. An ideal operation of CIP is expected to be implemented in such a manner:

1. when clicking the recipe button, the control interface displays the system performance based on previous cleaning operations and offline measurements, and reports if the selected recipe is able to complete the cleaning task in an efficient and economic manner;

2. when performing the cleaning, the abnormal detection approach triggers the alarm immediately when it happens, and the potential causes of anomalies and proposed actions are described;

3. after cleaning, a report is automatically generated including the cleaning duration, the chemical consumption, and the number of anomalies, as well as a self-evaluation of the result.

4.7 Conclusions

A three-level analysis approach was described to provide a benchmark to analyse historical data in CIP cycles. The case study analysed here was based on the cleaning of a fermenter in an industrial brewery. Reference models were established in order to evaluate if the future cleaning operations are performed normally or abnormally. The analysis approach is expected to be carried out prior to cleaning, during cleaning and at the end of the cleaning process.

In the demonstrated case of the cleaning of a brewery fermenter, a decreasing trend of the feed pump performance is observed, indicating the necessity of an overall inspection of the system. The process monitoring using multivariate analysis methods is able to detect the localized abnormal events in the process. Trajectory alignment is necessary to overcome time shifting between batches and hence improve the robustness of the model. Using the liquid volume consumption as an indicator variable to synchronize the data set is more efficient than DTW in terms of computation speed. Both Q-statistic and Hotelling's T^2 statistic can indicate the occurrence of an anomalous event. Contribution plots can help to diagnose the cause of an anomaly. When the cleaning is finished, the operators are advised to check the cleaning time or on−off ratio of the pump to evaluate if the cleaning has been performed consistently.

The application of the proposed analysis approach is not limited to the CIP operations of the brewery fermenter. The possible applications are to utilize historical knowledge to benefit the daily operations, the maintenance and optimization of the system, and the monitoring of new cycles, in order to gain a deeper understanding of the process and reduce cleaning costs. The model is flexible to involve more data to make it more informative. An ideal situation is to automatically detect and diagnose the anomalies in the system with the help of advanced monitoring and control systems.

List of Nomenclature in Chapter 4

The following nomenclature is only valid for this chapter. Some symbols are used in other chapters but with different meanings. Otherwise, the symbols are specifically explained in the text if there is no nomenclature in some chapter.

Roman Letters	
B	The threshold of Hotelling's T^2 statistic
c	The coefficient of the basic function
c_α	The normal deviation corresponding to the $(1-\alpha)$ percentile
C_Q	Contribution to the Q-statistic
C_{T^2}	Contribution to the Hotelling's T^2 statistic
e	Residual
F	The F-distribution value
h_0	A coefficient for computing the threshold of the Q-statistic
I	Number of batches
J	Number of time indices
$J[x]$	Roughness term
K	Number of variables
M	Number of principal components
p	Probability value
p_{km}	Loading for variable k in dimension m
P	Loading matrix
Q	Principal loading matrix
R	Number of batches in the reference set
S	Covariance matrix

t	Time, [s]
T	PCA scores
T^2	Hotelling's T^2 statistic
x	The predicted function in FDA
X	The matrix of variables
$\boldsymbol{y}$	The observed data set in FDA

Greek Letters

α	Significance level
σ_j	The jth eigenvalue
$\boldsymbol{\varepsilon}$	The noise term in FDA
Φ	Basic function
γ	Safety margin
η	The ratio of correct judgement
λ	Roughness penalty coefficient
δ^2	The threshold of the Q-statistic
θ_i	the ith coefficient for computing the threshold of the Q-statistic

CHAPTER 5

Simulations of Blending Phases in Pipe Systems Using CFD

In this chapter, CFD is used to simulate the blending phase problems in the rinsing of different pipe elements. The work was performed in collaboration with Alfa Laval Copenhagen A/S and Carlsberg Danmark A/S. Part of this chapter about the simulation of straight pipes has been published and reproduced based on the following article [134]:

CFD modelling of axial mixing in the intermediate and final rinses of cleaning-in-place procedures of straight pipes
Yang, J., Jensen, B. B. B., Nordkvist, M., Rasmussen, P., Gernaey, K. V., Krühne, U.
Journal of Food Engineering, 221: 95 - 105. (2018)
DOI: 10.1016/j.jfoodeng.2017.09.017

5.1 Introduction

5.1.1 Blending Phase Problems

Chapter 3 has presented that in the cleaning of pipes and tanks at the mapped brewery, nearly 60% of the cleaning costs attribute to the pipe cleaning operations. Most of the cleaning time and costs are spent on the alkaline/acid treatment, disinfection and three rinsing steps (two intermediate rinses and one final rinse). The recovery of the cleaning detergents can be up to 95% of the supply. In some industries, the final rinsing water can be partly recycled for the pre-rinse of the next CIP. The intermediate rinsing water is rarely recycled. Therefore, the overall recovery efficiency of rinsing water is very low, even less than 10%. Most of the rinsing water is directly disposed to drain.

Cleaning generates large amounts of waste water containing corrosive pollutants, nutrients, and potentially a considerable organic load. Furthermore, heat losses due to the discharge of hot water contribute significantly to the overall costs. Minimizing the consumption of resources (water, chemical and electrical energy, etc.) is of great importance

due to strict legislative and environmental regulations [135]. A number of studies have focused on the development of new cleaning agents, the effect of water quality and the optimization of chemical usage [1, 93, 136]. However, industrial applications of such technologies are still limited due to the complex alteration of existing equipment and the inestimable payback time. Operators prefer simple changes in operations without significant transformation of the existing processes. Therefore, reducing water consumption by optimizing the flow rate and rinsing time in rinsing steps and improving the recovery efficiency of cleaning agents becomes a practical solution for many food industries, as the operators can easily change and dynamically adapt these parameters at the control panel.

The objective of rinsing is to displace the residual cleaning agents (alkaline, acid and disinfectant) and reduce cross-contamination risks [6]. Such displacement of one liquid (chemical agent) with another liquid (water) occurs at the blending phase of the two liquids, where an axial mixing zone is created due to convection and diffusion phenomena [137]. The knowledge about axial mixing and displacement is of importance in order to ensure complete chemical removal at reduced water consumption.

5.1.2 CFD and Numerical Models

Section 2.6.2 has provided some applications of CFD in understanding and predicting fluid flow by predicting the wall shear stress (WSS) on surfaces. Nearly all of these CFD studies applied to CIP consider water as the medium to remove soils from the surfaces. There are, to our knowledge, no CFD investigations by other researchers about the intermediate or final rinses where water is mainly used to displace the cleaning agents. Compared with analytical mathematical models, the use of CFD models can get the information about mixing in both axial and radial directions. In some cases, CFD models can replace on-line measurements, as the installation of probes increases the capital costs and may introduce new areas that are difficult to clean. Moreover, CFD applies to complex geometries and is very helpful for the hygienic design of a pipe system.

In CFD simulations, the Navier-Stokes equation for incompressible flow reads:

$$\rho\Big(\frac{\partial u_i}{\partial t} + u_j\frac{\partial u_i}{\partial x_j}\Big) = -\frac{p}{\partial x_i} + \frac{\partial}{\partial x_j}\Big(\mu\frac{\partial u_i}{\partial x_j}\Big) \tag{5.1}$$

where ρ is the fluid density and μ is the dynamic viscosity. u, x and t are velocity, coordinate and time, respectively. The time-dependent convection-diffusion equation for a scalar transport with concentration C is as follows:

$$\frac{\partial C}{\partial t} + u_i\frac{\partial C}{\partial x_i} = \frac{\partial}{\partial x_i}\Big(D\frac{\partial C}{\partial x_i}\Big) \tag{5.2}$$

where D is the dispersion coefficient. In the case of turbulent flow, the dispersion consists principally of two contributions, caused by molecular diffusion and turbulent eddies. In liquid mixtures, the concentration diffusion flux J in the ith coordinate can be described as follows:

$$J_i = -\Big(D_0 + \frac{\nu_t}{Sc_t}\Big)\frac{\partial C}{\partial x_i} \tag{5.3}$$

where D_0 is the molecular diffusion coefficient; Sc_t is the turbulent Schmidt number calculated by the turbulent kinetic viscosity ν_t and the turbulent diffusivity D_t through $Sc_t = \nu_t / D_t$. Mathematically, dispersion can be treated in the same manner as molecular diffusion [138]. In a turbulent regime, the contribution of molecular diffusion is much less than that of turbulent eddies.

5.1.3 Objective of This Chapter

Pipe systems include various types of elements, e.g., straight pipes, bends, T-joints, expansions, contractions and valves (mixing valves, butterfly valves, ball valves, air-blow valves, etc.). The cleaning difficulties vary depending on the design of these elements and the operating conditions. Investigating single and simple geometries is an important step if a complex geometry with various pipe elements is going to be studied. Therefore, the purpose of this chapter is to simulate the blending phase problems, including axial mixing and the displacement phenomenon, in the intermediate and final rinses of CIP procedures for different pipe elements using CFD.

A detailed understanding of the blending phase problems in CIP supports the knowledge about the effects of flow patterns on the process. The minimal time required to completely displace the residual agents can be predicted. Furthermore, the total water consumption can be minimized by a proper combination of flow rate and rinsing time as well as by the implementation of efficient recovery plans.

This chapter describes two steps. The first step is to simulate the simplest straight pipe geometries. The results are validated using published empirical results based on an analytical mixing model for a turbulent flow regime, published in Yang et al. (2018) [134]. The second step is to simulate more complex geometries including bends, expansions, contractions and T-joints, in order to generate comparable results of various geometries. The latter step has been implemented with an education training purpose. All simulations were conducted by the attendees in the intensive CFD course (28831, Computational Fluid Dynamics in Chemical Engineering) at the Technical University of Denmark in January 2018. Such a pedagogical approach to ask students to solve relevant questions through individual exploration or collaboration in groups is called problem-based learning (PBL). However, this chapter mainly focuses on the scientific outputs from the students rather than the evaluation of students' performance.

5.2 Methods

5.2.1 Simulation of Straight Pipes

This section first introduces an analytical model to describe the axial mixing of two fluids in a pipe. Then a CFD model is developed. The results of the two approaches are compared in the Results and Discussion section.

5.2.1.1 Taylor's Analytical Model

The Taylor model (Equation 5.4) describes the axial dispersion of steady incompressible Newtonian fluids flowing in the laminar regime [139]. The model has then been extended to cover non-Newtonian fluids and turbulent flows [140, 141]:

$$C_m = \frac{C_0}{2}\Big(1 - erf\Big(\frac{x - u_0 t}{2\sqrt{Dt}}\Big)\Big) \tag{5.4}$$

where C_m is the average agent concentration at length x and time t, C_0 is the initial agent concentration, u_0 is the mean flow velocity, D is the (axial) dispersion coefficient, erf is the error function. In the process where water displaces the cleaning solution in a pipe, the boundary conditions are:

- when $t = 0$, $C = C_0$ at $x \geq 0$;
- when $t > 0$, $C = 0$ at $x = 0$.

The empirical correlation of the axial dispersion coefficient for turbulent flows based on experimental measurements, D, is according to Salmi et al. (2010) [138]:

$$\frac{D}{u_0 d} = \frac{3 \times 10^7}{Re^{2.1}} + \frac{1.35}{Re^{0.125}} \tag{5.5}$$

where d is the inner pipe diameter, $Re = du_0\rho/\mu$ is the Reynolds number. Under the studied flow conditions, which are described later, the second term on the right hand side in Equation 5.5 dominates the value of D. So the dependency of D on $u_0 d$ can also be approximated by a correlation of $(u_0 d)^{7/8}$.

5.2.1.2 Flow Domain and Mesh

A series of horizontal straight pipes of 28 m in length were simulated. The inner diameters of the pipes were 15.80, 26.64, 40.90, 77.90 and 154.10 mm, respectively, in accordance with the European pipe size standards of DN 15, 25, 40, 80 and 150 mm with the pipe wall thickness defined by the standard pipe schedule. The surface boundaries were modelled as smooth, which is required for food processing.

The geometries were simplified to be quarter sections (Figure 5.1), as the flow profiles were symmetric along the radial direction. Such a simplification reduced the computational time significantly compared with the simulation of a whole pipe geometry. This kind of treatment also retained high-quality cuboid mesh elements at the center of the pipes. Structured hexahedral meshes were made with the help of the meshing software ANSYS ICEM CFD 16.2. A mesh independence test was carried out and described in Section 5.2.1.4 in order to minimize the errors associated with the mesh size. The mesh layers in the near-wall regions were enhanced to capture the flow details close to the wall (see Figure 5.1). The resulting meshes had a fixed number of nodes in the axial direction (501 nodes) and varying numbers of layer nodes in the radial direction. The attained values of y^+, the dimensionless distance from the wall, were 27 - 67 and agreed with the requirement for the turbulence model applied. The resulted mesh density was 450 - 770 elements/mL.

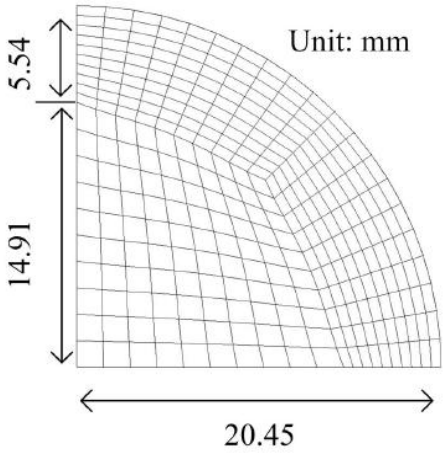

Figure 5.1: Structured mesh of the cross section of the pipe with inner diameter 40.90 mm (DN 40). The near-wall meshes were enhanced by fine layers. The geometry was simplified as a quarter section of the pipe in order to reduce computational time.

5.2.1.3 CFD Description

Water and the agent solution are miscible. The properties of the agent solution (i.e., density and viscosity) were assumed to be the same as water. Therefore, a single liquid phase simulation was performed in this study.

First, a steady-state simulation was performed using water to obtain the flow profiles. The inlet was set as plug flow with the mean flow velocities of 1.0, 1.5 and 2.0 m/s, corresponding to the standard working velocity range in industrial practices [142]. The Reynolds numbers were above 17,000. Thus, all the flows were fully turbulent. The outlet was defined with a relative pressure of 0 Pa. The effects of the turbulence intensity (Ti) and the turbulence length scale (Tl) at the inlet boundary are investigated in Section 5.2.1.4.

Subsequently, a transient simulation was performed using the steady-state results as initial conditions. The pipe was divided into two sections in order to eliminate the entrance effects under which the turbulent flow was not fully developed. It was crucial to introduce this additional length of the pipe, since a boundary condition at the inlet was chosen, where at any point of the inlet the same velocity was defined (plug flow). Therefore, a certain inlet length was needed, before the correct velocities in the radial direction were established. As shown in Figure 5.2, the first section was $-3 \leq x < 0$ m, where water was flushed from $t = 0$ and contacted with the agent solution at $x \geq 0$ m. The second section was $0 \leq x \leq 25$ m, where the cleaning agent components were dissolved in water with an initial concentration of 1 kg/m^3. The agent component was expressed as an additional volumetric variable, which could be transported through the flow via diffusion and convection, as indicated by Equations 5.2 and 5.3 (ANSYS CFX-Solver Theory Guide, ANSYS INC, 2013).

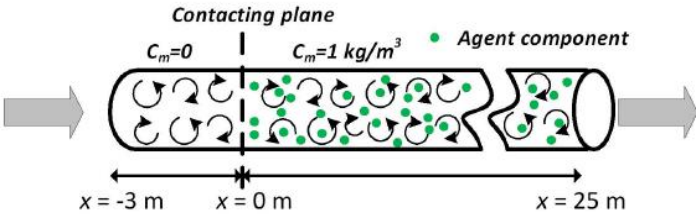

Figure 5.2: Description of the distribution of agent components within the pipe at $t = 0$. The agent components were dissolved in water with a concentration of 1 kg/m^3 at $x \geq 0$. Water was flushed from $x = -3$ m.

Buoyancy was not taken into account, because buoyancy did not contribute to axial mixing, especially when there was no density difference between the two fluids [141]. The axial dispersion coefficients were determined with the help of Equation 5.5. In the studied flow conditions, the D values range from $0.006 - 0.08$ m^2/s and the second term on the right hand side in Equation 5.5 contributes with more than 90% to the calculation of D.

The model was built with the help of ANSYS CFX version 16.2 using the standard $k - \varepsilon$ turbulence model with scalable wall functions. Steady-state simulations in the CFX software are pseudo transient simulations, where also a timescale has to be defined. This can be done automatically, which was our approach, or otherwise a time step has to be defined (physical timescale). The iterations were forced to run for minimum 500 steps, even though the convergence criteria (residual target MAX ≤ 0.00001) had been reached after around 100 steps. For the transient simulations, the Courant number is of fundamental importance to reflect the part of a mesh element that a solute traverses by advection in a time step. The definition is the product of the local velocity and the time step, divided by the mesh element characteristic length. In the simulations, the time step was 0.01 s, corresponding to the maximum Courant number of 0.42 - 0.92 for different pipe diameters and flow velocities.

5.2.1.4 Mesh Independence Test and Inlet Boundary Conditions

Table 5.1 shows 7 simulated cases that were carried out to minimize the errors associated with the mesh size and flow inlet conditions. The mesh study was performed by refining the mesh in a single radial direction (case 7) or in both radial and axial directions (case 6), and comparing the turbulence intensity near the wall and the average agent concentrations at different distances with the reference case 2. All studies were performed based on the inner pipe diameter of 40.90 mm (DN 40) and a flow velocity of 1.5 m/s.

In addition to the flow velocity, the turbulence at the inlet is defined by the turbulence intensity and the turbulence length scale [143]. In this study, the turbulence magnitude of the inlet was studied by comparing cases 1 - 5 in Table 5.1, with changing turbulence intensity (1 - 20%) and turbulence length scale (5 - 30% of the pipe diameter). This approach was similar to the study of the influence of the turbulence intensity at the inlet

Table 5.1: Parameters for the mesh study and for the influence of the turbulence intensity and the turbulence length scale. The inner pipe diameter is 40.90 mm (DN 40), the flow velocity is 1.5 m/s. Case 2 is the reference case that is selected for the following studies.

Case	Mesh indexes	No. of nodes in radial/axial directions	Ti_b, [%]	Tl_b, [% of diameter]	y^+	Max. Courant Number	Mean Courant number
1	Mesh 1	21/501	1	10	45	0.69	0.26
2	Mesh 1	21/501	5	10	45	0.69	0.26
3	Mesh 1	21/501	20	10	45	0.70	0.26
4	Mesh 1	21/501	5	5	45	0.69	0.26
5	Mesh 1	21/501	5	30	45	0.69	0.26
6	Mesh 2	29/751	5	10	32	1.04	0.39
7	Mesh 3	27/501	5	10	4	0.81	0.24

on wall shear stress fluctuations by Jensen (2007) [144].

5.2.2 Simulation of Complex Geometries

5.2.2.1 Geometries and Model Description

The complex geometries studied are listed in Table 5.2, including dimensions. The simulations of these geometries were designed as assignments in a CFD course with 24 attendees (either master or Ph.D students). Each geometry was chosen by at least one student and several geometries were modelled by two students.

Similar simulation approaches as straight pipes were performed but simplified for complex geometries. The investigated flow velocities were 1.5 or 3.0 m/s. The entrance length to eliminate any inlet effect was 10 times the inlet diameter instead of 3 m length for straight pipes. The outlet was placed 0.2 m downstream of the studied volume with a static pressure of 0 Pa. The axial dispersion coefficient through Equation 5.5 only applies to straight pipes where the Reynolds numbers are the same in different axial distances. However, for complex geometries, the values of the axial dispersion coefficient vary at different locations. Therefore, the dispersion coefficient in Equation 5.3 was obtained by defining the molecular diffusion coefficient $D_0 = 1 \cdot 10^{-9}$ m^2 s^{-1} and the turbulent Schmidt number $Sc_t = 0.7$ referring to the works done by others [141].

5.2.2.2 Calculation of Pressure Drop

The pressure drop is another critical characteristic parameter for describing the cleaning performance of long and complex pipe systems. A large pressure drop results in substantial power consumption to transfer the cleaning fluids. In the analytical approach, the following Bernoulli equation describes the impulse balance:

$$\frac{{u_1}^2}{2g} + \frac{P_1}{\rho g} + z_1 = \frac{{u_2}^2}{2g} + \frac{P_2}{\rho g} + z_2 + \triangle h_l \qquad 5.6$$

Table 5.2: Geometries of various pipe elements.

No.	Geometry	Description	No.	Geometry	Description
A	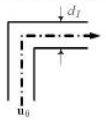	Squared corner	I	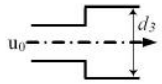	Sharp concentric expansion
B	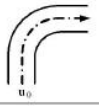	Round corner	J	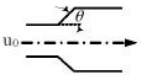	Gradual concentric expansion
C	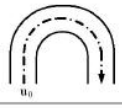	U-bend	K	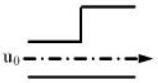	Sharp eccentric expansion
D	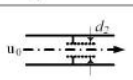	Orifice	L	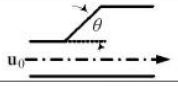	Gradual eccentric expansion
E	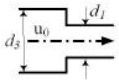	Sharp concentric contraction	M	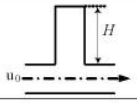	T-joint with direct entrance and exit
F	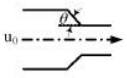	Gradual concentric contraction	N	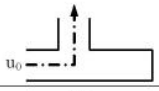	T-joint with exit perpendicular to entrance and dead zone
G	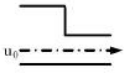	Sharp eccentric contraction	O	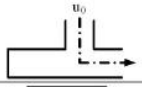	T-joint with entrance perpendicular to exit and dead zone
H	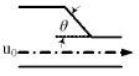	Gradual eccentric contraction	P	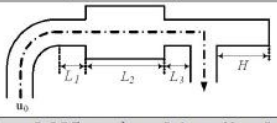	Complicated geometry combination (B, E, I, N)
Dimensions	$d_1 = 0.050\ m, d_2 = 0.025\ m, d_3 = 0.1\ m, H = 0.1\ m, L_1 = 0.1\ m,$ $L_2 = 0.25\ m, L_3 = 0.1\ m, u_0 = 1.5\ m/s, \theta = 45°$				

where P is the pressure, z is the height and g is the gravitational acceleration term. The subscripts 1 and 2 distinguish the inlet and outlet flows. $z_1 = z_2$ when the inlet and outlet are placed at the same height. The term $\triangle h_l$ denotes the head loss, including major loss h_{major} and minor loss h_{minor}. Major loss is caused by the friction between the fluid and the surface. For straight pipes, the major loss is expressed by the Darcy-Weisbach equation:

$$h_{major} = f\frac{L}{d}\frac{u^2}{2g} \tag{5.7}$$

where L is the pipe length and d is the inner diameter. The Darcy friction factor f depends on the Reynolds number and the relative roughness of surfaces. For smooth

pipes, the value of f can be approximated by the Blasius formula:

$$f = (100Re)^{-1/4} \tag{5.8}$$

The minor loss is caused by various pipe fitting elements that produce the changes in momentum. The minor loss can be calculated by:

$$h_{minor} = K\frac{u^2}{2g} \tag{5.9}$$

The resistance coefficient, K, varies with the type and size of pipe elements as well as the Reynolds number. For a system equipped with several straight pipes and pipe elements, it is necessary to put the pressure drop of each section together. Consequently, the analytical calculation of the pressure drop ($\triangle P_{Analytical}$) includes the sum of the three parts caused by velocity change, major loss and minor loss, as:

$$\triangle P_{Analytical} = P_1 - P_2 = \frac{\rho(\triangle u)^2}{2} + f\frac{\rho L}{2d}u^2 + K\frac{\rho}{2}u^2 \tag{5.10}$$

It is common to use an equivalent length of a straight pipe to quantify the minor loss of a complex pipe element. This equivalent length is helpful to design new CIP systems and to estimate the pressure drop and cleaning effectiveness when fluid has travelled through the complicated pipe work consisting of different elements. The equivalent length of straight pipe (L_{eq}) can be computed by assuming Equation 5.7 equals the minor loss from simulations via:

$$h_{minor,\,sim} = f\frac{L_{eq}}{d}\cdot\frac{u^2}{2g} \quad \Longrightarrow \quad \frac{L_{eq}}{d} = \frac{2g}{fu^2}\cdot h_{minor,\,sim} \tag{5.11}$$

5.3 Results and Discussion

5.3.1 Studies of Straight Pipes

5.3.1.1 Studies of Mesh Independence Test and Inlet Boundary Conditions

The predicted near-wall turbulence intensity initially drops, then rises, and reaches a constant value (ca. 0.056) apart from the pipe section covering the first 2 m after the entrance (as shown in Figure 5.3A). Comparing cases 6 and 7 with case 2, finer meshes in radial and axial directions lead to a larger turbulence intensity in the turbulent section, but the change is less than 1% of deviation in the fully developed flow section.

Equation 5.4 indicates that $C_m = C_0/2$ at the mid-plane, which is defined as the plane where the front of the water phase arrives when an ideal plug flow is assumed ($x = u_0 \cdot t$). Figure 5.3B illustrates the average agent concentrations at four mid-planes (1.5, 9, 15 and 21 m). It is found that all of the predicted values of C_m are lower than the theoretical value, which is mostly caused by the discretization error when a fluid domain is subdivided into a mesh. However, all of the deviations are less than 1% of the theoretical value calculated by Equation 5.4. In particular, cases 1 - 5 result in the same average agent

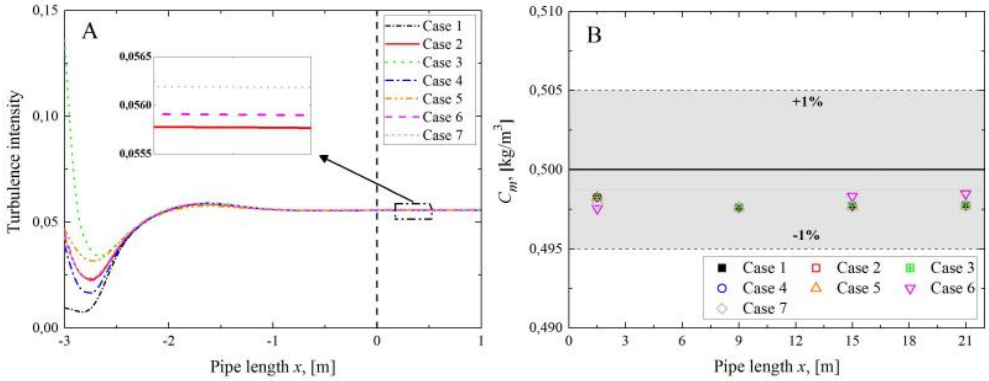

Figure 5.3: (A) Near-wall turbulence intensity (1 mm from the wall) and (B) average agent concentration at various mid-planes for different model cases. The inner pipe diameter is 40.90 mm (DN 40), the flow velocity is 1.5 m/s. The parameters for different cases are shown in Table 5.1.

concentration values (with precision 0.00001 kg/m^3) at the four mid-planes. Therefore, it can be concluded from Figure 5.3 that the differences caused by mesh sizes as well as the turbulence intensity and turbulence length scale are only limited to the initial 2 m pipe section, but are no longer observable from $x = 0$.

Hence, case 2 provides a sufficient mesh for this project. Extremely fine meshes like cases 6 and 7 may be counter-productive, because the mixing in the radial direction is not significant (see Figure 5.7) and flat mesh elements lead to low mesh quality in slender pipes. The results imply that the use of a 3 m pipe as entrance (Figure 5.2), is a reasonable measure to overcome the effects of entrance fluctuations. The meshes of other pipe diameters were made by fixing axial nodes similar to case 2 and adjusting radial nodes to result in identical layer size and y^+. The value of y^+ describes how coarse or fine of a mesh is at the boundary, a large value of which normally indicates a relatively coarse mesh and vice versa. The inlet boundary conditions are selected to $Ti = 5\%$ and $Tl = 10\%$ of the pipe diameter. When a new mesh and a new flow velocity were employed, the same validation approaches as demonstrated in Figure 5.3 were carried out in order to ensure that the flow was in a turbulent condition at $x = 0$ and $C_m \approx 0.5C_0$ at the mid-planes.

5.3.1.2 Comparison of the Taylor Model and CFD Simulations

Figure 5.4 shows the agent concentrations at the mean flow velocity of 1.5 m/s at $x = 15$ m and for a fixed rinsing time (10 s) at an arbitrary distance. The presented values are obtained from the Taylor model [139] and the CFD simulations. Figure 5.4A can be regarded as the displacement dynamics at the fixed plane during the rinsing period. Figure 5.4B can be considered as the agent distributions within the pipe after 10 s of rinsing.

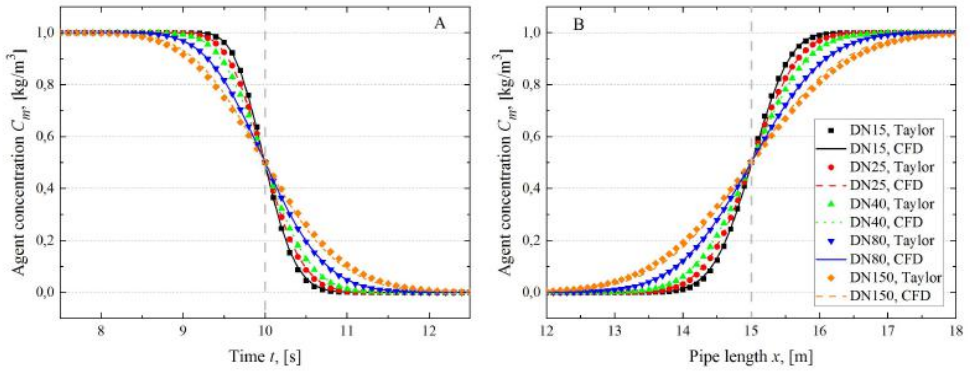

Figure 5.4: Comparison of the Taylor model and the CFD simulations at 1.5 m/s of flow velocity for (A) a fixed distance of 15 m with varied rinsing time, and (B) a fixed rinsing time of 10 s with varied distance.

The agent components transfer slower near the wall than in the center due to blunt velocity profiles (Figure 5.5). The longer tails in larger pipes (Figure 5.4) indicate that the agent components are axially mixed faster in the pipe center but slower near the wall than in smaller pipes. The mixing of agent molecules is a result of convection and diffusion [137]. According to Equation 5.5, the value of the axial dispersion coefficient increases with increasing pipe diameter when the flow is turbulent [138]. In Figure 5.5, the value of turbulent kinetic energy k is minimal at the center and increases towards the radial direction, and decreases near the wall, which is the same as Zhao et al. (2010) observed when simulating the mixing of two miscible liquids with different densities [141]. Considering the lower center velocity but larger axial diffusion for larger pipes, it can be concluded that the mixing of the agent components is governed by axial diffusion in the pipe center section, and by convection near the wall.

CFD successfully predicts the values which are calculated with help of the Taylor model [139]. The CFD model predicts accurately the analytical model in terms of the transient agent concentrations at different locations in the pipe. In addition to the Taylor model, the prediction of dispersion within a pipe by using CFD has also been verified to be successful by predicting Stegowski et al. (2013)'s experimental data [145] and the residence time distribution (RTD) theory [146]. The validations of the latter two approaches are provided in the supplementary material in Yang et al. (2018) [134] (DOI: 10.1016/j.jfoodeng.2017.09.017), which are not shown in this thesis. Therefore, the CFD model is used for further investigations of the displacement process and the mixing zone analysis.

5.3.1.3 Displacement Time

Three displacement times are defined in this work for different purposes:

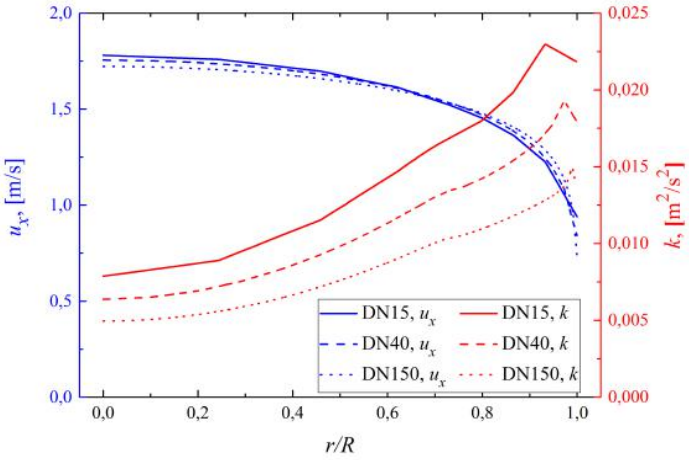

Figure 5.5: Axial velocity and turbulent kinetic energy at the distance of 15 m and for a mean flow velocity of 1.5 m/s for different pipe diameters. r/R is the dimensionless distance from the center of the pipe to the wall. u_x and k quantify the intensity of convection in axial direction when the radial and tangential velocities are not significant.

- $t_{1,plane}$ is the time when 1% of the agent is displaced by water at a fixed plane ($C_m = 0.99C_0$). It is assumed to be the detected start point of rinsing when measurements are employed to determine the agent concentration. The sensor is located at the flow downstream from where the plane lies;
- $t_{99,plane}$ is the minimum rinsing time to remove 99% of the agent components at the fixed plane ($C_m = 0.01C_0$). In practice, it is the apparent time where rinsing ends once the downstream measurement outputs reach the pre-defined rinsing criterion;
- $t_{99,volume}$ is the minimum rinsing time to remove 99% of the cleaning agent from the volume, which is the true time required to displace the agent components and to reduce contamination risks.

The selection of 99% as complete rinsing refers to Graßhoff (1983)'s work when studying the displacement of one liquid with another liquid during CIP [147]. Depending on the initial agent concentration and the requirement of rinsing in different industries, the minimum rinsing time may be defined to remove more or less than 99% of cleaning agent in order to achieve a safe level.

It is observed that the product of the displacement time and the mean flow velocity, $t_{1\ or\ 99} \cdot u_0$, is constant for different flow velocities, which can be correlated by a power function presented in Equation 5.12 with the inner pipe diameter as variable. Figure 5.6 illustrates $t_{1\ or\ 99} \cdot u_0$ against the inner pipe diameter at different length of pipe sections. The values of the correlation parameters for three pipe lengths (2, 15 and 24 m) are presented in Table 5.3. The small values of β indicate that the rinsing times are mainly

influenced by the flow velocity and pipe length, instead of the pipe diameter. In a CIP rinsing process, such correlations help to make predictions about when the recovery of agent should be stopped and when the recovery of rinsing water should be launched.

$$t_{1\ or\ 99} \cdot u_0 = \alpha \cdot d^{\beta} \tag{5.12}$$

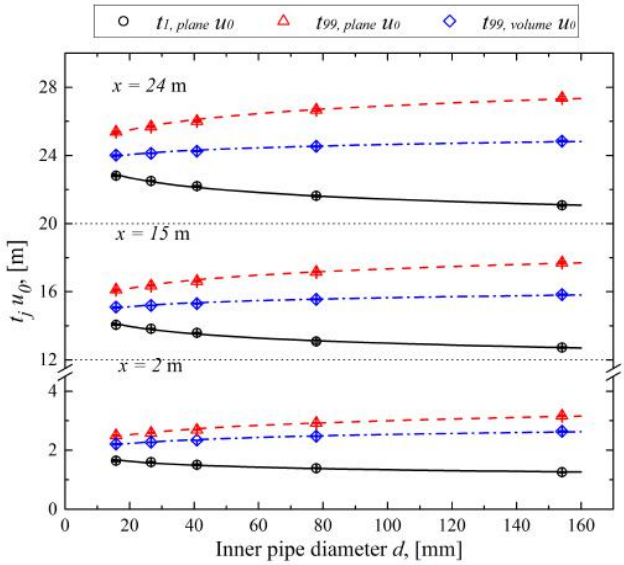

Figure 5.6: The product of displacement time and flow velocity for different pipe lengths. The marker values and error bars (too small to be seen) are from the average and standard deviation of $t_{1\ or\ 99} \cdot u_0$ at three flow velocities. The curves represent the values that are calculated by the power function in Equation 5.12.

An increase in pipe diameter not only speeds up the start of displacement, but also prolongs the termination of displacement. It is caused by the longer tailing distribution of agent components in the larger pipes as presented in Figure 5.4. The obtained minimum rinsing time values based on the fixed planes are greater than the values based on the volumes. It can be understood in such a way that when 99% of the cleaning agent is removed from the volume, the volume-weighted average agent concentration is 1% of the initial concentration. Meanwhile, agent concentrations near the inlet are lower than near the outlet. So the average agent concentration at the outlet plane is still above 1% at $t_{99,volume}$. In practice, the rinsing time can be determined by measuring the agent concentration downstream and the rinsing step stops exactly when the agent concentration reaches the pre-defined criterion. However, the apparent rinsing time in such a situation is still longer than the true requirement in order to reduce contamination risks.

Table 5.3: Correlation parameters of the product of displacement time and flow velocity for three pipe lengths by the power function as Equation 5.12. The unit of inner pipe diameter should be meter.

x, [m]	t, [s]	α, [m$^{1-\beta}$]	β	R^2
2	$t_{1,plane}$	1.01	-0.121	0.998
	$t_{99,plane}$	3.83	0.107	0.963
	$t_{99,volume}$	3.03	0.0788	0.966
15	$t_{1,plane}$	11.7	-0.0456	0.989
	$t_{99,plane}$	19.1	0.0422	0.978
	$t_{99,volume}$	16.4	0.0212	0.970
24	$t_{1,plane}$	19.8	-0.0354	0.996
	$t_{99,plane}$	29.1	0.0337	0.980
	$t_{99,volume}$	25.5	0.0152	0.971

5.3.1.4 Minimum Water Consumption for Rinsing

The minimum water consumption for an effective rinsing is the minimum requirement of water to reduce the amount of agent to such a low degree that the residues have no or only a minor effect on the following steps. In this study, the removal of 99% of agent components is assumed as a complete rinse. In order to compare the minimum consumption for different pipe diameters, a volume factor, F, is defined as the ratio between the minimum water consumption, V_{min}, and the pipe volume, V, as follows:

$$F = \frac{V_{min}}{V} = \frac{\pi d^2/4 \cdot u_0 \cdot t_{min}}{\pi d^2/4 \cdot x} = \frac{u_0 \cdot t_{99}}{x} \tag{5.13}$$

Equation 5.12 indicates that the value of $u_0 \cdot t_{99}$ only depends on the inner pipe diameter for a given pipe length. Therefore, according to Equation 5.13, the values of volume factors are independent of flow velocities as well. The increase in flow velocity reduces the rinsing time significantly, but it does not affect the minimum water consumption. However, if water also works as a medium to remove soils from surfaces, large flow velocities improve rinsing efficiency by destroying the structure between soils and surfaces by mechanical forces, i.e., shear stress [6]. The pipes of larger size lead to larger volume factors, as t_{99} increases with increasing inner pipe diameters. Both the numerator and denominator in Equation 5.13 increase for longer pipes, but the value of $u_0 \cdot t_{99}$ grows slower than x. Thus, the volume factors become smaller for longer pipes.

With decreasing pipe diameter and increasing pipe length, the volume factor values tend to the lower limit of 1, indicating that the minimum water consumption approaches the pipe volume. It can also be concluded that the calculated volume factors based on the downstream measurement are larger than the values based on the volume, which is the same trend as the illustrated rinsing time in Figure 5.6. Therefore, if the rinsing time is controlled by downstream measurements, the consumption of water is still 6 - 20% larger than the real demand to remove a certain amount of agent from the volume.

5.3.1.5 Minimum Volume of Waste Water

Recovering cleaning agent and rinsing water is an efficient solution to reduce the rinsing costs. For a given pipe length, the recovery plan can be made in the following manner:

1. The recovery of cleaning agent stops at $t_{1,plane}$. So the agent solution is still at a high concentration without dilution and can be reused with high activity;
2. The recovery of rinsing water starts at $t_{99,plane}$, as the rinsing water is less "polluted" by the agent components. The recovered water can be used for the pre-rinse of the next cleaning or for other applications where the water quality fits;
3. The effluent between $t_{1,plane}$ and $t_{99,plane}$ is a mixture of the agent solution and the rinsing water, which can be disposed to drain or a waste water treatment plant. The amount of effluent can be regarded as the minimum amount of waste water when the recovery is planned according to this manner.

The minimum volume of waste water is:

$$V_{Waste\ water} = \frac{\pi d^2}{4} \cdot u_0 \cdot t_{99,plane} - \frac{\pi d^2}{4} \cdot u_0 \cdot t_{1,plane} = \frac{\pi d^2}{4} \cdot \left(u_0 \cdot t_{99,plane} - u_0 \cdot t_{1,plane} \right) \quad 5.14$$

As indicated by Equation 5.12, the values of $u_0 \cdot t_{99,plane}$ and $u_0 \cdot t_{1,plane}$ only depend on the inner pipe diameter for a given pipe length. Therefore, the minimum volume of waste water increases as well when the pipe diameter increases.

5.3.1.6 Mixing Zone Length

Figure 5.7 shows the process when the agent is displaced by water in a 1 m pipe section within 2 s. The displacement occurs mainly in the axial direction. Mixing in radial direction is not significant when the flow is in the turbulent regime [142]. In this study, mixing length is defined as the distance from the leading edge where the agent concentration is 99% to the trailing edge where the agent concentration is 1%.

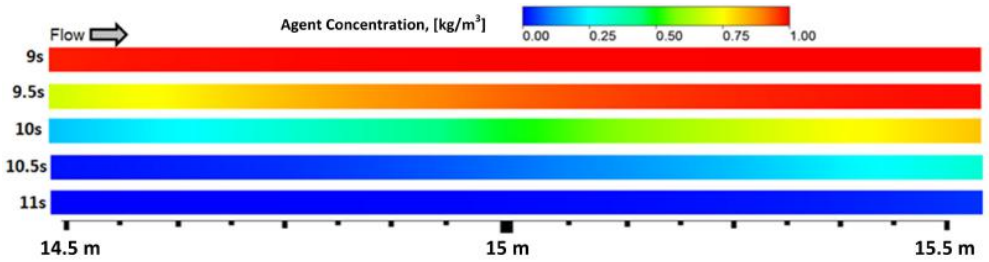

Figure 5.7: An example of agent distribution in a 1 m pipe section at different rinsing times. The inner pipe diameter is 26.64 mm (DN 25 mm), and the flow velocity is 1.5 m/s.

The study of mixing length is important for intermediate rinses, especially for long pipes. The usual practice is to completely displace the cleaning agent A by water before introducing another cleaning agent B. An alternative method is shown in Figure 5.8. Two

cleaning agents can be synchronously introduced with a proper interval between the two agents. A so-called intermediate rinse length is the sum of the mixing zone length of the agent A, the mixing zone length of the agent B and an intermediate length between two mixing zones. The intermediate length between two mixing zones can be minimized in order to reduce water consumption. Thus, the minimum requirement of intermediate rinsing water is the volume of two mixing zones which can be calculated from the mixing length.

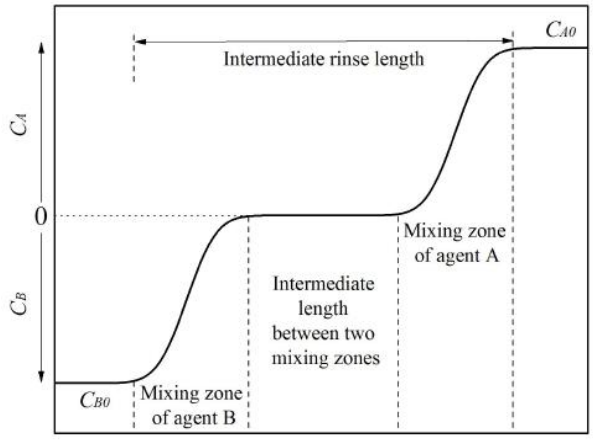

Figure 5.8: Intermediate rinse length between two cleaning agents.

Figure 5.9 demonstrates that the mixing length increases with rinsing time. The leading edge (above 0) and trailing edge (below 0) are symmetrically located on two sides of the mid-plane. Zhao et al. (2010) also observed that the increase in flow velocities contributes to greater mixing lengths when simulating the displacement of a heavier liquid with another lighter liquid [141].

According to the penetration theory of Higbie (1935), the mixing length of different species is dependent upon both the turbulent diffusivity and the contact time [141, 148, 149]:

$$l \propto 2\sqrt{D_t \cdot t} \tag{5.15}$$

where l is the mixing length, D_t is the turbulent diffusivity of the species. The right hand side term, $2\sqrt{D_t \cdot t}$, is called the characteristic length in mixing [150]. By replacing the turbulent diffusivity with the dispersion coefficient, Equation 5.15 also applies to the axial mixing of the CFD results as shown in Figure 5.10. The idea behind the correlation is that the penetration theory quantifies the component transfer using a similar error function as in Equation 5.4 [151]. On the basis of the correlation, it enables to predict the mixing lengths for longer rinsing times and various flow rates and pipe diameters.

For a given pipe length, the contacting time can be assumed as x/u_0, which is the mean residence time of rinsing water. Then the minimum requirement of intermediate rinsing

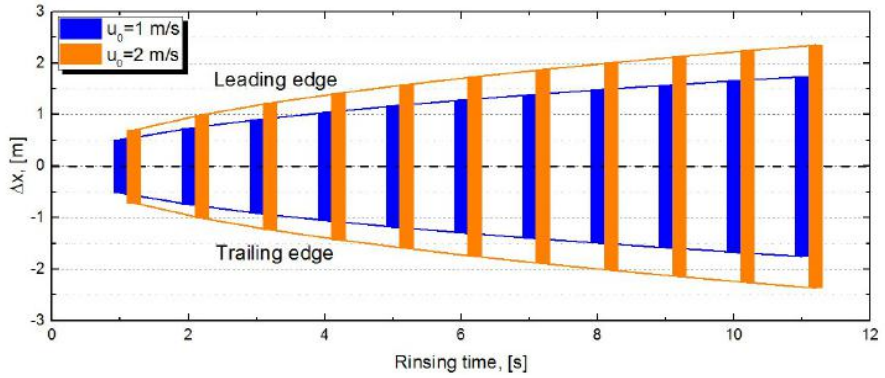

Figure 5.9: Dynamic mixing length of the 77.90 mm diameter (DN 80) pipe at 1 and 2 m/s. $\triangle x$ is the relative position of the leading edge (+) and the trailing edge (−) to the mid-plane ($x = u_0 \cdot t$).

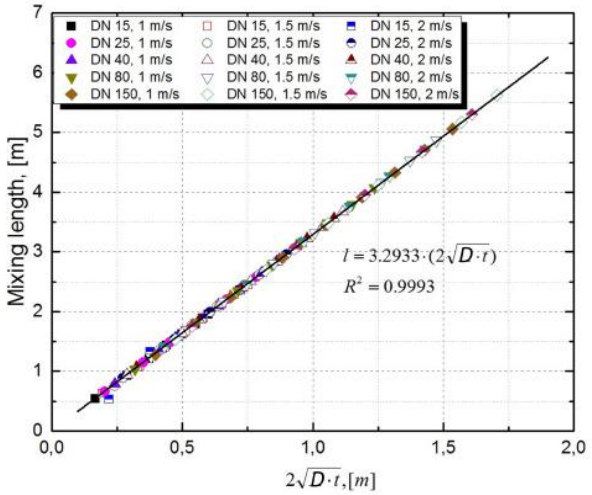

Figure 5.10: Correlation of the mixing length from simulations with the characteristic length, $2\sqrt{D \cdot t}$.

water can be calculated from the mixing length, as:

$$V_{Inter.\,rinse} = 2 \cdot \frac{\pi d^2}{4} \cdot l = 2 \cdot \frac{\pi d^2}{4} \cdot 3.29 \cdot \left(2\sqrt{D \cdot x/u_0}\right) = 3.29\pi d^2 \sqrt{D \cdot x/u_0} \qquad 5.16$$

Under the flow conditions in this study, the second right hand side term in Equation 5.5 dominates the value of D. Therefore, Equation 5.16 can be further simplified and

approximated as:

$$V_{Inter.\,rinse} \approx 3.29\pi d^2 \sqrt{1.35(u_0 d)^{0.875} \cdot (\mu/\rho)^{0.125} \cdot x/u_0} = 3.82\pi \sqrt{u_0^{0.375} d^{4.875} (\mu/\rho)^{0.125} x} \quad 5.17$$

5.3.2 Studies of Complex Geometries

The studies of complex geometries include two scenarios: (i) When water is the cleaning medium to detach soil materials from the surfaces, dead zones indicate the locations that are the most difficult to clean. These dead zones result in higher pressure drops than straight pipes. The identification of dead zones and the computation of pressure drops are achieved by the steady state simulations. (ii) When water is used to displace cleaning agents from the pipe fittings, which is the same as the studies of straight pipes, the minimum rinsing time and minimum water consumption can be obtained from the transient simulation results.

5.3.2.1 Dead Zone Identification

In cleaning operations, the removal of soil components from surfaces is insufficient when the local wall shear stress is below a critical value of 3 Pa [45]. Figure 5.11 shows an example of the predicted WSS of the complex geometry P (see Table 5.2) in comparison with the corresponding individual elements. The predicted WSS values for other geometries are provided in Appendix A. A number of conclusions can be drawn from the findings:

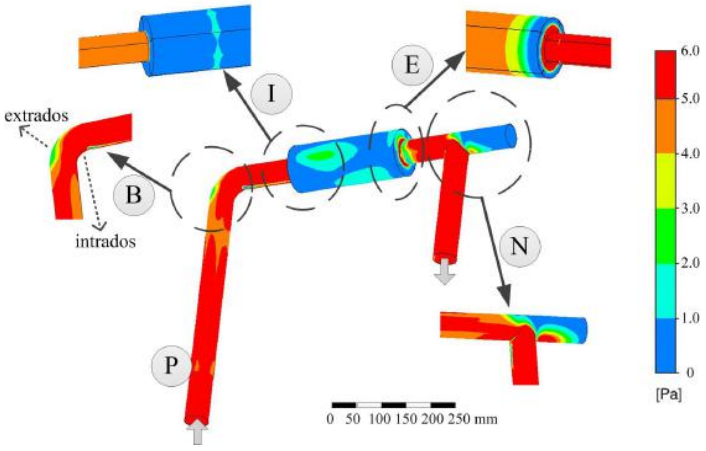

Figure 5.11: Predicted wall shear stress on the surfaces of five geometries.

- The extrados surface and the intrados surface of bends (see Figure 5.11) as well as both sides of orifices are difficult to clean. Furthermore, the dead zones also include the large pipe corners of contractions, the large pipe and connection of expansions,

and the dead legs of T-joints. All of these stagnant zones are formed due to either flow recirculation or the abandonment of main streams.

- With the flow velocity increasing from 1.5 to 3 m/s, the size of the dead zones is reduced but they cannot be avoided completely. This observation is in line with the simulations by Jensen et al. (2007) [102].
- Round corners and a gradual change in pipe diameter reduces the size of dead zones of bends and contractions, but have little impact on dead zones formed in pipe expansions.
- The T-joint for case N results in a smaller dead zone area than the other T-joint types.

The WSS of concentric expansions and contractions shown in Figure 5.12 are in agreement with the trend measured by Lelièvre et al. (2002) [56] and predicted by Jensen et al. (2005) [152], who both investigated the changeover of pipe diameters between 1 and 2 inch. For the sharp pipe contraction (Figure 5.12A), all studies observe a peak and dip of WSS at the interface. The observed pattern after the peak is more smooth for the gradual pipe contraction (Figure 5.12B). On the contrary, the decrease of WSS at the expansion interfaces is more straightforward. The slight raise of WSS downstream of the expansions shown in Figure 5.12C&D has also been previously reported by Jensen et al. (2005) [152] and Schöler et al. (2012) [153], indicating the location of the stream recirculation center. The gradual expansion in Figure 5.12D expresses a sharp reduction of WSS at the interface, which differs from the creeping decrease as measured by Lelièvre et al. (2002) [56] due to the large flow velocity applied in our study.

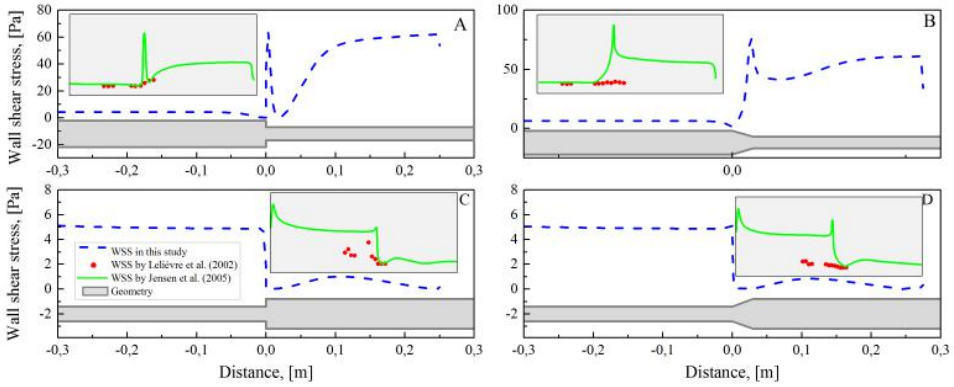

Figure 5.12: Predicted wall shear stress of four geometries: (A) sharp contraction, (B) gradual contraction, (C) sharp expansion and (D) gradual expansion. All flow directions are from left to right. The inset plots display the measurements by Lelièvre et al. (2002) [56] and the CFD simulations by Jensen et al. (2005) [152]. The latter two studies employed pipe diameter transitions of 0.023 - 0.046 m and an average flow velocity of 0.25 - 1.47 m/s.

5.3.2.2 Pressure Drop

The simulated pressure drops from inlet to outlet generated in the steady-state simulations were extracted in comparison with the analytical pressure drops by taking K values from Table 5.4 applied in Equation 5.9. According to Figure 5.13, the simulated pressure drops follow the same trend as the values based on the analytical approaches, with most of the figures in less than 50% or 30% of deviation. The most uncertainty of the analytical results comes from the determination of K, the value of which was obtained empirically in literature for specific types of pipe elements and flow conditions. Furthermore, the K values are derived based on stable flow profiles, where for instance the turbulence has been fully developed downstream of contractions or expansions. However, in some simulation cases (i.e., geometries I, J, K and L), the reserved length prior to the outlet is not long enough to establish stability. Thus, the resulted values of $\triangle P_{Sim}$ differ from the expected analytical solutions. However, the absolute pressure drops for these geometries are less than 103 Pa, meaning the high variation of these points displayed in the logarithmic plot in Figure 5.13 actually contains only minor absolute deviations.

Table 5.4: The resistance coefficient values, K, for different pipe elements

No.	K	Sources	No.	K	Sources
A	1.2	3-K model by Darby et al. (2017) [154]	I	0.6	Sudden expansion model by Rennels et al. (2012) [155]
B	0.4		J	0.6	Gradual expansion model by Darby et al. (2017) [154]
C	0.5		K	1.0	2-K model for exit by Darby et al. (2017) [154]
D	32.7	2-K model by Darby et al. (2017) [154]	L	0.7	15% higher than concentric expansion, according to Rennels et al. (2012) [155]
E	7.3	Sudden contraction model by Neutrium (2012) [156]	M	0.2	Flanged tee for line flow by Young et al. (2010) [157]
F	6.1	Gradual contraction model by Darby et al. (2017) [154]	N	1.0	Flanged tee for branch flow by Young et al. (2010) [157]
G	1.0	2-K model for entrance by Darby et al. (2017) [154]	O	1.0	
H	4.9	Contraction model by Darby et al. (2017) [154] with equivalent angle calculated by Rennels et al. (2012) [155]	P	9.3	Sum of K values for geometries B, E, I, N

The equivalent lengths of different pipe elements are displayed in Figure 5.14. It needs to be mentioned that the values of equivalent lengths depend significantly on the element

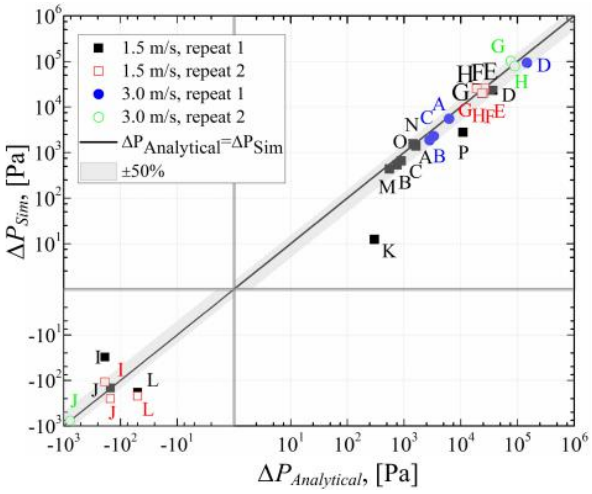

Figure 5.13: Predicted pressure drop by CFD against analytical solutions. "Repeat 1" and "Repeat 2" represent that the results are obtained by two different students.

geometries, the types of end connections, the flow conditions, etc. Therefore, the absolute values of L_{eq}/d in Figure 5.14 may differ from the figures in some literature but are in a reasonable range. For example, the L_{eq}/d values of geometries A, B, M and N/O are 57, 11, 5 and 58/56 in simulations, corresponding to 57, 30, 20 and 60 in the sources from the Crane Company (1978) [158]. According to the results in Figure 5.14, the existence of orifice (D) and sharp contractions (E and G) reduces pressure extremely. The use of gradual contractions (F and H) can also cause significant pressure drop to the system.

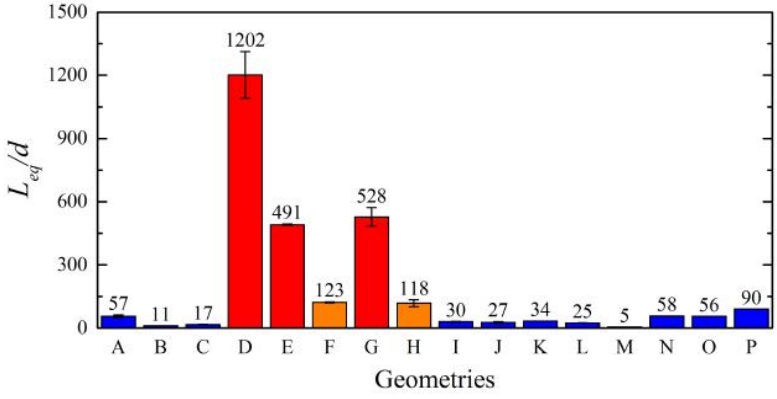

Figure 5.14: Equivalent length of different pipe elements simulated by CFD. The letters in the horizontal axis indicate the geometry numbers in Table 5.2.

The equivalent length of the complex geometry P cannot be simply calculated as the sum

of the equivalent lengths of the simple geometries B, E, I and N. The reason is that the pipe elements in the proposed geometry P are located so close to each other that the flow pattern differs from the cases where single elements are simulated.

The CFD approach is an effective method to investigate the pressure drop occurring in pipe systems. The analytical equation can only quantify the total pressure drop, while CFD can result in additional information such as the flow pattern and pressure gradient in cross sections. For future applications, the roughness of the pipe surface can be added to the model, with the friction factor obtained from the Moody chart. This roughness term can also be implemented in CFD codes.

5.3.2.3 Displacement Time

Figure 5.15 displays the predicted values of $t_{99,volume}$ and $t_{99,point}$ for different pipe elements. $t_{99,point}$ is defined as the time to displace 99% cleaning agent from a point located in the dead volume determined previously. According to the result, bends and contractions are easy to be rinsed, except the sharp eccentric contraction geometry (G). Pipe expansions, orifices and T-joint N are comparably hard to be flushed. T-joints M and O as well as the gradual eccentric expansion (L) are the most difficult to flush. For most geometries, the point-based displacement times are larger than the volume-based values, meaning that determining the displacement time by a local sensor is a safe way to validate the removal of a soluble agent component but causes slightly excessive waste. For the geometries B, G and H, a measurement-based displacement time is inadequate to reduce the overall agent concentration to a safe level. Moreover, a higher flow velocity shortens the displacement time significantly. However, the accuracy of the simulations performed by the students needs to be validated using experimental data, even though most replicated simulations performed by different students are quite similar. The location of the selected monitoring point is random, which proves to greatly affect the determination of $t_{99,point}$.

Graßhoff (1980) measured the displacement time to expel 99% of agent components from three types of T-joints of the same diameter as in this chapter, using a conductometric electrode installed at the end of the dead legs [159]. Table 5.5 shows that the predicted displacement times are in agreement with the range of experimental results except for geometry N. This deviation is mostly caused by the limitation of the standard $k-\varepsilon$ model to deal with strong recirculation flows within geometry N.

Figure 5.16 expresses the displacement process within the geometry P. The agent components at the round corner are displaced very fast. The pipe contraction can also be flushed after about 5 s. However, the agent components in the T-joint and particularly in the sharp expansion are difficult to be flushed. This trend agrees well with the simulations of the individual pipe elements as shown in Figure 5.15. However, the values of the displacement times differ due to the change of the flow patterns in the complex geometry P. The result indicates that the determination of rinsing end based on a local sensor at the T-joint (as shown in the top left graph of Figure 5.16) can give a false “clean” signal after about 10 s by ignoring the unremoved components in the upstream pipe transition.

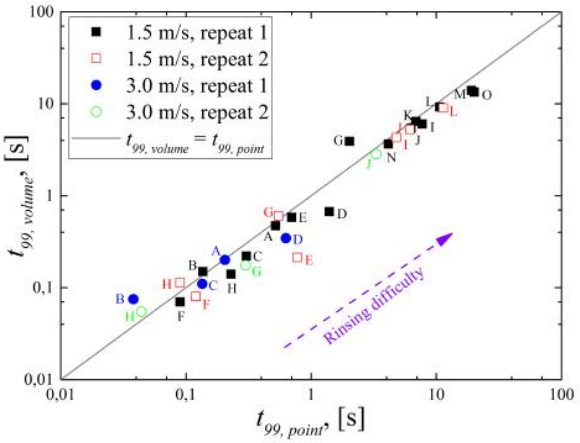

Figure 5.15: Predicted displacement times to remove 99% of agent components from the dead zone volume or from the monitoring point in the stagnant zone. "Repeat 1" and "Repeat 2" represent that the results were obtained from different students.

Table 5.5: Comparison of the predicted displacement times (1.5 m/s) in T-joints with the experimental results from Graßhoff (1980) [159]

Geometries	Experimental t_{99},[a] [s]		Simulated t_{99} at 1.5 m/s, [s]	
	1 m/s	2 m/s	$t_{99,point}$	$t_{99,volume}$
M	13.5	26.8	19.1	13.9
N	1.6	3.0	4.2	3.7
O	16.6	32.4	20.1	13.4

[a] The experiments by Graßhoff (1980) were performed with a pipe diameter of 0.050 m, a flow velocity of 1 or 2 m/s, and a water temperature of 50 °C [159].

5.3.2.4 Minimum Water Consumption for Rinsing

As shown in Figure 5.17A, increasing the flow velocity from 1.5 to 3.0 m/s can reduce the displacement time significantly without affecting the minimum water consumption. This observation is in line with previous studies when simulating straight pipes.

In this study, the dead zone volume is defined as 0.05 m upstream and 0.05 m downstream of the investigated geometry section. As indicated in Figure 5.17B, the minimum consumption of water is generally larger than the dead zone volume, except for one point of geometry B at 3.0 m/s. This could be explained as a numerical error because the displacement time to rinse geometry B is so short at 3.0 m/s (<0.05 s). As a result, the number is highly sensitive to the selected time step in the simulation. The values of volume factor F range from 1 to hundreds for geometries M and O, meaning that the water consumption to rinse a dead zone is multiple times its volume. Therefore, there is no doubt that dead zones should be avoided in hygienic design because a huge amount

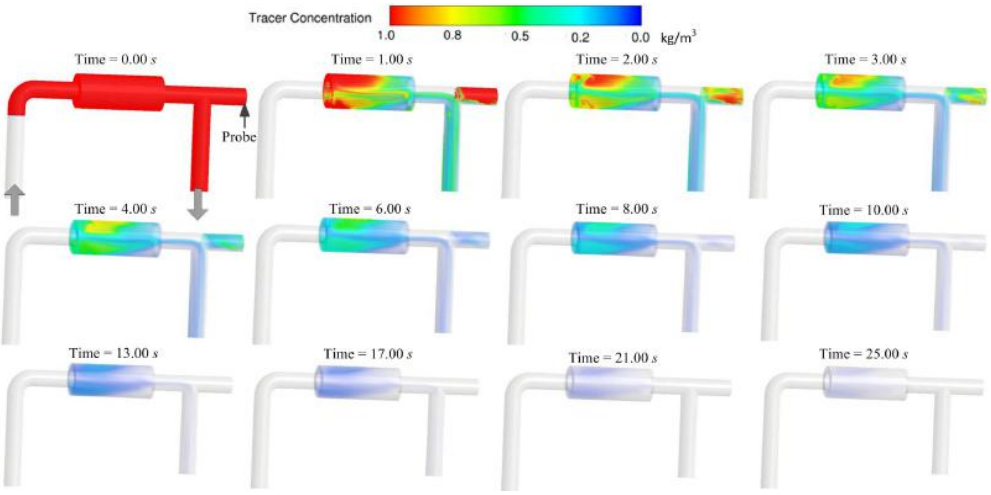

Figure 5.16: Displacement profiles of geometry P.

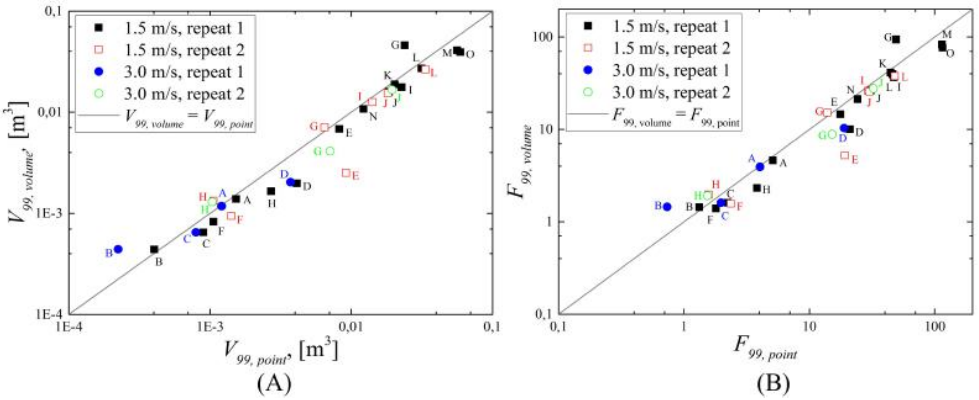

Figure 5.17: (A) Predicted water consumption to remove 99% of agent components from the dead zone volume or from the monitoring point in the stagnant zone and (B) predicted volume factors calculated by the volume-based displacement time and point-based displacement time. "Repeat 1" and "Repeat 2" represent that the results were obtained from different students.

of water is required to flush these parts.

5.4 Conclusions

The study of pipe rinsing is essential to optimize the cleaning operations and to improve the recovery of cleaning agent solutions and rinsing water. In this chapter, CFD is used to simulate the displacement of one water-like cleaning agent by water. The simulations

comprised two steps: the first is to simulate the simplest straight pipes; the second is to model different complex pipe elements.

For straight pipes, the simulation results were compared with the analytical Taylor model. The proposed CFD model for the description of agent concentrations at varying time points and locations in the pipes is found to give an excellent agreement with the analytical approach. The key findings can be summarized in the following:

1. The displacement times depend on the pipe diameters and flow velocities. The product of the displacement time and the mean flow velocity can be correlated by a power function with inner pipe diameter as independent variable.

2. The minimum water consumption for completely rinsing a pipe is slightly larger than the pipe volume. The minimum water consumption is not much influenced by changing flow velocities when the flows are fully turbulent.

3. A practical rinsing step can be controlled based on downstream measurement and rinsing stops when the measurement reaches the pre-defined criterion. However, the resulting time is still longer than required. The resulting water consumption is slightly larger than the minimum requirement in order to reduce contamination risks.

4. The minimum volume of waste water can be predicted from the displacement times, and is independent of the flow velocity.

5. Radial mixing is not significant during the displacement process. The mixing length varies with the pipe diameter, flow velocity and rinsing time. The values of the mixing lengths are proportional to the characteristic length ($2\sqrt{D \cdot t}$), which can be applied to calculate the minimum requirement of intermediate rinsing water.

For complex pipe elements, this study has for the first time compared the ability to clean various pipe geometries using CFD. This kind of comparison helps to understand critical features that determine the ability to clean a pipe. For example, dead zones mainly exist in areas where flow recirculation is strong. The size of dead zones can be reduced by employing smooth connection or a large flow velocity. However, dead zones cannot completely disappear. Simulated pressure drops are in line with the analytical solutions from literature. CFD can provide sufficient information to calculate the equivalent lengths of different pipe types in order to calculate pressure drops in a complicated pipe system. Increasing flow velocity can reduce the displacement time significantly but the minimum water consumption is not affected. The overall water consumption to rinse different geometries varies from 1 to hundreds of times the volume of a geometry. These results have laid the foundation for applying CFD to investigate geometries and flow conditions that are more complex. Some simulation results have been verified to be justifiable as compared to the experimental findings from other researchers. Therefore, the outcomes increase the confidence to use CFD to optimize the hygienic design of pipe systems and to improve the operational efficiency.

List of Nomenclature in Chapter 5

The following nomenclature is only valid for this chapter. Some symbols are used in other chapters but with different meanings. Otherwise, the symbols are specifically explained in the text if there is no nomenclature in some chapter.

Roman Letters

C_0	Initial agent concentration, [kg m^{-3}]
C_m	Average agent concentration, [kg m^{-3}]
C_μ	Model constant for solving the turbulence length scale and the dissipation rate of turbulence kinetic energy, dimensionless
d	Pipe diameter, [m]
d_1, d_2, d_3	Dimension of complex geometries, [m]
D	Dispersion coefficient of species, [m^2 s^{-1}]
D_0	Molecular diffusion coefficient of species, [m^2 s^{-1}]
D_t	Turbulent diffusivity of species, [m^2 s^{-1}]
f	Darcy friction factor, dimensionless
F	Volume factor, dimensionless
g	Gravity acceleration, [m s^{-2}]
h_{major}	Major loss, [m]
h_{minor}	Minor loss, [m]
H	Dimension of complex geometries, [m]
J	Concentration diffusion flux, [kg m^{-2} s^{-1}]
k	Turbulence kinetic energy, [m^2 s^{-2}]
K	Resistance coefficient, dimensionless
l	Mixing length, [m]
L	Pipe length, [m]
L_1, L_2, L_3	Dimension of complex geometries, [m]
L_{eq}	Equivalent length of straight pipe, [m]
p	Pressure in Navier-Stokes equation, [Pa]
P	Pressure, [Pa]
r	Radial coordinate, [m]
R	Pipe radius, [m]
Sc_t	Turbulent Schmidt number, dimensionless
t	Time, [s]
t_1	The time required for displacing 1% of agent by water, [s]
t_{99}	The time required for displacing 99% of agent by water, [s]
Ti	Turbulence intensity, dimensionless
Ti_b	Turbulence intensity at inlet, dimensionless
Tl	Turbulence length scale, [m]
Tl_b	Turbulence length scale at inlet, [m]
u	Flow velocity, [m s^{-1}]
u_0	Mean flow velocity, [m s^{-1}]
u_x	Axial flow velocity, [m s^{-1}]
u'	Fluctuating velocity, [m s^{-1}]
V	Pipe volume, [m^3]

$V_{Inter.\,rinse}$	Volume of intermediate rinsing water, [m^3]
V_{min}	Minimum water consumption, [m^3]
$V_{Wastewater}$	Volume of waste water, [m^3]
x	Pipe length, [m]
y^+	Wall distance for a wall-bound flow, dimensionless
z	Height, [m]

Greek Letters

α, β	Coefficients correlating the inner pipe diameter and the displacement time
ε	Dissipation rate of turbulence kinetic energy, [$m^2\ s^{-3}$]
θ	Angle of complex geometry, [°]
μ	Dynamic viscosity, [Pa s]
ν	Kinetic viscosity, [Pa s]
ρ	Density, [kg m^{-3}]

CHAPTER 6

Cleaning of Egg Yolk Soils from Tank Surfaces Using Burst Flows

In this chapter, burst techniques have been applied to clean tank surfaces soiled by egg yolk materials. The work was performed in collaboration with Alfa Laval Copenhagen A/S. This chapter of the thesis has been published and reproduced based on the following article [135]:

Investigation of the cleaning of egg yolk deposits from tank surfaces using continuous and pulsed flows
Yang, J., Kjellberg, K., Jensen, B. B. B., Nordkvist, M., Gernaey, K. V., Krühne, U.
Food and Bioproducts Processing, in press
DOI: 10.1016/j.fbp.2018.10.007

6.1 Introduction

Burst, or pulsed, cleaning in tank cleaning operations is performed by interrupting a continuous flow with several breaks between the shots of detergent. For tank cleaning, the term burst identifies the rectangular form of a pulse, meaning a two-level output of a flow rate. In this thesis, Sections 2.1.3 and 2.3 have described the perspectives of using burst flows to enhance tank cleaning performance by ensuring surface coverage and providing additional time for the soaking of soil materials. Consequently, it is anticipated to save chemical usage and henceforth reduce cleaning costs.

Conventionally, burst tank cleaning is mainly conducted to clean brewery fermenters to remove the foam and yeast deposit that remain on the wall after emptying the tank. In this technique, the water pre-rinse step that is customary in continuous cleaning is skipped. Instead, a burst of alkali solution is applied for wetting the soil layers followed by a pause to allow the detergent to react. This sequence is repeated several times. It has been reported that burst cleaning is able to reduce water and chemical consumption at the expense of longer cleaning time [6, 33, 160]. However, the mechanisms behind the improvement of tank cleaning by using burst or pulsed flows are still poorly understood,

because a standardized method for assessing the performance of tank cleaning is lacking [161].

The scientific literature has discussed how pulsed flows enhance the cleaning of denatured whey protein deposits in pipes [162] and annular tube heat exchangers [163]. Reduced chemical consumption was also found by exposing deposits to a chemical environment before water rinse [51]. CFD simulations [102, 164, 165] and the analytical approaches using Fourier series [166] have proved that the alteration of flow pattern, particularly flow reversal, intensifies the local wall shear stress and hence increases the cleaning efficiency. Furthermore, pulsed flow has been observed to play a positive role in the cleaning of filter media [167, 168]. For the cleaning of open surfaces, more xanthan soils are detached from vertical surfaces by using a pulsed water jet [169, 170].

However, implementing pulsed flows in tank cleaning operations differs from the processes investigated in the aforementioned studies:

1. The pulse technique used in tank cleaning is regularly performed by controlling the pump on or off rather than hydraulically generating a sinusoidal flow rate. The frequency (around 1 Hz) of changing the flow rate in the above-mentioned researches is extremely high for cleaning a tank, because the water flow coming from a jet device takes a period to reach the tank surface with stabilized high impact force.

2. The soil layers are soaked in the cleaning liquid environment between pulses when cleaning pipes, heat exchangers or filters. However, when cleaning a tank, the flow is one-way and most of the liquid flows downwards under gravity during breaks.

3. Changing the flow rate affects the performance of rotating cleaning devices since the rotational motion depends on the flow rate of liquid through the machine. The duration of each burst should ensure that all internal areas are covered by the cleaning liquid at least once. Moreover, the damage to pumps as a consequence of frequent start-up and shut-down has not been fully determined yet [44].

The aim of this chapter is to compare the cleaning of tank surfaces soiled by egg yolk using continuous or pulsed flows. Different process parameters (i.e., temperature, flow rate and alkali concentration) were investigated. The primary goal of using pulsed flow is to reduce liquid consumption and henceforth to reduce cleaning costs and environmental impact. In the end, this work provides a quantitative measure of performance to compare the cleaning results by using pulsed flows or conventional continuous flows.

6.2 Materials and Methods (Pilot-Scale)

6.2.1 Experimental Setup

The experiments were performed in a pilot-scale CIP system, as shown in Figure 6.1. The CIP system consisted of two storage tanks: one for alkali solution and one for fresh water. The test tank was made from transparent polyvinyl chloride (PVC). The dimensions of

the test tank were 50 cm diameter and 55 cm height with a 10 cm additional depth of a klopper torispherical bottom. Soiling materials were deposited on an extra soft stainless steel plate (type 304, roughness values Ra 0.17 ± 0.02 µm, 52 cm height, 30 cm width), which was dried in an oven before being bent and mounted along the tank wall with the help of two separated supports. Cleaning was performed using a single axis rotary spray head. The rotary spray head was located in the upper section of the test tank, as illustrated in Figure 6.2, resulting in the cleaning liquid distributing with a rotating fan. A digital camera was used to take photos of the test plate during cleaning.

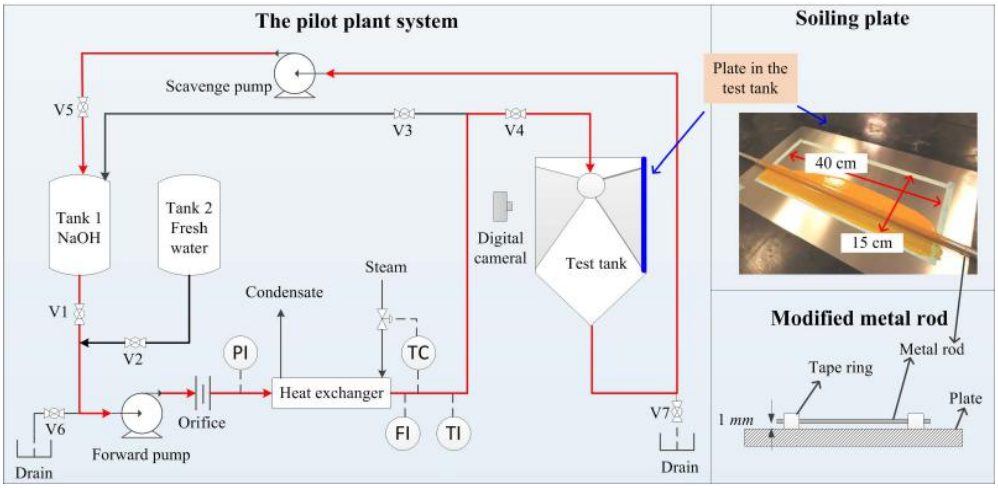

Figure 6.1: Schematic diagram of the pilot-scale setup, the soiling plate and the modified metal rod.

6.2.2 Soiling and Cleaning

Pasteurized egg yolk (Hedegaard, Denmark) was selected as the model soil in all experiments. Per 100 g, the soil contained 13 g protein, 24 g fat, 0.3 g carbohydrate and 0.1 g salt. According to the classification of cleaning problems in Figure 2.1 (see Chapter 2), egg yolk belongs to the type 3 soil, meaning chemicals are required to completely remove organic films. The soil was mixed with 1 % w/w riboflavin (Sigma-Aldrich, US) to improve the visual inspection of the cleaning efficiency. Only the center area of 40 × 15 cm^2 was covered by the soil materials. An even layer was achieved by spreading the soil material using a modified straight metal rod, which had been wrapped with tapes to form a 1 mm thickness ring on each end so a uniform layer could be obtained under the rod after spreading (see Figure 6.1). Then the soiled plate was dried in an oven with hot air to form uncooked (40 - 45 °C for 2 hours) or cooked (80 – 90 °C for 1 hour) soils before being mounted on the tank wall prior to cleaning. The protein structure of egg yolk was reported to aggregate when being heated up to 70 °C [20, 171]. The test plates were

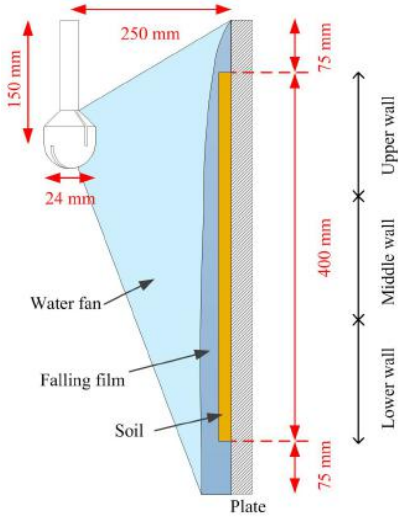

Figure 6.2: Illustration of cleaning by the single axis rotary spray head. The surface is divided into upper, middle and lower wall sections for analysis.

weighed before and after soiling, obtaining 16.8 ± 1.2 g uncooked soil or 16.4 ± 1.1 g cooked soil per plate, respectively. The variation of mass was within the range of ±7 %.

The cleaning procedure consisted of 10 min circulation of NaOH solution and 1 min final rinse with fresh water. The circulation of NaOH solution was performed according to four different approaches, as described in Figure 6.3:

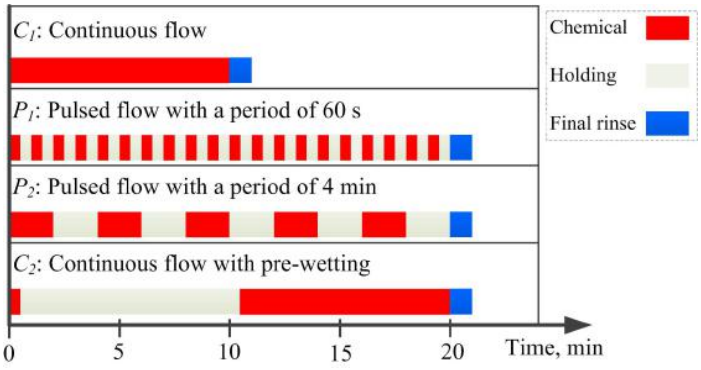

Figure 6.3: The four cleaning approaches applied in this study.

- Continuous flow (C_1): continuous 10 min flow before 1 min final rinse. The total cleaning time was 11 min;

- Pulsed flow with a period of 60 s (P_1): 30 s flow followed by 30 s break repeated for 20 times before the final rinse. The total cleaning time was 21 min;
- Pulsed flow with a period of 4 min (P_2): 2 min flow followed by 2 min break repeated for 5 times prior to the final rinse, with a total cleaning time of 21 min;
- Continuous flow with pre-wetting (C_2): 30 s flow followed by 10 min break and 9.5 min continuous flow before the final rinse. The total cleaning time was 21 min.

The cleaning results were evaluated by taking photos of the test plate during each break and after the final rinse. The first two approaches, C_1 and P_1, were mainly investigated. C_2 and P_2 were designed for comparison. The burst frequency of P_2 was more similar to the common industrial practices for tank cleaning operations. To reduce the damage to the pumps as a result of frequent start-up and shut-down, the forward flow was controlled by alternatively opening or closing the butterfly valves V3 and V4, resulting in the switch between flow circulation (during breaks) and cleaning. The scavenge pump started when the liquid was accumulated at the test tank bottom above a certain level. The examined parameters included temperature, flow rate and NaOH concentration, which are described in Section 6.2.4. All experiments were performed at least in duplicates.

6.2.3 Determination of Soiling Areas

The remaining soiling areas were calculated with the help of the image analysis toolbox in Matlab (MathWorks, US). The normalized remaining soiling area y was defined as the ratio of the remaining soiling area to the total initial soiling area, according to:

$$y = \frac{Remaining\ soiling\ area}{Total\ soiling\ area\ before\ cleaning} \tag{6.1}$$

So $y = 1$ denotes completely dirty and $y = 0$ denotes completely clean. The soiled plate was equally divided into three sections (upper, middle and lower wall) with 13.33 cm height for each (Figure 6.2). The different sections were analysed separately.

6.2.4 Factorial Experimental Design

As shown in Table 6.1, the effects of temperature T, flow rate FR and NaOH concentration C were evaluated in terms of the normalized remaining soiling area y. The experiments were executed in a random order with the intention to randomize experimental errors [172]. A second-order regression model for the actual variables x_i (indicating T, FR and C) was obtained by fitting the experimental results using Equation 6.2:

$$\hat{y} = \beta_0 + \sum_{j=1}^{3} \beta_j x_j + \sum_{j=1}^{3} \sum_{i<j} \beta_{ij} x_i x_j + \epsilon \tag{6.2}$$

where $\hat{y}$ is the predicted value of y. β_0, β_i and β_{ij} are the intercept, linear and interaction terms respectively and ϵ is the statistical error term. Adding one center point in the factorial experimental design helped to examine the significance of curvature effects on the model if a $\beta_{ii}{x_i}^2$ term was added.

Table 6.1: 2^3 factorial experimental design indicating the coded and actual values of variables

Runs	Coded levels of variables			Actual levels of variables		
	Temp. X_1	Flow rate X_2	Conc. X_3	Temp. T, [°C]	Flow rate FR, [m^3/h]	Conc. C, [kg/m^3]
Factorial points						
1	-1	-1	-1	25	0.9	1
2	1	-1	-1	55	0.9	1
3	-1	1	-1	25	1.5	1
4	1	1	-1	55	1.5	1
5	-1	-1	1	25	0.9	5
6	1	-1	1	55	0.9	5
7	-1	1	1	25	1.5	5
8	1	1	1	55	1.5	5
Center point						
9	0	0	0	40	1.2	3

6.2.5 Cost Model

The total costs of cleaning by alkali solution (δ_{Total}) were computed as the sum of the costs of fresh water ($\delta_{Fresh\ water}$), chemical ($\delta_{Chemical}$), electricity by pumps ($\delta_{Electricity}$) and sensible heat (δ_{Heat}). To calculate the cleaning costs that result in a certain amount of cleanliness, the following equation was used:

$$\begin{aligned} \frac{Cleaning\ costs}{Degree\ of\ cleaning} &= \frac{\delta_{Total}}{100 - 99 \cdot \tilde{y}} \\ &= \frac{\delta_{Fresh\ water} + \delta_{Chemical} + \delta_{Electricity} + \delta_{Heat}}{100 - 99 \cdot \tilde{y}} \end{aligned} \tag{6.3}$$

where $\tilde{y}$ is the corrected term of $\hat{y}$ by eliminating the unrealistic prediction errors as:

$$\tilde{y} = \begin{cases} 0 & \hat{y} < 0 \\ \hat{y} & 0 \leq \hat{y} \leq 1 \\ 1 & \hat{y} > 1 \end{cases} \tag{6.4}$$

A degree of cleaning (DoC) value of 100 represents that all soils are removed ($\tilde{y} = 0$), and the value of 1 represents that no soil is removed ($\tilde{y} = 1$). The costs of fresh water, chemical, electricity and sensible heat were calculated through Equations 6.5 to 6.8 (re-written from Equations 3.2 to 3.5), noting the term $t/3600$ converted the time unit from second to hour:

$$\delta_{Fresh\ water} = FR \cdot t/3600 \cdot \varphi_{Fresh\ water} \tag{6.5}$$

$$\delta_{Chemical} = FR \cdot t/3600 \cdot C \cdot \varphi_{Chemical} \tag{6.6}$$

$$\delta_{Electricity} = (P_f + P_s) \cdot t/3600 \cdot \varphi_{Electricity} \tag{6.7}$$

$$\delta_{Heat} = FR \cdot t/3600 \cdot \rho \cdot c_P \cdot (T - T_0) \cdot \varphi_{Heat} \tag{6.8}$$

where P_f and P_s are the powers of the forward and scavenge pumps, ρ (1,000 kg/m^3) is the density of water, c_P (4,185.5 J/(kg °C)) is the heat capacity of water and T_0 (25 °C) is room temperature. The unit cost of each item was selected based on the prices in Danish industries: $\varphi_{Fresh\,water}$ = 3.6 Euro/m^3 including waste water treatment, $\varphi_{Chemical}$ = 1 Euro/kg, $\varphi_{Electricity}$ = 0.09 Euro/(kWh), φ_{Heat} = 2.6·10^{-8} Euro/J.

6.3 Results and Discussion

6.3.1 Cleaning Dynamics

Figure 6.4 shows the normalized remaining soiling areas (of selected runs in Table 6.1, the results for all runs are provided in Appendix B) at different wall locations by using continuous flow C_1 and pulsed flow P_1. Fewer soils remain in the upper wall section than in the lower wall section at the same effective time, which is defined as the time when the liquid flow acts on the tank surface (actual cleaning time subtracted holding time). It means the fastest removal of deposit occurs in the upper part. As illustrated in Figure 6.2, the upper section is the closest to the rotary spray head and experiences the highest impact force from the droplets in the liquid fan. However, thicker falling films form in the lower section as liquid flows down under gravity, implying higher wall shear stress in the lower section than in the upper section. The phenomena of (i) higher shear force but slower cleaning rate in the lower wall section and (ii) lower shear force but faster cleaning rate in the upper wall section imply that the soil layers are mainly detached by the direct impact of liquid droplets instead of falling films.

The results in Figure 6.4 reveal that pulsed flows are able to remove more deposits from the tank wall than continuous flows at the same effective time. There are two explanations of the enhanced cleaning performance by pulsed flows: the increased holding time and the improved shear force. The holding time between two bursts can provide additional time for the diffusion of the alkali solution into the soil outer layer and therefore improves the reaction rate. In between two bursts, the outer layer of soiling materials swells and becomes weak, and is therefore more easily detached in the next burst [33]. For the cleaning by continuous flow, the impact force and falling film detach the outer swollen layer constantly. But this process is restricted by the rate of diffusion and swelling, so the mechanical force cannot remove as much soil as it can. However, for the cleaning by pulsed flow, the additional holding time between two pulses enables more soil layers to swell and thus removes more soil layers. The improved shear force is caused by the unstable falling film when stopping and starting a pulse. It is anticipated that a wavy film forms in the unsteady flow region. Consequently, the local maxima of wall shear stress, even local flow reversal, occur instantaneously at the front of the unstable free falling film [86, 90]. Therefore, during the cleaning by pulsed flow, the unstable falling film can contribute to the removal of soil materials by enhanced shear force. This effect is comparable to the pipe or filter cleaning operations where pulsed flows enhance local wall shear stress and hence improve the cleaning results [162, 168]. However, as discussed above, cleaning by falling film is less significant than by the direct impact from the liquid fan. Therefore, the improved shear force due to pulsed flow can contribute to cleaning

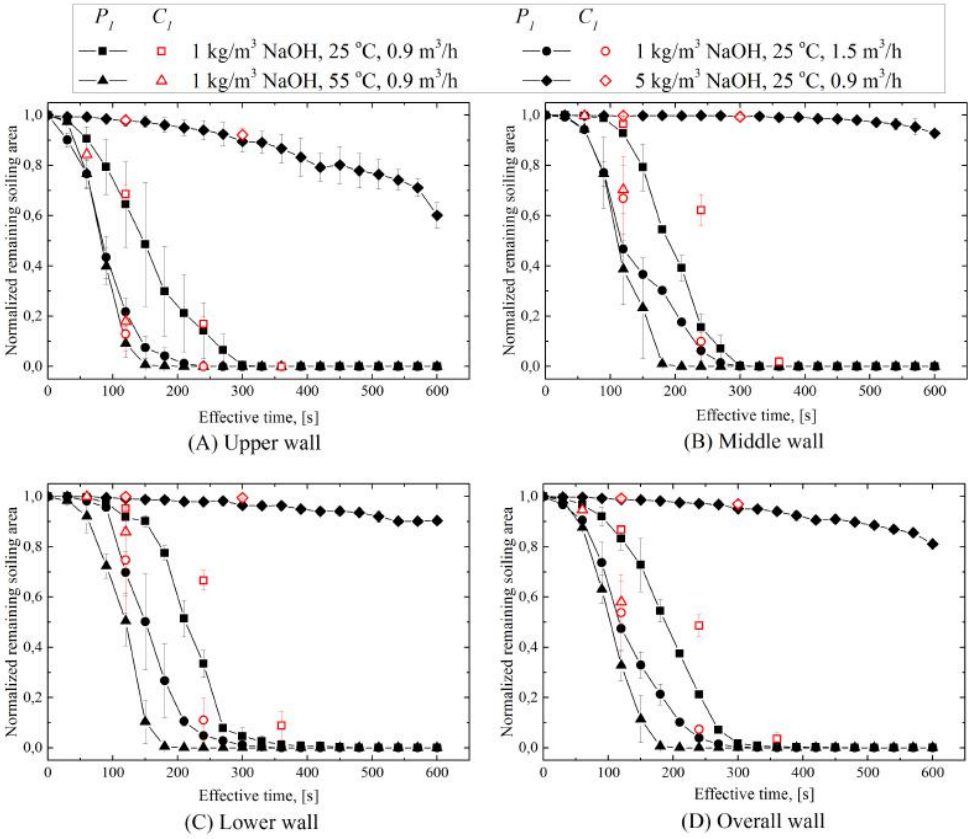

Figure 6.4: Removal of uncooked soils for different conditions of temperature, flow rate and NaOH concentration, by using continuous flow without pre-wetting (C_1) or pulsed flow of high frequency (P_1). Only the results of selected runs 1, 2, 3 and 5 in Table 6.1 are displayed. The results for all runs are displayed in Appendix B: (A) tank upper wall, (B) tank middle wall, (C) tank lower wall, (D) tank overall wall surface.

but is not the key factor.

The slopes in Figure 6.4 indicate the removal rate of uncooked egg yolk deposits by using pulsed flow (P_1). The cleaning dynamics by continuous flow (C_1) could be analyzed through the discrete observations and are shown in Figure 6.5. Typical three-phase cleaning dynamics are revealed: the cleaning rate is initially slow due to the swelling of soil, then chunks are removed at a constant rate, and finally the removal is limited at the decay phase. This profile is similar to the observations of Gillham et al. (2000) [162] and Goode et al. (2010) [42]. According to Figure 6.4, the most efficient cleaning occurs at low alkali concentration, high temperature and high flow rate. Among the tested parameters, the alkali concentration and temperature contribute most to the swelling and removal of

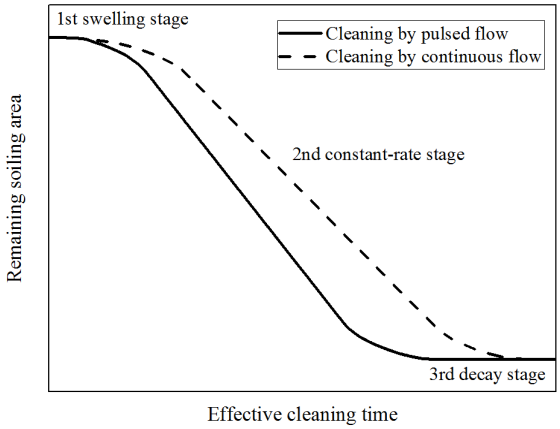

Figure 6.5: Cleaning dynamics by pulsed or continuous flow.

egg yolk samples, which is also reported by other research groups [20].

It is interesting to find that the increase in NaOH concentration from 1 to 5 kg/m^3 reduces the cleaning rate. The preliminary study has proved that the egg yolk soil cannot be cleaned by water only. Therefore, an optimal NaOH concentration should exist below 5 kg/m^3 to clean egg yolk. Helbig et al. (2018) studied the cleaning of egg yolk and explained that the removal occurred by diffusive dissolution or cohesive separation in low alkali concentration. In contrast, adhesive detachment occurred in high alkali concentration. Increasing alkali concentration below the optimal value favoured the hydrolysis of ester bonds and the breakup of hydrogen bonds within the lipoprotein, thereafter promoted the solubility of lipids. However, a further rise of NaOH concentration increased the interactions within the proteins by enhancing hydrogen bonding, hydrophobic interactions and disulfide bridges, leading to worse cleanability [39]. Furthermore, Bird et al. (1991, 1992) investigated the cleaning of another protein-based soil (cooked whey protein) and obtained an optimal alkali concentration and temperature as well. They explained that a high alkali concentration changed the deposit structure rapidly to form a very thick translucent layer, which was difficult to be removed. Scanning electron microscope (SEM) results proved that the structure became open with high voidage at the optimal concentration. But the voidage was reduced at even higher alkali concentration. In their study, the optimal conditions for cleaning cooked whey proteins were 50 °C and 5 kg/m^3 of NaOH solution. Above the optimal temperature, a chemical reaction occurred and the cleaning rate was reduced [16, 17].

Even though pulsed flow removes more deposits than continuous flow at the same effective time or at the same alkali consumption, it is necessary to emphasize that pulsed flow may reduce the time efficiency under the investigated flow conditions. Figure 6.6 rearranges an example from Figure 6.4 according to the actual cleaning time (effective time plus holding time), inferring that pulsed flow results in less soil removal in the actual timescale. In

some industries, saving cleaning time can benefit production significantly. Hence, an optimization of the pulsed flow parameters (e.g., frequency, ratio between pulse duration and duration of breaks in between pulses) is required in order to apply the technique into practice, or the cleaning by pulsed flow is more applicable to the cases where cleaning downtime is not critical.

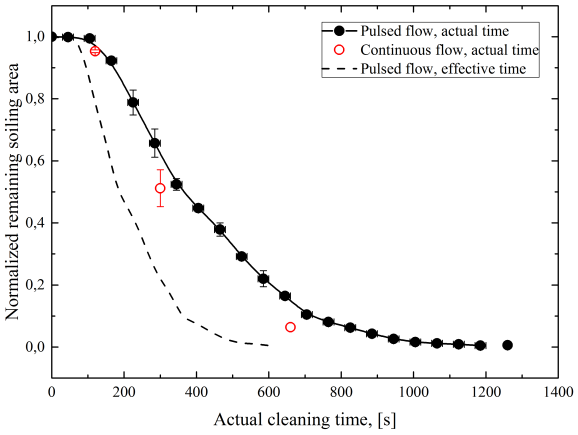

Figure 6.6: An example of cleaning dynamics (P_1 and C_1) based on actual cleaning time (effective cleaning time plus holding time). The cleaning conditions are: $T = 40$ °C, $FR = 1.2$ m^3/h, $C = 3$ kg/m^3. The dashed line is the cleaning profile using pulsed flow against effective time.

6.3.2 Statistical Comparison of Cleaning by Pulsed Flow or Continuous Flow

To quantitatively compare the effects of different parameters on the cleaning results, an analysis of variance (ANOVA) was applied to evaluate the significance of the constructed quadratic model (Equation 6.2) for pulsed flow cleaning (P_1) and continuous flow cleaning (C_1), respectively [172]. The cleaning results at the same effective cleaning time (2 min) were extracted from all cleaning runs. The statistical analysis was completed with the help of the JMP Software (SAS Institute, US) and the results are shown in Tables 6.2 and 6.3. The insignificant variables or interaction effects were removed by using stepwise regression control (SRC) to minimize the small-sample-size corrected version of the Akaike information criterion (AICc) (JMP 13.0.0 Help, SAS Institute). The remaining variables and interactions are significant at $P < 0.05$ (or $P < 0.1$ but the F value is very close to the criteria of $P < 0.05$). R^2 and Adj-R^2 explain the goodness of the model to fit the experimental data, and Pred-R^2 indicates how well the model fits new data [172]. The general range of R^2 is between 0.843 and 0.983, indicating that the models are adequate to describe the data satisfactorily [1]. The coefficients for the second-order regression model are listed in Table 6.4.

Table 6.2: Analysis for the cleaning of uncooked soil by using pulsed flow (P_1) at 2 min of effective time.

Source of variance	Upper wall		Middle wall		Lower wall		Overall wall	
	DF[a]	F	DF[a]	F	DF[a]	F	DF[a]	F
Model	5	44.62[c]	5	52.19[c]	5	29.39[c]	5	136.18[c]
X_1	1	13.40[c]	1	21.72[c]	1	28.15[c]	1	81.86[c]
X_2	1	7.65[d]	1	26.32[c]	1	11.19[c]	1	44.21[c]
X_3	1	183.85[c]	1	148.92[c]	1	74.35[c]	1	442.82[c]
X_1X_2	SRC[b]		SRC[b]		SRC[b]		SRC[b]	
X_1X_3	1	13.49[c]	1	33.79[c]	1	24.18[c]	1	79.30[c]
X_2X_3	1	4.72[e]	1	20.21[c]	1	9.06[d]	1	32.69[c]
Residual	12		12		12		12	
Lack of fit	3	2.30	3	0.83	3	6.71[d]	3	3.34
Pure error	9		9		9		9	
Total model	17		17		17		17	
R^2	0.949		0.956		0.924		0.983	
Adj-R^2	0.928		0.938		0.893		0.975	
Pred-R^2	0.865		0.917		0.849		0.968	

[a] DF: Degree of freedom
[b] SRC: Removed by "stepwise regression control" model
[c] $P \leq 0.01$
[d] $P \leq 0.05$
[e] $P \leq 0.1$

The results in Tables 6.2 and 6.3 show the effects of the investigated parameters on the cleaning behavior, and can be summarized as follows:

- For both cleaning approaches (continuous C_1 and pulsed P_1), the most important parameter of the cleaning process is the alkali concentration (X_3). Furthermore, the main effects of temperature (X_1) and flow rate (X_2) as well as the interactions between temperature and alkali concentration (X_1X_3) and between flow rate and alkali concentration (X_2X_3) are significant as well. The interaction between temperature and flow rate (X_1X_2) can, however, be eliminated.
- For pulsed flow cleaning, the effects of temperature and its interaction with alkali concentration are greater than the effects of flow rate and its interaction with alkali concentration. In contrast, the opposite is true for continuous flow cleaning.
- The quadratic curvature in the response model, implied by the lack-of-fit statistic, is insignificant or less significant compared with the other main factors or interactions. However, the current experimental design with only one replicated center point cannot identify which of the three variables exhibit curvature. An alternative design is to augment the 2^3 design with more axial runs, called a central composite design [1, 172]. Nonetheless, this study keeps the proposed design and model, because the curvature effect is less significant than the others in the studied ranges of conditions.

Table 6.3: Analysis for the cleaning of uncooked soil by using continuous flow (C_1) at 2 min of effective time.

Source of variance	Upper wall		Middle wall		Lower wall		Overall wall	
	DF[a]	F	DF[a]	F	DF[a]	F	DF[a]	F
Model	5	26.08[3]	5	16.45[3]	5	12.90[3]	5	23.09[3]
X_1	1	4.84[d]	1	10.32[3]	1	7.71[d]	1	10.30[3]
X_2	1	8.15[d]	1	12.91[3]	1	15.28[3]	1	14.33[3]
X_3	1	105.70[3]	1	36.24[3]	1	26.19[3]	1	69.77[3]
X_1X_2	SRC[b]		SRC[b]		SRC[b]		SRC[b]	
X_1X_3	1	5.69[d]	1	10.84[3]	1	4.68[e]	1	9.79[3]
X_2X_3	1	6.02[d]	1	11.95[3]	1	10.62[3]	1	11.26[3]
Residual	12		12		12		12	
Lack of fit	3	37.03[3]	3	4.04[d]	3	5.57[d]	3	3.51
Pure error	9		9		9		9	
Total model	17		17		17		17	
R^2	0.916		0.873		0.843		0.906	
Adj-R^2	0.881		0.820		0.778		0.867	
Pred-R^2	0.839		0.693		0.592		0.804	

[a] DF: Degree of freedom
[b] SRC: Removed by "stepwise regression control" model
[c] $P \leq 0.01$
[d] $P \leq 0.05$
[e] $P \leq 0.1$

Table 6.4: Parameter coefficients of the second-order regression model for uncooked soil.

Parameters	Pulsed flow P_1				Pulsed flow C_1			
	Upper	Middle	Lower	Overall	Upper	Middle	Lower	Overall
β_0	1.336	2.206	2.094	1.881	1.543	2.360	1.955	1.946
β_1, [°C^{-1}]	-0.016	-0.021	-0.021	-0.020	-0.013	-0.017	-0.010	-0.014
β_2, [m^{-3} h]	-0.528	-0.869	-0.653	-0.670	-0.756	-0.941	-0.731	-0.783
β_3, [kg^{-1} m^3]	-0.065	-0.234	-0.206	-0.169	-0.102	-0.267	-0.171	-0.179
β_{12}, [°C^{-1} m^{-3} h]	0	0	0	0	0	0	0	0
β_{13}, [°C^{-1} kg^{-1} m^3]	0.0032	0.0043	0.0041	0.0039	0.0028	0.0035	0.0018	0.0028
β_{23}, [h kg^{-1}]	0.0951	0.165	0.125	0.126	0.141	0.185	0.135	0.149

The improvement of cleaning by using pulsed flow can be quantified as the difference between the predicted normalized remaining soiling area by pulsed or continuous flows. Figure 6.7 plots the difference by fitting Equation 6.2 using the coefficients in Table 6.4. It is found that:

- The effects of pulsed flow on cleaning are generally positive in the studied ranges of parameters, meaning pulsed flow is able to remove more deposits from the tank wall compared with continuous flow.

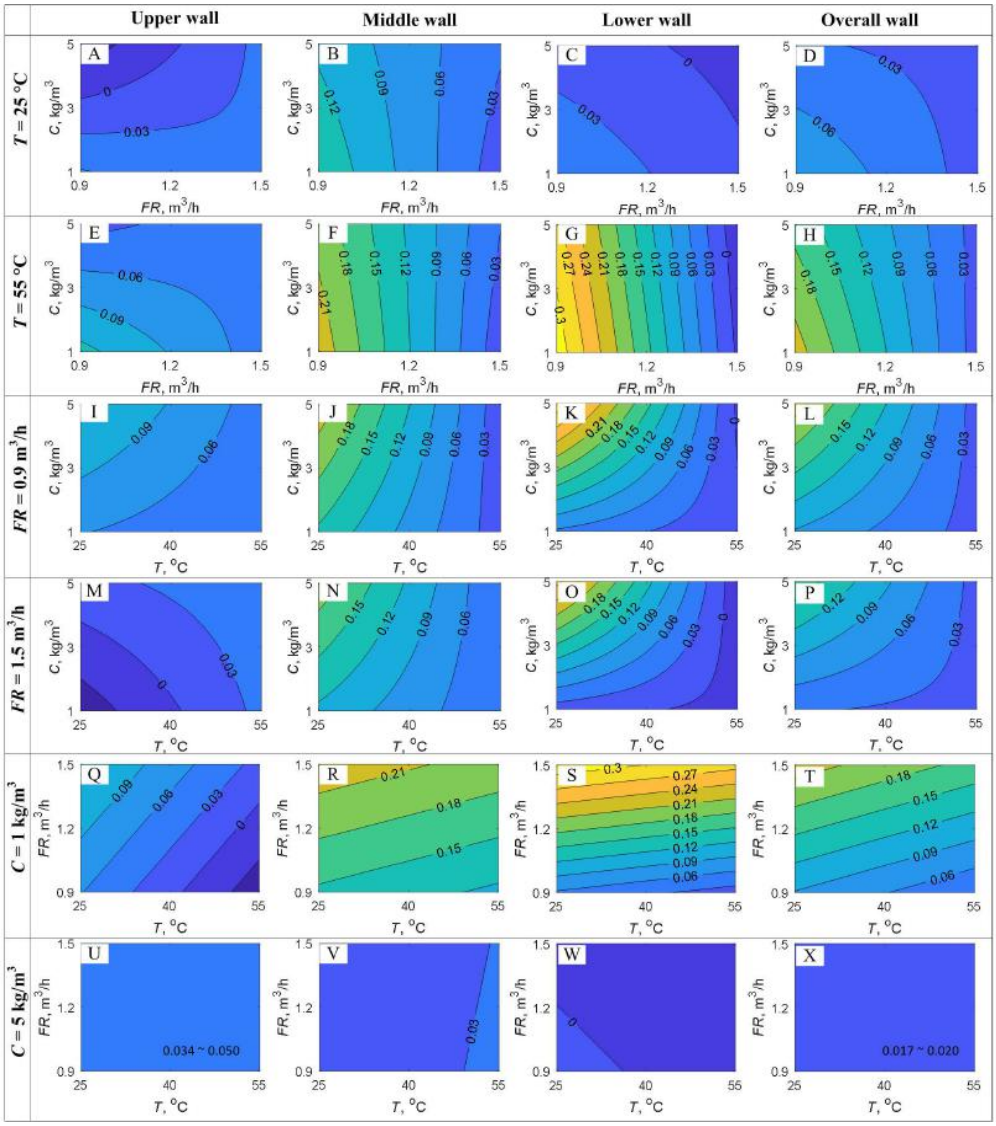

Figure 6.7: The difference of normalized remaining soiling area of uncooked soil between pulsed flow cleaning (P_1) and continuous flow cleaning (C_1). The results are based on an effective cleaning of 2 min. A positive value indicates that the effect of pulsed flow is positive. Yellow color denotes significant difference; dark blue color denotes insignificant difference.

- The difference between pulsed flow and continuous flow is more significant at high temperature and at low alkali concentration. The variation of the flow rate does not make a large difference between the two cleaning methods. This is because temperature and the alkali concentration are key factors contributing to reactions, which is in line with the idea of pulsed flow cleaning that allows a longer reaction time. Higher flow rates lead to greater mechanical impact, which, however, is not the limiting factor in this study because the applied flow rate is high enough to detach the swollen soils.

- The difference between the two cleaning approaches is less substantial at the upper wall section than at the lower wall section. The distance from the rotary spray head to the tank surface increases from the tank top to the bottom. Hence, the mechanical forces exhibited on the wall decline from the upper section to the lower section. As discussed above, the improvement of cleaning by pulsed flow is less affected by this impact. Therefore, the enhancement of cleaning by pulsed flow becomes less apparent at the upper wall section.

- For the lower wall section or the overall wall, the greatest improvement by using pulsed flow occurs at high temperature and low flow rate, or low alkali concentration and high flow rate. At low temperature and high alkali concentration, the contribution of pulsation is small.

6.3.3 Cleaning of Uncooked Soils with Different Pulsed or Continuous Approaches

Figure 6.8 compares the cleaning of uncooked soil deposits with different pulsed and continuous approaches. After the final rinse, the improvement of cleaning using pulsed flows is observed but not obvious in the upper and middle wall sections when compared with continuous flows. The reason is that only the pictures after final rinse were taken in the cleaning experiments by continuous flows, when most soil deposits have been removed. It has been indicated in Figure 6.5 that the improvement by pulsed flow is the most significant at the stage when chunks of deposits are removed at a constant rate (normally 150 - 500 s effective time for the upper and middle wall sections). Therefore, it is a logical deduction that a more clear difference between the pulsed and continuous approaches can be observed at some latent time points during alkali circulation. In Figure 6.8C, pulsed flow can remove ca. 15% more soils than continuous flow at the lower wall section. It confirms the hypothesis that a clear difference occurs before the cleaning approaches the end, as the cleaning of the lower wall section still lies in the constant-rate stage (illustrated in Figure 6.5) after final rinse.

Pulsed flow with a lower frequency (P_2) is less effective than that with a higher frequency (P_1) at the upper wall section, middle wall section and the overall surface. The repeated bursts of liquid contribute to the removal of the swollen soil layers instantly by mechanical forces, exposing the hard layers to fresh liquid in the next burst. However, the low impact forces at the lower wall section restrict the removal of the outer layer of soil [102], thereby the influence of pulse frequency is not significant. The resulted best cleaning performance

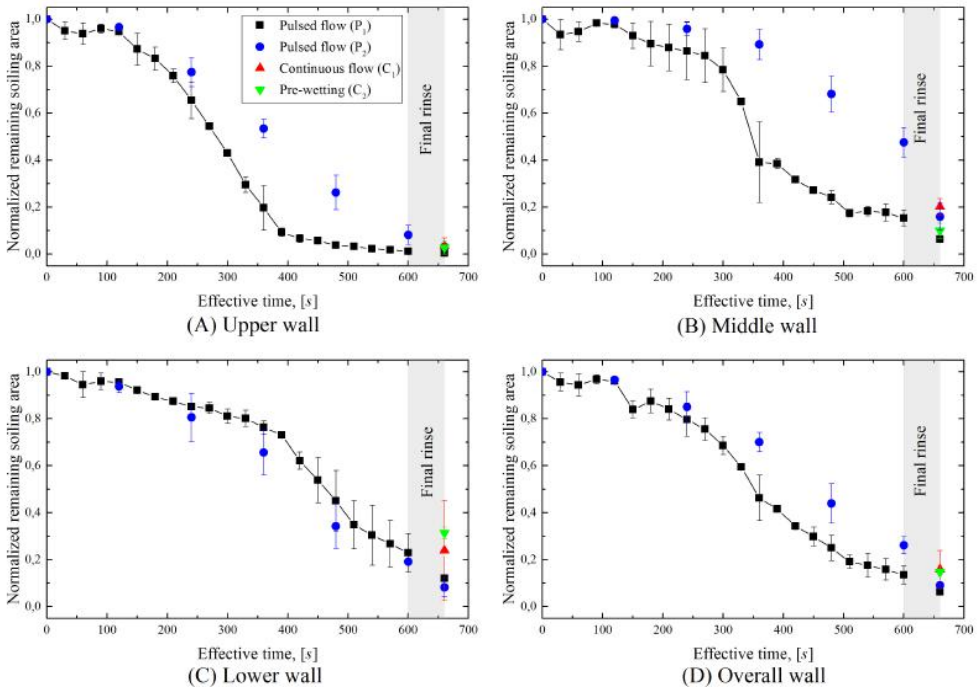

Figure 6.8: Comparison of cleaning uncooked soils with different continuous and pulsed approaches: (A) tank upper wall surface, (B) tank middle wall surface, (C) tank lower wall surface, (D) tank overall wall surface. The cleaning conditions are: $T = 55$ °C, $FR = 1.5$ m^3/h, $C = 5$ kg/m^3.

at the lower wall section by P_2 (Figure 6.8C) can be associated with the reasonable experimental deviations.

Gordon et al. (2012) suggested that pre-wetting protein soils before cleaning swells the soil layer initially and eases the following removal [21]. Lerch et al. (2013) compared the removal of the soluble ingredient riboflavin by falling films with or without pre-wetting, and found that the pre-wetting of dried soil achieved an enhanced cleaning [173]. Nonetheless, through comparing the cleaning results between continuous flow (C_1) and pre-wetting (C_2) as shown in Figure 6.8, the difference between normalized remaining soiling area to the overall wall is less than 2%. Therefore, the contribution of pre-wetting in this study is not apparent, because the water films are unable to attach to the vertical tank wall consistently as soaking, that is, by submerging soil layers in the liquid phase. As a result, pre-swelling is not substantively augmenting the cleaning.

The remaining soiling areas decrease at the effective cleaning time of 600 – 660 s in all wall sections, indicating that the final water rinse favours the removal of deposits as well. Some alkali solution remains in the CIP forward pipe at the initial period of the final rinse, whereas it is only a short period during the one-minute action. The results in

this study imply that mechanical forces rather than chemical reaction dominate the soil removal toward the end of the cleaning operation. Therefore, a more economic burst cleaning can be executed by short chemical shots in the beginning and then by water rinse in the end (not tested in this study).

6.3.4 Optimization of Cleaning

Optimizing a CIP procedure targets not only to minimize the consumption of resources but also to maximize the cleanliness at reduced costs. Figure 6.9 displays the cleaning costs per degree of cleaning at the optimal operating conditions. For pulsed flow cleaning, the most cost-efficient operation occurs at high temperature, low flow rate and low alkali concentration. On the contrary, the optimal conditions for continuous flow cleaning are high temperature, high flow rate and low alkali concentration. With both approaches, the chemical consumption is the main contribution to the overall costs whereas the cost of electricity is negligible, which is in accordance with previous findings when mapping CIP procedures in Chapter 3.

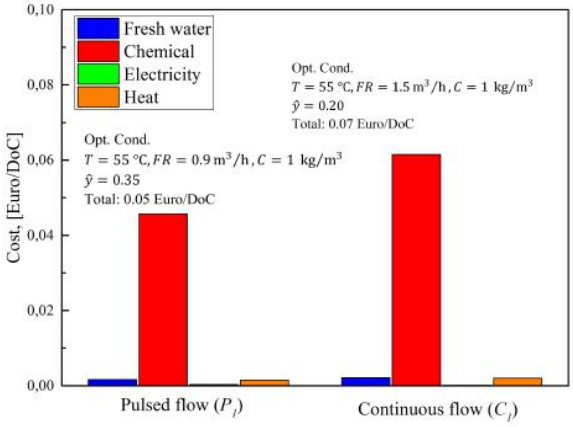

Figure 6.9: Comparison of the cleaning costs of uncooked soil by pulsed flow (P_1) and continuous flow (C_1) under optimal conditions. The degree of cleaning is defined at the effective cleaning time of 2 min.

As indicated in Figure 6.9, under the optimal cleaning conditions, pulsed flow reduces 25% of the cost to achieve per degree of cleanliness for cleaning uncooked soil. However, when performing cleaning under the most economical conditions, only 65% of soils are removed by the pulsed flow after 2 minutes. On the other hand, 80% of soil materials are removed by continuous flow after 2 minutes effective time at its optimal conditions. The difference is for the sake of higher flow rate when cleaning by continuous flow. Table 6.5 compares the total cleaning costs to remove 80% soil materials ($\hat{y} = 0.20$) from the surface by continuous flow or pulsed flow, where the flow conditions of pulsed flow are determined from the optimal conditions presented in Figure 6.9. The cost saving by pulsed flow is

21 - 31% compared to the cleaning by continuous flow. The generation of waste water is also lower when cleaning by pulsed flows. However, an increase in downtime should be considered when implementing burst cleaning in practice, as previously reported in Figure 6.6. It can still be concluded that tank cleaning by using pulsed flow makes the per unit consumption of cleaning detergent more valuable.

Table 6.5: Analysis for the cleaning of uncooked soil ($\hat{y} = 0.20$) by using continuous flow (C_1) at 2 min of effective time

Parameters	Continuous flow C_1	Pulsed flow P_1	
T, [°C]	55	55	55
FR, [m^3 h]	1.5	1.5	0.9
C, [kg m^{-3}]	1	1	1
Effective cleaning time[a], [s]	120	95	138
Actual cleaning time[a], [s]	120	185	258
Waste water volume[b], [m^3]	0.050	0.040	0.035
Total cost, [10^{-2} Euro/DoC]	6.6	5.2	4.6
Cost saving	-	21%	31%

[a] Effective cleaning time denotes the circulation time of alkali solution. Actual cleaning time is the sum of effective cleaning time and holding time.

[b] Alkaline solutions are circulated in experiments. Waste water volume is calculated as the product of flow rate and effective cleaning time, assuming chemical solutions are used without recycle.

6.3.5 Cleaning of Cooked Soils with Different Approaches

Figure 6.10 shows the cleaning results of cooked soils with different continuous and pulsed approaches. Larger soiling areas are obtained in all observations compared with the cleaning of uncooked soils at the same flow conditions (see Figure 6.8). The difference is caused by the nature of deposits that can strongly affect the cleaning behavior. Heating protein-based soil over its denaturation temperature makes the material harder to remove [21]. Some results of cleaning cooked soils are consistent with the results of cleaning uncooked soils: pulsed flow improves cleaning compared with continuous flow; higher pulse frequency favours the removal of deposits at the upper wall section compared to lower pulse frequency; the final rinse with water can detach the swollen soil when the cleaning tends to finish.

On the other hand, the influence of pulsed flows becomes more noticeable during the cleaning of cooked soil compared with the cleaning of uncooked soil. Taking the continuous flow cleaning C_1 as contrast, the cleanings performed by pulsed flow with low frequency (P_2) and pulsed flow with high frequency (P_1) can respectively improve the removal of deposits by 33.0% and 51.1% of the overall surface. However, the negative improvement by pre-wetting to the middle wall section can be associated with experimental deviations, as displayed in Figure 6.10B.

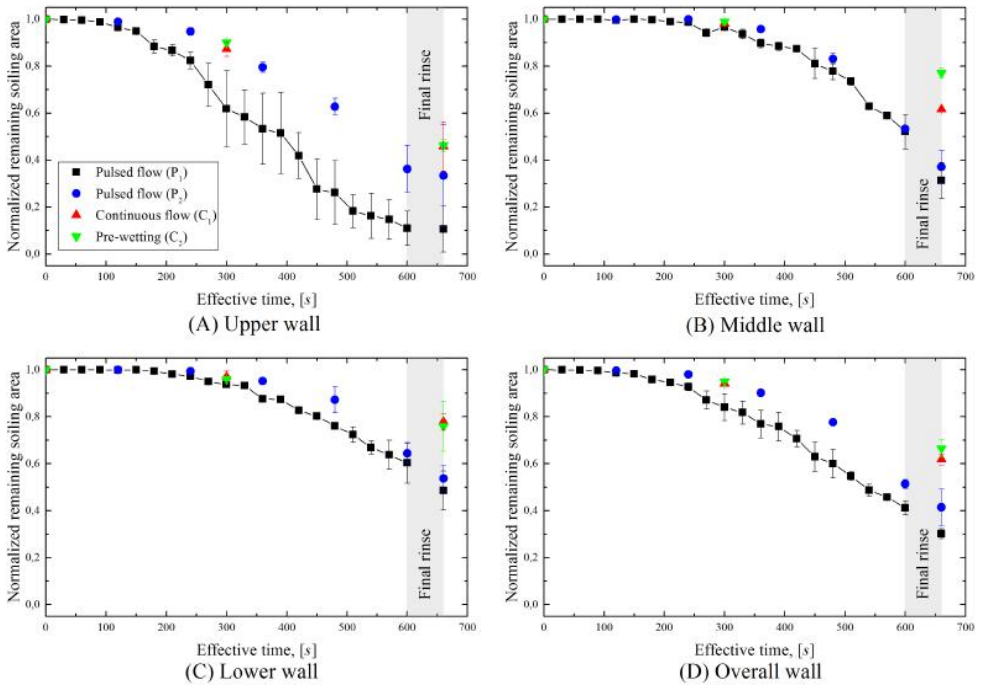

Figure 6.10: Comparison of cleaning cooked soils with different continuous and pulsed approaches: (A) tank upper wall surface, (B) tank middle wall surface, (C) tank lower wall surface, (D) tank overall wall surface. The cleaning conditions are: $T = 55$ °C, $FR = 1.5$ m^3/h, $C = 5$ kg/m^3.

6.3.6 Cleaning in a Large Scale Tank

Scale-up studies were performed in a 19 m^3 tank to examine the above-mentioned conclusions. The setup has been previously described by other researchers [78, 161]. Briefly speaking, the diameter of the test tank is 2.8 m (Figure 6.11A). A mobile CIP unit supplies liquid at pre-defined temperature and feed pressure. Egg yolk soils were spread on a separated bent plate using the same metal rod as in the pilot-scale experiments, forming soil layers of 1 mm thickness. A rectangle region of 55×24 cm^2 was marked for analysis, which was slightly smaller than the actual soiling area (Figure 6.11C). After three-day drying at room temperature, the plate was fixed on the tank wall and cleaned with help of a single axis rotary spray head (SaniMagnum 360°, Alfa Laval, Denmark), as illustrated in Figure 6.11B. The cleaning conditions were: NaOH concentration 1 or 5 kg/m^3, 25 ± 3 °C, 2 bar (corresponding to the flow rate of 11.4 m^3/h). The cleaning methods included continuous flow and pulsed flow (with a period of 60 s or 2 min). The effective cleaning time was 5 min. Most experiments were carried out once. One repetition of the burst cleaning at low NaOH concentration and low frequency proved the reproducibility of the experiments (5% difference). Therefore, the experimental error was assumed to be small,

taking ca. 10% by referring to the deviations in the pilot-scale experiments.

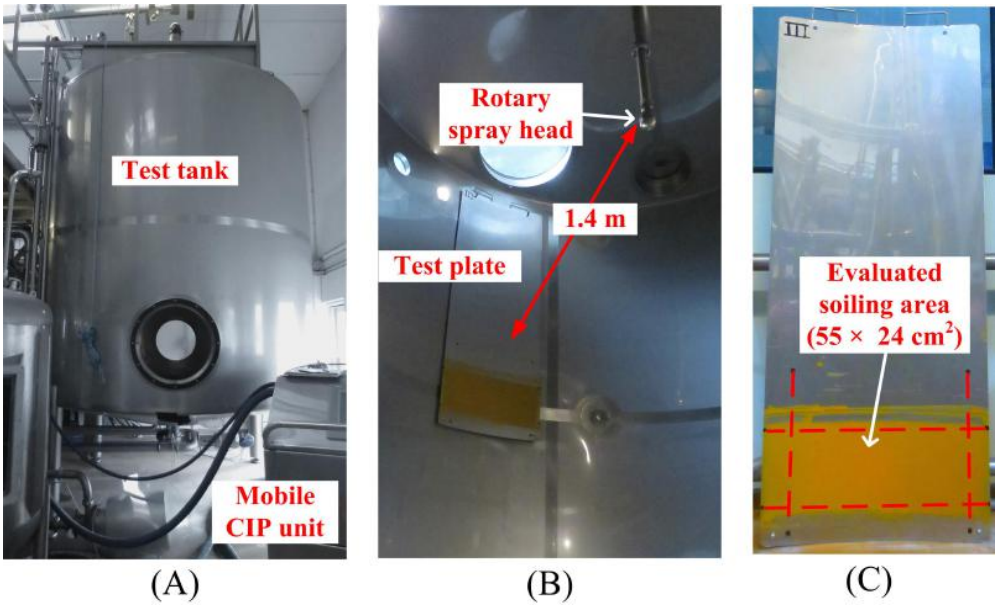

Figure 6.11: Photographs of the apparatus used for scale-up experiments: (A) the test tank, (B) the test plate and rotary spray head and (C) the investigated soiling area.

Figure 6.12 shows the photographs of the test plates using different methods. By comparing Figure 6.12B-D, the pulsed flow with a short period of 60 s removes all soils, leading to the best cleaning result at low NaOH concentration (1 kg/m^3). These results are consistent with the findings in pilot-scale tests. However, it is interesting to observe that the pulsed flow with the period of 2 min results in less cleanliness than the continuous flow, which can be attributed to reasonable experimental errors. As expected from previous findings, increasing the NaOH concentration to 5 kg/m^3 (Figure 6.12E and F) reduces the cleaning efficiency. Therefore, the conclusions drawn from pilot-scale experiments also apply to scale-up tests. That is, the pulsed flow with a short period and high frequency is the most efficient approach to remove egg yolk soils from the tank surfaces; high alkali concentration (up to 5 kg/m^3) contributes negatively to the removal of the studied soil type.

The above-mentioned work has shown that tank cleaning using pulsed flow offers an efficient approach to increase the usage efficiency of alkali solutions. Conventional burst cleaning practices can be further improved by shortening burst intervals and adding repetitions. The primary benefit of applying burst cleaning is to reduce cleaning costs and the environmental footprint. However, caution should be taken when generating bursts by frequent start-up and shut-down of pumps, because surge pressures are encountered when changing the pump between on-off status, which results in damages of centrifugal pumps and pipe systems. One solution to this problem is to equip a single seat valve with

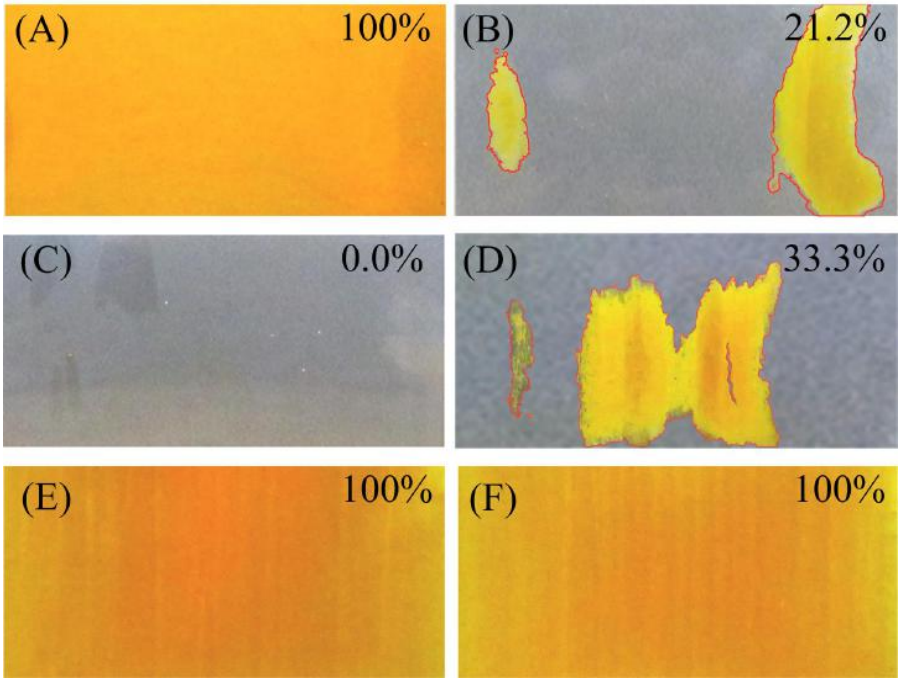

Figure 6.12: Photographs of the large scale test plate (evaluated area of 55 × 24 cm^2) (A) before cleaning, and after cleaning by (B) continuous flow at 1 kg/m^3 NaOH, (C) pulsed flow at 1 kg/m^3 NaOH with a period of 60 s, (D) pulsed flow at 1 kg/m^3 NaOH with a period of 2 min, (E) continuous flow at 5 kg/m^3 NaOH, and (F) pulsed flow at 5 kg/m^3 NaOH with a period of 60 s. The photos are taken after 5 min of effective cleaning time. The number on the upper right corners of each image indicates the percentage of soiling area, with ca. 10% deviation. To highlight the remaining soils, images (B) and (D) have been processed by blurring the plate surface to remove noises due to lighting.

a three body configuration (i.e. Alfa Laval Unique SSV Reverse Acting), which enables one flow channel to be closed while another channel is opened. As a result, the pump keeps running during the whole cleaning cycle, and the flow is switched between feeding and circulating. Another solution to protect facilities from frequent starting and stopping is to install a variable frequency drive (VFD) for controlling the gradual acceleration and deceleration of pumps, which avoids the damage caused by sharp alteration of pump status.

6.4 Conclusions

This study investigated the potential of using pulsed flow for improving the cleaning of tank surfaces soiled by egg yolk layers, as well as the effects of different process parameters (temperature, alkali concentration, flow rate) and soiling situations (denaturation or not)

on the cleaning results. The primary investigation was performed at pilot-scale, and the main findings were then examined in scale-up tests.

In the pilot-scale tests, the optimal conditions to remove egg yolk were low alkali concentration, high temperature and high flow rate. The interactions of alkali concentration with the other parameters affected the cleaning of the protein- and lipid-based soiling material as well. For a given effective circulation time of alkali solution, the remaining soiling areas, cleaned with continuous or pulsed flows, could be expressed using a second-order regression model. Pulsed flow with a high frequency resulted in more removal of soil deposits than that with a low pulsing frequency. The enhancement of cleaning by pulsed flow occurs primarily because the additional holding time is provided for soil layers to react and swell, which has the benefit that the materials become easy to remove in the next pulse of flow. Pre-wetting prior to continuous flow operation insignificantly improved the cleaning result. It was found that cooked soil material heated above its denaturation temperature made the soil more difficult to detach. However, the enhanced cleaning behavior by pulsed flow became more obvious when removing cooked soils.

The main findings at pilot-scale were also found in full scale tests. It was verified that the cleaning efficiency was highly improved by the pulsed flow with short period and high frequency. The negative contribution of high alkali concentration (5 kg/m^3) was still observed after scale-up. As a result, this work provided a quantitative measure to demonstrate that pulsed flow improves tank cleaning results by reducing the relative consumption of cleaning detergent in order to achieve a certain cleanliness.

List of Nomenclature in Chapter 6

The following nomenclature is only valid for this chapter. Some symbols are used in other chapters but with different meanings. Otherwise, the symbols are specifically explained in the text if there is no nomenclature in some chapter.

Roman Letters

c_P	Heat capacity of water, [J kg^{-1} °C^{-1}]
C	Alkali concentration, [kg m^{-3}]
F	F-value in ANOVA
FR	Flow rate, [m^3 h^{-1}]
P	P-value in hypothesis testing
P_f	Power of forward pump, [kW]
P_s	Power of scavenge pump, [kW]
T	Temperature, [°C]
T_0	Room temperature, [°C]
x_i	Actual variable i
X_i	Coded variable i
y	Normalized remaining soiling area
$\hat{y}$	Predicted value of y
$\tilde{y}$	Corrected term of $\hat{y}$

Greek Letters

β_0, β_i, β_{ij}	Coefficients in the second-order regression model
δ_i	Cleaning cost of item i
ϵ	Statistical error
ρ	Density, [kg m^{-3}]
φ_i	Unit cost of item i

CHAPTER 7

A Three-Stage Measurement-Based CIP System for Reducing Water Consumption

7.1 Introduction

In CIP operations, the terms recycling and recovery are to a certain extent identical, meaning that the cleaning liquid is reused more than once. Figure 7.1 illustrates three common CIP systems. For a single-use CIP system, the cleaning medium needs to be prepared freshly, and sent directly to drain after passing through the equipment and piping being cleaned. It reduces the possibility of cross-contamination and potential spore formation. However, it is expensive to operate. A partial recovery system recovers the detergent solution in the recovery tank for use in the next detergent or pre-rinse step. A full recovery system returns the cleaning fluid back to the supply tank [110]. Recovery systems are commonly applied in food industries because of lower energy requirement, lower water consumption and reduced chemical losses. Single-use CIP is normally seen where a high level of hygiene is required, like in the pharmaceutical industry [6].

Current CIP monitoring systems normally consist of conductivity probes, flow meters and temperature probes, etc., with the purpose to ensure that the system is under a state of control. The cleaning procedure is usually defined based on time, which means that the cleaning cycle starts when both temperature and conductivity measurements reach the critical points, and ends after a pre-defined period. If a recovery process is applied, the recovery starts when the conductivity output at the return flow reaches a set point or after the detergent has been added for a specific period [6]. However, a time-based CIP recipe generally consumes more resources than needed, because the allocated time

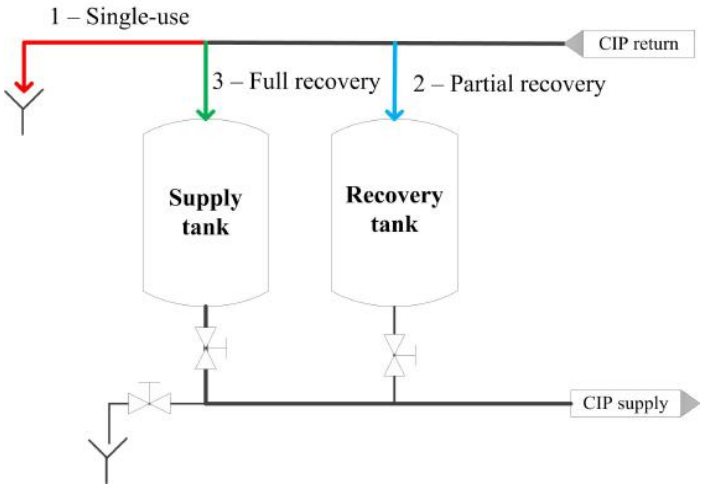

Figure 7.1: An illustration of common CIP systems for single-use, partial recovery or full recovery of cleaning liquid. For single-use and full recovery approaches, only one supply tank is required. For a partial recovery approach, two tanks are needed.

for cleaning is dictated by the worst case scenario. Therefore, a measurement-based CIP setup is potentially more efficient by performing cleaning based on need. In this way, the CIP cycle can stop when the system is clean, which may lead to reduced operating costs compared to a process based on time. A number of new CIP optimization systems have been developed to measure the residual level at the outlet or return flow [44, 58, 62, 66, 174]. The concept is to reduce cleaning time and water consumption by removing the ineffective cleaning phase when no pollution load is detected in the liquid phase.

The removal of deposits from a surface displays a tailing effect. That is, most of the soil materials are removed in the beginning and then the removal rate decreases until no more soil is removed, as discussed in Section 2.1.3 [34, 42, 58, 175]. As a result, the cleaning liquid contains lots of impurities initially, and becomes clearer and clearer toward the end of operation. Therefore, instead of only controlling the cleaning time, it is possible to further reduce water consumption by designing efficient recovery plans. In other words, the initial liquid with high pollution load can be sent to drain and only the clear liquid should be recovered and reused. In this way, most of the impurities are not accumulated in the recovery tank. As a consequence, the lifetime of the cleaning liquid can be prolonged. Meanwhile, the total volumetric loss of water is reduced. To the best of our knowledge, there are only a few studies, or at least very few publications, that discuss how to prolong the lifetime of recovered cleaning liquid. This knowledge gap is probably due to the fact that more attention has been paid to the benefits by improving the production efficiency, rather than attempting to achieve savings by reducing the cleaning costs.

This chapter investigates a measurement-based CIP system with special consideration of water recovery. Turbidity measurements are used as a tool to evaluate the quality of the

bulk cleaning liquid, which is a popular technique studied by many researchers [1, 58, 94]. The ultimate purpose is not only to reduce the cleaning time, but also to extend the lifetime of the cleaning liquid in order to reduce fresh water consumption.

7.2 Materials and Methods

7.2.1 Experimental Setup

The same pilot plant experimental setup as in Chapter 6 was used in this study, while the test modules were modified, as shown in Figure 7.2.

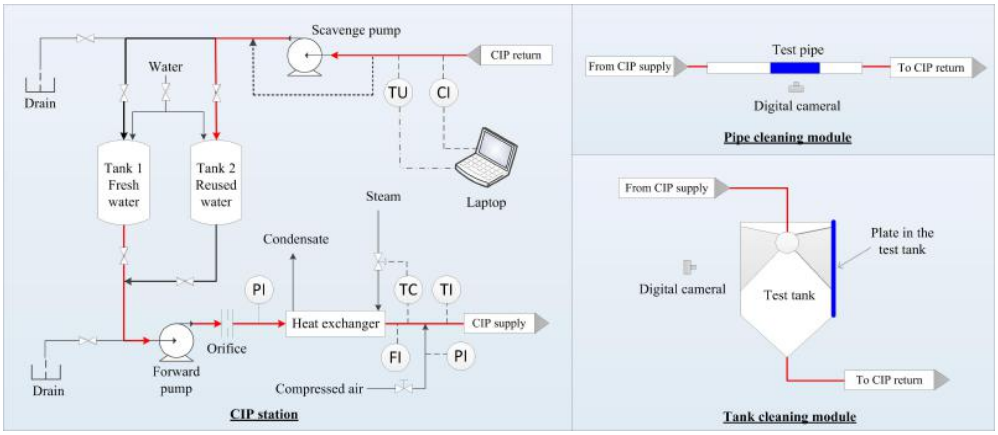

Figure 7.2: Pilot plant CIP system consisting of a CIP station, two test modules and a series of measurement points. The abbreviations include: PI - pressure indicator, FI - flow meter, TI - temperature sensor, TC – temperature controller, CI - conductivity sensor, TU - turbidity sensor.

The CIP station consisted of two tanks of 150 L to store the cleaning liquids, a frequency controlled CIP forward pump, a steam heat exchanger (though not used in the experiments) for controlling the temperature of the forward liquid, a scavenge pump to return the liquid, and various valves. Due to the large capacity of the forward pump, an additional exchangeable orifice was installed downstream of the forward pump in order to reduce the operating range. During the experiments, tank 1 was used to store fresh water, and tank 2 was used to store reused water. Compressed air was applied to remove any remaining liquid from the plant. The CIP station could be manually connected to the investigated testing modules through V-band clamps.

In this study, both pipe and tank cleaning operations were investigated. For pipe cleaning, two types of test pipes were made from transparent PVC and 316 stainless steel (SS), respectively. The pipes were 40 cm long with inner diameter 27.2 mm for PVC and inner diameter 29.6 mm for SS. To ensure a standardized flow through the test pipes, two

straight pipes of 1 m and 0.4 m length were inserted before and after the test section, respectively, which were larger than the requirement of a five-time-diameter length to stabilize flows [176]. After cleaning, the liquid was directed to the reuse tank or to drain bypassing the scavenge pump. For tank cleaning, the test tank (50 cm diameter, 55 cm height + 10 cm additional depth of a klopper torispherical bottom) surface was made from transparent PVC. To quantify and spread soils uniformly, two types of removable test plates were made from soft PVC and 304 stainless steel (50 cm height, 30 cm width). The SS plates were bend to the same radius as the tank wall. After soiling, the plates were fixed along the tank wall by two separated supports. The tank cleaning was performed with the help of a rotary spray head (the same as Figure 6.2). After cleaning, the liquid was led to the reuse water tank or to drain by the scavenge pump. A digital camera was used to record the tank cleaning and PVC pipe cleaning operations.

Apart from the steam valve, all valves were manually actuated. The CIP setup comprised two pressure indicators (PI), a flow meter (FI), temperature sensors (TI) and in addition to a controller (TC) for adjusting the steam flow to the heat exchanger. A conductivity sensor (CI, TetraCon 325, WTW, Weilheim, Germany) and a turbidity sensor (TU, STS01, Seli GmbH, Neuenkirchen, Germany) were installed at the outlet of the testing modules (ca. 50 cm away from the pipe module or ca. 1 m away from the tank bottom) and the data could be logged to a laptop for analysis.

7.2.2 Soiling

Mustard (First Price "staerk sennep") was used as model soil in all experiments. The ingredients were 48% water, 29% vinegar, 18% ground mustard seeds and 3% others. Per 100 g, the soil contained 4.8 g fat, 4.8 g protein, 3.5 g carbohydrate and 3.1 g salt. To soil the pipes, mustard was filled into the pipe. The two ends of the pipe were closed by two plastic caps. Then the filled pipe was weighed (w_1) and put immediately to the testing module after removing the caps. The two caps were weighed again (w_2), as some mustard stuck to the caps. The amount of mustard in the pipe was calculated as:

$$w_{soil} = w_1 - w_2 - w_0 \tag{7.1}$$

where w_0 is the weight of the dry pipe. The average mass of soils was 246.3 ± 3.3 g in the PVC pipe and 292.0 ± 13.1 g in the SS pipe.

To soil the plates, mustard was squeezed on the plate and spread out as smooth as possible using a glass wiper cleaning brush. The plate was only soiled from 5 to 45 cm height of the plate, because the top and bottom parts needed to be attached to the supports to be mounted on the tank wall. The mass of mustard was calculated as the difference between the weight of the plate before and after soiling, to be 115.1 ± 3.7 g, corresponding to 0.096 ± 0.003 g soil/cm^2 surface. The plate was left at room temperature for 3 hours. Then the plate was fixed to the tank wall for cleaning with the help of the supports.

7.2.3 Measurements

The cleanliness of cleaning water was measured by turbidity. The mustard residues on the surfaces could be visually observed or by analysing the recorded pictures. In addition, a swab-click-read method was applied to indicate whether protein residuals remained on the surface, which was performed according to the instruction manual of the Clean-Trace swab test (PRO100, 3M, Minnesota, US). The swab changed in color in the presence of protein. There are four degrees of color intensity that are used for assessing the degree of protein contamination: clean, questioned, contaminated, highly contaminated. In this study, only the first cleaning level was regarded as acceptable "clean".

Three cleaning levels were defined for different purposes:

1. Turbidity clean: The measured turbidity of the cleaning liquid at the return flow was below a user-defined criterion (20 NTU) and the cleaning liquid looked clear. As a reference, the turbidity of fresh cleaning water was ca. 3 NTU.

2. Visual clean: There was no visible mustard residue on the surface. However, very small traces could still exist.

3. Protein clean: There was no protein residue detectable on the test surface by using the swab-click-read method. The protein clean situation was assumed to be the true clean.

7.2.4 Cleaning

Mustard belongs to the group of weak soils which can be easily cleaned by only using water [59]. Therefore, only water was used as the cleaning agent. Two cleaning approaches were tested: (1) a single-use approach where fresh water was used and the cleaning water was not recycled, (2) a three-stage partial recovery approach where reused water was used for rinsing (first stage) and circulation (second stage), then fresh water was subsequently used with recovery (third stage). The procedures for the two approaches are described in Table 7.1. Considering practical issues, when performing the partial recovery experiments of plate cleaning, four SS plates and three PVC plates were tested alternatingly. All cleaning was conducted at room temperature.

7.2.5 Cleaning Costs

The costs of cleaning (δ_{CIP}) consisted of fresh water ($\delta_{Fresh\ water}$), heat (δ_{Heat}), electricity ($\delta_{Electricity}$), and the treatment of waste water ($\delta_{Waste\ water}$). If recovery was applied, the cost of water that was initially filled in the reused water tank ($\delta_{Initial\ fill\ in\ reused\ tank}$) was averaged into each operation by dividing with the number of times that the water was reused ($N_{Reuse\ times}$). A cost model of CIP is expressed in Equation 7.2.

$$\delta_{CIP} = \delta_{Fresh\ water} + \delta_{Waste\ water} + \frac{\delta_{Initial\ fill\ in\ reused\ tank}}{N_{Reuse\ times}} + \delta_{Electricity} + \delta_{Heat} \quad 7.2$$

Table 7.1: The cleaning procedures of single-use and partial recovery approaches

Single-use	Partial recovery
1. The forward pump started at a defined flow rate and timing started when liquid reached the test unit. The cleaning water was disposed to drain.	1. The first-stage rinse started at a defined flow rate by using reused water and timing started when liquid reached the test unit. The cleaning water was first disposed to drain (or collected in a bucket).
2. If performing tank cleaning, the scavenge pump started when the return pipe was filled with liquid.	2. When the turbidity measurement value was below a criterion (currently 100 NTU), the time was noted and the cleaning water started to be recycled through the reused water tank.
3. The cleaning process was performed.	3. The circulation was executed for 5 minutes for pipe cleaning, or 10 minutes for tank cleaning.
4. The forward pump was stopped when both turbidity clean and visual clean were reached. The scavenge pump was stopped when there was no liquid accumulation at the tank bottom.	4. The third stage rinse was performed by using fresh water (tank 1) for a duration that was not shorter than the length of the first stage rinse, until the turbidity value equalled the value of fresh water. The cleaning water was recycled to the reused water tank (tank 2).
5. The pipe or plate was dismantled for protein swab measurement.	5. Compressed air was injected to recycle liquid to the reused water tank.
	6. The liquid volume in the reused water tank and the amount of waste water were determined.
	7. The pipe or plate was dismantled for protein swab measurement.

In this study, no heat was used. Therefore, only the costs of fresh water, waste water treatment, initial water filling and electricity used by the pumps were considered. The unit costs of each item were the same as applied in Equations 6.5 and 6.7 in Chapter 6.

Four scenarios were defined in order to compare the cleaning costs by using different cleaning strategies, referring to Figure 7.1. Only the tank cleaning case was studied as an example for comparison.

- Scenario 1 - *Single-use*: The cleaning liquid was used once without recovery or reuse. The cleaning was performed by using fresh water and flushing for 15 minutes.
- Scenario 2 – *Full recovery*: The cleaning was performed by circulating water from

the reused water tank for 10 minutes. A final rinse was conducted by rinsing with fresh water for 5 minutes. All liquid was recovered.

- Scenario 3 – *Time-based partial recovery*: The three-stage partial recovery approach was applied. But there were no turbidity measurements to determine the rinsing time. The times for the first and third stages were both 5 minutes, which made sense because in industrial practices this time was set based on experience and the value was larger than the real demand. The circulation time was 10 minutes.

- Scenario 4 – *Measurement-based partial recovery*: The three-stage partial recovery approach used turbidity measurements to determine the rinsing time of the first stage. The third stage rinsing time corresponded to the first stage time. This scenario was the same as the partial recovery approach shown in Table 7.1.

7.3 Results and Discussion

7.3.1 Cleaning Time Against Flow Rate

In order to implement measurement-based CIP, it is desired that the surface is completely clean when the turbidity sensor detects a clear signal. In other words, the turbidity cleaning time should not be less than the visual cleaning time or even the protein cleaning time. Otherwise, the cleaning will stop erroneously even though the surface is still dirty.

The use of high flow velocities improves the cleaning performance and shortens the cleaning time by intensifying the local wall shear stress [102]. As shown in Figure 7.3A for pipe cleaning, the visual cleaning time at low velocity is much longer than the turbidity cleaning time, meaning that there are still harsh soils on the surface even though the bulk liquid is turbidity clear. The difference between visual cleaning time and turbidity cleaning time reduces with the increase in flow velocity. The turbidity cleaning time becomes larger than the visual cleaning time when the velocity is above 0.95 m/s, corresponding to a Reynolds number of 29,000. A further increase in flow velocity does not significantly contribute to reducing the cleaning time. The cleaning of SS pipes cannot be visually monitored on-line. However, when dismantling the SS pipes when the turbidity clean status is reached, large pieces of soils can still be observed on the inner pipe surface, as shown in Table 7.2. It means that for SS pipes the visual cleaning time is longer than the turbidity cleaning time, even at the largest investigated flow velocity. This attributes to the higher adhesion force of soil materials to the stainless steel surfaces than to PVC [177]. However, even though both the turbidity and visual clean status are finally achieved, the swab tests reveal that there are still protein traces remaining on the surfaces. Therefore, an even longer cleaning time is required than both turbidity and visual cleaning times in order to obtain complete cleanliness.

The turbidity cleaning times of plates are shown in Figure 7.3B. At 1 m^3/h, the turbidity cleaning time for PVC plate is shorter than for the stainless steel plate due to the tighter adhesion of the chosen soil on the SS surface [177]. However, the difference becomes insignificant at higher flow rates, which is in line with the observations in pipe cleaning

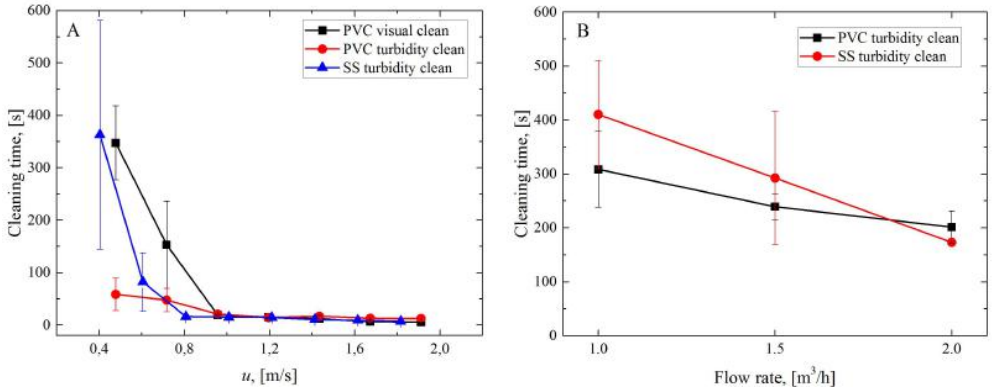

Figure 7.3: The cleaning time against the flow velocity/rate for (A) pipe cleaning and (B) tank cleaning by fresh water in single-use approach. The cleaning time and standard deviation were obtained from triplicate tests.

results as shown in Figure 7.3A. The soils are first removed from the top of the plate and later at the bottom (see Table 7.2), as the rotating spray head is closer to the top and results in relatively higher impact than at the bottom [6]. Cleaning stops when the turbidity value reaches the turbidity of fresh water. At this stage, there are still small amounts of visible soils present at the bottom of the test plates, as shown in Table 7.2. On the one hand, it is because the lower mechanical forces at the bottom impact the cleaning efficiency. On the other hand, the materials at the edges of the soiled area are drier than in the center due to a larger exposure surface and henceforth become even more difficult to clean.

Therefore, it can be concluded that only measuring the outlet liquid quality to determine the cleaning time is not safe enough even at the largest flow rate within the studied range. Longer cleaning time is required to completely remove soils from the surfaces. As a result, more fresh water will be consumed if the single-use approach is still retained.

7.3.2 Monitoring of Turbidity

The turbidity of water at the return flow during the single-use cleaning of the stainless steel plate is presented in Figure 7.4. The noise in the measurement signals is predominantly caused by entrained bubbles in liquid phase when the liquid is sucked from the tank bottom by the scavenge pump. The initial high turbidity and the subsequent long tailing with relatively low turbidity values indicate that the removal of soil materials occurs mostly at the initial stage. This trend is similar to the findings from Van Asselt et al. (2002) when monitoring turbidity during the cleaning of an evaporator in the dairy industry [58]. The cleaning time determined by the turbidity measurement decreases at high flow rates.

However, an unanticipated phenomenon occurs at the highest flow rate (2 L/min). That

Table 7.2: The results of visual observations and protein swab measurements when turbidity clean is achieved in rinsing water. All cleaning operations are performed by fresh water in single-use approach. The protein swab tests of plates are not displayed, as there are obvious soil deposits on the surfaces.

	Visual observation	Protein swab	Results
PVC pipe 1.43 m/s			The pipe is visual clean. But there are still inconspicuous traces on the surface. The protein swab reveals that the surface is still contaminated.
SS pipe 1.61 m/s			The pipe surface is still contaminated with soil residuals and protein even though the liquid is turbidity clean.
PVC plate 1.5 m^3/h		–	There are still soil deposits at the bottom of the PVC plate even though the liquid is turbidity clean.
SS plate 1.5 m^3/h		–	There are still soil deposits at the bottom of the SS plate even though the liquid is turbidity clean.

is, soil materials are observed on the surface of the rotary spray head after cleaning, which is caused by the bounced liquid. This means that the adhered soils on the cleaning device and accessory pipes can subsequently lead to contamination to the following processes. Even though cleaning devices are generally designed with self-cleaning capability [142], an extra amount of water is typically consumed to finish this task. Therefore, an excessively high flow rate should be avoided in this tank cleaning operation.

In common measurement-based CIP schemes, the period before the return liquid reaches the clean criterion is regarded as effective cleaning, after which it is regarded as unnecessary and ineffective cleaning. However, there are still possibly small amounts of deposits and traces on the surface when the turbidity measurement reveals a "clean" signal. One solution to achieve complete cleanliness is to continue rinsing using fresh water for a safe period until all traces are removed. But such an approach violates the original intention to control a CIP operation based on measurements, as more water will be consumed than what may be needed. Another solution to this problem is to apply a longer action by circulating reused water instead of fresh water, which is proposed in this study.

Figure 7.5 displays the water samples collected from the outlet of the test section. The liquid samples are less transparent and more turbid in the first four minutes. There are even visible deposits within the samples in the first two minutes. The samples taken from the fifth minute onward look as clear as fresh water, which means this water has

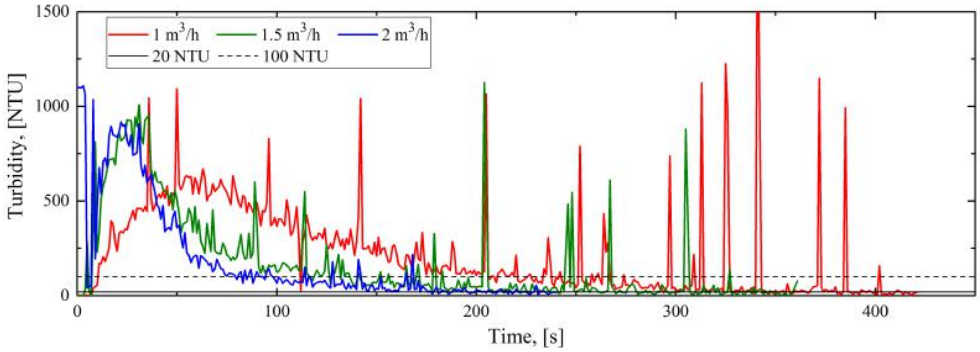

Figure 7.4: Monitoring of turbidity during the single-use cleaning of the stainless steel plate at different flow rates. The rinsing times for 1, 1.5 and 2 m^3/h are 7, 6 and 4 minutes, respectively.

the potential to be recycled and reused. Recycling too much water can accumulate soil in the liquid tank and shorten the lifetime of the reused water. Recycling a too low amount of water can cause unnecessary waste of high quality water and increase the operating costs. Therefore, it is meaningful to use turbidity as an indicator to assist in only recycling clear water, instead of dirty water. It is therefore necessary to define a turbidity criterion indicating when recycling starts. In this study, recycling starts when turbidity has reached a value below 100 NTU.

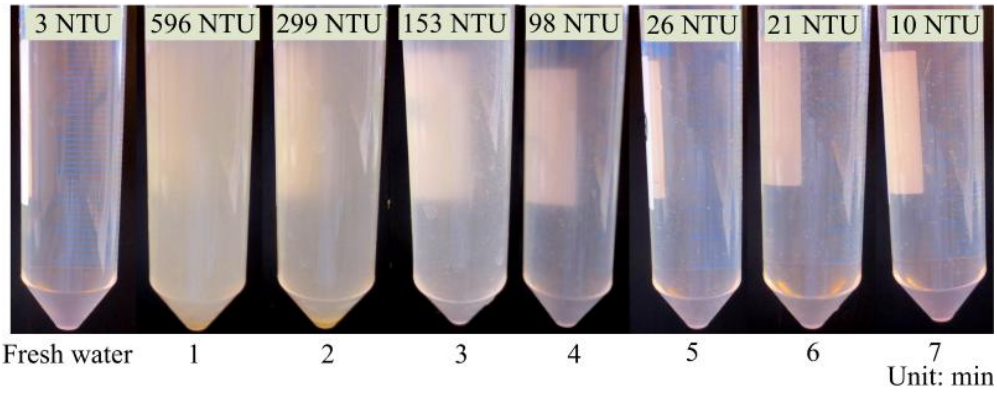

Figure 7.5: Visual observation of cleaning water samples collected from the outlet flow during the stainless steel plate cleaning at various cleaning times. The flow rate was 1 m^3/h. The labels on the pictures indicate the corresponding turbidity values of the water samples.

7.3.3 Recovery of Cleaning Water

The aim of this study is to implement a measurement-based CIP scheme combined with partial water recovery, as described in Table 7.1. It is anticipated that very low amounts of soils are accumulated in the reused water tank. In order to realize this purpose, the selected flow velocity should result in a turbidity cleaning time that is not shorter than the visual cleaning time. Besides, the optimal flow velocity for pipe cleaning is recommended to be larger than 1.5 m/s [6]. Therefore, the selected velocities are 1.67 m/s for the cleaning of PVC pipes (3.5 m^3/h) and 1.61 m/s for the cleaning of SS pipes (4 m^3/h) , respectively. The flow rate for tank cleaning is 1.5 m^3/h in order to avoid the adherence of soil materials on the surface of the cleaning device at higher flow rate.

It has been found that all tests using reused water can achieve the cleaning purpose, i.e., resulting in visually clean and protein clean surfaces. Table 7.3 demonstrates the partial recovery results in terms of the consumption of fresh water and the generation of waste water. The consumption of fresh water almost equals the generation of waste water. As a result, the volume of liquid in the reused water tank is nearly unchanged after several cleaning operations.

Table 7.3: Fresh water consumption and wastewater generation in partial recovery tests.

	Flow rate, [m^3/h]	Fresh water consumption, [10^{-3} m^3]	Waste water production, [10^{-3} m^3]
PVC pipes	3.5	15.45 ± 2.02	15.39 ± 1.35
SS pipes	4	10.32 ± 1.81	10.97 ± 1.89
PVC & SS plates	1.5	66.95 ± 9.19	65.60 ± 9.18

The turbidity of reused water increases after cleaning, as shown in Figure 7.6. After being reused for 10 times in pipe cleaning tests, the liquid still looks clear, meaning the liquid can be reused for more cleaning operations. For PVC pipes, the turbidity cleaning time is larger than the visual cleaning time. On the contrary, the visual cleaning time for SS pipes is larger than the turbidity cleaning time due to higher adhesion forces to the SS surface. If the recycle is controlled based on turbidity, there are more soils accumulated in the reuse water tank when cleaning SS pipes, leading to higher turbidity values in the recycled liquid. The turbidity of reused water for tank cleaning is higher than for pipe cleaning operations, because tank cleaning is more difficult than pipe flushing, especially at the tank bottom.

7.3.4 Comparing Cleaning Costs of Different Scenarios

Table 7.4 compares some practical issues and the resource consumptions by different cleaning scenarios defined in Section 7.2.5. The longest lifetime of reused water appears in the time-based partial recovery approach (scenario 3), as more fresh water is consumed than the measurement-based partial recovery approach (scenario 4). Both partial recovery scenarios keep a constant liquid volume in the reused water tank, which is very critical in industrial applications when considering the system stability and maintenance.

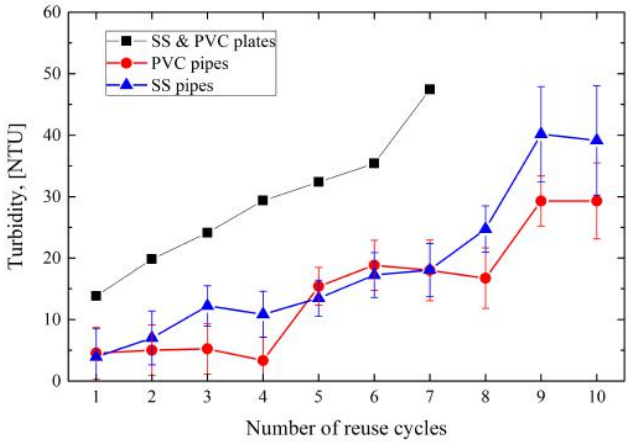

Figure 7.6: Turbidity of the reused water as a function of the number of reuse cycles.

A comparison of the operating costs of the different cleaning scenarios is summarized in Figure 7.7. Increasing the number of water reuse cycles reduces the operating costs, which, however, becomes less sensitive when the number of reuse cycles reaches a certain value. For all of the studied reuse cycles, the operating costs for the single-use approach (scenario 1) are much higher than for the recovery approaches, in spite of its potential to reduce cross contamination and spore formation. The measurement-based partial recovery approach leads to the lowest cleaning costs, because it results in the lowest fresh water consumption and waste water generation. It has been tested that the surface can be cleaned well (i.e., protein clean) when the rinsing time is over 15 minutes regardless of using fresh water or reused water. Therefore, even though the time-based partial recovery has a wider margin of safety than the measurement-based partial recovery due to the longer rinsing time, the real consumption in the time-based approach is actually more than needed.

The costs in Figure 7.7 are only presented for each cleaning operation. The costs for cleaning the reused water tank are not included. Once a full recovery approach (scenario 2) is applied, the water tank needs to be cleaned more frequently compared to applying partial recovery. However, in reality, cleaning the reused water tank is much easier and cheaper than cleaning the production tanks, because the dirt materials in the reused water tank are not as harsh as the product deposits.

The proposed three-stage partial recovery system in this study is investigated by only using water as cleaning medium. Similar approaches can also be applied to other cleaning steps with chemical treatment. In such as case a greater economic benefit can potentially be revealed. The concept of the measurement-based partial recovery approach is implemented to avoid the waste of fresh water in the fist-stage rinse and the third-stage rinse. If cleaning downtime is not a barrier for production, like in the brewery industry where fermentation takes one or two weeks but cleaning takes only hours, it is recommended to

Table 7.4: Comparison of tank cleaning for different scenarios. The flow rate was 1.5 m^3/h.

Scenario	Approach	Number of required tank(s)	Fresh water consumption, [kg/cleaning]	Waste water generation, [kg/cleaning]	Total cleaning time, [min/-cleaning]	Liquid volume in the reused water tank	Turbidity of water in the reused water tank	Reused water lifetime	Operation cost
1	Single-use	1	375	375	15	-	-	-	High
2	Full recovery	2	125	0	15	Increased	Highly increased	Short	Intermediate
3	Time-based partial recovery	2	125	125	20	Unchanged	Very slowly increased	Very long	Intermediate
4	Measurement-based partial recovery	2	∼67	∼67	∼16	Unchanged	Slowly increased	Long	Low

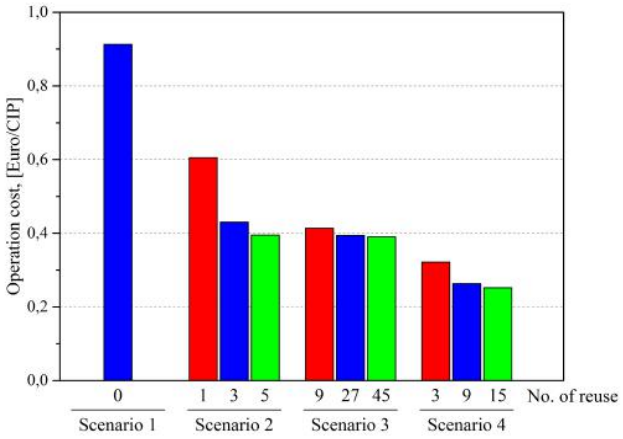

Figure 7.7: The cleaning operating costs for different scenarios for the tank cleaning at flow rate 1.5 m^3/h. Scenario 1: single-use; Scenario 2: full recovery; Scenario 3: time-based partial recovery; Scenario 4: measurement-based partial recovery. The selection of the number of reuse cycles are the approximations based on industrial practices or the capacity of the reused water tank.

circulate the cleaning liquid for longer time. The overall cleaning costs can be reduced by saving fresh water consumption and prolonging the lifetime of reused water. The costs of electricity consumption by the pumps are much lower than the costs of water (which has also been indicated previously by Figures 3.3 and 6.9). However, any change in the system and the reuse of water should be performed without compromising the cleaning quality.

7.4 Conclusions

Current measurement-based CIP operations aim to stop cleaning when the liquid phase is clean or when the quality of return liquid equals the quality of fresh liquid. Increasing the flow rate allows to reduce the cleaning time. However, inconspicuous traces can sometimes still exist on the surfaces to be cleaned even though the measurements indicate a "clean" signal. It is found that the cleaning water is very turbid in the beginning, and becomes clearer and clearer until the end of the cleaning operation. Therefore, it is a promising approach to recycle the clear liquid for reuse, in order to reduce the cleaning costs by extending the lifetime of reused water.

A three-stage measurement-based partial recovery approach is proposed in this chapter. In the first stage, reused water is used to remove bulk soils until the water quality reaches a pre-defined criterion. In the second stage, the fluid is circulated for a fixed period of time. The third stage uses fresh water for a duration that is not less than the first

stage, with all water recovered. As a result, the overall cleaning is performed for a sufficient period of time without increasing the consumption of fresh water. The water volume in the reused water tank keeps unchanged. So the cleaning water can be reused several times. The lifetime of the reused cleaning water can be prolonged by avoiding the accumulation of impurities in the reused water tank. Four scenarios are studied to compare the operating costs by conducting single-use or recovery approaches. The results reveal that the proposed measurement-based partial recovery allows savings between 30-70% of the cleaning costs compared with other approaches.

Even though the proposed approach is developed by only using water as cleaning medium, it is possible to apply this approach to other cleaning steps, where chemical solutions are used. Especially, the proposed procedure can be used for processes where cleaning downtime does not restrict the production efficiency.

List of Nomenclature in Chapter 7

The following nomenclature is only valid for this chapter. Some symbols are used in other chapters but with different meanings. Otherwise, the symbols are specifically explained in the text if there is no nomenclature in some chapter.

Roman Letters

$N_{Reuse\ times}$	Number of reuse cycles, dimensionless
w_0	Weight of dry pipe, [g]
w_1	Weight of filled pipe with caps, [g]
w_2	Weight of filled pipe without caps, [g]
w_{soil}	Weight of soil, [g]

Greek Letters

δ_i	Cleaning cost of item i

CHAPTER 8

Cleaning of Toothpaste from Vessel Surfaces by Impinging Liquid Jets and Falling Films

In the work presented in this chapter, the removal of a toothpaste soil from flat glass surfaces by using impinging liquid jets and falling films were studied. The model for the adhesive removal of soil layers by impinging water jets presented by Bhagat et al. (2017) [178] was applied to the case of toothpaste removal. This work was performed in collaboration with Professor Ian Wilson at the Department of Chemical Engineering and Biotechnology at the University of Cambridge in the UK, during my research visit to Ian's group in the summer of 2018. The author greatly appreciates the thoughtful discussions with Professor Wilson and Ph.D students Rajesh Bhagat, Rubens Rosario Fernandes and Melissa Chee in Cambridge.

8.1 Introduction

Liquid jets are widely used in cleaning operations to remove soil materials from internal tank surfaces or open surfaces of process equipment. Common jet devices for tank cleaning operations include the static spray ball and the rotary jet head, as described in Table 2.3. The selection of a suitable jet device relies on the design and process for which the surface is to be cleaned.

The flow pattern and cleaning behaviour associated with a single liquid jet have been investigated. These studies can be mainly categorized into two groups, as discussed in Section 2.5: (i) cleaning in the impingement area generally studies the flow behaviour and cleaning dynamics around the impingement point where the jet hits the surface [78, 80, 178, 179]; (ii) cleaning by falling films focuses on cleaning below the impingement point where the liquid flows down under gravity and wets a vertical or inclined wall [82,

83].

Wilson et al. (2012) presented a simple model of the radial flow region to predict the hydraulic jump radius and the minimum width of falling film based on momentum balances [72]. In the model of Wilson et al. (2012), the flow in the radial flow region is treated as a laminar film with parabolic velocity profile, which was revised by Bhagat et al. (2016) to include the development of laminar and turbulent boundary layers in the thin film [73]. The flow model has been used to develop an adhesive removal model to compute the momentum force at the cleaning front of soft-solid soil layers [75] and viscoplastic soil layers [77]. The removal model has been extended to include nozzle movement [76] and an angle of the jet to the wall [180]. Liquid losses due to jet breakup were included in an effective flow rate term when being applied for industrial tank cleaning [78].

This chapter applies the adhesive removal model reported by Wilson et al. (2014) and Bhagat et al. (2017) to the cleaning of a new soil type, namely toothpaste. In addition to considering cleaning by static and moving jets, as investigated in previous studies, this chapter develops the model by including the effect of soil soaking, and extends the model to the cleaning by falling films.

8.2 Model Description

8.2.1 Impinging Jet Introduced Flow Patterns

The flow pattern generated by a horizontal jet impinging on a vertical surface is illustrated in Figure 8.1. A radial flow zone (RFZ) is formed around the impingement point, where the liquid moves rapidly outwards and terminates at a hydraulic jump. In the RFZ, the effect of gravity is negligible. So the schematic in Figure 8.1A applies to a vertical jet impinging on a horizontal surface as well. Beyond the RFZ, gravity becomes the dominant force and the liquid flows downwards to result in a transition film zone. A rope or corona with varying thickness forms above the RFZ, containing the liquid from the hydraulic jump. The falling film is driven by gravity. It features two regions: (i) the outer bounding flow, which is the extension of the rope above the corona, and (ii) the inner section, here termed the core, of width W_c and thickness less than the rope. Further details of the falling film are given by Wang et al. (2013) [80, 83]. In cases where downward momentum is smaller than surface tension, the film width may narrow gradually to a thin tail, called rivulet flow, or the film splits, creating a dry patch (see Figure 2.5). The formation of different falling film types depends on flow properties and surface characteristics. In this study, only glass surfaces are used, where water flows stably out a long distance downwards before narrowing to a tail. Therefore, a pseudo stable gravity falling film of constant width is assumed.

The aim of this work was to develop a cleaning rate model for toothpaste, based on the adhesive removal theory reported by Wilson et al. (2014) and Bhagat et al. (2017) [75, 178]. The parameters of the model were obtained from the cleaning of soil materials using static impinging jets. Then the model and the parameters were applied to the cleaning of soil using moving jets and falling films.

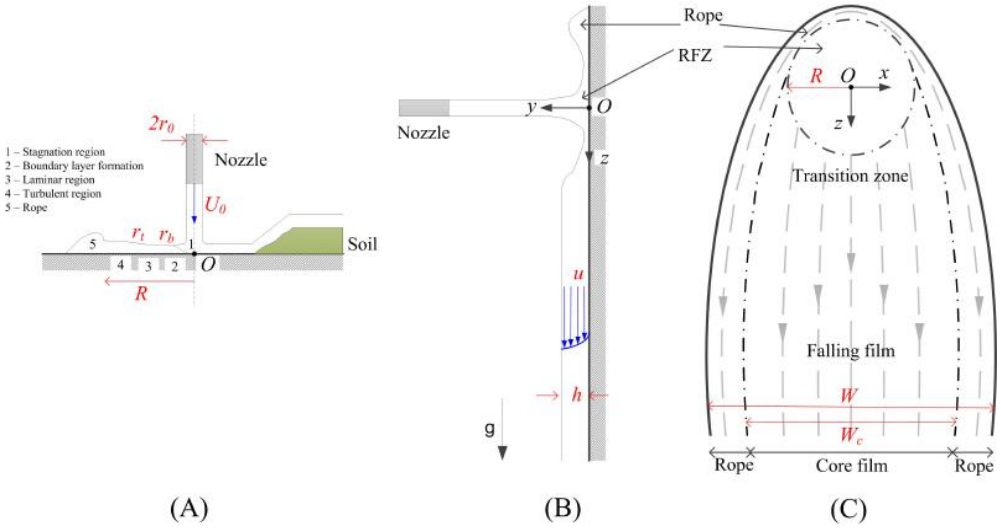

Figure 8.1: Schematic of the flow pattern formed by a horizontal impinging jet on a vertical wall: (A) radial flow zone with (right) and without (left) soil, (B) side view of radial flow zone and falling film, (C) front view of the radial flow zone and falling film. O marks the jet impingement point.

8.2.2 Adhesive Removal Model

According to the adhesive failure theory, the rate of removal is determined by the force acting on the soil at the soil-surface-liquid contact line [75]. The force is assumed to be the momentum in the liquid film at the cleaning front. The removal rate is given by:

$$\frac{da}{dt} = k'(M - M_y) \tag{8.1}$$

where a is the distance to the cleaning front from the impingement point at time t; k' is a lumped cleaning rate constant; M and M_y are the momentum of liquid per unit width and the yield momentum of soil that should be overcome for cleaning, respectively. The value of k' is related to the soil layer thickness and the soaking time. Since the same soil thickness was employed in the cleaning experiments in this study, there are two assumptions here: (i) k' is only dependent on soaking time t_{soak}, and (ii) the relationship between k' and t_{soak} is a linear dependency. Thus, the following equation reads:

$$k' = k_0 + k_1 \cdot t_{soak} \tag{8.2}$$

where k_0 and k_1 are constants, obtained through fitting experimental data. The momentum of liquid per unit width is calculated from:

$$M = \int_0^h \rho u^2 dy \tag{8.3}$$

where h is the water film thickness; ρ and u are the density and velocity of water, respectively. In the work of Wilson et al. (2014) [75], the yield momentum per unit width of the material, M_y, was not considered when cleaning soft-solid soils (polyvinyl acetate, xanthan gum, petroleum jelly) from polymethylmethacrylate (Perspex) and glass plates. Elsewhere, the term M_y was found to be important in the cleaning of viscoplastic materials [77], which are similar to the toothpaste soil used in this work. Here, since toothpaste is water soluble, the term M_y is assumed to be dependent on the soaking time as well.

8.2.3 Cleaning Model of Static Jet

Figure 8.1A illustrates the film flow around the impingement point on a vertical or horizontal flat surface. As shown in the left schematic of Figure 8.1A, the flow can be divided into four regions: (1) the stagnation region, (2) the boundary layer formation region (BLFR), (3) the laminar region, and (4) the turbulent region. The radial flow zone terminates at the hydraulic jump due to a balance between momentum and surface tension [73]. Beyond the jump liquid forms a rope.

In the stagnation region, the flow velocity equals the jet flow velocity U_0. In the BLFR, the local velocity grows from 0 at the non-slip wall across the boundary layer of thickness δ, above which is the stagnation region with a constant velocity U_0. The BLFR ends at radius r_b where the boundary layer reaches the film surface. Beyond r_b the liquid flows in a fully developed laminar film, which eventually becomes turbulent at r_t. The turbulent flow region ceases when the hydraulic jump occurs at R. The critical values of δ, r_b, r_t and R are given by Equations 8.4 to 8.7. The calculations of the momentum per unit width M used in this work are presented in Table 8.1, with more details given by Wilson et al. (2012) [72] and Bhagat et al. (2016) [73].

$$\delta = 2.12\sqrt{\mu r/\rho U_0} \tag{8.4}$$

$$r_b/d = 0.24{Re_j}^{1/3} \tag{8.5}$$

$$r_t/d = 0.2964{Re_j}^{1/3} \tag{8.6}$$

$$R = 0.276\left[\frac{\dot{m}^3}{\mu\rho\gamma(1-\cos\theta)}\right]^{1/4} \tag{8.7}$$

Here r is the radial coordinate, $\dot{m}$ is the mass flow rate, γ is the surface tension between liquid and vapour, and θ is the contact angle. The jet Reynolds number is defined as $Re_j = \rho d U_0/\mu$, with μ denoting the dynamic viscosity of the liquid.

8.2.4 Cleaning Model of Moving Jet

In the case where a horizontal jet strikes a moving vertical plate or vice versa, the point of impingement moves across the plate at a velocity v_{jet}. A roughly elliptical cleaning front ahead of the impingement point was modelled by Wilson et al. (2015) [76] and Glover et al. (2016) [77]. A moving coordinate system was applied so that the point of impingement was static and the soiled plate moved up or down at velocity $-v_{jet}$, as described in Figure 8.2. Point X, located at a distance a_X ahead of the jet impingement

Table 8.1: Summary of equations for calculating film thickness h, surface velocity U_s, velocity profile u and momentum per unit width M in the radial flow zone when cleaning by static jet. The equations are derived according to Bhagat et al. (2016) [73].

Regions	h, U_s and u	Momentum per unit width M
BLFR $r < r_b$	$h = 0.125/r + 1.06(rd/Re_j)^{1/2}$ $U_s = U_0$ $u = \begin{cases} U_0 f(\eta) & y < \delta \\ U_0 & y \geq \delta \end{cases}$	$M = \rho {U_0}^2 h - \rho {U_0}^2 \delta (C_1 - 1)$
Laminar $r_b < r < r_t$	$h = d\left[\frac{3.792}{Re_j}\left(\frac{r}{d}\right)^2 + 0.1975\left(\frac{d}{r}\right)\right]$ $U_s = \frac{U_0}{8C_2 \frac{hr}{d^2}}$ $u = U_s f(\eta)$	$M = C_1 \rho {U_s}^2 h$
Turbulent $r_t < r < R$	$h = \frac{0.0209d}{{Re_j}^{1/4}}\left(\frac{r}{d}\right)^{5/4} + (0.296 - 0.001356{Re_j}^{1/2})\left(\frac{d^2}{r}\right)$ $U_s = \frac{4Q}{7\pi r h}$ $u = U_s \eta^{1/7}$	$M = \frac{\rho \frac{64}{63} \frac{Q}{2\pi} U_0}{r\left[\frac{0.167}{{Re_j}^{0.125}}(\frac{r}{d})^{9/4} + (2.37 - 0.0108{Re_j}^{1/2})\right]}$

The equations used for calculation				
$\eta = y/\delta$	$f(\eta) = \eta - \frac{3}{2}\eta^2 + 4\eta^3 - \frac{5}{2}\eta^4$	$C_1 = \int_0^1 f(\eta)^2 d\eta$	$C_2 = \int_0^1 f(\eta) d\eta$	

point, is a stationary point where the cleaning rate equals the nozzle velocity. At point P, oriented at angle β to the direction of nozzle movement and at distance p from the origin, resolving the motion at steady state yields a non-linear differential equation [76].

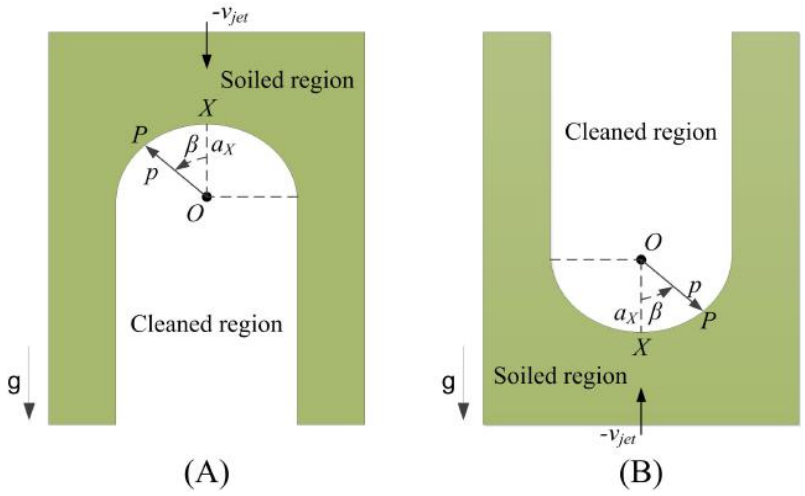

Figure 8.2: Model geometry for moving a horizontal nozzle impinging on a vertical plate. A moving coordinate system is applied so the point of impingement is static and the soiled plate moves downwards or upwards. (Reproduced based on Glover et al. (2016) [77])

Bhagat et al. (2017) provided three moving jet models to quantify the cleaning rate for different soil types, namely weak soils, strong soils and intermediate strength soils, according to the magnitude of p in Figure 8.2 [178]. In all cases, the cleaning front at point X obeys:

$$\frac{da}{dt} = v_{jet} \tag{8.8}$$

The relative strength of soils is associated with the flow pattern in the radial flow zone (see Figure 8.1A). That is, weak soils feature a large cleaning radius so the flow pattern at the cleaning front is nearly laminar or turbulent; strong soils result in a small cleaning radius, within the growing boundary layer. Different flow models apply in the two regions. The intermediate strength soils lie between weak soils and strong soils.

For an intermediate strength soil, the distance to the cleaning front at X, a_X, can be calculated by Equation 8.9:

$$\frac{da_X}{dt} = v_{jet} = \frac{\sigma}{a_X(A + Ba_X^3)} \tag{8.9}$$

where σ, A and B are groups of parameters related to the cleaning rate: $\sigma = 3k'\dot{m}U_0/5\pi$, $A = 1 - 10\pi\mu r_0/3\dot{m}$, $B = 10\pi\mu/3\dot{m}r_0^2$. Setting $p^* = p/a_X$ and $b_X = A/Ba_X^3$, the shape

of the cleaning front can be written in a dimensionless form as:

$$\frac{dp^*}{d\beta} = \frac{1}{\sin\beta}\left(\frac{b_X + 1}{b_X + p^{*3}}\right) - \frac{p^*}{\tan\beta} \tag{8.10}$$

The initial condition is that $p^* = 1$ at $\beta = 0$. The only unknown parameter needed to solve Equation 8.10 is the cleaning rate constant k', which can come either from the inspection of data generated by a static cleaning nozzle or by fitting the experimental results of the cleaning by moving jets. The cleaning models for other soil strengths can be found in Bhagat et al. (2017) [178].

8.2.5 Cleaning Model of Falling Film

The falling film is assumed to be laminar flow with a parabolic velocity profile:

$$u = \frac{\rho g}{2\mu}(2hy - y^2) \tag{8.11}$$

The average velocity in the film (U_{av}) is:

$$U_{av} = \frac{1}{h}\int_0^h u dy = \frac{\rho g h^2}{3\mu} \tag{8.12}$$

Based on Equations 8.3, 8.11 and 8.12, the momentum of film per unit width can be calculated via:

$$M = \frac{6}{5}\rho U_{av}^2 h \tag{8.13}$$

The water film thickness h can be calculated based on some assumptions. In Nusselt's theory, the film is purely viscous so a flat surface is assumed [84]. The mean film thickness is:

$$h_{Nusselt} = \left(\frac{3\mu q}{\rho g}\right)^{1/3} \tag{8.14}$$

where q is the volumetric flow rate per unit width; g is the gravitational acceleration term. The right term in Equation 8.14 can be re-written as the wetting rate of a falling film according to Equation 2.1. However, it has been found that wave inception occurs to liquid at a low flow rate. According to Kapitza's theory of wavy flow, the parabolic velocity profile also applies but the mean film thickness is given by [85]:

$$h_{Kapitza} = \left(\frac{2.4\mu q}{\rho g}\right)^{1/3} \approx 0.928 h_{Nusselt} \tag{8.15}$$

Therefore, based on Equations 8.14 and 8.15, the Nusselt film is ca. 7% thicker than the Kapitza film. For water, Nusselt's and Kapitza's theories are valid when the film Reynolds number ($Re_f = 4\rho q/\mu$) is less than 1,160 [85]. Since ropes exist on both edges of the falling film, with a thickness much larger than the core film (as indicated in Figure 8.1C), only the momentum per unit width in the core film region is calculated. In the core film, the volumetric flow rate per unit width q is estimated by $q = f_c Q/W_c$, where the width of core film W_c comes from experimental observations. The fraction of volumetric flow rate in the core film f_c is assumed to be 50% of the overall volumetric flow rate Q by ignoring flow splash [80].

8.3 Materials and Methods

8.3.1 Rheology

The rheology of the toothpaste (Advanced White, Colgate, US) was measured on a rotational rheometer (Kinexus lab+, Malvern Panalytical, UK) using a parallel plate measuring system at 20 °C with 1 mm gap. The solid content of the toothpaste sample was 62.1 ± 4.5 % w/w. The measurements included undiluted or diluted (10–50 % extra water weight) toothpaste samples without a pre-shear, as well as undiluted toothpaste with a pre-shear at 5 Pa for 3 min (referring to Table 8.3). The selection of pre-shear conditions referred to the wall shear stress of the falling film at the studied flow rate range (ca. 3 Pa). Firstly, an oscillatory time sweep applied an amplitude oscillation stress of 0.1 Pa at a frequency of 1 Hz for 3 min in order to probe the understanding of the viscous and elastic characteristics of the materials. Then, a stress sweep increased the stress from 0.25 Pa until the material yielded. The hysteresis of the original sample was also studied to test the macro- or micro-structural rearrangement of the material with time. It was carried out with shear rate initially ascending and subsequently descending between 0.01 and 100 s^{-1}.

8.3.2 Millimanipulation

The millimanipulation device has been described by Magens et al. (2017) [181]. As shown schematically in Figure 8.3, the toothpaste sample was spread on a glass plate (5×5 cm) with a known thickness of δ_{soil}, and pushed by a blade at a set velocity v_{blade} with a defined gap distance to the plate surface δ_{gap}. In reality, the blade was static but the soiled plate mounted in a chamber moved towards the blade at $-v_{blade}$, where the minus sign means the plate moving velocity is opposite to the pseudo blade velocity. The force imposed on the blade was measured by a force transducer (HBM S2M, Germany). The width of the blade tip W_{blade} was 0.140 ± 0.017 mm, scanned by a confocal thickness sensor (CTS, IFS 2405-3, Micro-Epsilon, Germany) system. More details of the device can be found in Magens et al. (2017) [181].

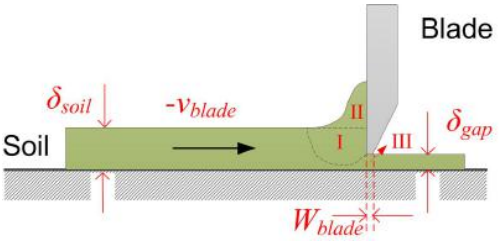

Figure 8.3: Schematic of the millimanipulation device. In the experiments, the blade is static and the soiled plate moves towards the blade. Three regions denote the three components of the measured force: (I) to deform the material, (II) to displace the deformed material, (III) to overcome the shear resistance in the gap.

Millimanipulation was performed to investigate the removal force by varying soil thickness, gap distance, and soil types (soaked or not). Measurements were made at different blade velocities (0.1, 1, 5 and 10 mm/s). To prepare the soaked soil sample, the chamber where the soiled plate was mounted was filled with deionized water and emptied immediately after 3 min using a syringe. In the measurement, the soil deformed and accumulated in front of the blade, as indicated in Figure 8.3. The force measured by the sensor included three components: (i) that to deform materials ahead of the blade, (ii) that to displace the deformed materials, and (iii) that to overcome the shear resistance under the tip of the blade. The shear force per unit width (region III in Figure 8.3), $F_{W,\,shear}$, could be determined through the shear stress (τ) by:

$$F_{W,\,shear} = \frac{\tau A_{blade}}{L_{blade}} = \frac{\eta_{app}\dot{\gamma} L_{blade} W_{blade}}{L_{blade}} = \eta_{app}\dot{\gamma} W_{blade} \tag{8.16}$$

where the apparent viscosity η_{app} was read from the rheology measurement at a given apparent shear rate $\dot{\gamma} = v_{blade}/\delta_{gap}$. A_{blade} and L_{blade} were the area and the length of the blade tip, respectively. The combined force of deforming and displacing the soil materials ahead of the blade was defined as the normal force (regions I and II in Figure 8.3), determined by:

$$F_{W,\,normal} = F_W - F_{W,\,shear} \tag{8.17}$$

The design of the experiments in the millimanipulation test is shown in Table 8.2.

Table 8.2: Investigated millimanipulation test conditions. All tests were made at different blade velocities from 0.1 to 10 mm/s.

Investigated parameters	Fixed parameters	Varied parameters
Soil thickness	Soil: original toothpaste $\delta_{gap} = 100$ µm	δ_{soil} =200, 500, 700 µm
Gap distance	Soil: original toothpaste $\delta_{soil} = 500$ µm	δ_{gap} =50, 100, 200, 400 µm
Soil type	$\delta_{gap} = 50$ µm $\delta_{soil} = 500$ µm	Soil: original toothpaste and toothpaste soaked for 3 min

8.3.3 Impinging Jet Apparatus and Experimental Design

The pilot-scale apparatus has been previously described by Glover et al. (2016) [77]. The test plates were transparent glasses (360 × 600 mm, 150 × 150 mm), which were used as vertical or horizontal walls, respectively. The plates were coated by toothpaste before being mounted prior to cleaning. Even soil layers were prepared by dragging a blade over the plate with fixed and known clearance between the blade and the plate. The resulting soil layers were approximately 500 µm thick and a mass coverage 0.059 ± 0.004 g/cm^2 on the plates.

Cleaning experiments were performed immediately (with ca. 3 min preparation) after soiling in order to avoid drying. Cleaning was performed with water jets generated

by a brass nozzle of 2 mm diameter (d). The nozzle position could be adjusted to be horizontal or vertical, perpendicular to the test plate. Single-use deionized water at room temperature (22 ± 2 °C) was used in all tests. In all experiments, an interrupter was located between the nozzle and the soiled plate initially while the flow was set and stabilized. The interrupter was then removed and timing started.

Video recordings of jet impingement and cleaning were made by placing the camera (Nikon D3300 D-SLR, Japan) on the reverse side of the vertical plate or above the horizontal plate. Images were processed using the image analysis toolbox in Matlab (MathWorks, US).

Three cleaning approaches were performed: cleaning by static jets, cleaning by moving jets, and cleaning by falling films. The details of each cleaning approach are introduced in the following sections.

8.3.4 Film Thickness

Falling film thickness was measured by the CTS system. The principle of measuring multiple layer thickness is that the sensor projects a polychromatic white light spot on the target transparent surface, focusing each wavelength at a specific distance with controlled chromatic aberration (see Figure 8.4). The sensor receives the light that is reflected from each interface and transfers it to the controller (ConfocalDT controller 2461, Micro-Epsilon, Ortenburg, Germany). Spectral analysis is then conducted to calculate the distance between the interfaces and therewith the thickness of each layer [182].

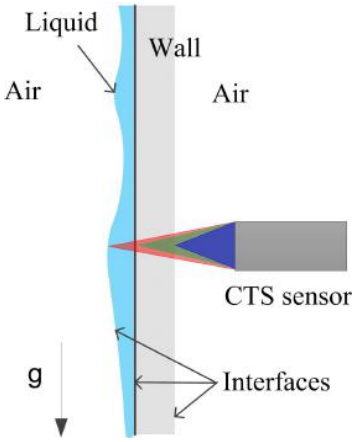

Figure 8.4: CTS system for measuring gravity film thickness.

The measurement was performed by impinging water on a vertical plate made from transparent Perspex (thickness ca. 5 mm). The flow rate was 2 L/min. The sensor was installed on the opposite side of the plate and 15 cm below the impingement point. The system could only measure the film thickness at one fixed point at a time. The CTS

was fixed on a manual translation stage, and the sensor moved horizontally to measure the film thickness at discrete locations. The measurement spanned the film region from one rope to another, sampling at an interval of every ca. 2 mm. The sample frequency was 10 Hz. The film thickness was determined as the average value over a ca. 20 s span.

8.3.5 Cleaning by Static Jets

The glass plate of dimension 150 × 150 mm was used in static jet cleaning tests. The soiled plate was placed horizontally in a basin, and located on aluminium blocks to get a ca. 2 cm gap from the bottom. Both non-soaked and soaked soils were studied. In order to soak the soil prior to cleaning, deionized water was poured into the basin to submerse the soiled plate. The water was removed after 1–10 min.

The flow rate was 2 L/min ($Re_j = 21,200$). The vertical jet impinged on the soil layer directly in the centre of the plate. The digital camera was placed above to record the cleaning process.

One more test with a vertical plate and a horizontal jet was performed in the same condition to clean non-soaked soil in order to investigate the effect of gravity on the cleaning performance by the impinging jet. A circular cleaning front was found in all tests. The variation of the radius of the cleaning front was analysed.

8.3.6 Cleaning by Moving Jets

The large glass plate of dimension 360 × 600 mm was soiled and mounted vertically on an aluminium frame. The nozzle remained horizontal and stationary. The plate moved upwards (1.25 cm/s) or downwards (1.5 cm/s), driven by a motor in order to generate relative motion between the plate and the nozzle.

The jet could impinge initially either directly on the soil layer, or above/below the soil region, as illustrated in Figure 8.5A-C. Two different cleaning phenomena were created, which are discussed later.

Only non-soaked soil was studied when the plate moved downwards (the jet moved relatively upwards). Both non-soaked and soaked soils were investigated when the plate moved upwards (the jet moved relatively downwards).

To soak the soil, a falling film was generated by impinging water above the soiled region for 1 or 2 minutes, as illustrated in Figure 8.5A. No soil was removed during the two-minute soaking period, and the soil layer was covered by a water film. After soaking, the upward movement of the plate began. The digital camera was placed on the reverse side of the transparent plate to record the cleaning process. The width of the cleaning path and the shape of the cleaning front were analysed.

8.3.7 Cleaning by Falling Films

The large glass plate was mounted vertically on an aluminium frame, with a soiled region 15 - 30 cm below the impingement point, as shown in Figure 8.5A. The examined flow

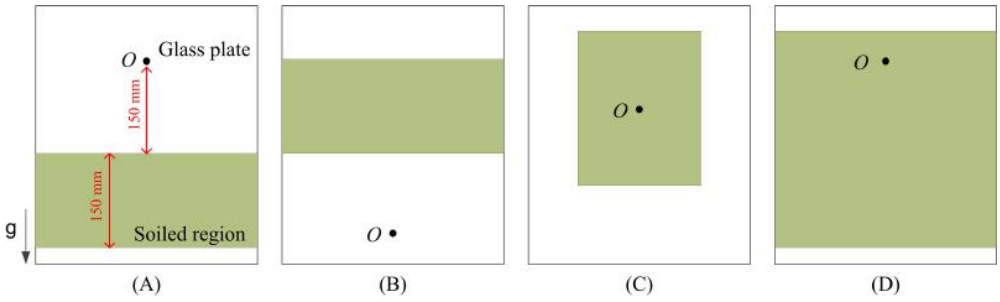

Figure 8.5: Four soiled regions and impinging points in the experiments of cleaning by moving jets and falling films. (A) Impinging above the soiled region, for the cleaning when the nozzle moves downwards (plate moves upwards) and the cleaning only by falling films. (B) Impinging below the soiled region, for the cleaning when the nozzle moves upwards (plate moves downwards). (C) Impinging on the soiled region, for the cleaning when the nozzle moves either downwards or upwards (plate moves either upwards or downwards). (D) Cleaning a plate where the whole surface is covered by toothpaste.

rates ranged from 0.6 – 2.5 L/min, corresponding to jet Reynolds numbers of 6,300 – 26,500. The video recorded from the reverse side of the plate was analysed to determine the progress of cleaning.

The plate could be divided into cleaned and uncleaned regions (see Figure 8.6). The cleaning occurred by three different means: (i) falling films, (ii) ropes and (iii) flow channels. Cleaning by ropes happened very quickly due to a larger flow rate in these regions compared with the core film. Flow channels appeared spontaneously in all tests, by which soil materials were removed slower than by ropes but faster than by core falling films. An example for the development of flow channels is provided in Appendix C.

Morison et al. (2002) used a wetting rate term to quantify the peripheral mass flow rate by $\Gamma = \dot{m}/W$ [82]. In this chapter, a revised definition of the wetting rate in the core film was given by $\Gamma_{core} = f_c\dot{m}/W_c$. The wetting rate in the ropes was estimated by $\Gamma_{rope} = (1 - f_c)\dot{m}/[(W - W_c)/2]$. The resulting wetting rates in the studied flow rate range were $\Gamma_{core} = 0.064 - 0.012$ kg/(m s) and $\Gamma_{rope} = 0.192 - 0.451$ kg/(m s). The wetting rate in flow channels lay in between the two ranges.

Only cleaning times within the core film region were analysed. As illustrated in Figure 8.6, the core film region was divided into a series of 1×1 cm squares. The cleaning time was manually determined in two ways: the grid-based cleaning time $t_{clean,\,grid}$ denoted the time when the vertex of grids became clean (i.e., the intersections of the vertical lines and horizontal lines in Figure 8.6); the line-based cleaning time $t_{clean,\,line}$ denoted that the cleaning front reached the respective horizontal line. Therefore, at a given height, $t_{clean,\,grid}$ contained groups of cleaning times including the information of cleaning by both core film and flow channels. $t_{clean,\,line}$ was only one time value that was required to clean the harshest soil by core film at the height.

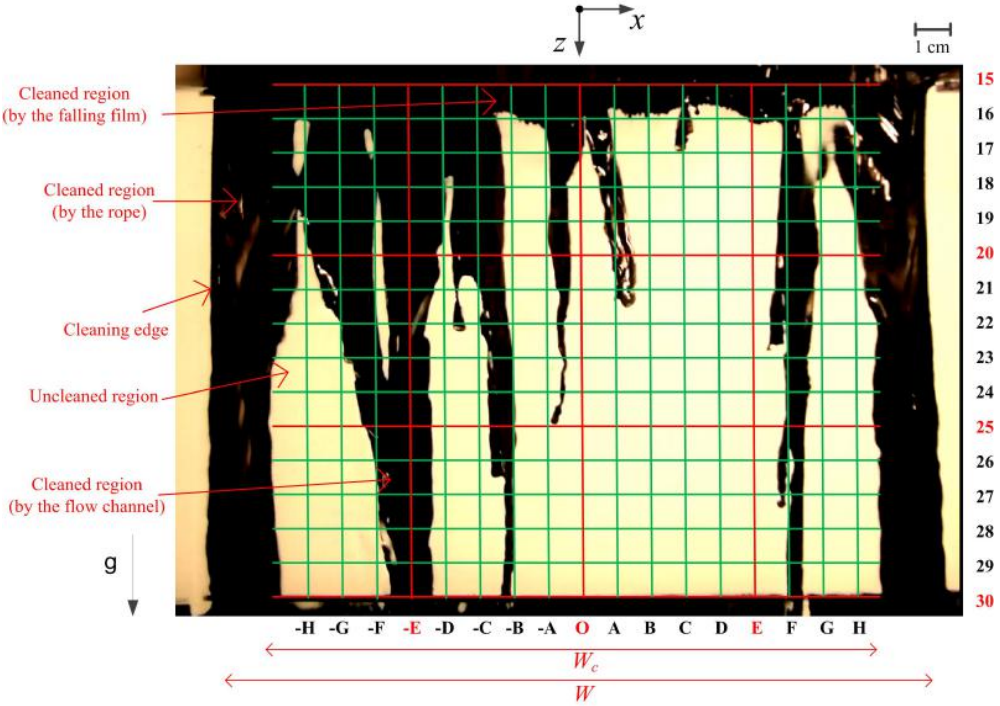

Figure 8.6: Example of cleaning by falling films. The soiled region was a rectangular board from 15 - 30 cm below the impingement point. The flow rate was 2 L/min, and the cleaning time was 200 s. Dark regions are cleaned areas.

8.4 Results and Discussion

8.4.1 Rheology Measurement

Figure 8.7 shows the rheological properties of the toothpaste. In the oscillatory time sweep measurement, the elastic modulus (G') and viscous modulus (G'') are nearly constant within the measurement period. Therefore, Figure 8.7A shows the average shear modulus at different dilutions or solid contents. A higher G' than G'' indicates that the toothpaste can be regarded as mainly elastic at the low shear stress. After dilution, both the elastic and viscous modulus decreases, implying that less force is required to deform the material. Pre-shearing can reduce both shear moduli, but the effect is less significant than dilution. The results for the apparent viscosity are shown in Figure 8.7B. The undiluted and diluted toothpastes exhibit shear thinning behaviour, meaning that the apparent viscosity decreases with the increase in shear rate. The hysteresis of the undiluted sample indicates a permanent deformation of the material. Dilution can significantly change the apparent viscosity of the material. However, pre-shearing the material at 5 Pa for 3 min does not affect the apparent viscosity very much.

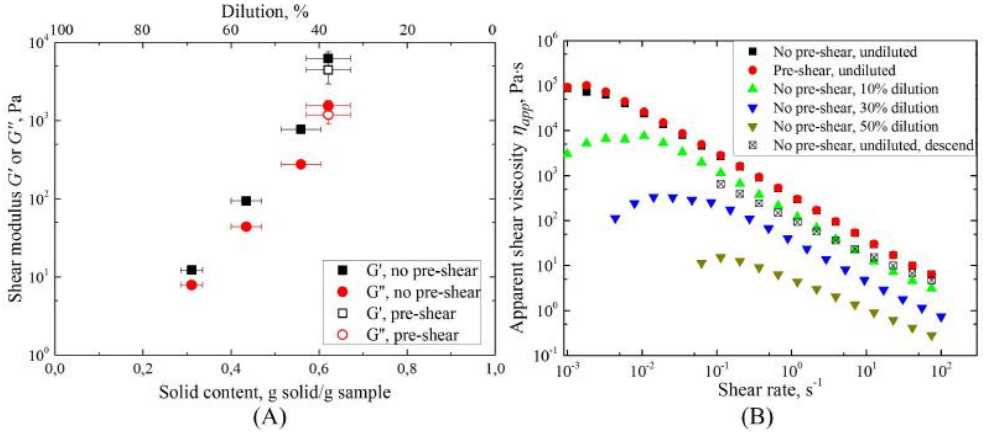

Figure 8.7: (A) shear modulus of toothpaste samples measured by oscillatory time sweep at a constant oscillation stress of 0.1 Pa and a frequency of 1 Hz and (B) stress sweep of toothpaste samples, and the hysteresis of the original toothpaste. Ascending shear stress was applied in the measurements if not identified as "descend".

The measured phase angle ($\chi = \arctan(G''/G')$) and yield stress are presented in Table 8.3. The yield stress is determined as the shear stress at which the apparent viscosity starts to decline sharply in the "shear stress vs. viscosity" plot (not shown). According to Table 8.3, diluting toothpaste reduces the yield stress extremely. As a result, the deposit becomes easier to remove after dilution or soaking.

Table 8.3: Rheological properties of toothpaste materials

Samples	Phase angle χ, [°]	Yield stress τ_y, [Pa]
Without pre-shear, undiluted	13.7 ± 0.8	179 ± 1
With pre-shear, undiluted	15.2 ± 1.6	160 ± 6
Without pre-shear, 10% dilution	19.4 ± 0.2	66.5 ± 7.5
Without pre-shear, 30% dilution	24.9 ± 0.3	15.3 ± 0.7
Without pre-shear, 50% dilution	32.8 ± 0.2	1.65 ± 0.05

8.4.2 Millimanipulation Measurement

Figure 8.8A displays the shear force (Equation 8.16) and normal force (Equation 8.17) against the removal force determined by millimanipulation. The scale of the normal force is much larger than the scale of the shear force, meaning that more than 99% of the measured force is applied to deform and displace the soil in front of the blade rather than to overcome the shear force under the blade tip. The measured millimanipulation force per unit width, F_W, increases with the increase in the soil thickness ahead of the blade ($\delta_{soil} - \delta_{gap}$) and the blade velocity (v_{blade}). An arrangement of the measurement

data in Figure 8.8A demonstrates that the measured removal force is proportional to the volumetric removal rate of soil that is displaced by the blade, as presented in Figure 8.8B.

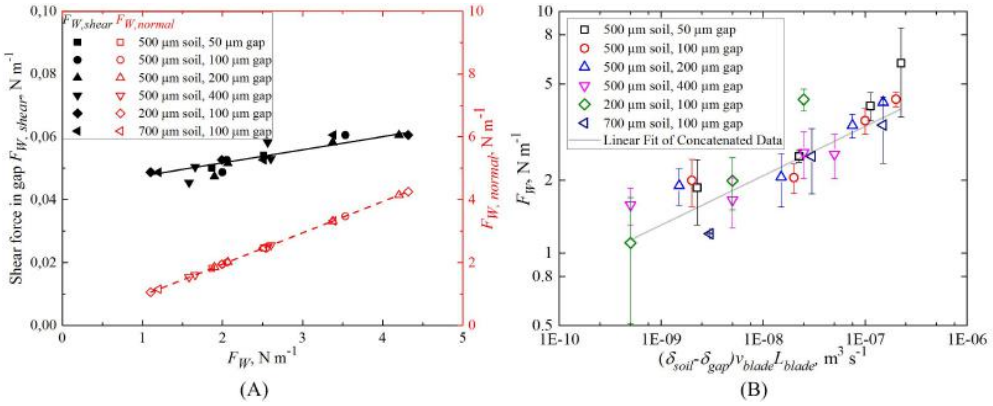

Figure 8.8: (A) Shear force and normal force against the force measured by millimanipulation and (B) displaced volume of toothpaste against the force measured by millimanipulation. The error bar indicates the standard deviation of at least three measurements.

The impact of soaking is assessed by comparing F_W to remove original toothpaste with the force to remove the soil that has been immersed in water for 3 min prior to manipulation. According to Figure 8.9, the removal force decreases significantly after soaking. There are noticeable amounts of residual materials on the test plates after the blade has passed, indicating that the adhesive force between soil and surface is relatively larger than the cohesive bound within the soil matrix. The amount of remaining toothpaste declines after soaking. Therefore, both the adhesive and cohesive interactions have decreased greatly. The results are in line with the findings by other researchers who observed a reduced removal force after immersing a carbohydrate-fat food soil in a detergent solution for a set time [26].

8.4.3 Cleaning Behaviour - Static Jet

Figure 8.10A summarises the cleaning rate of the toothpaste layer (δ_{soil}=500 µm) on a horizontal plate by a vertical jet at a fixed flow rate (2 L/min). The toothpaste samples were soaked for different times before cleaning was started. The momentum per unit width (M) in the horizontal axis of Figure 8.10A is calculated using the equations in Table 8.1. According to Equation 8.1, the slopes and intercepts in Figure 8.10A represent the cleaning rate constant k' and the product of k' and the yield momentum term M_y, respectively.

As shown in Figure 8.10B, the value of the cleaning rate constant increases significantly after soaking, which can be expressed as a linear function using the soaking time t_{soak} as

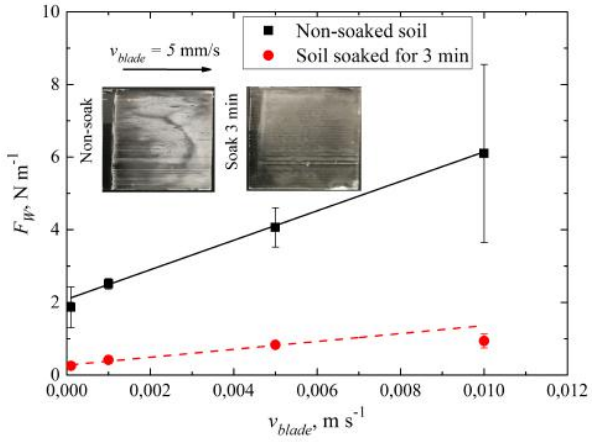

Figure 8.9: Effect of soaking on the force measured by millimanipulation. The photographs show the remained soils after measurement. The soil thickness is 500 µm. The gap distance of the blade is 50 µm. The error bar (the error bars for some points are too small to see) indicates the standard deviation of at least three measurements.

variable. The intercept term $k'M_y$ rises and drops with the soaking time. The value of M_y can be computed as the quotient of the intercepts and slopes of fitting curves from Figure 8.10A. M_y decreases with soaking time, which can be expressed by an exponential function. However, as indicated in Figure 8.10B, the deviations of M_y are extremely larger than the absolute values because the errors of k' and $k'M_y$ can be propagated to the calculation of M_y. Therefore, it is reasonable to summarize the decreasing trend of M_y against soaking time, but the exact values are subject to high uncertainty.

One more test of cleaning original toothpaste from a vertical plate by a horizontal jet confirmed that the cleaning rate constant does not change with the jet direction (data not shown). Hence, the resulted k' values from Figure 8.10B can be employed to cleaning toothpaste from vertical plates.

For most experiments in Figure 8.10 (except the cleaning with soaking for 10 min), the radius of the cleaning region grows as a circle with cleaning time, then forms unstable fingers (see Figure 8.11), finally terminates at a maximal radius. The radius where fingers start to appear and the corresponding momentum per unit width are plotted in Figure 8.11. When a finger forms, the water film passes underneath the soil layer and rolls the soil up. The finger radius, which is smaller than the radius of the hydraulic jump, increases linearly with the soaking time. The hypothesis is that the appearance of fingers is related to the stability of fluid at the liquid-liquid interface [183] and the yield momentum of soil material. However, the existing study cannot provide enough evidence to test the hypothesis. More investigations are required to explain the mechanism of finger formation, which, however, is not within the scope of this study.

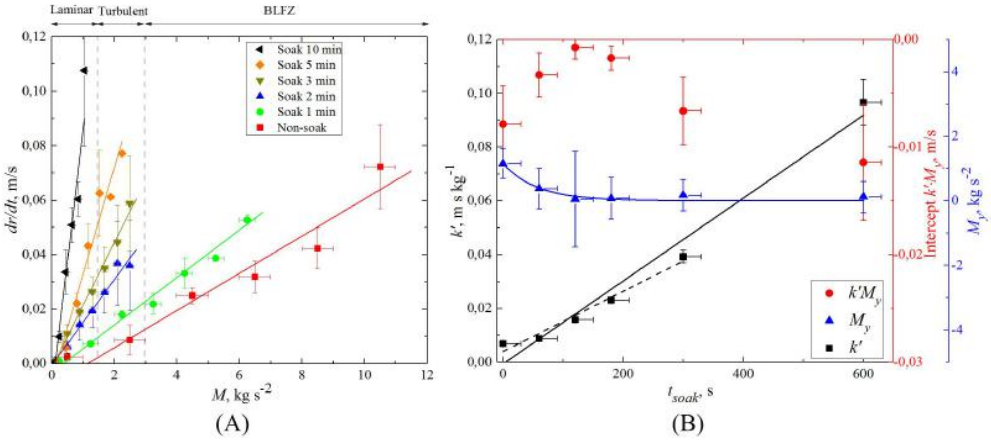

Figure 8.10: (A) Cleaning rate of toothpaste samples by static jets, plotted against the momentum per unit width. The slopes of fitted curves give the lumped cleaning rate constant k'. (B) Effects of soaking time on the lumped cleaning rate constant k', the intercept $k'M_y$ and the yield momentum required to clean the soil material, M_y.

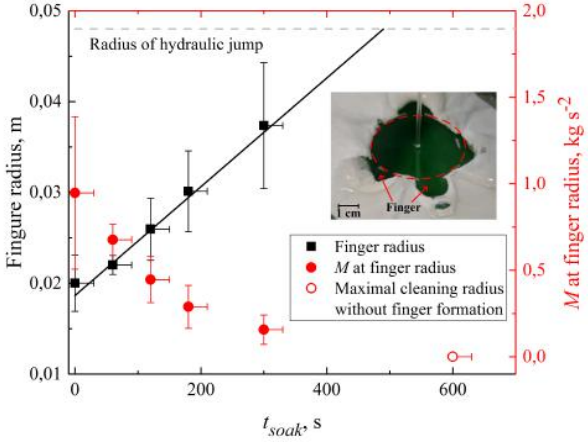

Figure 8.11: Effect of soaking time on the radius when the figure starts to form, and the momentum at the onset of figure radius. The photograph displays an example of a finger.

8.4.4 Cleaning Behaviour - Moving Jet

The cleaning of non-soaked toothpaste by moving jets occurs by two mechanisms:

1. When the water jet initially impinges outside the soiled region and moves towards the soil, the thin water film can invade the interface between the soil and plate surface, detaching the soil layer via roll-up (Figure 8.12A&C).

2. When the water jet initially impinges on the soil layer, the material is dislodged and yields an inclined cleaning front (Figure 8.12B&D). The area is much smaller than the removal by roll-up. This mechanism is the same as presented in previous studies where the adhesive removal model was investigated by other researchers [75, 76, 77].

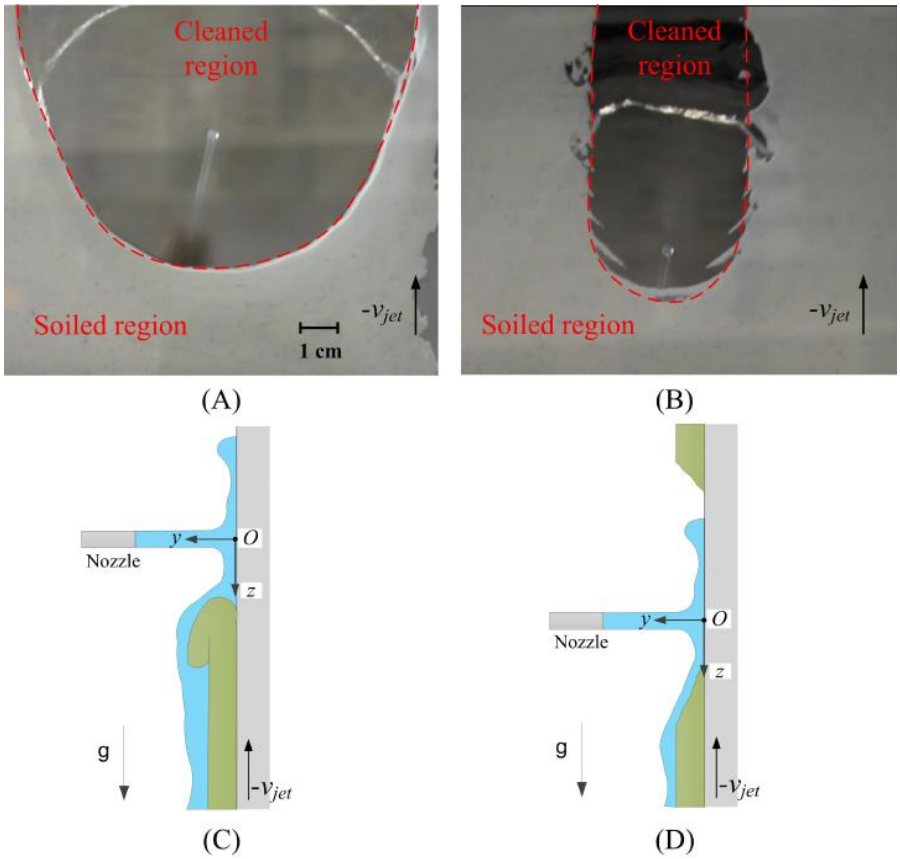

Figure 8.12: Two mechanisms of cleaning non-soaked toothpaste by moving jets: (A) and (C) are roll-up when the jet initially hits outside the soiled region; (B) and (D) are adhesive removal when the jet initially hits the soiled region. (A) and (B) are photos recorded in experiments. (C) and (D) are schematic diagrams of two mechanisms.

When impinging water above the soiled region for 1 to 2 minutes with a static nozzle, the soiled region is covered by water films but no soil is removed. This phenomenon is discussed in Section 8.4.6. When the nozzle moves down afterwards, only adhesive removal occurs. Therefore, only the cleaning results by adhesive removal are analysed further.

Bhagat et al. (2017) defined three soil types (weak, strong, intermediate strength) when developing the adhesive cleaning model by moving jets [178]. However, the criterion to distinguish a soil type is still empirically determined. All of the three models have been considered to fit the cleaning of toothpaste in this study, taking the values of k' and M_y from the results of cleaning by static jets in Figure 8.10B. It is found that the model for intermediate strength soil type (using Equations 8.9 and 8.10) gave the best fit to the experimental results, as presented in Figure 8.13.

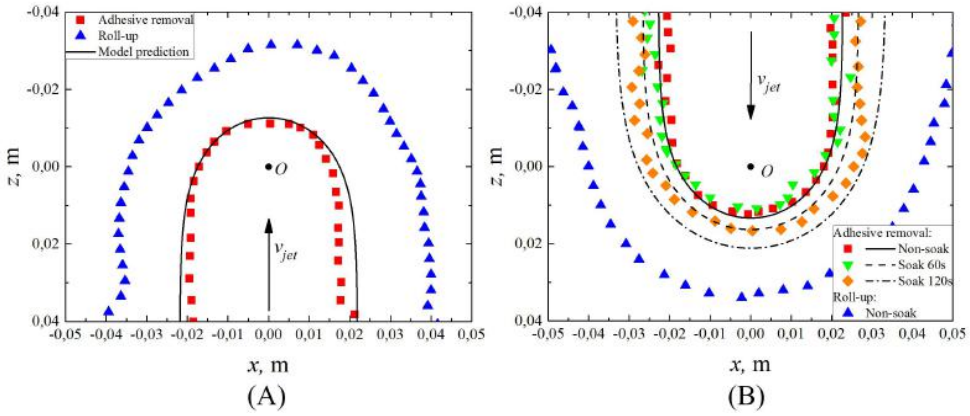

Figure 8.13: Shape of the cleaning front obtained by experiments and predictions: (A) plate moves downwards at 1.5 cm/s (jet moves upwards); (B) plate moves upwards at 1.25 cm/s (jet moves downwards).

The predicted cleaning widths for soaked soils when the jet moves downwards (Figure 8.13B) are slightly larger than the experimental observations. There are two explanations for the over-prediction of the cleaning width of soaked toothpaste. First, when the soil is soaked, the material becomes weaker and thereafter the intermediate strength soil model does not apply. However, the weak soil model given by Bhagat et al. (2017) still predicts larger cleaning radii than the measurements (data not shown). Second, it can be associated with the incomplete soaking by a falling film (Figure 8.13B) compared to the complete soaking achieved by submerging soils in water (Figure 8.10). As a result, using the cleaning parameters from the cleaning by static jets can over-estimate the actual cleaning rate when the soils are soaked by falling films.

Therefore, the moving jet model combined with the intermediate strength soil model presented by Bhagat et al. (2017) can well predict the cleaning width of non-soaked toothpaste, but slightly over-predicts the cleaning width of soaked toothpaste.

8.4.5 Measurement of Film Thickness

Figure 8.14 shows the film thickness measured using the CTS on a Perspex plate. The presence of ropes is evident on both edges of the film. The mean thickness of the core

film is nearly constant, which agrees well with the thickness predicted by the Kapitza film model (Equation 8.15). The Nusselt film model (Equation 8.14) slightly over-predicts the film thickness by ca. 17%, indicating that the waves on the falling film need to be considered to accurately compute the film thickness. Regular wavy flow was observed during all cleaning experiments. This is reflected in the percentiles of film thickness presented in Figure 8.14. In the core film, most thickness measurements ($75^{\text{th}}/25^{\text{th}}$ percentiles) lie within 8% of the average thickness measured by the CTS. The intensity of waves denoted by the difference of the 99^{th} and 1^{st} percentiles is ca. 160% of the average film thickness.

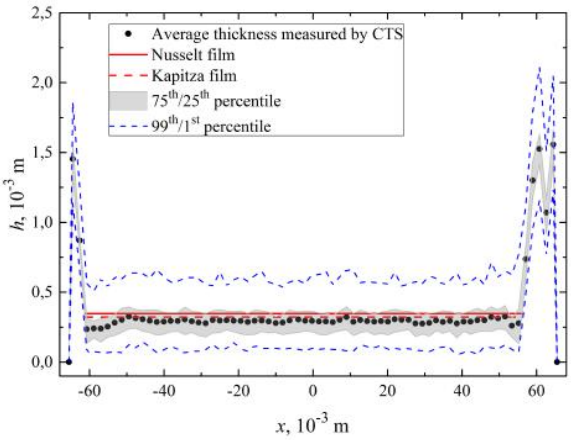

Figure 8.14: Film thickness determined by the CTS system. The plate material is Perspex; the flow rate is 2 L/min; the measurement location is 15 cm downstream of the impingement point. The Reynolds number in the core film is $Re_f = 70$. The $75^{\text{th}}/25^{\text{th}}$ percentiles can represent the measurement range of most samples. The $99^{\text{th}}/1^{\text{st}}$ percentiles can represent the maximal and minimal film thickness, respectively.

In Figure 8.14, only two points are measured for the left rope compared to five points for the right rope. This is because the CTS thickness measurement sensor can only determine the distances from the sensor lens to the different interfaces as illustrated in Figure 8.4. The thickness of the transparent plate and the liquid film are calculated as the distance between two relevant interfaces. However, the range of liquid film measurements by the CTS is limited to ca. 3 mm, which is still related to the distance to the plate and the thickness of the transparent plate. The other measurements for the left rope are discarded since the local rope thickness is beyond the measurement range or measured with high uncertainty.

8.4.6 Cleaning Behaviour - Falling Film

Figure 8.15A displays a typical result of cleaning times in the core film. Channel flows (indicated in Figure 8.6 and Appendix C) were present in all cleaning tests, contributing

to fast cleaning in some areas. The location and size of the flow channels were random when repeating the experiments. As a result, the number of grid vertexes cleaned by flow channels varied between batches. It is found in Figure 8.15A that there are more grids cleaned by channels at the top area (small z) than at the low area (large z). The remaining areas are cleaned by falling films. Line-based cleaning times are determined as the time when there is no more visual soils above each horizontal line, which can be regarded as the longest period to detach the soil layer from a given plate height. Therefore, the cleaning times determined by lines are commonly longer than those determined by grids.

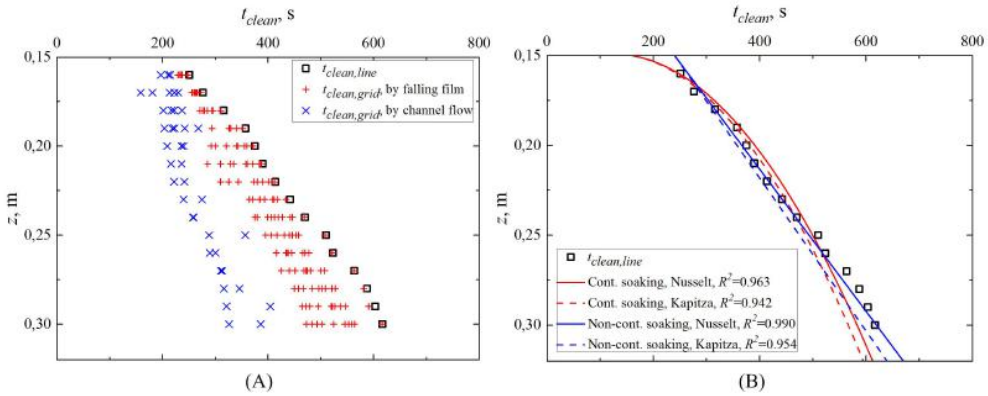

Figure 8.15: (A) An example of cleaning times determined by grids or lines, and (B) fitting the line-based cleaning times using the adhesive removal model. The flow rate is 1 L/min.

The cleaning front does not move initially, indicated by the nearly 3 min delay of the first cleaning time detected in Figure 8.15A. This could be due to either the soaking of soil to reduce the yield momentum M_y or the pre-shear of soil to decrease the yield stress. The rheology measurements have confirmed that pre-shearing the soil material at the shear stress of the falling film for 3 min only reduces the yield stress of toothpaste insignificantly (Table 8.3). Therefore, a more reasonable explanation of the delay of the cleaning start is that the soil needs to be soaked initially until the yield stress or yield momentum is lower than that imposed by the falling film. The time when the cleaning front starts to move downwards is defined as t_i.

Soaking by falling films can occur in two modes. A continuous soaking means the soil layer is constantly covered by water films from the beginning to the end of the cleaning (left locus in Figure 8.16). In this case, the cleaning rate constant k' keeps increasing and the yield momentum term M_y keeps decreasing throughout the whole cleaning period. On the other hand, a non-continuous soaking indicates that the soil layer is only covered by water before flow channels start to appear. Once a large channel forms, most liquid near the channel accumulates towards the channel direction (right locus in Figure 8.16). As a result, the neighbouring soil layers are no longer soaked in liquid. In this manner, the cleaning rate constant k' and the yield momentum term M_y change in the beginning, and keep unchanged subsequently.

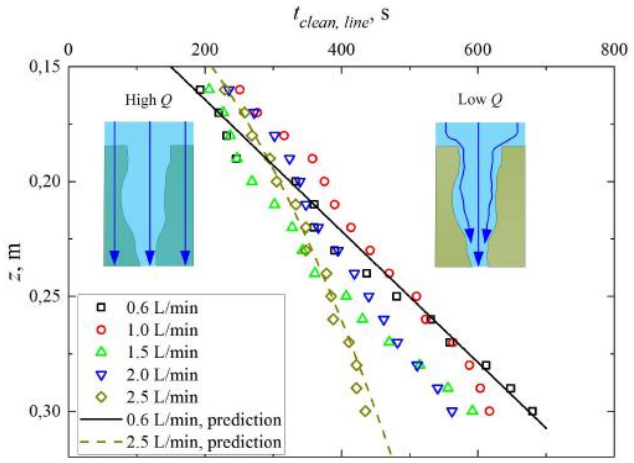

Figure 8.16: Line-based cleaning times at different flow rates as well as the adhesive removal model. At 0.6 L/min, only initial soaking applies with t_i=150 s and $M_y = 0.5M$. At 2.5 L/min, continuous soaking applies with t_i = 210 s and $M_y = 0.7M$. The film thickness is determined according to Kapitza's theory.

In the example in Figure 8.15B, both continuous and non-continuous soaking modes are modelled to fit the line-based cleaning times. The slopes of the fitting curves represent the value of the lumped cleaning rate constant k', which comes from the experimental results in the cleaning by static jets (refer to Figure 8.10B and Equation 8.2). The predicted cleaning times based on the Nusselt film are generally longer compared with the Kapitza film. This is because the Nusselt film results in thicker films, lower flow velocities and consequently smaller momentum forces on the soil layers (Equation 8.3) when the overall flow rate is assumed constant.

When the soil is continuously soaked, the cleaning rate increases as the soil material becomes weaker and weaker to remove. In the other case, when the soil is non-continuously soaked, the cleaning rate is constant. Thus, the cleaning curve is a straight line. For the example presented in Figure 8.15 (at a volumetric flow rate 1 L/min), the non-continuous soaking mode can describe the removal dynamics better. However, when the flow rate increases up to 2.5 L/min, the continuous soaking approach gives a more accurate description of experimental observations, as shown in Figure 8.16.

Therefore, the mechanism of cleaning toothpaste soil from vertical surfaces by (core) falling films can be described as follows:

1. The initial yield momentum of the soil is larger than the momentum of the falling film, so soil starts with soaking but is not removed. The liquid flows over the soil layer.

2. At t_i, the yield momentum of the soaked soil is smaller than the momentum of the

falling film. The toothpaste soil starts to be removed by adhesive failure. Channel flow appears at the same time or earlier.

3. At low flow rates, all liquid flows down through channels, so only the cleaning front and channel boundaries are contacted with liquid. The rest of the soil layer is not further soaked. Therefore, the cleaning front moves down at a constant rate.

4. At high flow rates, a fraction of the liquid flows through the channels and the remainder flows over the soil layer. The liquid continues soaking the soil and the cleaning rate keeps increasing.

Flow channels are formed when the liquid film tears a small gap of the soil layer and the neighbouring liquid accumulates toward the gap direction. As a result, the flow rate in the flow channel increases. According to Figure 8.16, the transition between non-continuous soaking and continuous soaking occurs at a flow rate of 2 - 2.5 L/min, corresponding to a wetting rate Γ_{core} = 0.097 - 0.112 kg/(m s). This critical range is much lower than the standard by ASME BPE, which requires 0.517 - 0.617 kg/(m s) wetting rate for cleaning vertical cylindrical vessels with static spray devices [184].

One more cleaning test was performed with the whole plate covered by toothpaste (see Figure 8.5D), in order to compare with the results where only the downstream plate is soiled and cleaned solely by a falling film. As shown in Figure 8.17, cleaning starts around the impingement point immediately after the water jet touches the soil layer. The cleaned area expands outwards and downwards. Flow channels with high flow rates can peel off the neighbouring soil layers rapidly. The slowest cleaning region is regarded as adhesive removal where the developed model in this study applies. The boundary of the final cleaned region indicates the footprint of the water film. The line-based cleaning time to clean to 30 cm downstream of the impingement point is around 550 s, in comparison with 583 ± 22 s when the plate is only soiled at 15 - 30 cm downstream. Thus, the cleaning times determined from these two different initial soiling areas are very similar. The slight difference can be caused by experimental deviations, since the position and size of the flow channels differ in every experiment.

To sum up, the momentums of water films are significantly different between the impingement area (> 0.1 kg s^{-2}) and the falling film (< 0.05 kg s^{-2}). It has been shown that the adhesive model developed by Wilson et al. (2012) [72] and Bhagat et al. (2017) [178] for cleaning near the impingement region also applies to the cleaning by falling films. However, there are still some challenges to use the model to the cleaning of toothpaste by falling films: firstly, the value of the yield momentum of toothpaste after soaking is highly uncertain, which requires a more accurate method for exact determination; secondly, the soaking mechanism of toothpaste by falling films differs from that by submerging soils in water, which leads to great deviations when taking the model parameters from the cleaning by static jets to the cleaning by falling films; thirdly, the initial delay of the cleaning front moving down is caused by the soaking of soil, the period of which is related to the flow conditions but the detailed mechanism behind this is not completely understood yet.

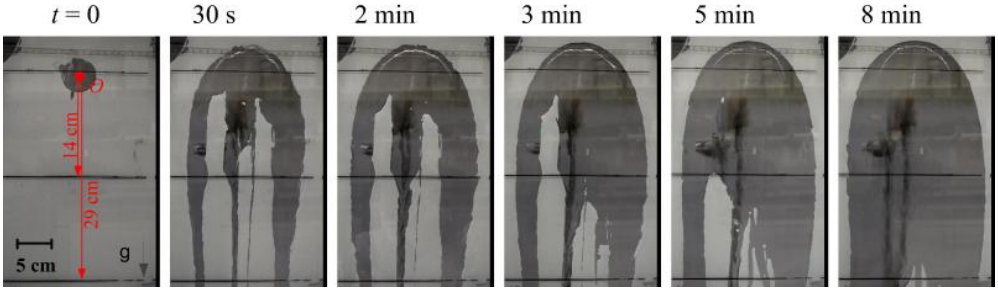

Figure 8.17: Cleaning a plate fully covered by toothpaste with flow rate $Q = 2$ L/min. Even though the distances from the impingement point to the black lines are 14 and 29 cm as shown in the left picture, the cleaning time is determined based on 30 cm downwards the impingement point for comparing with the cleaning experiments with falling films.

8.5 Conclusions

The cleaning of toothpaste soils from glass surfaces by impinging liquid jets has been studied in this chapter. The adhesive failure model investigated by Wilson et al. (2012) [72] and Bhagat et al. (2017) [178] is used to describe the cleaning dynamics. The effect of soaking and the cleaning by falling films are firstly integrated into the existing model.

The toothpaste used in this study exhibits viscoplastic properties and shear-thinning behaviour. The yield stress decreases sharply when the sample is diluted with water. Pre-shearing toothpaste only reduces the yield stress slightly. The removal force measured by millimanipulation mostly comes from the resistance to deform and push soil forward instead of shearing under the blade. The total removal force is linear to the volumetric removal rate of soil by the blade. The cohesive force within the soil matrix is stronger than the adhesive interaction between the soil and the plate surface. Both forces decrease significantly after the soil is soaked in water for a set time, indicating the easier removal of toothpaste after soaking.

The cleaning rate constant and yield momentum of the soil for different soaking times obtained from the cleaning by static jets are used in the following cleaning studies by moving jets and falling films. The cleaning rate constant increases linearly with soaking time. The yield momentum of the soil decreases after soaking, indicating that a weaker force is required for removal.

For the cleaning by moving jets, two removal mechanisms are revealed, depending on whether the soil is soaked and where the water jet initially hits the target. For non-soaked soils, if the jet initially hits outside the soiled area, the soil layers are separated rapidly by roll-up. However, if the jet initially acts on the soiled region, the soil is detached by adhesive removal. Only the latter mechanism happens to soaked soils. The proposed model in this study only applies to the cleaning by adhesive removal. The model successfully predicts the cleaning profile of non-soaked toothpaste assuming an intermediate strength soil type according to Bhagat et al. (2017) [178]. However, soaking toothpaste by falling films is complicated, resulting in the slight over-prediction of the

cleaning width according to the model.

The adhesive model developed from the cleaning around the impingement point can also apply to the cleaning by falling films. Kapitza's theory results in a more accurate prediction of the falling film thickness because of the presence of wavy flow. The existence of flow channels can speed up the removal of some local areas. But the removal rate in the hardest removal area can be predicted by the adhesive model. It takes a period for the cleaning front to start moving down since the soil needs to be soaked until the yield momentum is less than the flow momentum. At low flow rates (less than 0.097 - 0.112 kg/(m s) wetting rate of core film), the soaking effect terminates when the cleaning front moves down or large flow channels form, as most liquid accumulates towards the flow channels and the soil layer is no longer exposed to a water film. On the other hand, when the flow rate is above the transition wetting rate, a continuous soaking effect works on the soil layer until cleaning ends. The line-based cleaning time resulted from the plate that is fully covered by soil is close to the cleaning time when only soiling the area below the impingement point. In the present model, some challenges should be resolved for more accurate prediction of cleaning by falling films, including the determination of the yield momentum after soaking, the mechanism of toothpaste soaking by falling films, and the initial delay of the cleaning front moving down.

List of Nomenclature in Chapter 8

The following nomenclature is only valid for this chapter. Some symbols are used in other chapters but with different meanings. Otherwise, the symbols are specifically explained in the text if there is no nomenclature in some chapter.

Roman Letters

a	Cleaning distance, [m]
a_X	Distance to cleaning front on moving jet path, [m]
A	Cleaning rate parameter defined by $A = 1 - 10\pi\mu r_0/3\dot{m}$, dimensionless
A_{blade}	Area of millimanipulation blade tip, [m^2]
B	Cleaning rate parameter defined by $B = 10\pi\mu/3\dot{m}r_0^2$, dimensionless
C_1	Constant defined by $C_1 = \int_0^1 f(\eta)^2 d\eta$, dimensionless
C_2	Constant defined by $C_2 = \int_0^1 f(\eta) d\eta$, dimensionless
d	Jet diameter, [m]
f_c	Fraction of flow in core film, dimensionless
F_W	Force per unit width measured by millimanipulation, [N m^{-1}]
$F_{W,\,normal}$	Normal force per unit width, [N m^{-1}]
$F_{W,\,shear}$	Shear force per unit width, [N m^{-1}]
g	Gravitational acceleration, [m s^{-2}]
G'	Elastic modulus, [Pa]
G''	Viscous modulus, [Pa]
h	Film thickness, [m]

$h_{Kapitza}$	Mean film thickness based on Kapitza's theory, [m]
$h_{Nusselt}$	Mean film thickness based on Nusselt's theory, [m]
k_0	Lumped cleaning rate constant without soaking, [m s kg^{-1}]
k_1	Lumped cleaning rate constant per soaking time, [m kg^{-1}]
k'	Lumped cleaning rate constant, [m s kg^{-1}]
L_{blade}	Length of the millimanipulation contacting with soil, [m]
$\dot{m}$	Mass flow rate, [kg s^{-1}]
M	Momentum per unit width, [kg s^{-2}]
M_y	Yield momentum per unit width of material, [kg s^{-2}]
p	Radial distance to cleaning front, [m]
p^*	Dimensionless radial distance to cleaning front, dimensionless
q	Volumetric flow rate per unit width, [m^2 s^{-1}]
Q	Volumetric flow rate, [m^3 s^{-1}]
r	Radial coordinate, [m]
r_0	Nozzle radius, [m]
r_b	Radius where boundary layer reaches the surface, [m]
r_t	Transition radius from laminar to turbulent flow, [m]
R	Radius of impingement region, [m]
Re_f	Film Reynolds number defined by $Re_f = 4\rho q/\mu$, dimensionless
Re_j	Jet Reynolds number, dimensionless
t	Time, [s]
$t_{clean,\,grid}$	Cleaning time based on grid, [s]
$t_{clean,\,line}$	Cleaning time based on line, [s]
t_{soak}	Soaking time, [s]
u	Flow velocity, [m s^{-1}]
U_0	Mean flow velocity from jet, [m s^{-1}]
U_{av}	Mean flow velocity, [m s^{-1}]
U_s	Surface flow velocity, [m s^{-1}]
v_{blade}	Millimanipulation blade velocity, [m s^{-1}]
v_{jet}	Jet velocity, [m s^{-1}]
W	Falling film width, [m]
W_{blade}	Width of the millimanipulation blade, [m]
W_c	Core film width, [m]
$x,\ y,\ z$	Coordinates, [m]

Greek Letters

β	Angle to direction of nozzle motion, dimensionless
γ	Surface tension (liquid/vapour), [N m^{-1}]
$\dot{\gamma}$	Apparent shear rate, [s^{-1}]
δ	Boundary layer thickness, [m]
δ_{soil}	Soil thickness, [m]
δ_{gap}	Gap distance of millimanipulation blade, [m]
η	Distance normal to the wall defined by $\eta = y/\delta$, dimensionless
η_{app}	Apparent viscosity, [Pa s]
θ	Contact angle, dimensionless
μ	Dynamic viscosity, [Pa s]

ρ	Density, [kg m^{-3}]
σ	Cleaning rate parameter defined by $\sigma = 3k'\dot{m}U_0/5\pi$, [m^2 s^{-1}]
τ_y	Yield stress, [Pa]
χ	Phase angle, [°]
Γ	Wetting rate, [kg m^{-1} s^{-1}]
Γ_{core}	Wetting rate in core film, [kg m^{-1} s^{-1}]
Γ_{rope}	Wetting rate in rope, [kg m^{-1} s^{-1}]

Part III

Conclusions and Perspectives

CHAPTER 9

Overall Conclusions

The primary topic of this Ph.D work was to investigate different approaches for reducing resource consumption and cleaning costs during CIP operations. In the mapping study in a brewery, it was shown that most of the cleaning time and the main cleaning costs are spent on the cleaning detergent steps. The recovery of cleaning detergents can reduce the cleaning costs significantly. The annual cleaning costs for pipes are higher than the costs of tank cleaning operations, because the former occurs more frequently than the latter. The main findings in the brewery and the suggestions for implementing best practice are useful to improve the CIP systems in other industries where similar processes are used.

Analysing the historical data from the CIP of a brewery fermenter provides a benchmark that allows use of the historical cleaning data to improve the CIP operations in the future. In the presented case, a three-level analysis approach was used to evaluate a CIP system or operation to be normal or abnormal online or offline. Univariate analysis was applied in the first and third levels for assessing the CIP performance before and after the batch, respectively. Multivariate analysis was used in the second level of analysis to locally indicate the occurrence of anomalous events. The implementation of the analysis approach has significant potential to automatically detect the deviations and anomalies in future CIP cycles and to optimize the cleaning process.

CFD is a powerful tool to simulate the displacement of cleaning agent by water in pipe systems during the intermediate and final rinse steps in the cleaning of pipes. Based on the results from CFD simulations, it was found that dead zones mainly exist in the areas where flow recirculation is strong. The size of dead zones can be reduced by employing smooth connections or large flow velocities, but the occurrence of dead zones cannot be completely avoided. Increasing the flow velocity is able to reduce the rinsing time, but the overall water consumption is merely changed by varying flow velocity. In most situations, determining the rinsing time based on a local measurement is a safe way to avoid contamination risks, but is not the most economic way to minimise the actual water consumption. Furthermore, CFD supplements the traditional empirical approach to compute the pressure drop and equivalent length of different pipe elements. Summarizing, the present study proves that CFD is a helpful tool to optimize the hygienic design of pipe systems and to improve the cleaning efficiency.

Cleaning tank surfaces using pulsed flows has potentials to save cleaning costs. For the cleaning of tank surface soiled by egg yolk soil, pulsed flow is able to remove more deposits than continuous flow at the same consumption of alkaline solution, but at the expense of longer actual cleaning time. The enhancement of the cleaning effect by pulsed flow occurs

primarily because additional time is provided for soil layers to swell. Then the materials become easy to remove in the next pulse of flow. The most efficient burst technique is pulsing with high frequency and short period. Pre-wetting prior to continuous flow shows no significant improvement of the cleaning result. Cooking the soiling material above its denaturation temperature makes the soil more difficult to detach. For cleaning egg yolk by alkaline solution, the optimal cleaning conditions are high flow rate, high temperature (below denaturation temperature), and low alkali concentration. The main findings in pilot scale tests are also found in scale-up tests.

Common measurement-based CIP aims to control the cleaning time when there is no detectable soil in the liquid phase. However, there is still a risk that inconspicuous traces exist even though the measurement indicates a clear signal. Instead of extending the cleaning time using fresh water, a three-stage measurement-based partial recovery approach was designed with a turbidity sensor applied to measure the water quality. Reused water is utilised in the first stage to remove bulk soils and sent to drain directly. When the water is relatively clear, the circulation of reused water is started for a pre-defined period to detach all small traces from the surfaces. Fresh water is then used in the third stage to remove all remaining dirt, and is then recycled for the next cleaning. In this manner, the overall cleaning is performed for a sufficient period without increasing the consumption of fresh water. The water volume in the reused water tank keeps unchanged. So the cleaning water can be reused several times. The lifetime of the reused cleaning water can be prolonged by avoiding the accumulation of impurities in the reused water tank. The cleaning costs of the proposed three-stage measurement-based partial recovery approach yield the most economic scenario compared with single-use, full recovery, and time-based partial recovery approaches.

The cleaning of toothpaste soils from glass surfaces by impinging liquid jets and falling films can be predicted by the adhesive failure model investigated by Wilson et al. (2012) and Bhagat et al. (2017). This thesis is the first work to integrate the effect of soaking and the cleaning by falling films into the existing model. Toothpaste exhibits viscoplastic properties and shear-thinning behaviour. The soil becomes easier to remove after dilution or soaking. Pre-shearing the soil prior to cleaning is less important than soaking. The cleaning rate constant and yield momentum of soil for different soaking times obtained from the cleaning by static jets can be used in the cleaning studies by moving jets and falling films. However, the mechanism of cleaning non-soaked toothpaste by moving jets depends on whether the soil is soaked and where the water jet initially hits the target, resulting in the removal by either roll-up or adhesive removal. Only the latter mechanism applies to the removal of soaked soils. For the cleaning by falling films, Kapitza's theory results in more accurate prediction of falling film thickness than Nusselt' theory due to the presence of wavy flow. At low flow rate, the soil is non-continuously soaked until the cleaning front moves down or large flow channels appear. When the flow rate is above the transition wetting rate, a continuous soaking effect acts on the soil layer until cleaning ends.

CHAPTER 10

Perspectives

The objective of this Ph.D work was to investigate the opportunities for improving CIP operations, with particular focus on the CIP practices in brewery or similar industries. This chapter consists of two sections: the first summarizes the suggestions of future work based on the studies in Chapters 4 to 8; the second section provides other state-of-the-art techniques to improve the performance of CIP operations in industrial applications.

10.1 Suggestions for Future Work

Chapters 4 to 8 present independent case studies. The future work suggested in this section is also organised by chapter:

1. The three-level analysis approach in Chapter 4 can be applied to other CIP systems than the cleaning of brewery fermenters. With more data integrated into the proposed model, particularly water quality measurement, it should be possible to predict the end point of cleaning. Furthermore, the present study only indicates the occurrence of anomalies in a cleaning process and the likely causes. A detailed trouble-shooting approach is required to diagnose the root cause of an anomaly.

2. Part of the simulations of pipe cleaning and rinsing using CFD (Chapter 5) has been validated using analytical approaches and experimental results available in the literature. More experiments are needed to compare with the simulations of various pipe elements. Considering the numerous combinations of geometries, sizes and flow conditions, etc., a more practical solution is to focus on an existing pipe system and identify the most difficult cleaning part for analysis.

3. The enhancement of cleaning by pulsed flow was examined by cleaning egg yolk soils by alkaline solutions in Chapter 6. Egg yolk is a complicated soil type because of its denaturation property at high alkaline concentration and at high temperature. Therefore, a more simple soil type could be useful for further investigations of burst techniques in tank cleaning. Besides, the burst parameters (e.g., frequency, ratio of effective and holding times) can be optimized for removing more deposits per unit cost of cleaning resources.

4. The measurement-based partial recovery CIP system presented in Chapter 7 only uses water as cleaning medium. Similar approaches can be applied to other cleaning steps where chemicals are utilised. The lifetime of the cleaning liquid depends on

various factors like the type of deposits to be cleaned and quality requirement. Therefore, the determination of liquid lifetime is another important characteristic for evaluating the cost saving in CIP recovery processes.

5. The flow rates of liquid jets (indicated by the wetting rate of liquid film) in Chapter 8 are much lower than the recommendation for cleaning large tank vessels by the ASME BPE standard. Therefore, some phenomena (i.e., non-continuous soaking by falling films) may not occur after scaling up. It is worth investigating the different soaking approaches of toothpaste described in Chapter 8, such as dilution with water, submersing under water, soaking by falling films.

10.2 Other Opportunities for Improving Industrial CIP Operations

10.2.1 Smart Scheduling of Production and Cleaning

Cleaning has often been regarded as a supplementary activity executed after present production or before a new production. As a result, plenty of studies have focused on how to improve the productivity instead of how to save costs from cleaning, even though people universally agree that magnificent resource savings can be achieved through the efficient implementation of CIP. In fact, the cleaning costs can be hugely decreased, or at least avoid being wasted, by smartly scheduling production and cleaning plans. For instance:

- Immediate cleaning after production can avoid the formation of hard-to-clean soils. Soil materials become more difficult to clean after a long holding period because of soil drying, reaction and microbial growth, etc. Therefore, soils should be cleaned immediately after production to avoid unnecessary waste of cleaning resources.

- Avoiding long waiting time between two production batches can reduce unnecessary repeated cleaning cycles. Once some equipment is held for long time, for example two weeks for brewery fermenters, it is required to conduct cleaning before usage. A smart scheduling of production and facility utilisation should avoid this kind of long holding time and therewith needless cleaning.

- Identical or similar products can be allocated for production together. When the same or similar products are produced by the same facility, cleaning can be avoided or performed after a number of batches. It is also possible to execute a short cleaning recipe between alteration instead of long and expensive recipes, which can save cleaning costs significantly.

- Low-contaminated production can be planned prior to high-contaminated production. In such a manner, the cleaning between two production batches can be performed using a simple recipe. A good example is that when producing normal cola

and sugar-free cola, a fast cleaning is needed when producing sugar-free before normal cola, in comparison to a complex cleaning recipe when planning normal cola ahead of sugar-free cola.

10.2.2 Membrane Technology

Membrane processes have become an integral part of food processing, and are used to separate a liquid feed stream into two separate streams, namely permeate and retentate. This separation is mainly driven by the pressure difference across the membrane. As the filtration continues, the membrane and pores are gradually filled with feed components with high solid level, which consequently decreases the separation efficiency. Therefore, the cleaning of membranes have become more and more important in order to restore production capacity [6], especially for the reverse osmosis (RO) elements with small holes. This cleaning is commonly done by CIP with various types of cleaning agent such as caustic, acid, proteolytic enzymes and proprietary additives (surfactants and sequestrants), due to the complex matrix of fouling layers. The cleaning of membrane systems is recommended to be performed separately from other equipment to avoid inter-contamination. Trans-membrane pressure (TMP) is one of the key characteristics to assess membrane fouling and cleaning.

Another application of membrane systems is to treat waste water and water for reuse by recovering cleaning detergent compounds from CIP processes [185, 186, 187]. For example, Suárez et al. (2015) used a nanofiltration pilot plant to recover the CIP solution in an industrial yoghurt factory. Membranes retained nearly 90% of the chemical oxygen demand (COD). The permeates could be reused in the CIP plant without reducing the cleaning efficiency. The fresh detergent savings were around 18% [61]. Another study by Dresch et al. (2001) compared the continuous and discontinuous approaches to integrate a nanofiltration system in a CIP process to recover alkaline solution in the dairy industry. Whatever the selected integrated process, the COD level in the CIP tank stabilized at a level depending on the membrane area, which, however, was much lower than the COD content in commonly recycled CIP systems without membrane regeneration [188].

10.2.3 Novel Cleaning Agents

10.2.3.1 Enzyme-Based Cleaner

Enzymatic cleaning is advantageous to the environment because less aggressive conditions are required and a lower amount of salt is released compared to the traditional alkali treatment [189]. In a recent study, a 2-stage CIP operation was investigated by Chutrakul et al. (2018) to soak coconut milk fouling. Using surfactant linear alkylbenzene sulfonates (stage 1) prior to cellulase treatment (stage 2) could remove the foulants to a similar extent compared with only using NaOH solution for the same soaking time. The enzymatic approach is superior to the alkaline approach because of the lower temperature and lower pH required by the enzyme, and the biodegradability of surfactant and cellulase [190].

10.2.3.2 Electrolysed Water

Electrolysed water is an effective cleaning and sanitizing agent. Compared with conventional chemical sanitizers, electrolysed water has the advantages of low risk to produce and little addition of toxic heavy metals. Electrolysed water can be generated by the electrolysis of a dilute NaCl solution using two electrodes. Traditionally, the cathode and anode electrodes are separated by membranes. In the anode cell, water reacts with the anode electrode, producing oxygen and hydrogen ions. Chlorine ions can also react with the electrode, generating chlorine gas and hypochlorous acid (HOCl). This solution is called acidic electrolysed water with a pH value of 2.7 or lower. Acidic electrolysed water is able to inactivate a variety of bacterial pathogens on the surfaces of food processing equipment [136]. Compared with traditional chlorine-based solutions, electrolysed water is more effective in killing microbes, hence, lower concentration is required. Novel technology allows to generate electrolysed water without using a membrane to separate the cathode and anode electrodes. Thereby, neutral electrolysed water is produced with low risk of corrosion of processing equipment and low irritation to operators [191].

10.2.4 Pigging Technology

Pushing a piston through a pipe, commonly known as pigging, is an efficient technique to recover the product from a pipeline and clean the pipe wall. Conventionally, solid pigs with simple geometries are propelled by compressed air, water or another liquid through the pipes with a uniform diameter. Clever mechanical design and the use of compliant materials have extended the application of pigging to the pipelines with minor geometry changes. However, there are still barriers when installing a pigging system to an existing production line, due to the existence of valves, sensors, heat exchangers, pumps, etc.

An innovative method of pigging is to use crushed ice rather than a solid to remove viscous products and fouling. According to Quarini (2002), a mixture of ice particles and water with a freezing point depressant is pumped through various geometries, including straight pipes, bends, T-joints, static mixers, orifices and plate heat exchangers, etc. The ice-pigging technique can never get stuck even at the most complex heat exchanger geometry. The use of water has considerable environmental benefits [192, 193]. However, The biggest challenge to limit the application of ice-pigging is the high costs to make and store ice [59].

Part IV

Appendices

APPENDIX A

Dead Zone Identifications of Various Pipe Elements by CFD

This appendix displays the wall shear stress of complex pipe elements simulated by CFD in Chapter 5. A dead zone can be regarded as the area where local wall shear stress is less than 3 Pa [45].

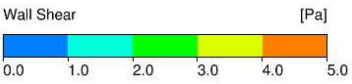

Geometries	Descriptions	Wall shear stress
A	1.5 m/s	
A	3.0 m/s	

B	1.5 m/s	
B	3.0 m/s	
C	1.5 m/s	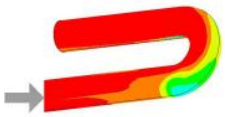
C	3.0 m/s	
D	1.5 m/s	
D	3.0 m/s	
E	1.5 m/s	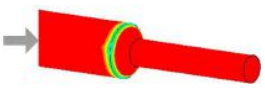
F	1.5 m/s	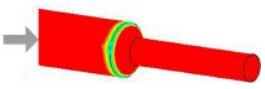

G	1.5 m/s	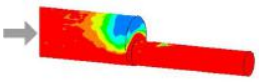
G	3.0 m/s	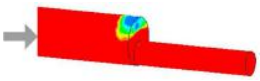
H	1.5 m/s	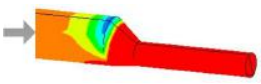
H	3.0 m/s	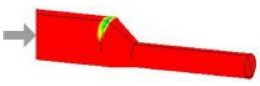
I	1.5 m/s	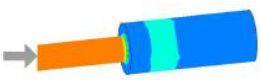
J	1.5 m/s	
J	3.0 m/s	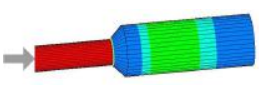
K	1.5 m/s	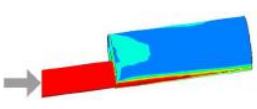

L	1.5 m/s	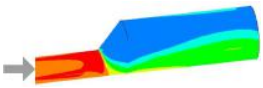
M	1.5 m/s	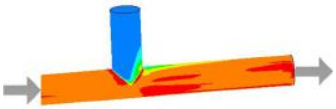
N	1.5 m/s	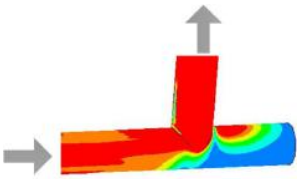
O	1.5 m/s	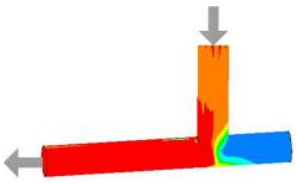
P	1.5 m/s, views from two perspectives	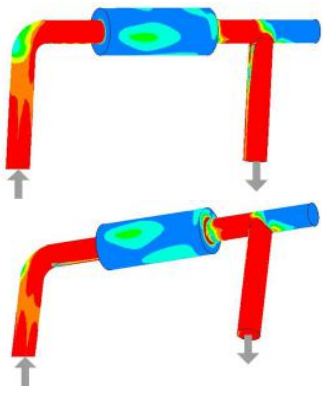

APPENDIX B

Cleaning Dynamics of Egg Yolk Soils from Tank Surfaces (All Data)

This appendix is an extension of Figure 6.4 in Chapter 6, showing the removal of uncooked egg yolk soils from tank surfaces under all experimental conditions.

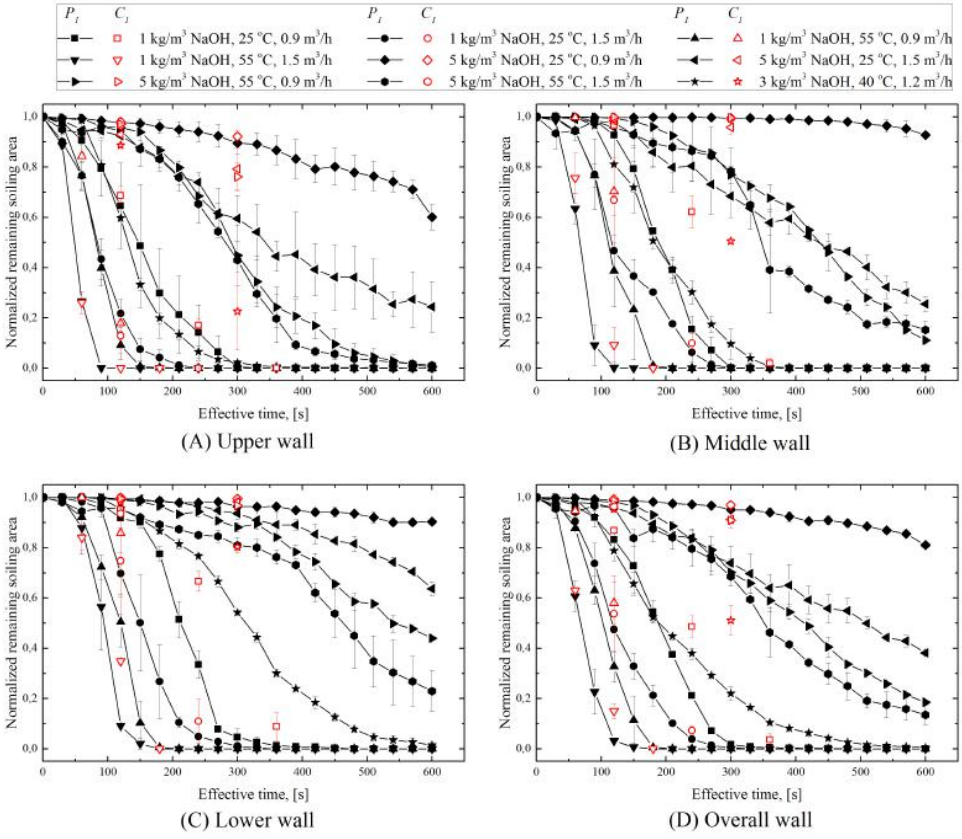

Figure B.1: Removal of uncooked soils for all runs under different conditions of temperature, flow rate and NaOH concentration, by using continuous flow without pre-wetting (C_1) or pulsed flow in short period and high frequency (P_1): (A) tank upper wall, (B) tank middle wall, (C) tank lower wall, (D) tank overall wall surface.

APPENDIX C

The Development of Flow Channels During the Cleaning of Toothpaste by Falling Films

This appendix displays the development of flow channels during the cleaning of toothpaste by falling films in Chapter 8. Flow channels appear spontaneously in all experiments with flow rate ranging from 0.6 - 2.5 L/min. In the flow channel region, the soiled material is removed slower than by a rope but faster than by a falling film. Flow channels form before the cleaning front starts to move.

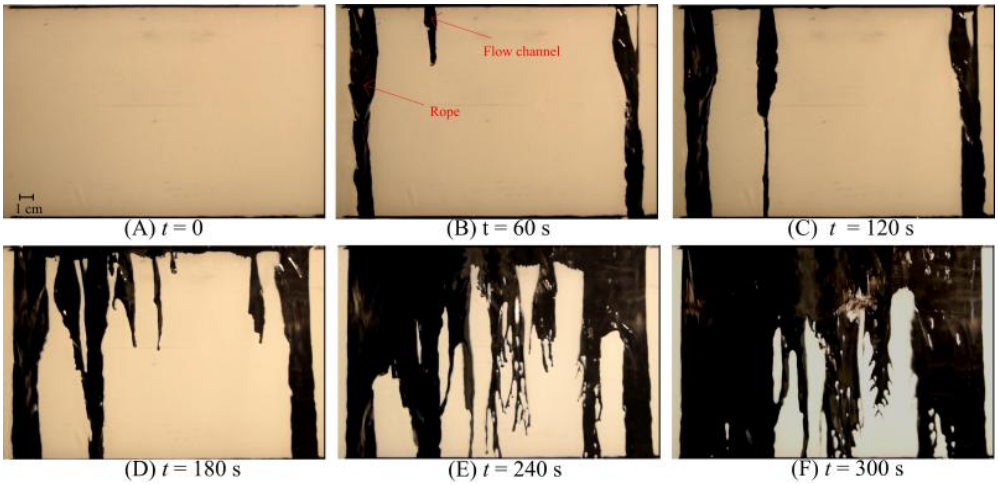

Figure C.1: The development of flow channels during the cleaning of toothpaste by falling films. The example is at flow rate 2 L/min, the same condition as in Figure 8.6. (A) Cleaning starts. (B) Flow channel starts to form, but the cleaning front does not move. (C) Flow channel grows, but the cleaning front does not move. (D) More flow channels form, and the cleaning front starts to move. (E) More flow channels grow, and the cleaning front moves fast. (E) More areas are cleaned.

List of Publications

Peer-reviewed manuscripts

Yang, J., Jensen, B. B. B., Nordkvist, M., Rasmussen, P., Pedersen, B., Kokholm, A., Jensen, L., Gernaey, K. V., Krühne, U. (2018). Anomaly Analysis in Cleaning-in-Place Operations of an Industrial Brewery Fermenter. *Industrial and Engineering Chemistry Research*, 57 (38): 12871 - 12883.
DOI: 10.1021/acs.iecr.8b02417

Yang, J., Jensen, B. B. B., Nordkvist, M., Rasmussen, P., Gernaey, K. V., Krühne, U. (2018). CFD modelling of axial mixing in the intermediate and final rinses of cleaning-in-place procedures of straight pipes. *Journal of Food Engineering*, 221: 95 - 105.
DOI: 10.1016/j.jfoodeng.2017.09.017

Yang, J., Kjellberg, K., Jensen, B. B. B., Nordkvist, M., Gernaey, K. V., Krühne, U. (2018). Investigation of the cleaning of egg yolk deposits from tank surfaces using continuous and pulsed flows. *Food and Bioproducts Processing*, in press.
DOI: 10.1016/j.fbp.2018.10.007

Conference proceedings and abstracts

Yang, J., Kjellberg, K., Jensen, B.B.B., Nordkvist, M., Gernaey, K.V., Krühne U. (2018). Cleaning of tank surfaces fouled by egg yolk. 17 – 20 April 2018, *Fouling and Cleaning in Food Processing Conference*, Lund, Sweden. Accepted for oral presentation and proceeding publication.

Yang, J., Gernaey, K., Krühne, U., Rasmussen, P., Kokholm, A., Nordkvist, M. (2018). Industrial cleaning-in-place processes in brewery – a systematic mapping study. 30 January 2018, *12th Annual Water Research Meeting of Danish Water Forum*, Copenhagen, Denmark. Accepted for oral presentation and abstract publication.

Yang, J., Nordkvist, M., Gernaey, K. V., Krühne, U. (2017). Anomaly Detection and Diagnosis Using Multivariate Analysis Tools in Industrial Cleaning-in-Place Operations. 12 – 14 June 2017, *IChemE Advances in Process Automation and Control 2017*, Birmingham, UK. Accepted for oral presentation.

Yang, J., Gernaey, K. V., Krühne, U. (2016). Simulation of Axial Mixing by CFD during the Rinse of CIP procedures. 2 - 3 Nov. 2016, *EHEDG World Congress on Hygienic Engineering and Design 2016*, Herning, Denmark. Accepted for poster presentation and proceeding publication.

Bibliography

[1] I Palabiyik et al. “Minimising the environmental footprint of industrial-scaled cleaning processes by optimisation of a novel clean-in-place system protocol”. In: *Journal of Cleaner Production* 108 (2015), pages 1009–1018.

[2] TR Bott. *Fouling notebook*. Institution of Chemical Engineers, 1990.

[3] L Melo, TR Bott, and CA Bernardo. *Fouling science and technology*. Volume 145. Springer Science & Business Media, 2012.

[4] B Jude and E Lemaire. “How to optimize clean-in-place (cip) processes in food and beverage operations”. In: *Scheider Electric* (2013).

[5] DA Seiberling. *Clean-in-place for biopharmaceutical processes*. CRC Press, 2007.

[6] AY Tamime. *Cleaning-in-Place: dairy, food and beverage operations*. 3rd edition. Ayr, UK: Blackwell, 2008, page 272.

[7] EHEDG Secretariat. *EHEDG Yearbook 2016/2017*. 2017.

[8] JE Frantsen and TE Mathiesen. “Specifying stainless steel surfaces for the brewery, dairy and pharmaceutical sectors”. In: *Corrosion 2009* (2009).

[9] HLM Lelieveld, MA Mostert, and J Holah. *Handbook of hygiene control in the food industry*. 1st edition. Cambridge, UK: Woodhead Publishing, 2005, page 744.

[10] DW Sun. *Computational fluid dynamics in food processing*. CRC Press, 2007.

[11] Erwin, AP and A Graßhoff. “Cleaning and Sanitation”. In: *Handbook of Food Engineering*. Edited by DR Heldman and DB Lund. Second Edi. CRC Press, 2006. Chapter 14, pages 929–975.

[12] PJ Fryer, GK Christian, and W Liu. “How hygiene happens: physics and chemistry of cleaning”. In: *International Journal of Dairy Technology* 59.2 (2006), pages 76–84.

[13] I Palabiyik. “Investigation of fluid mechanical removal in the cleaning process”. PhD thesis. University of Birmingham, 2013.

[14] B Van der Bruggen and L Braeken. “The challenge of zero discharge: from water balance to regeneration”. In: *Desalination* 188.1-3 (2006), pages 177–183.

[15] PJ Fryer and K Asteriadou. “A prototype cleaning map: a classification of industrial cleaning processes”. In: *Trends in Food Science & Technology* 20.6-7 (2009), pages 255–262.

[16] MR Bird and PJ Fryer. "Experimental study of the cleaning of surfaces fouled by whey proteins". In: *Food and Bioproducts Processing* 69.1 (1991), pages 13–21.

[17] MR Bird and PJ Fryer. "An analytical model for the cleaning of food process plant". In: *Food Engineering in a Computer Climate*. Taylor & Francis. 1992, pages 325–330.

[18] N Akhtar et al. "Matching the nano-to the meso-scale: Measuring deposit–surface interactions with atomic force microscopy and micromanipulation". In: *Food and Bioproducts Processing* 88.4 (2010), pages 341–348.

[19] ZK Xu et al. "Assessing the impact of germination and sporulation conditions on the adhesion of bacillus spores to glass and stainless steel by fluid dynamic gauging". In: *Journal of Food Science* 82.11 (2017), pages 2614–2625.

[20] R Pérez-Mohedano, N Letzelter, and S Bakalis. "Swelling and hydration studies on egg yolk samples via scanning fluid dynamic gauge and gravimetric tests". In: *Journal of Food Engineering* 169 (2016), pages 101–113.

[21] PW Gordon et al. "Elucidating enzyme-based cleaning of protein soils (gelatine and egg yolk) using a scanning fluid dynamic gauge". In: *Chemical Engineering Research and Design* 90.1 (2012), pages 162–171.

[22] P Saikhwan et al. "Swelling and dissolution in cleaning of whey protein gels". In: *Food and Bioproducts Processing* 88.4 (2010), pages 375–383.

[23] TR Tuladhar, WR Paterson, and DI Wilson. "Investigation of alkaline cleaning-in-place of whey protein deposits using dynamic gauging". In: *Food and Bioproducts Processing* 80.3 (2002), pages 199–214.

[24] WJ Liu et al. "Quantification of the local protein content in hydrogels undergoing swelling and dissolution at alkaline pH using fluorescence microscopy". In: *Food and Bioprocess Technology* 11.3 (2018), pages 572–584.

[25] WW Liu et al. "Quantification of the cleaning of egg albumin deposits using micromanipulation and direct observation techniques". In: *Journal of Food Engineering* 78.1 (2007), pages 217–224.

[26] GL Cuckston et al. "Quantifying the effect of solution formulation on the removal of soft solid food deposits from stainless steel substrates". In: *Journal of Food Engineering* (2019).

[27] DM Phinney et al. "Identification of residual nano-scale foulant material on stainless steel using atomic force microscopy after clean in place". In: *Journal of Food Engineering* 214 (2017), pages 236–244.

[28] PA Cole et al. "Comparison of cleaning of toothpaste from surfaces and pilot scale pipework". In: *Food and Bioproducts Processing* 88.4 (2010), pages 392–400.

[29] S Gunasekaran and MM Ak. "Dynamic oscillatory shear testing of foods—selected applications". In: *Trends in Food Science & Technology* 11.3 (2000), pages 115–127.

[30] W Hu et al. "Micromechanical characterization of hydrogels undergoing swelling and dissolution at alkaline pH". In: *Gels* 3.4 (2017), page 44.

[31] DI Wilson. “Challenges in cleaning: recent developments and future prospects”. In: *Heat Transfer Engineering* 26.1 (2005), pages 51–59.

[32] M Joppa et al. “Prediction of cleaning by means of computational fluid dynamics: implication of the pre-wetting of a swellable soil”. In: *Proceedings of International Conference on Heat Exchanger Fouling and Cleaning XII*. 2017.

[33] K Kjellberg. “Rotary jet head ‘burst’ cleaning technology delivers significant savings in cleaning costs”. In: *EHEDG Yearbook 2015/2016* (2016), pages 96–98.

[34] PJ Fryer, PT Robbins, and K Asteriadou. “Current knowledge in hygienic design: can we minimise fouling and speed cleaning?” In: *Advances in Food Process Engineering Research and Applications*. Springer, 2013, pages 209–227.

[35] I Palabiyik et al. “Flow regimes in the emptying of pipes filled with a Herschel–Bulkley fluid”. In: *Chemical Engineering Research and Design* 92.11 (2014), pages 2201–2212.

[36] A van Asselt and M Fox. *How to improve and control the performance of CIP processes*. 2012. URL: `https://www.youtube.com/watch?v=rY1Vh28scNQ`.

[37] W Liu et al. “Identification of cohesive and adhesive effects in the cleaning of food fouling deposits”. In: *Innovative Food Science & Emerging Technologies* 7.4 (2006), pages 263–269.

[38] Y Chisti. “Modern systems of plant cleaning”. In: *Encyclopedia of Food Microbiology* 3 (1999), pages 1806–1815.

[39] M Helbig et al. “Laboratory methods to predict the cleaning behaviour in a flow channel exemplified by egg yolk layer”. In: *Foulig and Cleaning in Food Processing 2018*. Lund, Sweden, 2018, pages 149–166.

[40] J Piepiórka-Stepuk, J Diakun, and M Jakubowski. “The parameters of cleaning a CIP system affected energy consumption and cleaning efficiency of the plate heat exchanger”. In: *Chemical and Process Engineering* 38.1 (2017), pages 111–120.

[41] NI Khalid et al. “Design of a test rig for cleaning studies and evaluation of laboratory-scale experiments using pink guava puree as a fouling deposit model”. In: *Journal of Food Process Engineering* 38.6 (2015), pages 583–593.

[42] KR Goode et al. “Characterising the cleaning mechanisms of yeast and the implications for Cleaning In Place (CIP)”. In: *Food and Bioproducts processing* 88.4 (2010), pages 365–374.

[43] MY Fan, DM Phinney, and DR Heldman. “The impact of clean-in-place parameters on rinse water effectiveness and efficiency”. In: *Journal of Food Engineering* 222 (2018), pages 276–283.

[44] KR Goode et al. “The effect of temperature on adhesion forces between surfaces and model foods containing whey protein and sugar”. In: *Journal of Food Engineering* 118.4 (2013), pages 371–379.

[45] BBB Jensen and A Friis. “Critical wall shear stress for the EHEDG test method”. In: *Chemical Engineering and Processing: Process Intensification* 43.7 (2004), pages 831–840.

[46] K Asteriadou et al. “Improving cleaning of industrial heat inducted food and beverages deposits: a scientific approach to practice”. In: *Proceedings of International Conference on Heat Exchanger Fouling and Cleaning VIII*. June. 2009, pages 158–164.

[47] CR Gillham et al. “Cleaning-in-place of whey protein fouling deposits: mechanisms controlling cleaning”. In: *Food and Bioproducts Processing* 77.2 (1999), pages 127–136.

[48] JG Detry et al. “Flow rate dependency of critical wall shear stress in a radial-flow cell”. In: *Journal of Food Engineering* 92.1 (2009), pages 86–99.

[49] NI Khalid et al. “Alkaline cleaning-in-place of pink guava puree fouling deposit using lab-scale cleaning test rig”. In: *Agriculture and Agricultural Science Procedia* 2 (2014), pages 280–288.

[50] GK Christian, SD Changani, and PJ Fryer. “The effect of adding minerals on fouling from whey protein concentrate: development of a model fouling fluid for a plate heat exchanger”. In: *Food and Bioproducts Processing* 80.4 (2002), pages 231–239.

[51] GK Christian and PJ Fryer. “The effect of pulsing cleaning chemicals on the cleaning of whey protein deposits”. In: *Food and Bioproducts Processing* 84.4 (2006), pages 320–328.

[52] T Truong et al. “The use of a heat flux sensor for in-line monitoring of fouling of non-heated surfaces”. In: *Food and Bioproducts Processing* 80.4 (2002), pages 260–269.

[53] SRS Dev et al. “Optimization and modeling of an electrolyzed oxidizing water based clean-in-place technique for farm milking systems using a pilot-scale milking system”. In: *Journal of Food Engineering* 135 (2014), pages 1–10.

[54] M Scholander. *Handbook: Cleaning in Place, A guide to Cleaning Technology in the Food Processing Industry*. Technical report. Lund, Sweden: Tetra Pak, 2015, page 40.

[55] S Kumari and PK Sarkar. “In vitro model study for biofilm formation by Bacillus cereus in dairy chilling tanks and optimization of clean-in-place (CIP) regimes using response surface methodology”. In: *Food Control* 36.1 (2014), pages 153–158.

[56] C Lelièvre et al. “Cleaning in place: effect of local wall shear stress variation on bacterial removal from stainless steel equipment”. In: *Chemical Engineering Science* 57.8 (2002), pages 1287–1297.

[57] MY Fan, DM Phinney, and DR Heldman. “Effectiveness of rinse water during in-place cleaning of stainless steel pipe lines”. In: *Journal of Food Science* 80.7 (2015), E1490–E1497.

[58] AJ Van Asselt, G Van Houwelingen, and MC Te Giffel. “Monitoring system for improving cleaning efficiency of cleaning-in-place processes in dairy environments”. In: *Food and Bioproducts Processing* 80.4 (2002), pages 276–280.

[59] KR Goode. “Characterising the cleaning behaviour of brewery foulants-to minimise the cost of cleaning in place operations.” PhD thesis. University of Birmingham, 2012.

[60] V Melero et al. “Experimental investigation about rinse water consumption of a CIP process applied to a shell and tube exchanger”. In: *Advanced Materials Research*. Volume 785. Trans Tech Publ. 2013, pages 1294–1298.

[61] L Suárez, MA Diez, and FA Riera. “Recovery of detergents in food industry: an industrial approach”. In: *Desalination and Water Treatment* 56.4 (2015), pages 967–976.

[62] K Bader et al. “Online total organic carbon (TOC) as a process analytical technology for cleaning validation risk management”. In: *Pharmaceutical Engineering* 29.1 (2009), pages 8–20.

[63] E Wallhäußer et al. “Determination of cleaning end of dairy protein fouling using an online system combining ultrasonic and classification methods”. In: *Food and Bioprocess Technology* 7.2 (2014), pages 506–515.

[64] M Henningsson et al. “CFD simulation and ERT visualization of the displacement of yoghurt by water on industrial scale”. In: *Journal of Food Engineering* 80.1 (2007), pages 166–175.

[65] Ecolab. *3D TRASAR Technology for CIP*. Technical report. Ecolab USA Inc., 2017, page 3.

[66] A van Asselt. *Cleaning Optimization OptCIP©: Reduce Cleaning Time and Production Costs*. Technical report. Ede, Netherlands: NIZO food research B.V., 2014, page 2.

[67] Anderson,D. *Conductivity Measurement: Critical for Clean-in-Place Systems*. Technical report. Irvine, Canada: Emerson Process Management, 2007, page 4.

[68] SP Lin and RD Reitz. “Drop and spray formation from a liquid jet”. In: *Annual Review of Fluid Mechanics* 30.1 (1998), pages 85–105.

[69] RP Grant and S Middleman. “Newtonian jet stability”. In: *AIChE Journal* 12.4 (1966), pages 669–678.

[70] A Chillman, M Ramulu, and M Hashish. “A general overview of waterjet surface treatment modeling”. In: *American WJTA Conference and Expo*. 2009.

[71] E Fuchs et al. “Influence of the nozzle distance on the cleaning result compared to the jet break up and the mechanical forces on an industrial scale”. In: *Fouling and Cleaning in Food Processing 2018*. Lund, Sweden, 2018.

[72] DI Wilson et al. “Surface flow and drainage films created by horizontal impinging liquid jets”. In: *Chemical Engineering Science* 68.1 (2012), pages 449–460.

[73] RK Bhagat and DI Wilson. “Flow in the thin film created by a coherent turbulent water jet impinging on a vertical wall”. In: *Chemical Engineering Science* 152 (2016), pages 606–623.

[74] MWL Chee et al. “Impinging jet cleaning of tank walls: effect of jet length, wall curvature and related phenomena”. In: *Food and Bioproducts Processing* (2018).

[75] DI Wilson et al. “Cleaning of soft-solid soil layers on vertical and horizontal surfaces by stationary coherent impinging liquid jets”. In: *Chemical Engineering Science* 109 (2014), pages 183–196.

[76] DI Wilson et al. “Cleaning of a model food soil from horizontal plates by a moving vertical water jet”. In: *Chemical Engineering Science* 123 (2015), pages 450–459.

[77] HW Glover et al. “Cleaning of complex soil layers on vertical walls by fixed and moving impinging liquid jets”. In: *Journal of Food Engineering* 178 (2016), pages 95–109.

[78] NF Damkjær et al. “Flow pattern and cleaning performance of a stationary liquid jet operating at conditions relevant for industrial tank cleaning”. In: *Food and Bioproducts Processing* 101 (2017), pages 145–156.

[79] SK Bhunia and JH Lienhard. “Splattering during turbulent liquid jet impingement on solid targets”. In: *Journal of Fluids Engineering* 116.2 (1994), pages 338–344.

[80] T Wang et al. “Flow patterns and draining films created by horizontal and inclined coherent water jets impinging on vertical walls”. In: *Chemical Engineering Science* 102 (2013), pages 585–601.

[81] DE Hartley and W Murgatroyd. “Criteria for the break-up of thin liquid layers flowing isothermally over solid surfaces”. In: *International Journal of Heat and Mass Transfer* 7.9 (1964), pages 1003–1015.

[82] KR Morison and RJ Thorpe. “Liquid distribution from cleaning-in-place sprayballs”. In: *Food and Bioproducts Processing* 80.4 (2002), pages 270–275.

[83] T Wang, JF Davidson, and DI Wilson. “Effect of surfactant on flow patterns and draining films created by a static horizontal liquid jet impinging on a vertical surface at low flow rates”. In: *Chemical Engineering Science* 88 (2013), pages 79–94.

[84] W Nusselt. “Die Oberflachenkondesation des Wasserdamffes”. In: *Zeitschrift des Vereines Deutscher Ingenieure* 60 (1916), pages 541–546.

[85] S Portalski. “Studies of falling liquid film flow film thickness on a smooth vertical plate”. In: *Chemical Engineering Science* 18.12 (1963), pages 787–804.

[86] J Tihon et al. “Solitary waves on inclined films: their characteristics and the effects on wall shear stress”. In: *Experiments in Fluids* 41.1 (2006), pages 79–89.

[87] E Fuchs et al. “An experimental comparison of film flow parameters and cleaning behaviour of falling liquid films for different tilt angles”. In: *Food and Bioproducts Processing* 93 (2015), pages 318–326.

[88] E Fuchs et al. “Influence of the film flow characteristic on the cleaning behaviour”. In: *International Conference on Heat Exchanger Fouling and Cleaning X*. 2013, pages 09–14.

[89] W Aouad et al. “Particle image velocimetry and modelling of horizontal coherent liquid jets impinging on and draining down a vertical wall”. In: *Experimental Thermal and Fluid Science* 74 (2016), pages 429–443.

[90] J Tihon et al. “Electrodiffusion detection of the near-wall flow reversal in liquid films at the regime of solitary waves”. In: *Journal of Applied Electrochemistry* 33.7 (2003), pages 577–587.

[91] JR Landel, H McEvoy, and SB Dalziel. “Cleaning of viscous drops on a flat inclined surface using gravity-driven film flows”. In: *Food and Bioproducts Processing* 93 (2015), pages 310–317.

[92] AI Khuri and S Mukhopadhyay. “Response surface methodology”. In: *Wiley Interdisciplinary Reviews: Computational Statistics* 2.2 (2010), pages 128–149.

[93] E Jurado Alameda et al. “Cleaning of starchy soils in clean-in-Place (CIP) systems: relationship between contact angle and detergency”. In: *Journal of Dispersion Science and Technology* 37.3 (2016), pages 317–325.

[94] J Piepiórka-Stepuk, J Diakun, and S Mierzejewska. “Poly-optimization of cleaning conditions for pipe systems and plate heat exchangers contaminated with hot milk using the Cleaning In Place method”. In: *Journal of Cleaner Production* 112 (2016), pages 946–952.

[95] E Martin, G Montague, and P Robbins. “A quality by design approach to process plant cleaning”. In: *Chemical Engineering Research and Design* 91.6 (2013), pages 1095–1105.

[96] D McCarthy. “Modern trends in CIP automation.” In: *Food Quality and Safety* August (2015), pages 23–25.

[97] A Yang et al. “Towards improved cleaning of FMCG plants: a model-based approach”. In: *Computer Aided Chemical Engineering* 25 (2008), page 1161.

[98] XM Wang et al. “Mathematical modeling and cycle time reduction of deposit removal from stainless steel pipeline during cleaning-in-place of milking system with electrolyzed oxidizing water”. In: *Journal of Food Engineering* 170 (2016), pages 144–159.

[99] C Lelièvre et al. “Cleaning-in-Place: modelling of cleaning kinetics of pipes soiled by Bacillus spores assuming a process combining removal and deposition”. In: *Food and Bioproducts Processing* 80.4 (2002), pages 305–311.

[100] BBB Jensen et al. “Predicting cleaning: Estimate fluctuations in signal from electrochemical wall shear stress measurements using CFD”. In: *Fouling, Cleaning & Disinfection in Food Processing*. Department of Chemical Engineering, University of Cambridge. 2006, pages 130–137.

[101] BBB Jensen and A Friis. “Predicting the cleanability of mix-proof valves by use of wall shear stress”. In: *Journal of Food Process Engineering* 28.2 (2005), pages 89–106.

[102] BBB Jensen, M Stenby, and DF Nielsen. “Improving the cleaning effect by changing average velocity”. In: *Trends in Food Science and Technology* 18.Suppl. 1 (2007).

[103] GZ Li et al. “Improving the efficiency of ‘clean-in-place’ procedures using a four-lobed swirl pipe: a numerical investigation”. In: *Computers & Fluids* 108 (2015), pages 116–128.

[104] GZ Li et al. “Optimization of a four-lobed swirl pipe for clean-in-place procedures”. In: *ICCE 2015: International Conference on Clean Energy*. 2015, page 561.

[105] GZ Li et al. “Large eddy simulation and Reynolds-averaged Navier–Stokes based modelling of geometrically induced swirl flows applied for the better understanding of Clean-In-Place procedures”. In: *Food and Bioproducts Processing* 104 (2017), pages 77–93.

[106] KR Davey, S Chandrakash, and BK O’Neill. “A new risk analysis of Clean-In-Place milk processing”. In: *Food Control* 29.1 (2013), pages 248–253.

[107] H Xin. “A study of the mechanisms of chemical cleaning of milk protein fouling deposits using a model material (whey protein concentrate gel)”. PhD thesis. ResearchSpace@ Auckland, 2003.

[108] H Xin, XD Chen, and N Özkan. “Removal of a model protein foulant from metal surfaces”. In: *AIChE Journal* 50.8 (2004), pages 1961–1973.

[109] KR Davey, S Chandrakash, and BK O’Neill. “A Friday 13th failure assessment of clean-in-place removal of whey protein deposits from metal surfaces with auto-set cleaning times”. In: *Chemical Engineering Science* 126 (2015), pages 106–115.

[110] A Hill. *Brewing microbiology: Managing microbes, ensuring quality and valorising waste*. Woodhead Publishing, 2015.

[111] *Great brewing process*. URL: `https://carlsbergmyanmar.com.mm/en/beers-you-love/great-brewing-process/`.

[112] Hatlar Group Pty Ltd. *Clean-in-place best practice guidelines-Part I: Compare CIP with best practice*. Technical report August. Melbourne, Australia, 2010, page 40.

[113] JF Yang et al. “Anomaly analysis in cleaning-in-place operations of an industrial brewery fermenter”. In: *Industrial & Engineering Chemistry Research* 57.38 (2018), pages 12871–12883.

[114] LH Chiang, EL Russell, and RD Braatz. *Fault detection and diagnosis in industrial systems*. 2001.

[115] K Roy et al. “Multivariate statistical monitoring as applied to clean-in-place (CIP) and steam-in-place (SIP) operations in biopharmaceutical manufacturing”. In: *Biotechnology Progress* 30.2 (2014), pages 505–515.

[116] H Trevor, T Robert, and JH Friedman. *The elements of statistical learning: data mining, inference, and prediction*. 2009.

[117] C Undey and A Cinar. “Statistical monitoring of multistage, multiphase batch processes”. In: *IEEE Control Systems* 22.5 (2002), pages 40–52.

[118] J Ramsay. “Functional data analysis”. In: *Encyclopedia of Statistics in Behavioral Science* (2005).

[119] J Ramsay, G Hooker, and S Graves. *Functional data analysis with R and MATLAB*. Springer Science & Business Media, 2009.

[120] P Nomikos and JF MacGregor. “Multivariate SPC charts for monitoring batch processes”. In: *Technometrics* 37.1 (1995), pages 41–59.

[121] EJ Keogh and MJ Pazzani. “Derivative dynamic time warping”. In: *Proceedings of the 2001 SIAM International Conference on Data Mining*. SIAM. 2001, pages 1–11.

[122] SW Wang and F Xiao. “AHU sensor fault diagnosis using principal component analysis method”. In: *Energy and Buildings* 36.2 (2004), pages 147–160.

[123] C Ündey, S Ertunç, and A Çınar. “Online batch/fed-batch process performance monitoring, quality prediction, and variable-contribution analysis for diagnosis”. In: *Industrial & Engineering Chemistry Research* 42.20 (2003), pages 4645–4658.

[124] S Wold et al. “Modelling and diagnostics of batch processes and analogous kinetic experiments”. In: *Chemometrics and Intelligent Laboratory Systems* 44.1-2 (1998), pages 331–340.

[125] SP Gurden et al. “A comparison of multiway regression and scaling methods”. In: *Chemometrics and Intelligent Laboratory Systems* 59.1-2 (2001), pages 121–136.

[126] Ch Zhao and FR Gao. “Fault-relevant principal component analysis (FPCA) method for multivariate statistical modeling and process monitoring”. In: *Chemometrics and Intelligent Laboratory Systems* 133 (2014), pages 1–16.

[127] P Miller, RE Swanson, and CE Heckler. “Contribution plots: a missing link in multivariate quality control”. In: *Applied Mathematics and Computer Science* 8.4 (1998), pages 775–792.

[128] ME Celebi and K Aydin. *Unsupervised learning algorithms*. Springer, 2016.

[129] RP Singh and DR Heldman. *Introduction to Food Engineering*. 5th edition. Academic Press, 2014, page 892.

[130] A Lehman et al. *JMP for basic univariate and multivariate statistics: Methods for researchers and social scientists*. SAS Institute, 2013.

[131] JA Westerhuis, SP Gurden, and AK Smilde. “Generalized contribution plots in multivariate statistical process monitoring”. In: *Chemometrics and Intelligent Laboratory Systems* 51.1 (2000), pages 95–114.

[132] P Van den Kerkhof et al. “Analysis of smearing-out in contribution plot based fault isolation for statistical process control”. In: *Chemical Engineering Science* 104 (2013), pages 285–293.

[133] A Kassidas, JF MacGregor, and PA Taylor. “Synchronization of batch trajectories using dynamic time warping”. In: *AIChE Journal* 44.4 (1998), page 864.

[134] JF Yang et al. “CFD modelling of axial mixing in the intermediate and final rinses of cleaning-in-place procedures of straight pipes”. In: *Journal of Food Engineering* 221 (2018), pages 95–105.

[135] JF Yang et al. “Investigation of the cleaning of egg yolk deposits from tank surfaces using continuous and pulsed flows”. In: *Food and Bioproducts Processing* (2018).

[136] L Chen et al. “Cleaning in place with onsite-generated electrolysed oxidizing water for water-saving disinfection in breweries”. In: *Journal of the Institute of Brewing* 118.4 (2012), pages 401–405.

[137] J Wiklund, M Stading, and C Trägårdh. "Monitoring liquid displacement of model and industrial fluids in pipes by in-line ultrasonic rheometry". In: *Journal of Food Engineering* 99.3 (2010), pages 330–337.

[138] TO Salmi, JP Mikkola, and JP Warna. *Chemical reaction engineering and reactor technology*. CRC Press, 2010.

[139] GI Taylor. "Dispersion of soluble matter in solvent flowing slowly through a tube". In: *Proceedings of the Royal Society A* 219.1137 (1953), pages 186–203.

[140] O Levenspiel. "Longitudinal mixing of fluids flowing in circular pipes". In: *Industrial & Engineering Chemistry* 50.3 (1958), pages 343–346.

[141] LL Zhao, J Derksen, and R Gupta. "Simulations of axial mixing of liquids in a long horizontal pipe for industrial applications". In: *Energy & Fuels* 24.11 (2010), pages 5844–5850.

[142] Y Chisti and M Moo-Young. "Clean-in-place systems for industrial bioreactors: design, validation and operation". In: *Journal of Industrial Microbiology* 13.4 (1994), pages 201–207.

[143] DC Wilcox. *Turbulence Modeling for CFD*. DCW Industries, 20016.

[144] BBB Jensen. "Numerical study of influence of inlet turbulence parameters on turbulence intensity in the flow domain: incompressible flow in pipe system". In: *Proceedings of the Institution of Mechanical Engineers, Part E: Journal of Process Mechanical Engineering* 221.4 (2007), pages 177–186.

[145] Z Stegowski et al. "Dispersion determination in a turbulent pipe flow using radiotracer data and CFD analysis". In: *Computers & Fluids* 79 (2013), pages 77–81.

[146] B James and F Ollis David. *Biochemical Engineering Fundamentals*. Mc Grow Hill Book Company, 1986.

[147] A Graßhoff. "Toträume in CIP-gereinigten Rohrleitungssystemen". In: *Deutsche Milchwirtschaft* 13 (1983), pages 407–414.

[148] R Higbie. "The rate of absorption of a pure gas into a still liquid during short periods of exposure". In: *Transactions of AIChE* 31 (1935), pages 365–389.

[149] EP Van Elk, MC Knaap, and GF Versteeg. "Application of the penetration theory for gas–liquid mass transfer without liquid bulk: differences with systems with a bulk". In: *Chemical Engineering Research and Design* 85.4 (2007), pages 516–524.

[150] K Ekambara and JB Joshi. "Axial mixing in laminar pipe flows". In: *Chemical Engineering Science* 59.18 (2004), pages 3929–3944.

[151] M Assar et al. "A new approach to analyze entrance region mass transfer within a falling film". In: *Heat and Mass Transfer* 50.5 (2014), pages 651–660.

[152] BBB Jensen et al. "Local wall shear stress variations predicted by computational fluid dynamics for hygienic design". In: *Food and Bioproducts Processing* 83.1 (2005), pages 53–60.

[153] M Schöler et al. "Local analysis of cleaning mechanisms in CIP processes". In: *Food and Bioproducts Processing* 90.4 (2012), pages 858–866.

[154] R Darby and RP Chhabra. *Chemical Engineering Fluid Mechanics*. Edited by R Darby and RP Chhabra. 3rd edition. CRC Press, 2017, page 555.

[155] DC Rennels and HM Hudson. *Pipe Flow: A Practical and Comprehensive Guide*. John Wiley & Sons, 2012.

[156] Neutrium. *Pressure loss from fittings - expansion and reduction in pipe size*. URL: `https://neutrium.net/fluid_flow/pressure-loss-from-fittings-expansion-and-reduction-in-pipe-size/`.

[157] DF Young et al. *A Brief Introduction to Fluid Mechanics*. John Wiley & Sons, 2010.

[158] Crane Company. *Flow of fluids through valves, fittings, and pipe*. 410. Crane Company, 1978.

[159] A Graßhoff. "Untersuchungen zum Stromungsverhalten von Flussigkeiten in zylindrischen Totraumen von Rorhleitungssystemen". In: *Die Kieler Milchwirtschaft Forschungs* 32.4 (1980), pages 273–298.

[160] DE Briggs et al. *Brewing: science and practice*. Elsevier, 2004.

[161] M Stenby, MW Dethlefsen, BBB Jensen, et al. "New test method for rotating spray head performance in tank cleaning". In: *World Congress on Hygienic Engineering & Design*. 2011, pages 40–43.

[162] CR Gillham et al. "Enhanced cleaning of whey protein soils using pulsed flows". In: *Journal of Food Engineering* 46.3 (2000), pages 199–209.

[163] K Bode et al. "Pulsed flow cleaning of whey protein fouling layers". In: *Proceedings of 6th International Conference on Heat Exchanger Fouling and Cleaning - Challenges and Opportunities*. Volume 2. 25. Kloster Irsee, Germany, The Berkeley Electronic Press, 2005, pages 165–173.

[164] W Augustin et al. "Pulsed flow for enhanced cleaning in food processing". In: *Food and Bioproducts Processing* 88.4 (2010), pages 384–391.

[165] H Föste et al. "Modeling and validation of the mechanism of pulsed flow cleaning". In: *Heat Transfer Engineering* 34.8-9 (2013), pages 753–760.

[166] MS Celnik et al. "Analytical approaches for calculation of shear stress enhancement in laminar pulsed flows". In: *Proceedings of 6th International Conference on Heat Exchanger Fouling and Cleaning - Challenges and Opportunities*. Kloster Irsee, 2005, pages 174–182.

[167] B Olayiwola and P Walzel. "Effects of in-phase oscillation of retentate and filtrate in crossflow filtration at low Reynolds number". In: *Journal of Membrane Science* 345.1-2 (2009), pages 36–46.

[168] C Weidemann, S Vogt, and H Nirschl. "Cleaning of filter media by pulsed flow–Establishment of dimensionless operation numbers describing the cleaning result". In: *Journal of Food Engineering* 132 (2014), pages 29–38.

[169] E Fuchs et al. "Erhöhung der Reinigungseffizienz bei der Cleaning-in-Place-Reinigung durch diskontinuierliche Flüssigkeitsstrahlen". In: *Chemie Ingenieur Technik* 89.8 (2017), pages 1072–1082.

[170] H Stoye et al. “Untersuchungen zur Steigerung der Reinigungseffizienz durch pulsierende Spritzreinigung”. In: *Chemie Ingenieur Technik* 86.5 (2014), pages 707–713.

[171] M Le Denmat, M Anton, and G Gandemer. “Protein denaturation and emulsifying properties of plasma and granules of egg yolk as related to heat treatment”. In: *Journal of Food Science* 64.2 (1999), pages 194–197.

[172] DC Montgomery. *Design and Analysis of Experiments*. 8th edition. John Wiley & Sons, Inc., 2012, page 757.

[173] K Lerch et al. “Cleanability of surfaces from active pharmaceutical ingredient surrogate riboflavin by falling film”. In: *Chemie Ingenieur Technik* 85.3 (2013), pages 323–332.

[174] *Diversey CIPTEC*. URL: `https://www.diversey.com/food-care/diversey-knowledge-based-services/diversey-ciptec`.

[175] L Pettigrew et al. “Optimisation of water usage in a brewery clean-in-place system using reference nets”. In: *Journal of Cleaner Production* 87 (2015), pages 583–593.

[176] JT Holah et al. “A method for assessing the in-place cleanability of food-processing equipment”. In: *Trends in Food Science & Technology* 18 (January 2007), S54–S58.

[177] T Varzakas and C Tzia. *Handbook of food processing: food safety, quality, and manufacturing processes*. CRC Press, 2015.

[178] RK Bhagat, AM Perera, and DI Wilson. “Cleaning vessel walls by moving water jets: Simple models and supporting experiments”. In: *Food and Bioproducts Processing* 102 (2017), pages 31–54.

[179] H Köhler et al. “Study on the application of cleaning models with high speed water jets to CIP-processes”. In: *Tehnički Vjesnik* 23.2 (2016), pages 349–355.

[180] T Wang, JF Davidson, and DI Wilson. “Flow patterns and cleaning behaviour of horizontal liquid jets impinging on angled walls”. In: *Food and Bioproducts Processing* 93 (2015), pages 333–342.

[181] OM Magens et al. “Adhesion and cleaning of foods with complex structure: Effect of oil content and fluoropolymer coating characteristics on the detachment of cake from baking surfaces”. In: *Journal of Food Engineering* 197 (2017), pages 48–59.

[182] Micro-Epsilon. “Instruction Manual: confocalDT 2451/2461/2471”. Ortenburg, Germany, 2016.

[183] TT Hsu et al. “Role of fluid elasticity on the dynamics of rinsing flow by an impinging jet”. In: *Physics of Fluids* 23.3 (2011), page 033101.

[184] The American Society of Mechanical Engineers. *ASME BPE-2016: Bioprocessing Equipment*. Standard. 2016.

[185] G Götz et al. “Adjustment of the wastewater matrix for optimization of membrane systems applied for water reuse in breweries”. In: *Journal of Membrane Science* 465 (2014), pages 68–77.

[186] K Loganathan, P Chelme-Ayala, and MG El-Din. "Pilot-scale study on the treatment of basal aquifer water using ultrafiltration, reverse osmosis and evaporation/crystallization to achieve zero-liquid discharge". In: *Journal of Environmental Management* 165 (2016), pages 213–223.

[187] L Suárez et al. "Membrane technology for the recovery of detergent compounds: a review". In: *Journal of Industrial and Engineering Chemistry* 18.6 (2012), pages 1859–1873.

[188] M Dresch, G Daufin, and B Chaufer. "Integrated membrane regeneration process for dairy cleaning-in-place". In: *Separation and Purification Technology* 22 (2001), pages 181–191.

[189] T Paul et al. "Smart cleaning-in-place process through crude keratinase: an eco-friendly cleaning techniques towards dairy industries". In: *Journal of Cleaner Production* 76 (2014), pages 140–153.

[190] T Chutrakul et al. "Enzyme-based integrated solution to cleaning of coconut milk foulants". In: *Food and Bioproducts Processing* (2018).

[191] R Jiménez-Pichardo et al. "Evaluation of electrolyzed water as cleaning and disinfection agent on stainless steel as a model surface in the dairy industry". In: *Food Control* 60 (2016), pages 320–328.

[192] J Quarini. "Ice-pigging to reduce and remove fouling and to achieve clean-in-place". In: *Applied Thermal Engineering* 22.7 (2002), pages 747–753.

[193] EA Ainslie et al. "Heat exchanger cleaning using ice pigging". In: *Proceedings of International Conference on Heat Exchanger Fouling and Cleaning VIII*. 2009, pages 433–438.

Process and Systems Engineering Centre (PROSYS)
Department of Chemical and Biochemical Engineering
Technical University of Denmark
Søltofts Plads, Building 229
DK - 2800 Kgs. Lyngby
Denmark

Phone: +45 45 25 28 00
Web: www.kt.dtu.dk/forskning/prosys